Aspects géotechniques des pieux de fondation énergétiques

Neda Yavari

UNIVERSITÉ PARIS-EST

Thèse pour obtenir le grade de

Docteur de l'Université Paris-Est

discipline : Géotechnique

Présentée par

Neda YAVARI

Aspects géotechniques des pieux de fondation énergétiques

Centre d'Enseignement et de Recherche en Mécanique des Sols (CERMES)
Laboratoire Navier

Soutenue le 27 Novembre 2014

JURY

Hussein MROUEH	Université de Lille	Rapporteur
Luc THOREL	IFSTTAR	Rapporteur
Farimah MASROURI	Université de Lorraine	Examinatrice
Jean-Michel PEREIRA	École des Ponts ParisTech	Examinateur
Ghazi HASSEN	École des Ponts ParisTech	Examinateur
Anh-Minh TANG	École des Ponts ParisTech	Directeur de thèse

ACKNOWLEDGEMENTS

First and foremost, I wish to thank my research director, Dr. Anh Minh Tang for being supportive from the very first days I began working on the project. His expertise, understanding and patience, added considerably to my graduate experience. I would have been lost without his detailed plan. I am also deeply thankful to my co-director, Dr. Jean-Michel Pereira, for his inspiring guidance, sound advice and good ideas especially throughout my thesis-writing period. My sincere gratitude also goes to Dr. Ghazi Hassen for supervising me throughout the numerical study, for everything I learned, for his ideas and pertinent suggestions. Intelligence, wisdom, problem solving skills and human qualities of the supervision team made me cherish every moment of this work, even the hardest ones.

I am grateful to members of the jury, Prof. Farimah Masrouri, Prof. Hussein Mroueh and Dr. Luc Thorel, for agreeing to read the manuscript and to participate in the defence of this thesis; their remarks and constructive criticism were of great help.

I would like to express my appreciation to the French National Research Agency for funding this PhD thesis.

My sincere thanks also go to the laboratory's technical support staff ; Emmanuel De Laure, Hocine Delmi, Baptiste Chabot, Xavier Boulay and Marine Lemaire. Without their permanent support, unquestionable skills, understanding and helpfulness the experimental part of this work would definitely not have been possible. Thanks to all the CERMES members, for providing a stimulating environment. My special gratitude to my friends, Hamza Menaceur and Nicolaine Agofack for their moral support.

I would especially like to thank the French Institute of Science and Technology for Transport, Development and Networks (IFSTTAR) for supplying one of the most important experimental apparatuses and all the technical support. Appreciation is extended to Dr. Alain Le Kouby and Mr. Jean-Louis Tacita. Special thanks to Dr. Emmanuel Bourgeois for useful discussions and technical aids on the utilised finite element program.

My loving thanks to my husband, *Arash*, for his never-failing sympathy and encouragement, for always being there to help and support me, and for always being patient with me. Thanks for '*teaching*' me how to enjoy the delights and dangers of this adventure : writing the thesis.

To conclude this introduction with Iran, where the most basic source of my life meaning resides: my family. I am hugely thankful to the unconditional support of my parents. As always, I find myself *speechless* when it comes to them. I just want to assure them that I feel more deeply than ever that *the more I learn, the less I know*. My sisterly thanks to *Sara*, for ‘seeing me through the hard times that we have had’, for her ‘loyal heart’.

To my father,

To my mother,

To Arash & Sara……

ABSTRACT

Energy pile efficiency has been tested and validated by numerous studies from environmental and energy-related points of view until now. Nevertheless, energy pile technology is still more or less unknown and rarely applied in construction, especially in France compared to other European countries. The chief reason for this lack of attention might be the limited knowledge of the impact of the coupled thermo-mechanical loading on the behaviour of the pile and that of the surrounding soil. This thesis aims to study the geotechnical aspects of energy piles through physical modelling and some numerical investigations.

A physical model is developed in order to better identify the soil/pile interaction under thermo-mechanical loading. The model is made up of a small pile equipped with a heat exchanger loop embedded in compacted soil. The pile was once installed in dry sand and then in saturated clay; it was then loaded mechanically and was subjected to thermal cycles. The effect of mechanical load value, number of thermal cycles and soil type is studied. The results show the appearance of irreversible settlements during thermal cycles, whose quantity increases as the pile head load increases. Total pressure in the soil close to the pile surface does not change by cooling and heating, while total pressure below the pile increases gradually as thermal cycles proceed. This is in accordance with the permanent downward movement of the pile within thermal cycles. Experiments also show the evolution of axial force profiles with temperature, axial force in the pile increases by cooling and decreases by heating.

In another part of the experimental work, focus shifted to the soil/pile interface. The shear behaviour of the soil (the same as the soils used above) and that of the soil/concrete interface was evaluated at different temperatures. To do this, a conventional shear apparatus was equipped with a temperature control system. Soil (and soil/concrete interface) was subjected to a rather low range of stress. Thermal consolidation was performed according to a special protocol. It was observed that the soil friction angle and cohesion do not change considerably relative to temperature.

The numerical study was initiated by simulating existing tests in the literature on energy piles through a finite element code well-known to engineers, applying a simplified method. The thermal load was simulated by imposing volumetric strains calculated from the coefficient of thermal expansion of the material on the pile. The method successfully simulates the behaviour of some full-scale energy piles in terms of axial strain and pile head displacement. The results highlight the important role played by the pile thermal volume change on the mechanical behaviour of the energy pile under various thermo-mechanical loadings. In the

second stage, another numerical code with the possibility of including temperature effects was used for modelling the tests formerly performed on the physical model. Thus, compared to the first numerical attempts, the soil thermal volume change is also taken into account. The numerical results were compared with the experimental ones obtained from physical modelling. It was deduced that the numerical model could simulate correctly the pile behaviour under purely mechanical loading. Also, simulating thermo-mechanical tests, a good estimation of heat conduction in the soil was achieved numerically. Regarding the mechanical behaviour of the pile under thermal cycles, the numerical model adequately predicts the gradual ratcheting of the pile as observed in the experiments. However in terms of axial force distribution in the pile, the results from numerical modelling are different from the physical one.

Key words: energy pile, thermo-mechanical loading, dry sand, saturated clay, physical modelling, shear behaviour, soil/concrete interface, numerical modelling, heating/cooling cycle

RÉSUMÉ

L'efficacité de pieux géothermiques (e.g. énergétiques) a été examinée et validée par de nombreuses études à partir de points de vue environnemental et energétique jusqu'à présent. Néanmoins, la technologie des pieux géothermiques est encore peu connue et rarement appliquée dans la construction, notamment en France comparée à d'autres pays européens. La raison principale du manque d'attention peut être la connaissance limitée sur les impacts du chargement thermomécanique sur le comportement du pieu et celui du sol environnant. Cette thèse vise à étudier les aspects géotechniques des pieux géothermiques grâce aux modélisations physique et numérique.

Un modèle physique est développé afin de mieux connaitre l'interaction sol/pieu sous chargement thermomécanique. Le modèle est composé d'un pieu énergétique équipé des tubes d'échangeur de chaleur, installé dans un sol compacté. Le pieu a d'abord été installé dans un sable sec, puis dans une argile saturée ; il a ensuite été chargé mécaniquement et soumis à des cycles thermiques. L'effet de la charge mécanique, du nombre de cycles thermiques et du type de sol a été étudié. Les résultats montrent la génération de tassements irréversibles au cours des cycles thermiques, dont la quantité augmente avec l'augmentation de la charge en tête du pieu. La pression totale dans le sol à proximité de la surface du pieu ne change pas par refroidissement et chauffage, tandis que la pression totale au-dessous du pieu augmente progressivement à mesure que les cycles thermiques poursuivent. Les expériences montrent aussi l'évolution des profils de la force axiale avec la température ; la force axiale dans le pieu augmente pendant le refroidissement et diminue pendant l'échauffement.

Les comportements au cisaillement du sol (mêmes sols que ceux utilisés dans la première partie) ainsi que de l'interface sol/béton ont été évalués à différentes températures. Pour ce faire, un appareil de cisaillement conventionnel a été équipé d'un système de contrôle de température. Le sol (et l'interface sol/béton) a été soumis à une gamme de contraintes relativement faibles. La consolidation thermique a été effectuée selon un protocole particulier. Il a été observé que l'angle de frottement et la cohésion de matériaux utilisés ne changent pas sensiblement avec température.

L'étude numérique a débuté par la simulation d'essais existants dans la littérature sur des pieux énergétiques en appliquant une méthode simplifiée via un code de calcul basé sur la méthode des éléments finis et assez répandu dans la profession. Le changement de la température est simulé en imposant au pieu des déformations volumétriques calculées à partir du coefficient de dilatation thermique du matériau. La méthode prédit correctement le comportement de certains pieux énergétiques à grande échelle en termes de contrainte axiale

et de déplacement en tête du pieu. Les résultats mettent en évidence le rôle important joué par le changement de volume du pieu induit par les variations thermiques sur son comportement mécanique. Dans un second temps, un autre code de calcul offrant la possibilité d'inclure les effets thermique a été utilisé pour la modélisation des essais effectués auparavant sur le modèle physique. Ainsi, en comparant aux modélisations numériques précédemment expliquées, le changement de volume du sol induit par les variations de température est également pris en compte. Les résultats numériques et expérimentaux sont ainsi comparés. On en déduit que le modèle numérique est capable de prédire le comportement des pieux sous chargement purement mécanique. En outre, en simulant des essais thermomécaniques, une bonne estimation du transfert thermique dans le sol est obtenue. En ce qui concerne le comportement mécanique du pieu au cours de cycles thermiques, le modèle numérique prédit bien le tassement progressif du pieu. Cependant, en termes de répartition de la force axiale, on obtient des résultats contradictoires.

Mots-clés: pieu énergétique, chargement thermomécanique, sable sec, argile saturée, modélisation physique, cisaillement, interface sol/béton, modélisation numérique, cycle de chauffage/refroidissement

PUBLICATIONS

- **Yavari, N.**, Tang, A.M., Pereira, J.M., Hassen, G. 2014. A simple method for numerical modelling of mechanical behaviour of an energy pile. Géotechnique Letters 4: 119-124.
- **Yavari, N.**, Tang, A.M., Pereira, J.M., Hassen, G. 2014. Experimental study on the mechanical behaviour of a heat exchanger pile using physical modelling. Acta Geotechnica 9(3): 385–398.
- Tang, A.M., Pereira, J.M., Hassen, G., **Yavari, N.** 2013. Behaviour of Heat-Exchanger Piles from Physical Modelling. Chapter 4, Energy Geostructures: Innovation in Underground Engineering (Eds. Laloui & Di Donna), pp. 79 -97.
- Hassen, G., Pereira, J.M., Tang, A.M., **Yavari, N.** 2014. Etude du comportement des pieux échangeurs de chaleur par modélisation physique. Chapitre 4, Géostructure Énergétiques (Eds. Laloui & Di Donna), pp. 99-115.
- Tang, A.M., Pereira, J.M., Hassen, G., **Yavari, N.** 2013. Mechanical behaviour of energy piles. Proceedings of the 2nd International Conference on Geotechnics for Sustainable Development (Geotec Hanoi 2013).
- Tang, A.M., Pereira, J.M., Hassen, G., **Yavari, N.**, Kalantidou, A. 2013. Studying the mechanical behaviour of energy pile physical model. Proceedings of the French-Vietnamese conference on “Construction and Sustainable Development”, CIGOS 2013. No. 22.
- **Yavari, N.**, Tang, A.M., Pereira, J.M., Hassen, G. 2015. Modelling the mechanical behaviour of an energy pile. 16th European Conference on Soil Mechanics and Geotechnical Engineering (accepted).
- **Yavari, N.**, Tang, A.M., Pereira, J.M., Hassen, G. 2012. A physical model for studying the mechanical behaviour of heat exchanger pile. ALERT Geomaterials Workshop 2012.
- Pereira, J.M., Tang, A.M., Hassen, G., **Yavari, N.** 2013. Mechanical behaviour of a heat exchanger pile: physical and numerical modelling. Geoengineering Energy Geo-Storage, Weimar, Germany.

TABLE OF CONTENTS

LIST OF FIGURES

LIST OF TABLES

NOMENCLATURE

Greek symbols

α	coefficient of linear thermal expansion ($10^{-6} / °C^{-1}$)
α_n	creep parameter (mm)
α_v	coefficient of volumetric thermal expansion ($10^{-6} / °C^{-1}$)
β	gauge factor
γ	unit weight (kN / m^3)
$\underline{\Gamma}^d$	stress vector
Δ_i	displacement (mm)
ΔT	temperature change (°C)
ε	strain (10^{-6})
$d\lambda$	plastic multiplier
ν	Poisson's ration
ρ	density (Mg / m^3)
ρ_s	particle density (Mg / m^3)
$\underline{\underline{\sigma}}$	stress tensor
σ_n	normal stress (kPa)
τ	shear stress (kPa)
φ	friction angle (°)
ψ	dilation angle (°)

Roman letters

c	cohesion (kPa)

C_v	volumetric heat capacity
$\mathbb{C}$	fourth-order isotropic linear elastic stiffness tensor
D_{50}	median grain size of soil (mm)
e_{max}	maximum void ratio
e_{min}	minimum void ratio
E	elastic modulus (MPa)
H	sample height (mm)
g	gravitational acceleration (m/s^2)
k	thermal conductivity ($W/m°C$)
K	soil hydraulic conductivity (m/s)
K_0	coefficient of lateral earth pressure at rest
K_w	bulk modulus of water (MPa)
n	porosity
P	axial force (kPa)
q	heat flux
S_i	pile head displacement at time I (mm)
t	time (s)
T	temperature(°C)
$\underline{u}$	displacement vector
$V_{\max}$	shear rate (μm/min)
K_0	coefficient of lateral earth pressure at rest
Z	depth (mm)

GENERAL INTRODUCTION

Sustainable development implies reducing any reliance on the technical usage of current energy resources and shifting to others which are known to be clean, environmental friendly and renewable, if properly explored. Geothermal energy is a clean energy resource which does not contribute to global warming emissions. Heat contained in shallow ground can be used by means of a heat pump to cool or heat buildings, since the temperature inside the ground remains stable all year long (Brandl, 2013). In most European countries, this temperature varies between 10°C and 15°C and remains constant below 10 m in depth (Adam & Markiewicz, 2009). Therefore, in summer, the ground is cooler than ambient air and can act as an air conditioner, whereas in winter, the ground is warmer than the air and can be used to heat a building.

Many technologies have been developed to take advantage of geothermal energy, among which energy piles have gained particular attention during the last three decades. Energy piles are double-function piles working simultaneously as conventional deep foundations and heat exchangers. Energy piles contain polyethylene loops within which a heat carrier fluid (generally a mixture of water and glycol) circulates. Loops are connected to a heat pump by means of which in winter, the heat transfer fluid with a temperature of about 4° C is fed into the pile. It is warmed up and then injected back to the building with a higher temperature. The operation is inversed in summer: the fluid with a temperature close to 30° C is injected into the pile and comes back to the building with a lower temperature. Experiments highlight the efficiency of energy piles especially for heating of large industrial or office buildings. Also during summer months, instead of using chillers such buildings can very economically be cooled by running only a circulation pump in the system (Vuataz *et al.*, 2003).

Although justified and accepted from energy and environmental points of view (De Moel *et al.*, 2010), the application of this construction technique is hindered particularly because of the lack of a clear vision of the structural integrity of the pile under heating and cooling cycles.

Subjecting the pile to coupled mechanical and thermal cycles could indeed have important impact on the pile's structural behaviour. It is important to understand what effects heating and cooling cycles have on the behaviour of the foundations in order to determine their long-term structural stability: a) expansion and contraction of the pile subjected to heating and

cooling cycles together with; b) thermal volume change in the surrounding soil; c) and dependency of mechanical properties of the pile and the soil to temperature. These effects lead to changing the pile/soil interaction, which results in the variation of axial stress distribution in the pile and reduction of adhesion forces at the pile's interface. The thermo-mechanical response of the soil/pile interface need to be understood for developing appropriate design practices and standards, which propose economically optimised methods.

The objective of this Ph.D. thesis is to improve knowledge of the geotechnical aspects of heat exchanger piles through physical and numerical modelling. Experimental work consists in the development of a small-scale model in the laboratory and in the implementation of shear tests on soil and soil/pile interface in a modified shear box. The numerical study aims to examine the ability of current commercial codes to simulate energy piles including real scale and small scale ones.

Chapter 1 reviews the literature on different aspects of energy piles with a focus on their geotechnical aspects. The thermo-mechanical behaviour of soils is included. The shear behaviour of soil and soil/pile interface, without and with temperature changes, is highlighted. Different types of tests conducted on energy piles from in situ to laboratory scale are reviewed and major observations are discussed. Numerical studies performed on energy piles are pointed out afterwards. A brief introduction to the limited number of standards and design approaches on energy piles is also provided, which highlights the large deficit in current knowledge of this technology.

The second chapter presents the experiments on a small-scale energy pile. The model pile and its instrumentation are presented. Transducers used and soil materials are discussed in detail. Experimental procedure is explained afterwards.

The experimental results obtained from the physical model are presented in Chapter 3. The response of the pile was investigated by measuring the pile head's displacement, the pile's temperature and the pile's axial strain. The effects induced in the soil during mechanical and thermo-mechanical loading were explored via the measurement of temperature and total pressure.

The fourth chapter concerns shear tests on soil and soil/concrete interface at controlled temperature. Shear box equipment, materials and sensors used are presented. Thermo-mechanical loading paths are discussed. The results are analysed in order to evaluate the effect of temperature on the shear behaviour of sand, clay and clay/concrete interface.

The last chapter discusses numerical modelling performed on energy piles. Two finite element codes (Plaxis and Cesar-LCPC) commonly used by engineers in foundation design

are applied. As a first approach, a decoupling method was proposed whose validity is examined by modelling real scale and small-scale tests via Plaxis. Thereafter, the other commercial code in which temperature effects are also included, is utilised for modelling the pile in the small-scale model developed. The manuscript concludes by presenting general conclusions and perspectives.

CHAPTER 1

LITERATURE REVIEW

1.1 Introduction

The important environmental issue of reducing CO_2 emissions and the fact that the energy sources are limited have led to strengthening the classic idea of using renewable energies. One generally accepted concept is paying attention to the geothermal energy and extracting the energy stored below the earth's surface for heating purposes in winter and injecting the thermal energy back to the earth for cooling purposes in summer. Energy piles were introduced to the industry in the 1980's and could be considered as dual-purpose structural elements, that transfer the building loads to the ground (as other classical deep foundations) and exchange the ground/building heat as geothermal boreholes. Coupled effects of thermo-mechanical loading could have questionable impact on the mechanical behaviour of the soil and that of soil/pile interface, which could affect the pile behaviour.

Within this chapter, thermo-active geo-structures in general, and energy piles in particular are first presented. Energy piles are then discussed from energy-related and environmental points of view, according to different studies on this subject. Focus was put afterwards on geotechnical aspects of energy piles, which include the mechanical effects of heating and cooling on the soil/pile interface and on the surrounding soil. The experiments performed without and with temperature changes aiming at characterising both soil behaviour under thermo-mechanical loading and soil/pile interface response were reviewed. This literature review was extended to the study of soil/pile interaction in energy piles via experiments and numerical models. In experimental studies, the test procedure is explained and some important results are presented. Regarding the numerical studies, the models adopted, the numerical procedure and illustrative results are summarised. Finally, the existing energy piles design approaches and their limitations are discussed.

1.2 Thermo-active ground structures

More than 40% of the total energy consumed in Europe is used for heating, ventilation and air conditioning in residential and commercial buildings (Katzenbach *et al*., 2008). The main sources of this energy are fossil fuels which have major environmental impact on one hand and are finite resources on the other. It seems therefore vital to shift from conventional energy sources to low carbon renewable ones.

Geothermal energy could provide a clean and reliable energy source and help significantly in reducing carbon dioxide (CO_2) and other greenhouse gases emissions. Thermal energy stored at depths of 3 to 4 km could be used for electricity production. However this technique is relatively complicated and expensive. Shallower depths provide a good potential for energy storage or extraction, considering that the underground temperature variations stabilise at a depth of 10-20 m (Sanner, 2001), even if ground temperature at very shallow depths does not exceed 30°C (BRGM, 2005). Implementation of geothermal energy at these depths seems to be efficient for space heating and cooling purposes especially in structures with low thermal requirements.

Piles, diaphragm walls, boreholes, slabs, retaining walls and tunnel linings could be transformed into thermo-active geo-structures taking advantage of their structural concrete elements, which are connected to the ground, and considering the relatively high thermal conductivity of concrete. To make the heat exchange possible, concrete elements which are in contact with the underground are equipped with polyethylene pipes containing a heat carrier fluid. Concrete elements are connected to a second network of pipes integrated in other structural elements (which could be walls and roofs in the case of a building). Heat exchange, between the structure and the ground during different seasons, is carried out by the circulation of the heat carrier fluid. As a consequence, heat recovered from the structure through the second network of pipes is injected into the soil during summer and inversely, heat is extracted from the ground and transferred to the structure (again through the mentioned network of pipes) during winter (Brandl, 2006; Banks, 2008; Boënnec, 2009; Adam & Markiewicz, 2009). The technology could be applied in heating and cooling of conventional buildings, pavements, bridge decks and metro stations. As well-known projects, Laizer tunnel in Vienna (Austria), Dock Madfield terminal at Zurich airport (Switzerland), Main Tower in Frankfurt (Germany), One New Change building and Crossrail Project in London (UK) and more recently Shanghai Tower in Shanghai (China) could be mentioned (Pahud *et al*., 1999; Di Donna & Laloui, 2013*a*; Brandl 2006; Brandl 2013).

1.3 Energy piles

It is now more than 30 years that geothermal energy is being obtained from deep foundations known as geothermal, heat exchanger or energy piles (Brandl, 2006). Energy piles transfer the building loads to the ground and exchange the ground and building heat at the same time (Figure 1.1). The technology was inaugurated in Austria and spread first to other European countries and more recently to USA and Asian countries (Amis & Loveridge, 2014; Di Donna & Laloui, 2013*a*).

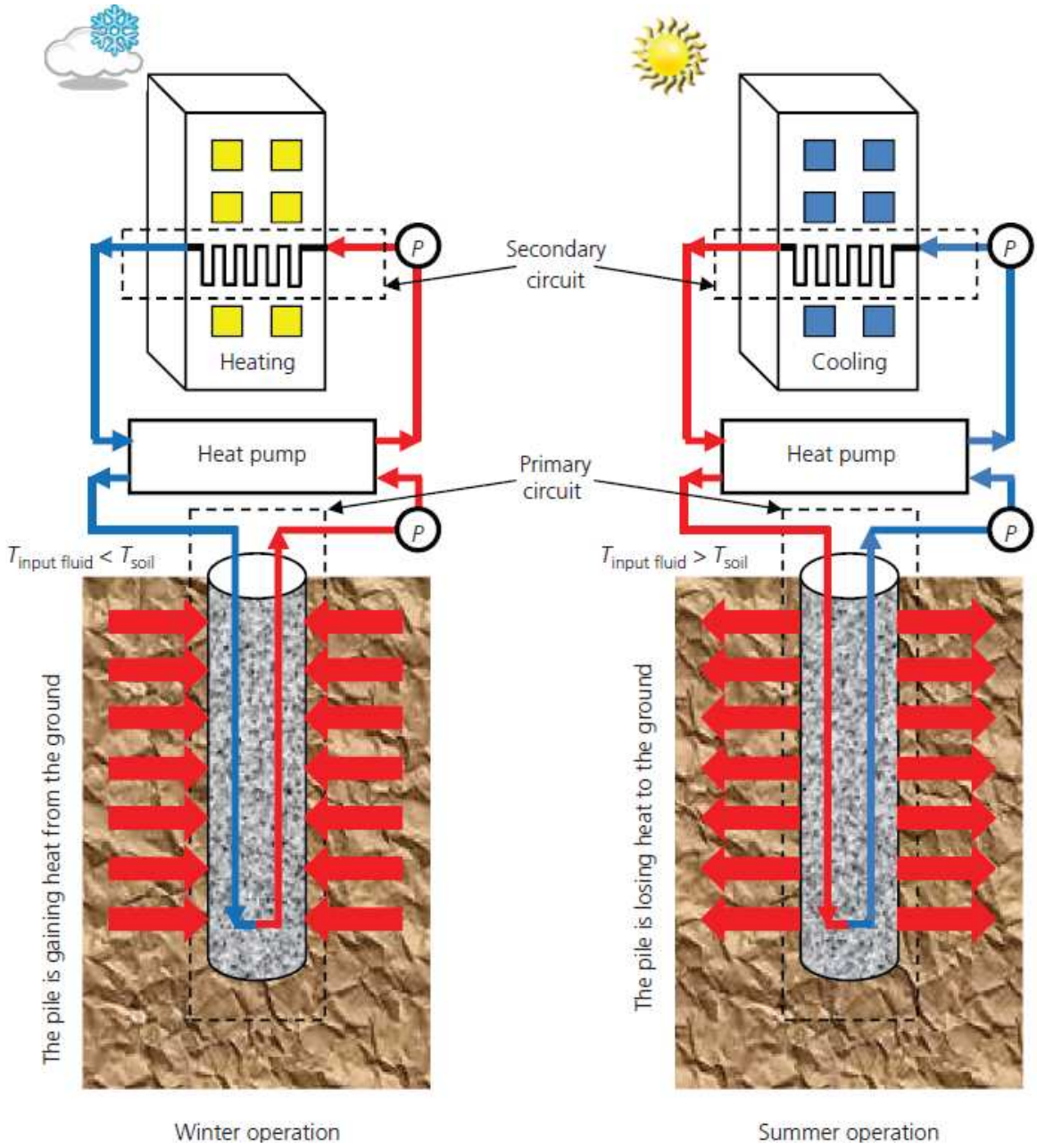

Figure 1.1 Heat exchanger pile performance during cold and hot periods of the year (Abuel Naga *et al.*, 2014)

Similar to conventional thermal boreholes, geothermal pipe loops filled with a heat carrier fluid, are inserted into the pile at the same time that the reinforcement cage is embedded. Usually, the system is accompanied by a heat pump which helps not only to circulate water, but also to increase the fluid's temperature from 10-15°C up to 25°C-35°C (Brandl, 2013).

That way, 15% to 25% of thermal needs of a building could be provided (Amis & Loveridge, 2014) while the electricity consumption of the heat pumps integrated with energy piles is only 25% to 30% of the building total electricity requirements (Ebnöther, 2008). The heat, which could be extracted from the ground through a one meter long-energy pile, varies between 20 W and 75 W (Ebnöther, 2008). Heat transfer rate is greater in piles with larger diameters (Amis & Loveridge, 2014) and in soils with higher thermal conductivity (Ebnöther, 2008). The heat that could be extracted from or injected into the ground depends on many parameters, mainly: the viscosity, heat conductivity and specific heat capacity of the heat carrier fluid; the dimension of the internal pipes; flow velocity within the pipes; difference between the inlet and outlet temperature values; thermal properties, hydraulic conditions and density of the soil; and the ground water level and its direction (Yari & Javani, 2007; Lee & Lam, 2007; Ma & Grabe, 2010; Dupray *et al*., 2014; Brandl, 2013; Stwart & McCartney, 2013; Dupray *et al*., 2014). There exist limited guidelines in terms of upper and lower temperature of the heat carrier fluid. It is highly recommended that the temperature imposed to the pile should not fall below zero, in order to prevent freezing at the soil/pile interface (SIA, 2005; Brandl, 2006; Loveridge & Powrie, 2013; Boënnec, 2009; GHSP, 2012). Regarding the upper temperature, it does not exceed 40°C in practice (Brandl, 2006; SIA, 2005).

Until now, energy piles have been studied from different points of view. A great part of the work has been focusing on energy-related aspects. Heat transfer regimes, thermal properties of soils, effect of pipes shape on system efficiency and effect of ground water level have been considered in the work of De Moel *et al*. (2010), Esen *et al*. (2009), Yari & Javani (2007) and Diao *et al*. (2004). Special care should be taken in order not to disturb the energy balance of the system (Arson *et al*., 2013; Loveridge & Powrie, 2013): heating and cooling loads should be similar enough. In other words, the same heat quantity extracted from the ground in winter should be injected into it in summer. Otherwise, the excess heat extraction could lead to ground freezing (Loveridge & Powrie, 2013; Boënnec, 2009; Cervera, 2013). In cold regions where heating requirements are dominant and risk of freezing is higher, other energy sources as solar energy should be used to compensate the excess heat extraction (Cervera, 2013). Arson *et al*. (2013) considered the particular case of an initially non-saturated soil. In such a case, heating and cooling loads applied to the pile could induce drying and wetting cycles to the surrounding

soil. This could be risky especially in expansive clayey soils, which undergo shrinkage by drying and swell by wetting. The volume changes applied to the soil in that way could lead to 'debonding' at pile interface. With respect to mechanical effects of this loss of adhesion, pile side friction decreases. In terms of energy loss, the created gap could play an insulating role and helps to break energy balance (Arson *et al*., 2013). Freeze-thaw cycles resulting from the imbalanced energy consumption, would cause structural damages to the pile and the soil (Katzenbach *et al*., 2013).

Although economic, eco-friendly and compatible with sustainable development, energy foundations have not gained the attention they deserved in the construction world, which could be directly related to lack of knowledge of their mechanical performance. Coupling effects of thermo-mechanical loading have been less examined which could be related not only to the complexity of the thermo-mechanical behaviour of the soil/pile system, but also to the difficulty of testing procedures.

Subjecting the pile to heating/cooling cycles could have important consequences, such as reducing the adhesion forces at pile interface, altering the axial stress distribution along the pile, inducing thermal consolidation and thermal volume change in the surrounding soil, etc. (Fromentin *et al*., 1999; Amatya *et al*., 2012; Arson *et al*. 2013; Akrouch *et al*., 2014; Murphy *et al*., 2014; Pasten & Santamarina, 2014; Yavari *et al*., 2014*a*&*b*). Soil mechanical parameters could also be affected by temperature changes (Cekerevac, 2003) and should not be ignored.

1.4 Thermo-mechanical behaviour of soils

Thermo-mechanical behaviour of soils has been a major research topic during the past two decades. Related researches apply to all underground structures which are subjected to thermal changes, including radioactive waste disposals, energy geo-structures, oil reservoirs, and high-voltage cables buried in soils (Cekeravac 2003; Brandl 2006; Abuel-Naga *et al*., 2007; Hueckel *et al*., 2009; Cui *et al*., 2009). Geological radioactive waste disposals submit the soil to high temperatures for a long period of time. The soil temperature varies from its initial state up to around 80°C (Graham *et al*., 2001; Tang *et al*., 2007). Thermal effects on the host geological formations, which are mainly clayey soils, could be important. In the case of energy geo-structures, such as walls and foundation piles, the soil temperature can vary from 5°C up to 40°C (Brandl, 2006; Boënnec, 2009), while greater difference between the upper and lower temperatures was considered in some studies in order to examine the worst case scenario (Bourne-Webb *et al*., 2009; Vega & McCartney, 2014).

Experimental studies on thermo-mechanical behaviour of soils are mostly based on modified oedometric or triaxial cells. The apparatus is generally equipped with a temperature control system and the soil temperature is changed indirectly. According to Cekerevac (2003), the difference between the apparatus developed in different studies is the temperature control method. Moritz (1995) used a triaxial apparatus, filled the cell with water and placed heating elements inside it. Clayey specimens were heated under drained and undrained conditions and then they were loaded until failure under undrained conditions. Tests were carried out at 8°C, 40°C and 70°C, while no experimental results are available at 8°C because of disturbance due to sampling problem. Cekerevac (2003) developed a triaxial apparatus based on the same principles as Baldi *et al*. (1985), Kuntiwattanakul *et al*. (1995) and Savvidou & Britto (1995). Thermally resistant rings were placed around the triaxial cell to control the temperature. Drained heating was performed between 22°C and 90°C. In the work of Abuel-Naga *et al*. (2007) an electric heater was attached to the outer oedometer ring. Water temperature was changed between 25°C and 95°C and clay samples were subjected to thermal cycles. Other heating methods consist of placing electric heating coil around a triaxial cell (Sultan *et al*., 2002; Monfared *et al*., 2011; Mohajerani *et al*., 2014) or immersing the cell in a thermostat bath (Tang *et al*., 2007). The temperature range applied in these studies was between 20°C and 80°C. It is worth noting that few work has been done in the temperature range lower than 20°C.

Different tests show that the thermo-mechanical behaviour of the soil depends strongly on the applied thermo-mechanical loading path. Heating under undrained conditions leads to increase in pore-water pressure and soil thermal expansion (Graham *et al*., 2001; Monfared *et al*., 2011; Mohajerani *et al*., 2014). Heating normally consolidated clay under drained condition induces thermal consolidation (Cui *et al*., 2000; Cekerevac & Laloui, 2004; Abuel-Naga *et al*., 2007). On the other hand, heating the soil at low stress induces thermal expansion. Subsequent mechanical loading shows a lower pre-consolidation stress at higher temperature (Sultan *et al*., 2002; Cekerevac & Laloui, 2004). Various constitutive models have been developed to describe the volumetric thermo-mechanical behaviour of clayey soils (Hong *et al*., 2013).

In terms of temperature effect on shear strength, conflicting results could be detected from the literature review. Cui *et al*. (2000) argued that the effects of temperature on shear strength of clay are strongly dependent on the volume change induced by heating. On one hand, thermal expansion leads to a decrease of soil strength; on the other hand, the thermal contraction hardens the soil and makes the shear strength increase. According to Hamidi *et al*. (2014), heating could make the friction angle decrease, increase or remain unchanged. The soil shear

behaviour is again found to be dependent on its mineralogy and the loading history. The same observation on friction angle was made by Cekerevac (2003), as illustrated in Figure 1.2.

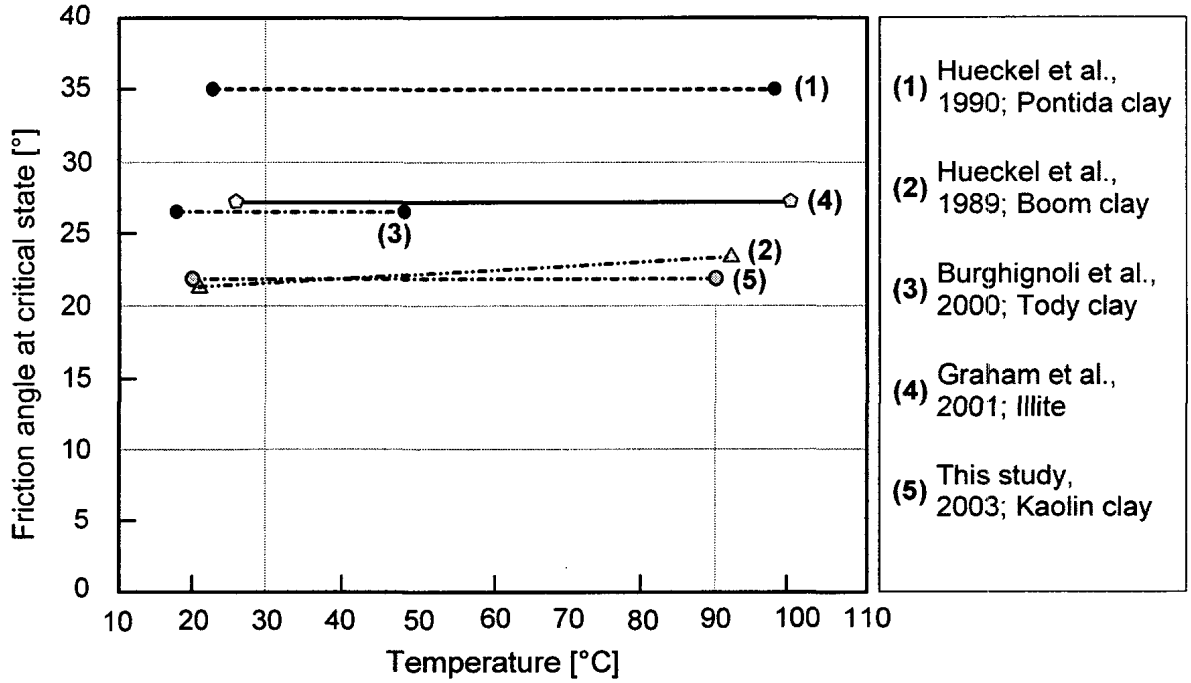

Figure 1.2 Evolution of soil internal friction angle with temperature (Cekerevac, 2003)

While various existing studies focus on the thermo-mechanical behaviour of clay, few work could be found on temperature effects on sand. Thermal consolidation tests performed by Recordon (1993) on fine sand in the range of 2°C and 40°C show that the compressibility parameters (compression index, modulus and over-consolidation ratio) are independent of temperature. The same observation was made by Saix *et al.* (2000) on clayey silty sand between 30°C and 70°C.

In the context of the energy piles, Franchomme *et al.* (2013) developed a mini penetration test which helps to rapidly determine temperature effects on cone tip resistance and shear resistance of the soil. The soil used was a mixture of Kaolin clay and Hostun sand. Two cones with a 60° apex, length of 250 mm and diameters of 10 and 12 mm were penetrated in the compacted sample with a rate of 30 mm/s. Tests were first performed on samples with an initial temperature of 20°C. Samples were then thermally cured at 1°C, 30°C and 50°C and tests were repeated. The experimental results show that in the range between 1°C and 30°C, effect of temperature on the penetration test parameters was negligible. At higher temperature values up to 50°C, water content decreased and tip and shear resistances increased. Eslami *et al.* (2014) performed pressuremeter tests on illitic soil at 20°C and 40°C. Soil was compacted in a container (600 mm in diameter and 800 mm in height) at a water content of 31.3% and a target

dry density of 1.29 Mg/m3. Steel tubes were welded to the outer surface of the soil container. A mixture of water and ethylene-glycol at a controlled temperature was circulated in the tubes. A mini pressuremeter with length of 340 mm and diameter of 22 mm was utilised. Pressure was increased by increments of 25 kPa for at least 1 minute. The results show low dependency of pressuremeter modulus to temperature in the tested range, while creep pressure and limit pressure values decreased when soil was heated from 20°C to 40°C. Also, pressuremeter curves indicate elastic limit shrinkage by heating.

Vega & McCartney (2014) studied the behaviour of saturated Bonny silt under heating and cooling cycles induced by energy geo-structures. Soil specimens were loaded to normally consolidated conditions in a modified thermal oedometer cell, then unloaded to different OCR values. Four thermal cycles were then conducted under a maximum temperature change of 75°C, during which soil was first heated then it underwent 'unassisted' cooling (which could also be known as the 'recovery' phase, see Kalantidou *et al*., 2012). Thermal axial strain versus temperature change for different OCR values is shown in Figure 1.3. The results show the contraction of normally consolidated specimens and the expansion of over-consolidated ones by the initial heating. The subsequent cooling led to elastic contraction of both normally consolidated and over-consolidated specimens. By the thermal phases that follow, all the specimens showed increasing additional irreversible volume change while the effects were more pronounced on the normally consolidated specimen. According to the authors, these observations disaffirm the applicability of current thermo-elasto-plastic models on the prediction of the long term behaviour of the soil under cyclic thermal loading, as they predict that the first heating produces plastic contraction in a soil specimen close to normally consolidated conditions, while subsequent heating and cooling cycles result in elastic volume change (Campanella & Mitchell, 1968; Laloui & Cekerevac, 2003; Cui *et al*., 2000).

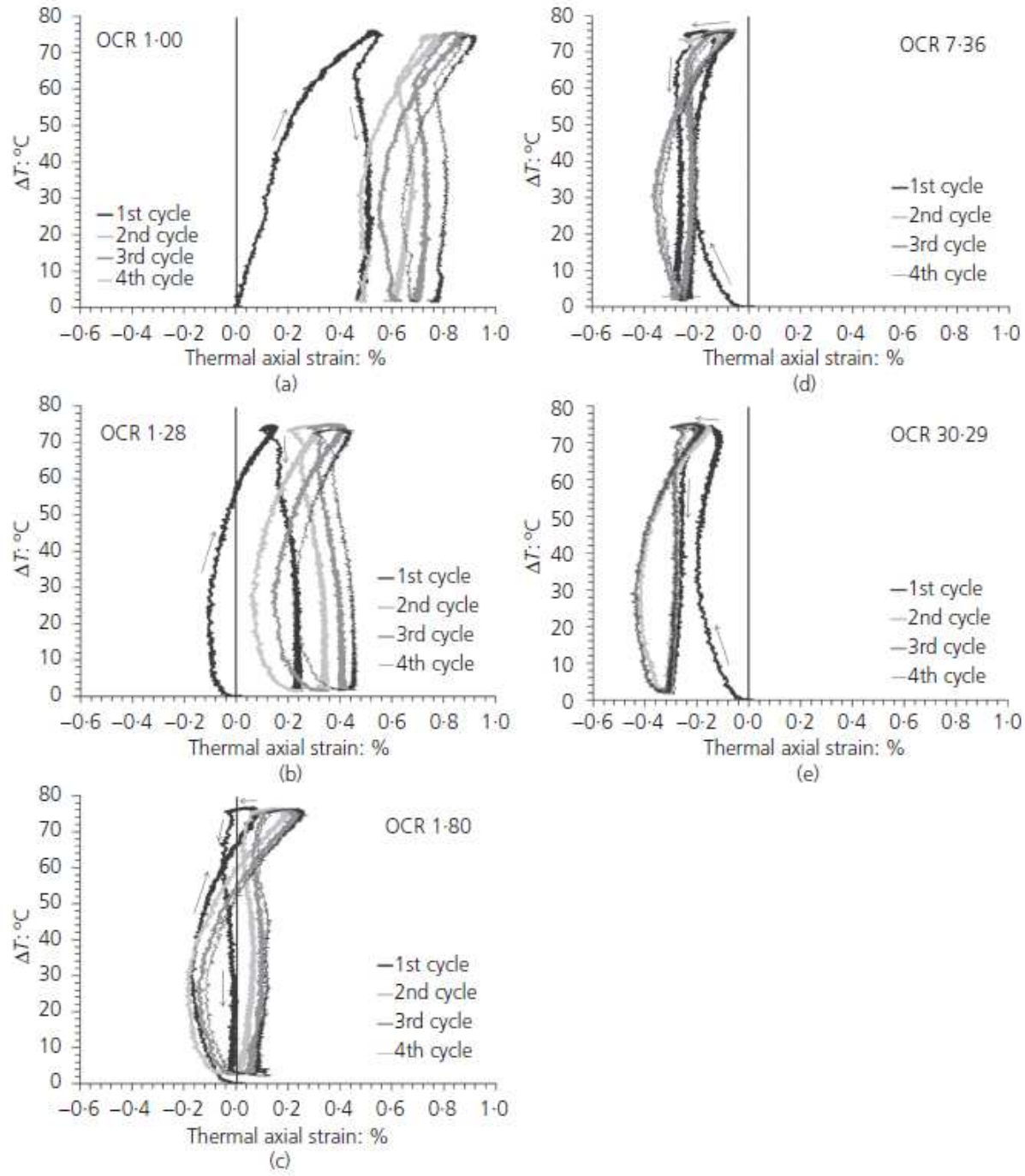

Figure 1.3 Axial strain versus temperature changes for different OCR values (Vega & McCartney, 2014)

1.5 Soil and soil/structure interface shear behaviour

Shear tests have been widely used in order to evaluate the shear behavior of soil itself and that of soil/structure interface. In the concerned studies, in general, first the shear strength of the soil is evaluated, then the soil is sheared against another surface and the two mechanisms are compared. As Lemos & Vaughan (2000) deduced from literature, shear strength found on sand/structure interfaces is always smaller than that of sand. When the roughness of the

interface is similar to the grains size, the shear strength will approach to the values observed during sand/sand shear tests. When sand is sheared, the shear behaviour depends on the density. In dense sands, peak strength is generally observed. Regarding the volume change, there exists a short contracting phase followed by a dilating one. In loose sands no peak could be identified and volume change remains contracting (Figure 1.4). On the contrary, the residual shear behaviour of clayey soils and clay/structure interfaces depends on their clay fraction. According to Lupini *et al*. (1981), three shear modes exist in clayey soils: sliding, turbulent and transitional. When clay fraction is dominant and the granular particles are dispersed, reoriented platy particles of clay could form a shear zone between the aggregates. Clay particles will slide on each other and shear will happen. In this case, shear failure is of brittle type. Reversely, when granular particles are dominant, enough space between larger particles, which could help creating the shear zone, does not exist. Thus shear will happen by rotation of the rotund particles and the shear mechanism is of turbulent mode. In this mode shear is of non-brittle type. There exist also a third mechanism, transitional type, in which the two mentioned modes could be observed at the same time. Lemos & Vaughan (2000) also stated that in high clay content clays, the shear residual resistance at interface is close to that of clay and it does not depend on surface roughness.

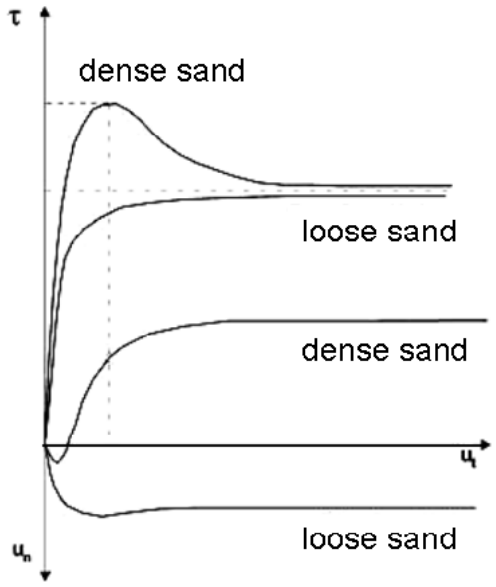

Figure 1.4 Typical interface response (Said, 2006)

Direct shear apparatus, simple shear apparatus and ring shear apparatus are usually used to study the shear behaviour of soil or soil/structure interface. Tsubakihara & Kishida (1993) used

a direct shear type and a shear box type apparatus in order to investigate the shear behavior of normally consolidated Kawasaki clay/steel interface. The shear box type used is shown in Figure 1.5. Steel plates with different roughness values were used. It was found that there exists a critical roughness beyond which shear failure occurs within the clay layer. Below the critical value, sliding at the interface occurs.

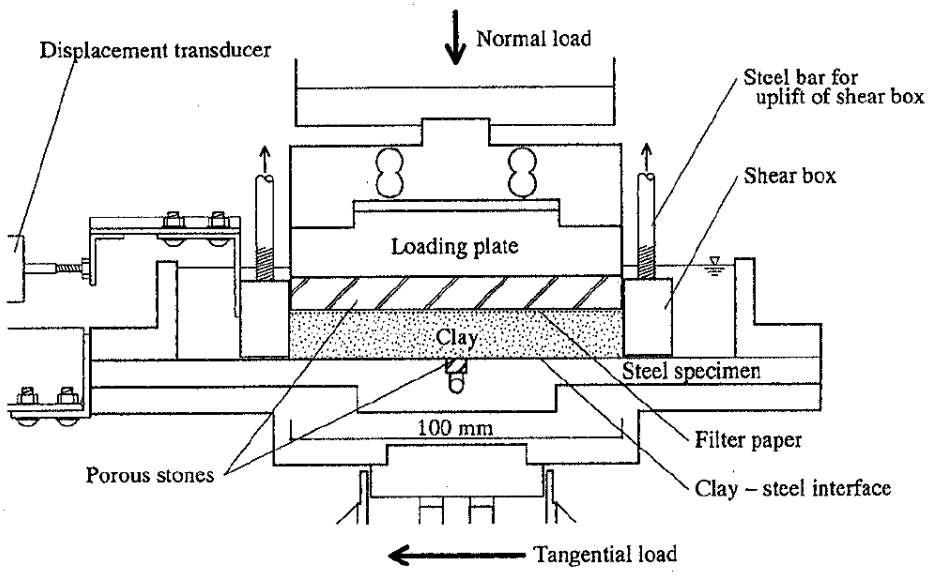

Figure 1.5 Direct shear box apparatus used by Tsubakihara & Kishida (1993)

In Tsubakihara *et al.* (1993), the authors studied normally consolidated clays with different sand fractions. The same observation on the existence of a critical roughness value was made. The value was found to be larger for mixtures with higher sand fraction. Hammoud & Boumekik (2006) in their work on a ring shear test, confirm the existence of a critical range of roughness. Below the lower limit, shearing occurs by sliding at the interface and above the upper limit shearing occurs within the soil. For the roughness values within the two limits, shearing is of an intermediate mode, which is a composition of internal shearing and sliding. It has to be noted that they have worked on different clayey soils and steel and concrete interfaces. Shakir & Zhu (2009) performed simple and direct shear tests on unsaturated clay/concrete interface. Concrete surfaces from smooth to rough were prepared in the lower box. Clay was then compacted at different water contents in the upper box. Shear deformation and shear sliding displacements were evaluated. The results show the significant effect of water content on different shear modes, which are depicted in Figure 1.6. According to them, a clay sample with low water content might behave as a quasi-solid material and failure occurs rather by sliding at

the interface. While more water content makes the soil body go under deformation when it is sheared.

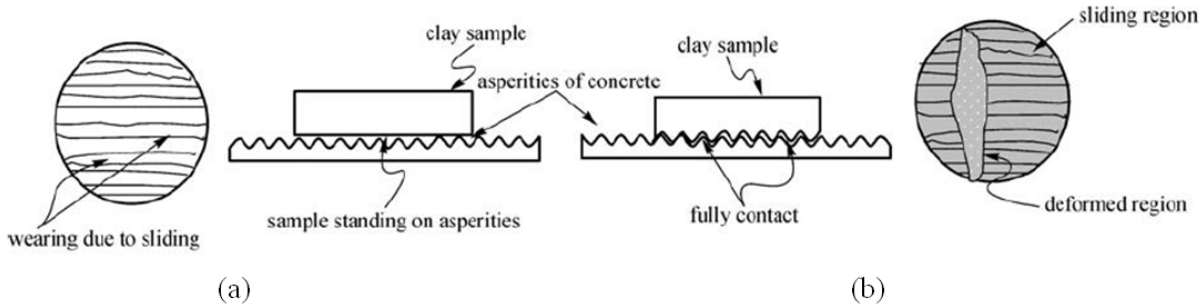

Figure 1.6 Failure mechanism in (a) clay with w_c = 10%, σ_n = 50 kPa, 100 kPa, 150 kPa; (b) clay with w_c = 21%, σ_n = 150 kPa (Shakir & Zhu, 2009)

Dove & Jarrett (2002), through direct shear tests on sand/structure interface investigated the effect of asperity height and angle on strength dilatancy behavior. They conclude that when the asperity height approaches the median grain size and asperity spacing is between one and three times the median grain size, the interface has the maximum efficiency; efficiency is defined as the ratio between the interface friction angle and the soil friction angle. Rouaiguia (2010) applied a modified shear box to evaluate the residual shear strength of clay alone and that of clay/structure interfaces. Six different clays were first sheared alone and then against two surfaces with different roughness values: glass which was relatively smooth (with an average roughness of 0.005 μm) and sandstone rock which was rougher (with an average roughness of 10.0 μm). The samples underwent forward and backward shear cycles. The results on the shear stress versus horizontal displacement show that the shear strength of clay/structure interfaces was smaller than that of clay (Figure 1.7, Figure 1.8). It was also found that the shear mode (whether it was sliding, turbulent or transitional) changed with the surface roughness.

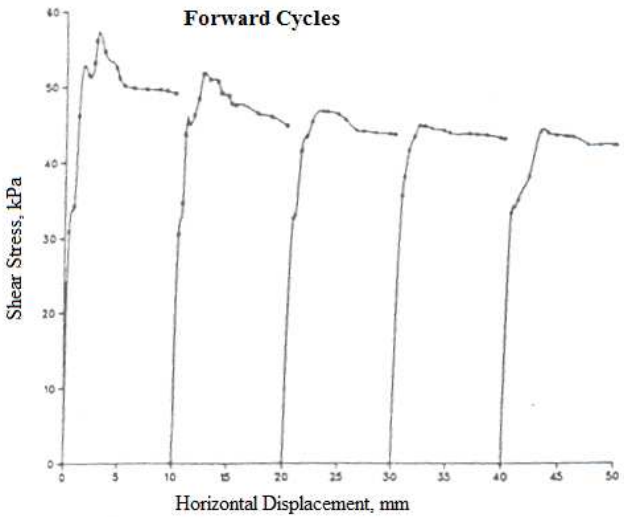

Figure 1.7 Stress-displacement relationship for kaolin/kaolin interface (Rouaiguia, 2010)

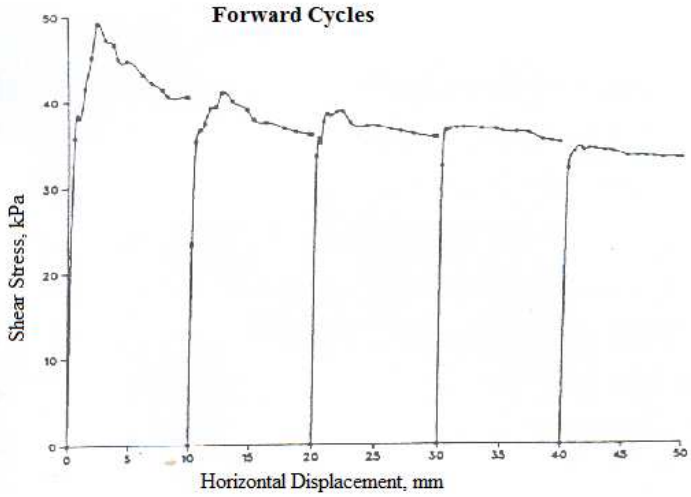

Figure 1.8 Stress-displacement relationship for kaolin/sandstone rock interface (Rouaiguia, 2010)

In general, smooth surface promoted sliding shear. For both interfaces, the strength dropped quickly once the peak strength was reached. Smaller shear strength was observed when smoother surface was used. Taha & Fall (2013) used a direct shear apparatus to study the behaviour of sensitive marine clay/concrete interface. Concrete samples were prepared with three different roughness values which varied between 6.5 μm and 20 μm. The results show an increase in the friction angle as concrete roughness increased (Figure 1.9). Also, interface shear strength was higher than that of the utilised clay.

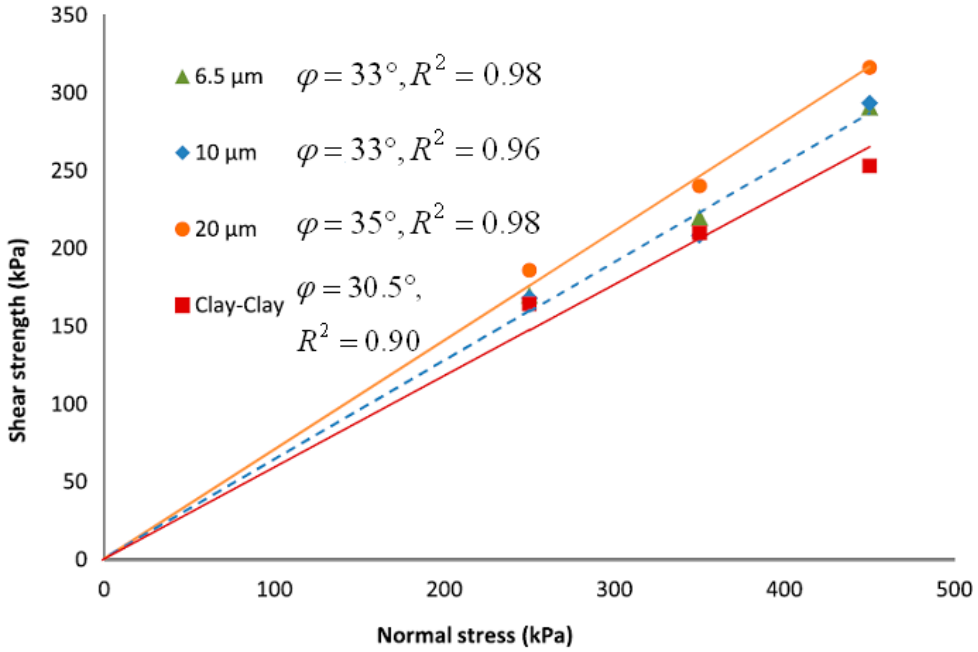

Figure 1.9 Shear strength envelope of clay and clay/concrete interface with different roughness values (Taha & Fall, 2013)

Di Donna & Laloui (2013*b*) equipped the shear box with a heating system and investigated the shear behaviour of soil and soil/concrete interface at 20°C and 60°C. Tests were conducted under three normal loads of 50 kPa, 100 kPa and 150 kPa. The results of illite clay and illite/concrete interface are shown in Figure 1.10. Tests on illite clay were only performed at 20°C. By increasing the temperature to 60°C, shear resistance at illite/concrete interface increased (Figure 1.10*a*). The authors argue that this increase might be explained by thermal consolidation of clay. With respect to the failure envelope (Figure 1.10*b*), illite clay and illite/concrete interface had the same friction angle at critical state at ambient temperature. The illite/concrete interface friction angle at critical state decreased slightly with temperature, while the peak value increased between 20°C and 60°C. Regarding the cohesion value on illite/concrete interface, a significant increase in critical state and peak values could be observed as the temperature increased from 20°C to 60°C. Also, at a constant temperature value, peak and critical state values were close to each other.

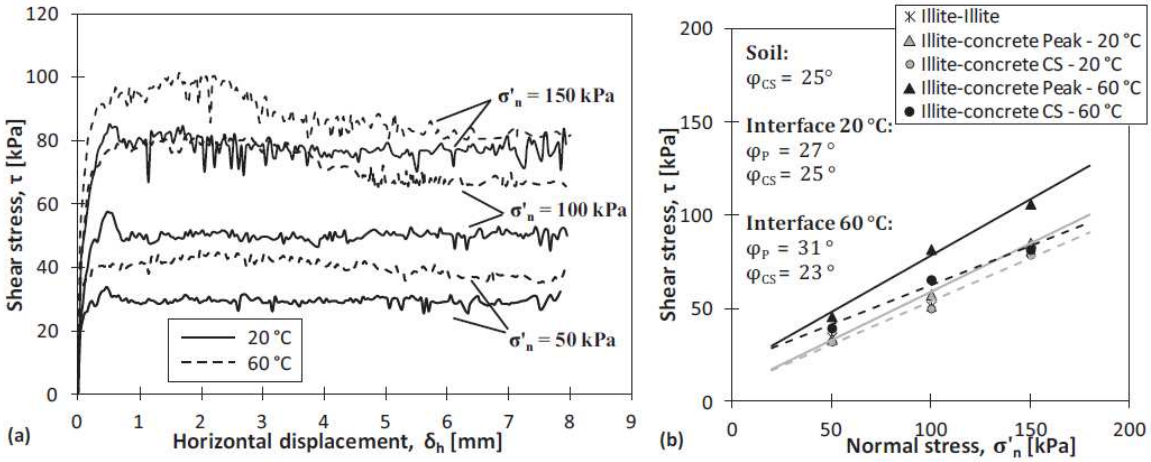

Figure 1.10 Experimental results on illite clay/concrete interface at different temperature values (Di Donna and Laloui, 2013*b*) (a) Shear stress versus horizontal displacement (b) Shear strength envelope

1.6 Soil/pile interaction in energy piles

The behaviour of a soil/pile system under thermo-mechanical solicitation could be investigated through experiments and/or numerical simulations. Experiments could be conducted at different scales, from real scales to laboratory ones. Below, different tests performed within the context of energy piles are first summarised. Then the numerical methods which are mostly validated on the basis of limited existing experiments are discussed.

1.6.1 Full-scale testing

For studying the thermo-mechanical behaviour of energy piles, one of the first methods was performing in situ experiments. Laloui *et al*. (1999) conducted full scale tests on one of the piles of a four-story building under construction on EPFL campus in Lausanne, Switzerland. Pile toe lied on molasses, while the head was topped by the weight of the building that gradually increased by adding each floor. Seven tests were conducted under a constant load value, which varied between 0 kN and 1300 kN. The geological profile and the pile instrumentation could be seen in Figure 1.11*a*. One U-shaped polyethylene tube, which was fixed in the pile during casting, let the heat carrier fluid (water in this case) circulate along the pile. The pile was equipped with vibrating strain gauges (VWSG) and optical fibre sensors (FOS) as well as a load cell at pile toe for measuring vertical and radial strains, temperature and load. At each stage of construction, a temperature change was imposed to the pile, which was equal to 22 °C in the first test and 15 °C in the six others. Pile was cooled down naturally, by stopping the fluid circulation at the elevated temperature. Observations confirmed the evolution of axial strain along the pile under thermo-mechanical loads. Results

also show the elastic behaviour of the pile during thermal cycles. In another study, conducted by Bourne-Webb *et al*. (2009) at Lambeth College in London (UK), one of the working piles, which had been used for verifying the design and also a heat sink pile, were equipped as energy piles. Piles toes lied on London clay while their heads were free. More detail on soil profile could be observed in Figure 1.11*b*. The heat sink pile was not loaded mechanically; it was uniquely subjected to thermal cycles. The main test pile was of diameter of 0.6 m and length of 23 m (Figure 1.11*b*) and was instrumented by vibrating-wire strain gauges (VWSG) and optical fibre sensors (OFS). Pile was loaded by 1800 kN of axial load at head, then it was unloaded and reloaded this time by 1200 kN. The temperature of the fluid circulating in the pile was varied between -2.5°C and 36°C. Pile was first cooled and then heated.

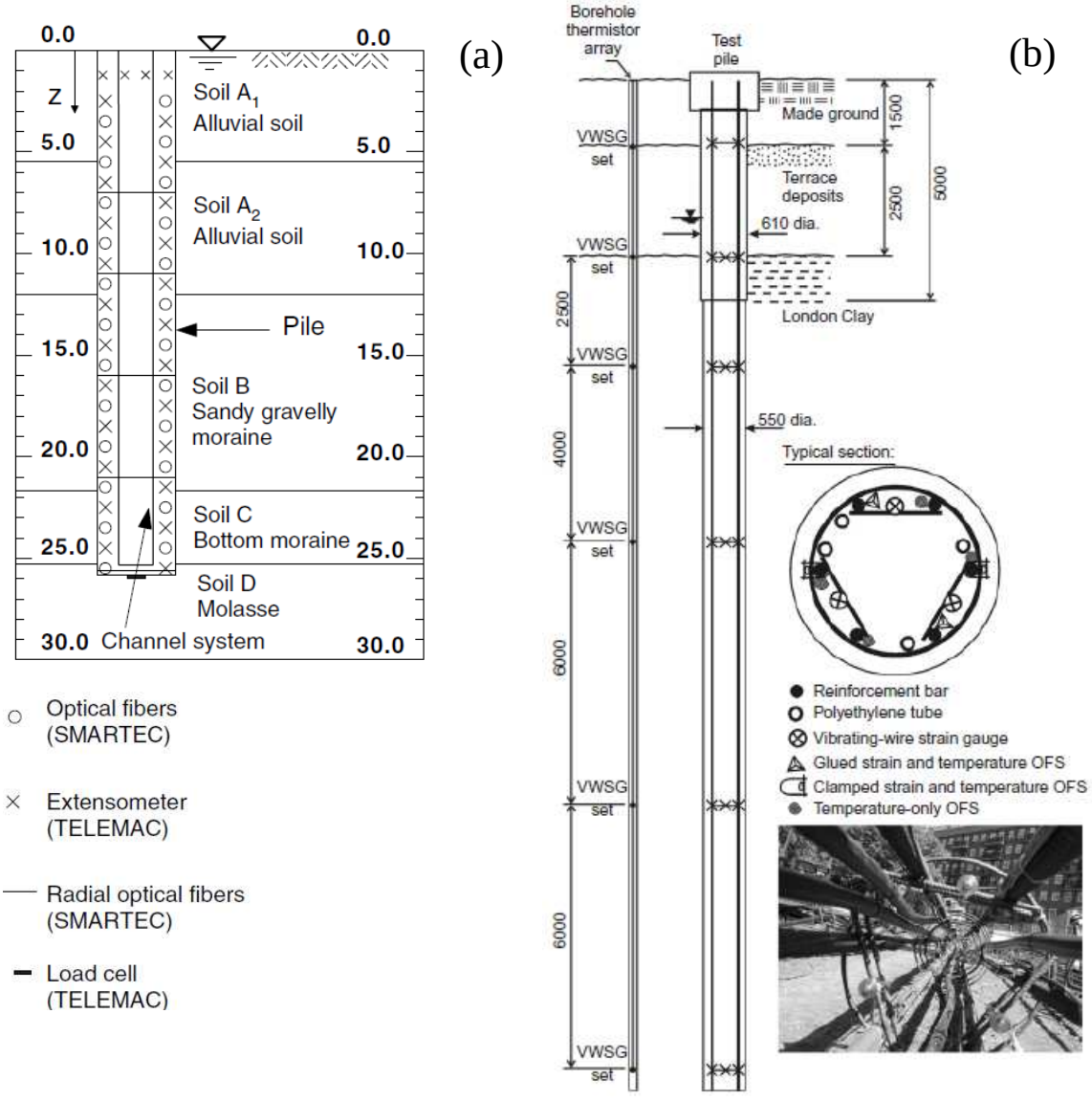

Figure 1.11 Geological formation and pile instrumentation at test locations: (a) Lausanne (Laloui *et al*., 2006) (b) London (Bourne-Webb *et al*., 2009)

In general, thermally induced stress in the pile is due to restrained strains. If a free pile is subjected to a temperature change of ΔT, a total strain of $\alpha\Delta T$ will be observed inside it, where α is the coefficient of thermal expansion. Is it noted that herein a free pile is a pile only blocked at its toe, with no load at its head and no soil around. When the pile is placed in the ground, owing to soil/pile interaction, it does not expand or contract freely. As a result, the observed strains in the pile will be less than $\alpha\Delta T$. Under a thermo-mechanical loading, the measured strain is composed of thermal and mechanical components:

$$\varepsilon_{measured} = \varepsilon_{mechanical} + \varepsilon_{thermal} \tag{1.1}$$

Thus, thermal strain could be estimated as below:

$$\varepsilon_{thermal} = \varepsilon_{measured} - \varepsilon_{mechanical} \tag{1.2}$$

Any restrained strain induces thermal force in the pile. The thermally induced axial force is then calculated using the following equation:

$$P_T = EA(\varepsilon_{thermal} - \alpha\Delta T) \tag{1.3}$$

The mechanical force and strain are directly related, assuming linear elasticity via Hooke's Law:

$$P_M = EA\varepsilon_{mechanical} \tag{1.4}$$

The total thermo-mechanical axial force is the sum of mechanical and thermal forces:

$$P_{total} = P_M + P_T = EA(\varepsilon_{measured} - \alpha\Delta T) \tag{1.5}$$

In full scale tests, '$\varepsilon_{measured}$' is the strain value recorded by the strain gauges during the test. In order to evaluate axial force in the pile, Equation 1.5 was applied.

Analysis of the experimental data in the work of Laloui *et al*. (1999) showed a significant increase in compressive axial force in the pile by heating (Figure 1.12). Axial force at pile toe was more influenced and was twice greater than in the case of purely mechanical loading. The mobilised friction increased considerably when the pile was heated. In the full scale test performed by Bourne-Webb *et al*. (2009) compressive axial force in the pile increased by heating and decreased by cooling, while pile toe was less affected (Figure 1.13). During heating, the mobilised shaft resistance increased in the upper part of the pile and decreased in the lower part. The trend reversed by cooling. Compression stress and force are respectively accounted for negatively in Figure 1.12 and positively in Figure 1.13. It is recalled that OFS stands for optical fibre sensors and VWSG for vibrating-wire strain gauges.

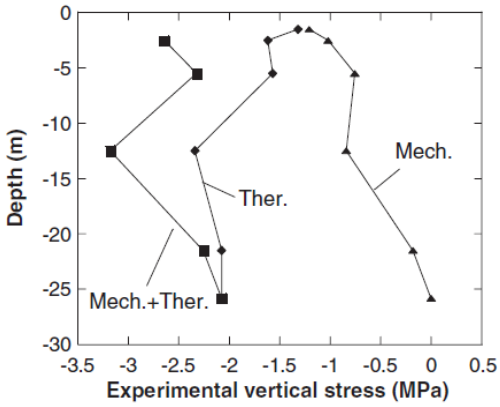

Figure 1.12 Axial force distribution in the pile in the last test in Lausanne test series (Laloui *et al*., 2006)

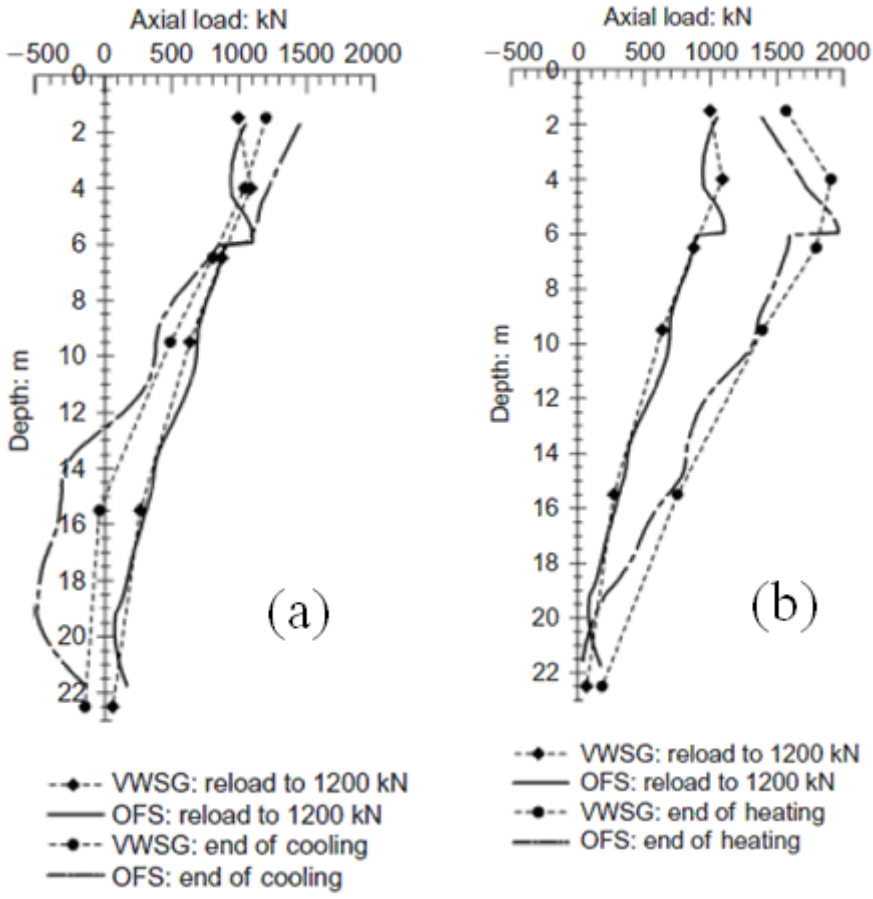

Figure 1.13 Axial force distribution in the main pile in London test: (a) at the end of cooling (b) at the end of heating (Bourne-Webb *et al*., 2009)

As a research project in Bad Schallerbach, Austria, one energy pile of a large rehabilitation center has been studied. The building foundation was equipped with 143 energy piles in this case. The piles were equipped with high-density polyethylene tubes, which contained a

mixture of water and antifreeze. The test pile was of diameter of 1.2 m and length of 9 m and its toe was located on highly-fissured clayey, sandy silt. Pile toe and head were equipped with pressure cells. Test pile was put under control for one year, starting from winter. Total temperature change was about 22°C. According to Brandl's report (2006), axial strain distribution along the pile varied as temperature increased. Higher strains could be detected at pile toe. Analysis performed by Amatya *et al*. (2012) show that higher additional compressive forces were produced in the upper part of the pile, while pile toe was not very influenced, indicating that the pile was little restrained by its toe. Very limited data have been published on this case.

The experimental results measured in the three mentioned field trials were summarised and compared by Amatya *et al*. (2012). According to them, the magnitude of thermally induced axial forces depends on end restraint, soil conditions and thermal load. Thermal loading changes the mobilised side friction significantly. Side friction is more dependent on temperature changes in stiff clayey soils (than soft clayey ones), as it was the case in London pile.

McCartney & Murphy (2012) investigated the behavior of two foundation piles (named as A and B), planned for a residential building in Denver, Colorado, which have been converted to energy piles. The two piles had the same diameter of 0.91 m and their toe stood on clay stone. Vibrating wire strain gauges and thermistors were attached to the piles at the levels shown in Figure 1.14.

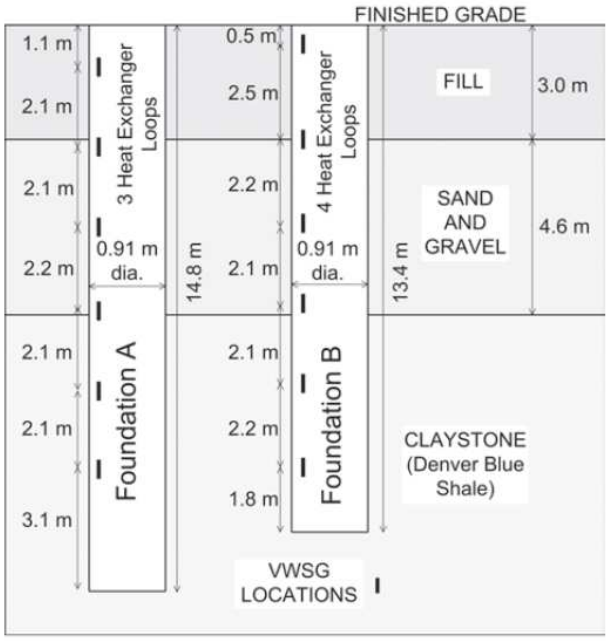

Figure 1.14 Ground profile and foundation instrumentation in the test conducted in Denver, Colorado (McCartney & Murphy, 2012)

During one year of typical operation, piles temperature was changed between 1.7°C and 32.2°C, while it was not mechanically loaded. The experimental data show the uniformity of temperature distribution in the pile. The induced thermal stress was calculated using the same derivation as shown before (Equations 1.1 to 1.6). Thermal strains were corrected as follows:

$$\varepsilon_{thermal} = \varepsilon_{measured} - \varepsilon_{mechanical} + \alpha_s \Delta T \quad (1.7)$$

where α_s is the coefficient of thermal expansion of the steel wire in strain gauges. Thermally induced stress profiles in foundations A and B are shown in Figure 1.15. It is noted that compression is expressed by positive sign. Similar to previous in situ observations, heating led to an increase in compressive forces while cooling had an inverse effect. However the authors conclude that the magnitude of the thermal axial stresses was below axial design loads and no major concern existed on structural damage. Further investigations were needed on tensile strains magnitude and development around the pile toe.

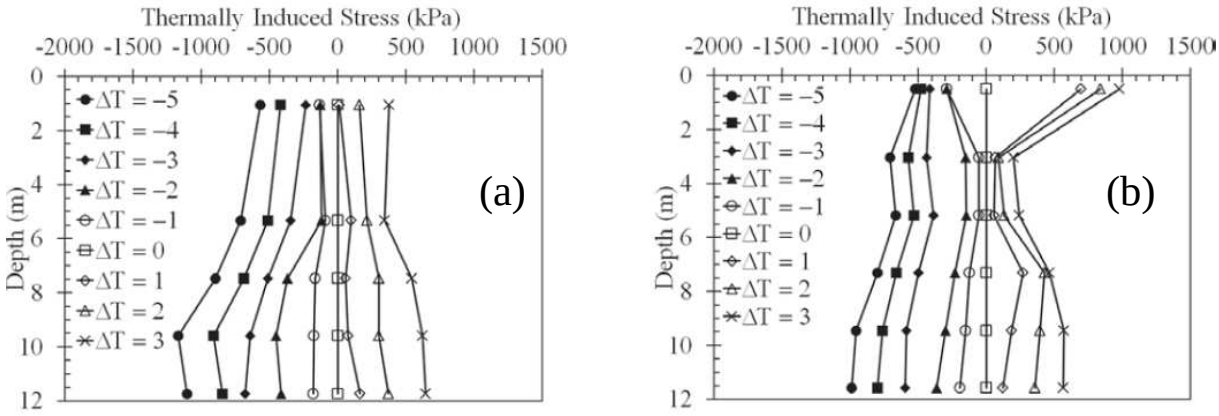

Figure 1.15 Thermal axial stress in (a) Foundation A; (b) Foundation B (McCartney & Murphy, 2012)

In a more recent full-scale test, Akrouch *et al*. (2014) examined the behaviour of an energy pile in high-plasticity stiff clay on an experimental site on the campus of Texas A&M University, at College station, Texas. The pile was of diameter of 0.18 m and length of 5.5 m (Figure 1.16). U-shaped pipe loops were inserted into the pile and water with a controlled temperature circulated inside them. The pile was instrumented with 6 strain gauges and thermocouples to track the developed strains and temperature changes and dial gauges to record pile head displacement. Strain gauges were of full Wheatstone bridge type with temperature compensation. To follow temperature changes in the soil, thermocouples were installed in a borehole at 0.5 m from the pile. A load cell showed the pile head load value at each time. Air temperature and relative humidity sensors were also used to monitor the

ambient conditions. Five Tension tests under tension forces of 40 up to 256 kN were conducted.

The pile was loaded mechanically for 1 hour, then it was subjected to temperature changes by starting hot water circulation in the internal tubes. Pile's temperature change was between +10°C and +15°C. Heating period was set to 4 hours. The pile was unloaded afterwards and on the next day the next test started. The results show that the thermal strains induced led to a very slight variation in axial load distribution in the pile (Figure 1.17*a*). Temperature distribution in the pile was not uniform which was attributed to the shallow depth of the pile that makes it more sensitive to air temperature fluctuations. More interesting results were obtained in terms of creep. Pile displacement under mechanical loading seemed to stabilise after 1 hour; while heating made the creep re-increase with a greater viscous exponent parameter (Figure 1.17*b*). Assuming that the pile was subjected to heating during its whole life, it was estimated that in a horizon of 50 years, a typical energy pile in a clayey soil undergoes an extreme displacement value which is 2.35 times the displacement of a conventional pile.

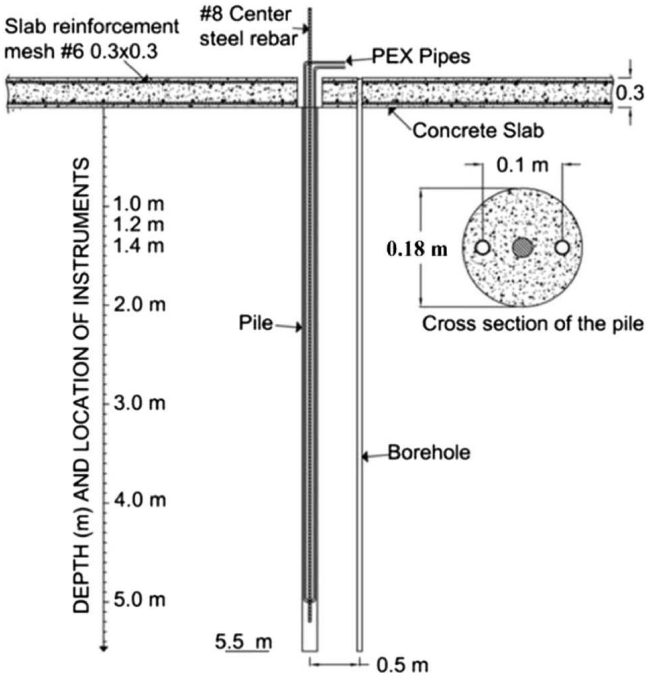

Figure 1.16 Cross section and plan view of the pile in Texas experiment (Akrouch *et al*., 2014)

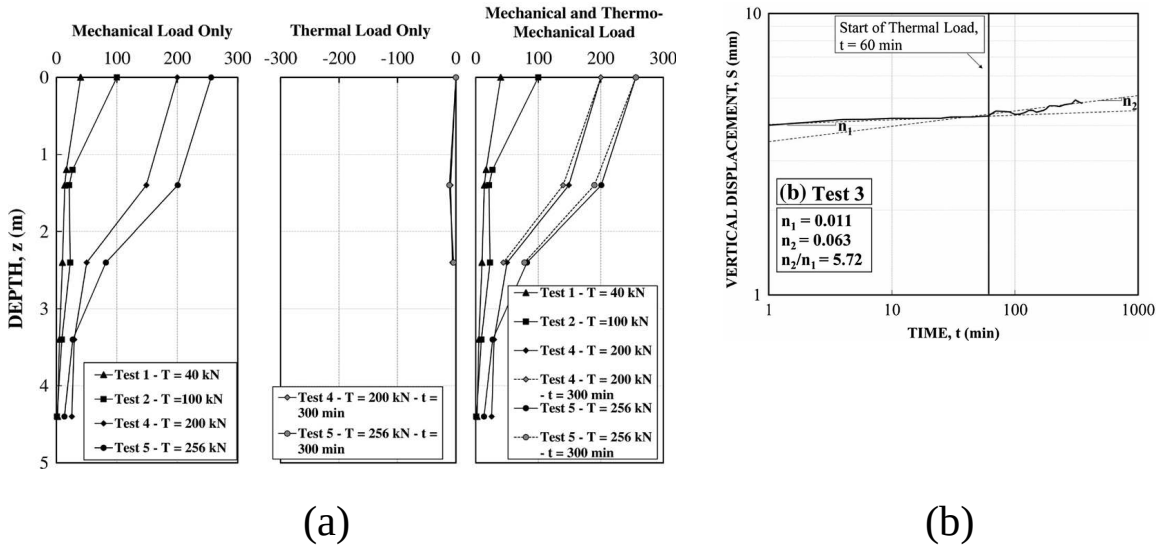

(a) (b)

Figure 1.17 Experimental results of Texas test (a) Axial force distribution in the pile (b) Vertical displacement in mechanical and thermal phases in test under 150 kN of tension load (Akrouch *et al.*, 2014)

Murphy *et al*. (2014) conducted studies on energy foundation piles of a one-story building at US Air Force Academy, Colorado. Regarding the soil profile, the first 3 meters were made of fill and dense sand. From this depth on, sandstone was extended to the maximum depth explored via tests. All the eight piles were equipped with heat exchanger pipe loops. Piles were of diameter of 0.61 m and length of 15.2 m and they were different in the heat exchanger pipe loops configuration. Three of eight piles were instrumented with vibrating wire strain gauges (VWSG). Each VWSG contained a thermistor to monitor the temperature changes inside the pile. Soil temperature was tracked by thermistor strings, which were installed in the boreholes drilled around two of the piles, with the radial distance of 1.2 m from each other. A thermal loading procedure was defined in order not to heat all the eight piles rapidly. Doing so, a ΔT of 18°C was applied to the piles during a heating and cooling (recovery) cycle. According to the experimental results which are shown in Figure 1.18, heating induced thermal expansion in the pile.

The behaviour of the pile remained thermo-elastic. The temperature change was uniform along the pile. The effect of pile top restraint could not be neglected; the corner pile (denoted by ‘Foundation 3’ in Figure 1.18), which was less restraint by its head, underwent lower thermal stress than the pile located in the middle of the wall (Foundation 1). Also, greater displacement was detected during cooling in the corner pile comparing to the middle one.

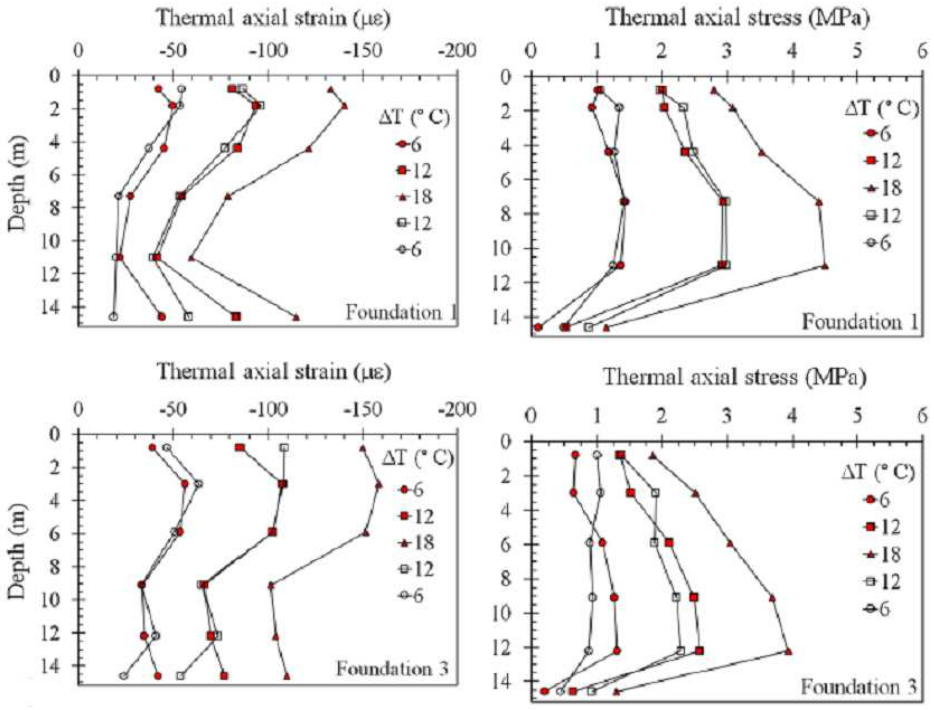

Figure 1.18 Thermal axial strain and stress during heating (red) and cooling (open) measured in Foundation 1 and Foundation 3 (Murphy *et al*., 2014)

In general, in situ tests are powerful tools as they provide an insight on real conditions under real scales. However they are expensive and rather time consuming.

1.6.2 Physical modelling

Physical modelling is one of the most usual approaches to investigate the behaviour of pile foundations. Below, the most important categories and their application in studies concerning energy piles are reviewed.

1.6.2.1 Centrifuge physical modelling

The centrifuge could be used in scale modelling of any large-scale nonlinear problem for which gravity is a primary driving force. According to Sakr & El Naggar (2003), the main advantage of centrifuge modelling is that this method can simulate the linear increase of the effective stress with depth. Centrifuge modelling has been widely used in investigation of pile's performance in different soils (Zhang et al., 1998; Horikoshi *et al*., 2003; Thorel *et al*., 2008.; Fioravante, 2011; Okyay *et al*., 2014). McCartney & Rosenberg (2011) used this method to study the response of thermo-active foundations. Four concrete piles with 379 mm length and 76.1 mm diameter were pre-cast in a cylindrical metal container with a height of 500 mm and a diameter of 381 mm. A U-shaped metal tube was installed in the piles to

conduct the heat carrier fluid (which was a silicone fluid). Two layers of silty soil were first compacted in the container at a dry unit weight of 17.2 kN/m^3. The piles were placed inside the container and the compaction was continued. A loading frame was made around the container and loads between 0 kN and 1000 kN were applied to the top of the foundations by a horizontally-mounted electric motor. Tests were performed at an acceleration level of 24g to represent 24 times larger piles (9.1 m length and 1.8 m diameter). More detail on the model set up could be seen in Figure 1.19.

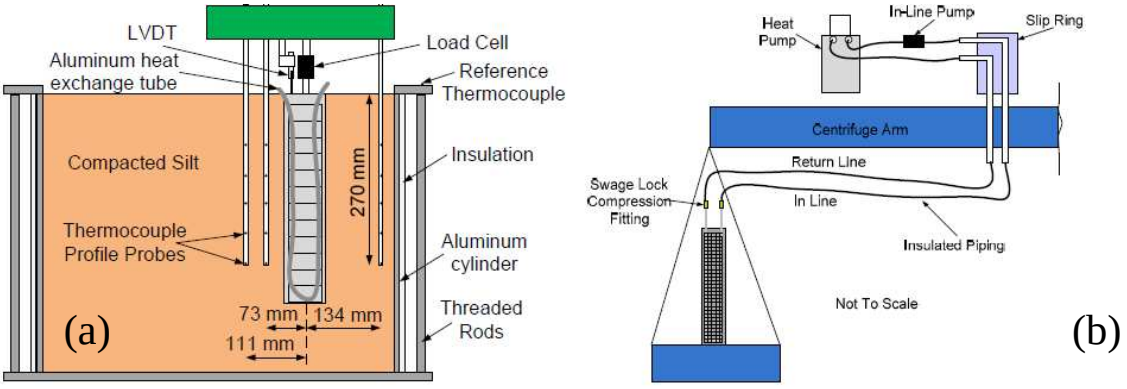

Figure 1.19 (a) Schematic of the centrifuge-scale testing setup at the University of Colorado; (b) Schematic of foundation and heat pump setup (McCartney & Rosenberg, 2011)

Loading was performed at a controlled displacement rate of 0.2 mm/min until a displacement of 5 mm. Three tests were performed at constant temperatures of 15°C, 44°C and 56°C. The results show that by heating the pile, its axial capacity has increased. Experimental results on the model pile were transformed to the identical values on a prototype pile by applying associated scale factors. The results are shown in Figure 1.20.

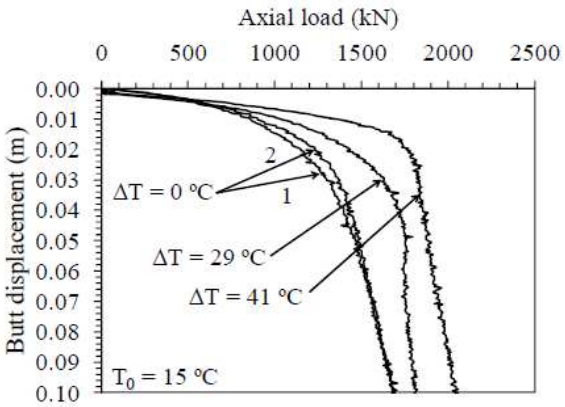

Figure 1.20 Load-settlement curves for model foundations in prototype scale in the work of McCartney & Rosenberg (2011)

In a more recent work on centrifuge modelling (Stewart & McCartney, 2014), an energy pile with a diameter of 50.8 mm and length of 533 mm was pre-cast outside the silty soil. It was then placed in the container by its toe fixed to the bottom of it. The pile was instrumented with strain gauges and thermocouples. LVDTs were placed on top of the pile and also at different distances from the pile on soil surface. Thermal probes were installed in the soil at radial distances of 140, 216 and 292 mm from the pile and thermocouples were put inside at different soil levels. Figure 1.21 could be referred for more detail.

Three heat exchanger loops were inserted in the pile and connected to the heating/cooling circulator. The pile was first loaded to the axial stress of 384 kPa which simulated the load of the building, then heated by increments. Once the pile temperature reached 40°C, the cooling phase was applied, down to 10°C. Four thermal cycles were applied to the pile. The results were presented at model and prototype scale. Axial load distribution in the pile at the prototype scale could be observed in Figure 1.22. As could be seen, heating induced thermal stresses in the pile. The stress values reduced during cooling while forces were still compressive. A perfect thermo-elastic behaviour was observed as a response to thermal cycles.

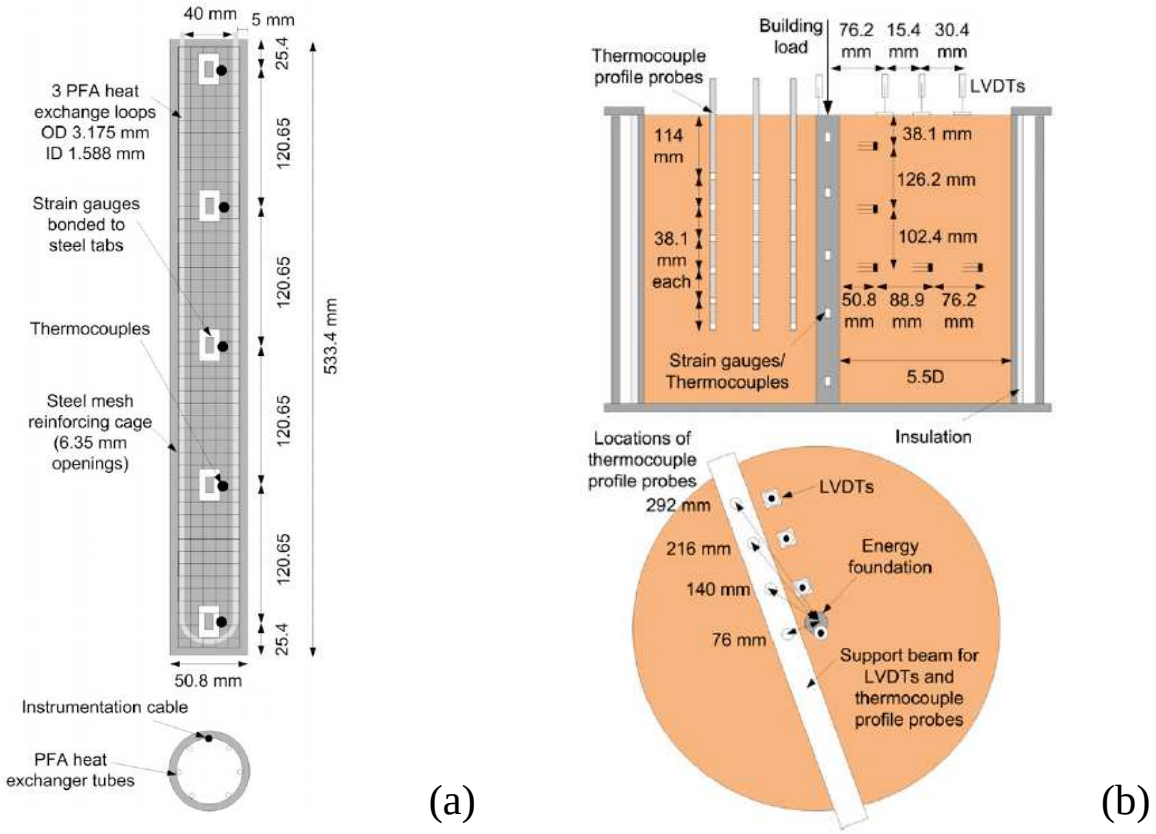

Figure 1.21 Physical modelling of energy pile: (a) the model pile; (b) and the corresponding instrumentation (Stewart & McCartney, 2014**)**

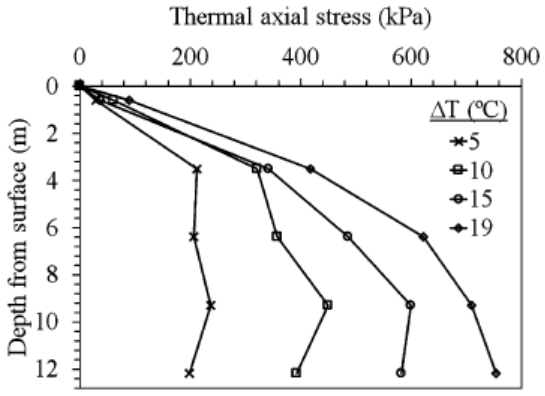

Figure 1.22 Axial load distribution in prototype scale in the work of Stewart & McCartney (2014)

The centrifuges are useful equipments giving the best simulation of real scale conditions but they are expensive. One major concern in centrifugation while energy piles are concerned is heat diffusion in the soil. According to Krishnaiah & Singh (2004) the time required for obtaining the same temperature in the soil in the model is much less than the corresponding time in the prototype, which means that during the same period of time a greater volume of the surrounding soil is affected by pile temperature (Stewart & McCartney, 2014) in a model which is not representative of the prototype conditions.

1.6.2.2 Calibration chambers

Calibration chambers have been widely used in foundation studies. The possibility of performing tests under known stress-strain histories and also controlled boundary conditions, make them interesting instruments in simulating in situ tests (Holden, 1991). On the other hand, because of the limited size of the chamber, the measured bearing capacities may be different from real ones. As a result, the diameters of the pile and the chamber should be chosen in the way that the mutual effects of the pile and the chamber are minimised (Paik & Salgado, 2004). According to Parkin & Lunne (1982), in order to minimise the boundary effects, the ratio between chamber diameter and pile diameter should be at least 20 in loose sands and 50 in dense sands. Calibration chambers could be rigid or flexible wall type (Chin & Poulos 1996; Weinstein, 2008). It is not easy to control lateral stress in rigid walled chambers, so very large chambers are needed to minimise the effects of the wall type (Weinstein, 2008). According to Holden (1991) better simulation of stress and strain is possible in smaller but flexible chambers. Relation between the pile dimensions and the grain size, known as scale effects, could also influence the pile response. Studies show that lateral friction is independent of scale effect when the pile diameter is 100 times the median grain

size (Weinstein, 2008). Even if calibration chambers are usually used in foundation studies, this method has not yet been applied to study energy piles.

1.6.2.3 Small-scale tests

Wang *et al*. (2011) developed a laboratory scale energy pile model to study the effect of temperature on the shaft resistance (see Figure 1.23). The model pile was a steel tube with external diameter of 25.4 mm. The soil container was a steel cylinder with diameter of 272 mm. Temperature changes were applied with a heating element fixed inside the pile. A loading frame was designed to accommodate the model pile and the loading machine. Temperature transducers were distributed in various positions inside the soil specimen and also on the pile surface. Loading/unloading cycles were conducted on the model pile before and after heating. The results show the significant effect of temperature on the shaft resistance: as the temperature increased from 18°C to 28°C, shaft resistance decreased from 0.05 kN to 0.02 kN in the case when the pile was embedded in fine sand.

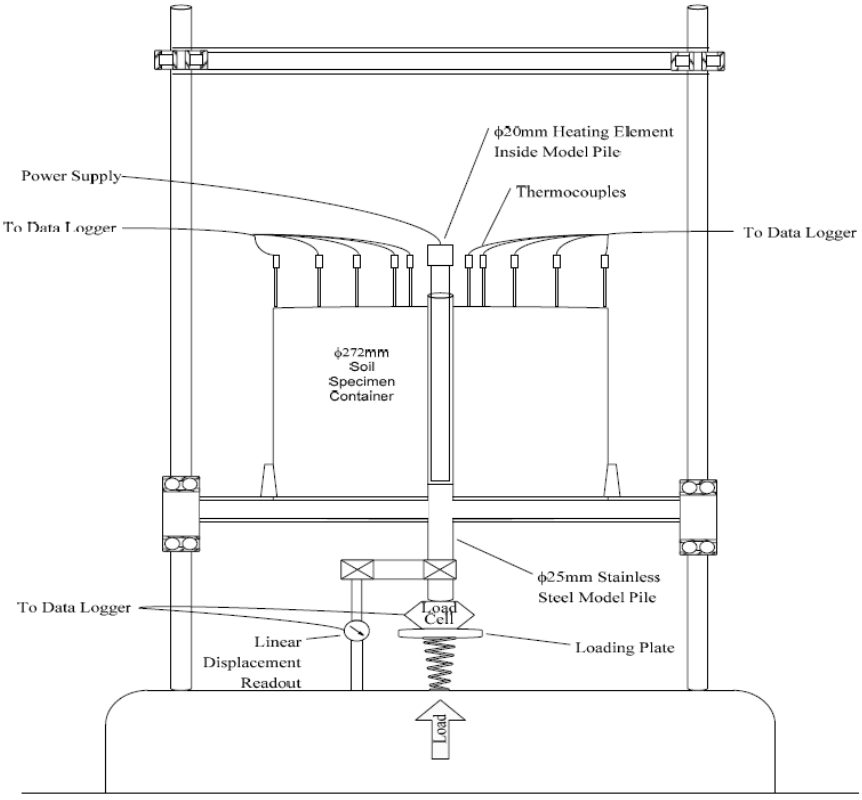

Figure 1.23 Laboratory scale testing apparatus (Wang *et al*., 2011)

Kalantidou *et al*. (2012) developed a small-scale physical model to study the mechanical behaviour of an energy pile. The pile, which was a metal tube with a length of 800 mm and a

diameter of 20 mm, was equipped with a U-shaped tube containing water. A temperature transducer was put inside the pile to track its temperature. A displacement transducer was fixed on the pile head (Figure 1.24). The model pile was first loaded axially and then its temperature was varied between 25°C and 50°C (successive heating and cooling cycles). Pile head displacement was monitored during the test. Behaviour of the pile was studied under different axial loads. Displacement-temperature curves show that under lighter loads pile behaviour remained thermo-elastic, while under heavier loads irreversible deformations were observed. The experimental curves obtained under 200 N (40% of the pile's ultimate load) and 500 N (95% of the pile's ultimate load) of pile head load are shown in Figure 1.25.

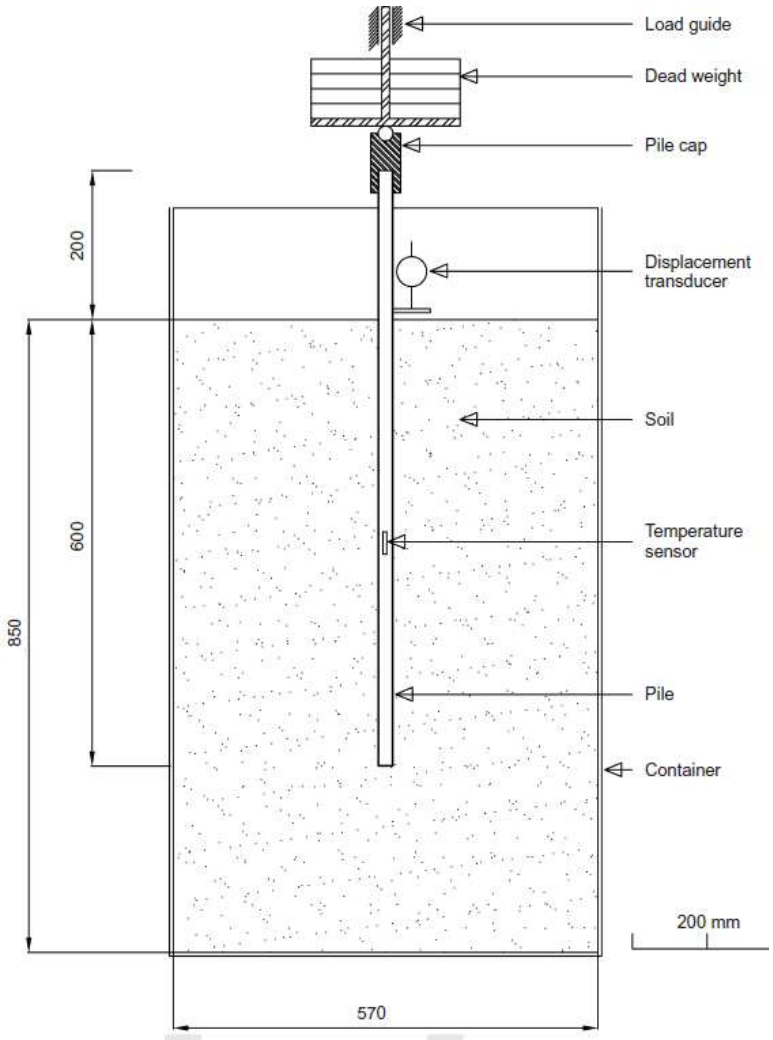

Figure 1.24 Experimental set-up (Kalantidou *et al*., 2012)

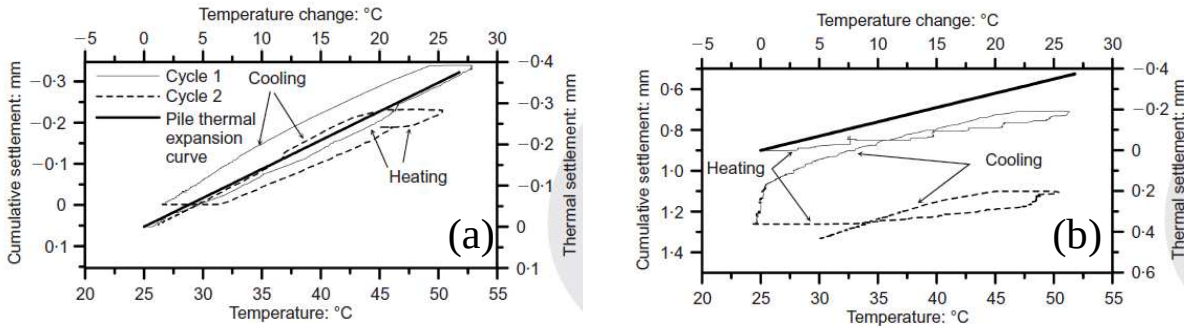

Figure 1.25 Pile temperature versus pile temperature under the pile head load of: (a) 200 N (b) 500 N (Kalantidou *et al*., 2012)

Comparing to other experimental methods, small-scale tests are easier to handle, quicker and cheaper and could be used for research purposes, if properly designed and performed. The fact that they are also repeatable, which is essential in these occasions, could not be neglected. On the contrary, poor simulation of boundary conditions and the workability of the model only in low stress ranges could be considered as disadvantages of this type of tests (Mayne *et al*., 2009).

1.6.3 Numerical modelling

Developing numerical codes to simulate the behaviour of energy piles seems attractive especially to engineers. However these kind of studies are not numerous for many reasons, particularly the complexity to extend existing geotechnical numerical codes to account for coupled thermo-mechanical behaviour. The numerical problem is composed of two principal parts: modelling the heat propagation from the pile into the soil and modelling the mechanical behaviour of the pile. Different analytical solutions on the heat propagation around geothermal boreholes have been developed (Yang *et al*., 2014; Arson *et al*., 2013; He, 2012; Li & Lai, 2012; Bandos *et al*., 2009). Heat diffuses radially out from a source, which is a borehole, with time. The analytical heat diffusion models are generally based on point source, line source or cylindrical surface source solutions (Li & Lai, 2012). From this point of view, geothermal piles could be modelled in the same way as a geothermal borehole; the models are based on the line source assumption (Arson *et al*., 2013). Li & Lai (2012) state that application of a cylindrical surface or spiral line model is closer to the case of a geothermal pile. On the contrary, the studies on the mechanical behaviour of geothermal piles stay limited. Finite element approaches such as the ones suggested by Laloui *et al*. (2006) and Suryatriyastuti *et al*. (2012) are based on thermo-hydro-mechanical models. The evolutions of pore water pressure and heat flow are governed by coupled equations of mass and energy

conservation and mechanical equilibrium. Finite element codes Gefdyn (Laloui *et al*., 2006) and Flac3D (Suryatriyastuti *et al*., 2012) are used to solve the complex system of equations in the mentioned studies. In the work of Laloui *et al*. (2006), Druker-Prager thermo-elasto-plastic model was used to simulate the behaviour of the soil. The concrete pile was modelled as a thermo-elastic material. The soil/pile interface was considered to be perfectly rough. The modelled pile was loaded thermally in one test and thermo-mechanically in other ones and results were compared to the experimental data obtained during an in situ test. The authors observed an acceptable consistency between the two sets of results (Figure 1.26).

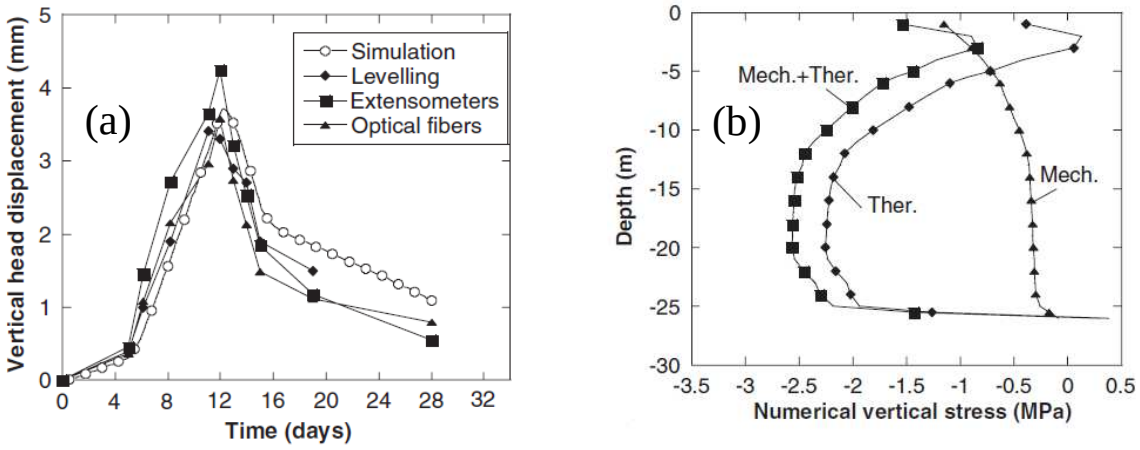

Figure 1.26 (a) Pile displacement in test 1 in Lausanne test (b) Numerical axial force distribution in the pile in Lausanne test (to be compared to Figure 1.12) (Laloui *et al*., 2006)

Suryatriastuti *et al*. (2012) modelled a pile under thermal loading and without mechanical loading on pile head. Contrary to the previous work, both pile and soil were modelled as thermo-elastic materials. In order to evaluate the effect of soil/pile contact, two types of interface were considered: a perfect contact and an elastic perfectly plastic frictional interface model. The results on thermal diffusion showed high thermal gradients at the interface in the second model, which highlights the role of contact nodes on thermal transfer. From the mechanical point of view, pile contraction while cooling and its expansion while heating induced soil surface settlement and heave in both models. Magnitude of thermally-induced displacements along the pile was almost the same in both cases. Heating increased the compressive stresses while cooling produced tensile stresses in the pile. This trend was observed in the results of both models while stress quantities were more important in the full contact interface one. In another work, Suryatriastuti (2013) applied a mechanical load to the

pile head and subjected the pile to numerous thermal cycles through a 3D model. This time, pile and soil were modelled as linear elastic and nonlinear elastic materials, respectively. Interface elements were added to the model. As the interface constitutive model, the Modjoin law was chosen, which includes soil non-linearity, cyclic degradation and the interface dilatancy. The enhanced Modjoin law was used to control cyclic degradation (including strain accommodation and stress relaxation). The pile was subjected to twelve cooling and heating cycles by $\Delta T = \pm 10°C$. The simulations were run once on a free head pile and then on a restrained head one. It is noted that a free head pile was subjected to a constant head load during loading cycles while in a restrained pile, the pile head displacement did not change with cycles. Pile head settlement versus thermal cycles resulting from simulation of a free head pile is shown in Figure 1.27*a*. Pile heaved when it was heated and settled when it was cooled. Pile head thermal settlement after twelve cycles reached 30% of the mechanical settlement. Head load variation of the simulated restrained pile is exhibited in Figure 1.27*b*. During each cycle pile head load decreased by cooling and increased by heating, while it decreased progressively through the 12 cycles. Axial force distribution in the free head pile and the restrained head one are shown in Figure 1.28*a* and Figure 1.28*b*. Axial force decreased in both piles by the first cooling and tensile forces were generated. It increased afterwards during the subsequent heating. As thermal cycles proceeded, compressive forces continude to increase in the free head pile because of interface resistance degradation, while in the restrained head one, a decreasing tendency governed the pile axial force distribution evolution.

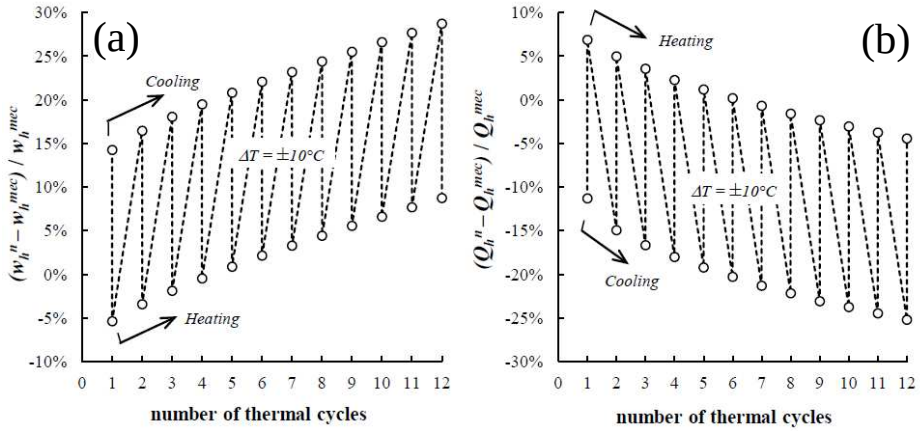

Figure 1.27 Pile head reaction to thermal cycles: (a) settlement variation in the free head pile (b) head force variation in the restrained head pile (Suryatriastuti, 2013)

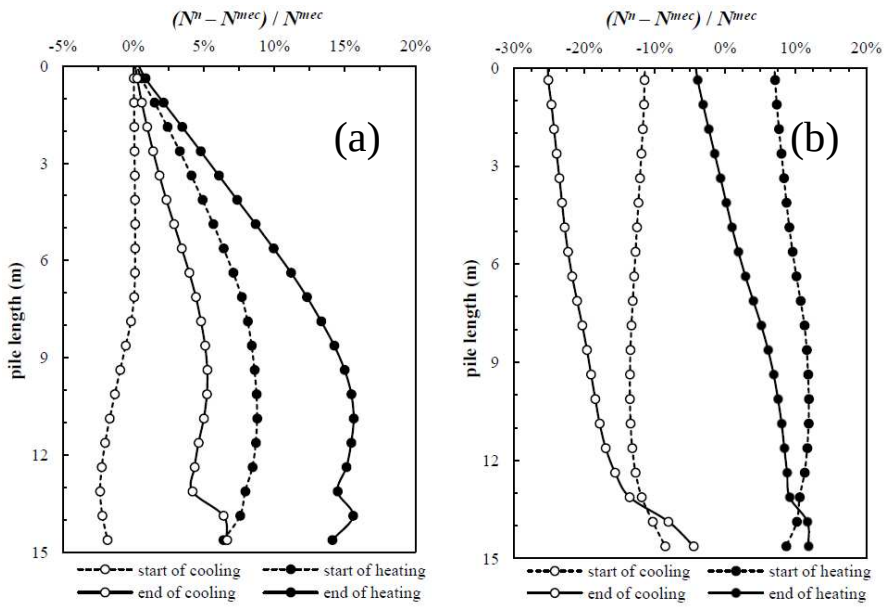

Figure 1.28 Axial force distribution in the (a) free head pile (b) restrained head pile (Suryatriastuti, 2013)

Saggu & Chakraborty (2014*a*), in their numerical studies on energy piles in sand, chose a constitutive model for sand, known as CASM, which considers the current state of the soil and its evolution by means of a parameter which depends on the current and critical void ratio. Pile behaviour was considered to be linear elastic. At the interface zone, frictional contact was considered in tangential direction and hard contact with zero penetration in normal direction. The model was implemented in the finite element software Abaqus. No interface elements were used; the mesh was refined close to the pile. A parametric study was then conducted to evaluate the effect of soil density, pile end restraint condition, coefficient of earth pressure at rest, pile dimensions, thermal load magnitude and soil thermal parameters and friction angle on the behaviour of a pile subjected to heating. No mechanical load was applied to the pile head. Between the parameters tested, the pile's response was observed to be more sensitive to its length and to the density of the soil. Independently of the pile head and toe restraint, the coefficient of lateral pressure of the soil increased by heating, which was known to be due to thermal expansion of the pile and compaction of the soil. In another work, Saggu & Chakraborty (2014*b*) studied the behaviour of a pile under a constant mechanical load and several thermal cycles, through a nonlinear transient finite element analysis. The soil was modelled using the Mohr-Coulomb constitutive model while a concrete damage plasticity model (originally proposed by Lubliner *et al*., 1989) was considered for the pile. The mesh was refined at the soil/pile interface with the same considerations as in their previous work. Similar to their former study four cases were considered: floating pile in loose sand, floating

pile in dense sand, end restrained pile in loose sand and end restrained pile in dense sand. Pile behaviour was modelled under different mechanical load values and considering 50 thermal cycles between 21°C and 35°C, with each cycle lasting 28 days. The duration of 28 days had been chosen in order to be compatible with the test performed by Laloui *et al.* (2003). At the end of the first heating/cooling cycle, axial stress in the floating pile was the same as that under purely mechanical loading. The observation remained the same until the fiftieth cycle. The authors deduce that in this case the mechanical load governed the behaviour of the pile. In dense sand, compressive axial stress increased by the first thermal cycle, while as expected, pile toe was more affected in the end-restrained pile. As thermal cycles proceeded, compressive axial stress in the pile in dense sand decreased. The effect of cooling and heating was less significant in loose sand. Regarding the axial stress variation in the soil at soil/pile interface, the authors deduce that in dense sand, the excess axial stress produced by heating was transferred to the soil while this transfer happened less efficiently in loose sand.

Knellwolf *et al*. (2011) proposed a less complex iterative routine which is based on load transfer method. Using the t-z and q-z curves suggested by Frank & Zhao (1982), first they analysed the pile under purely mechanical loading. t-z and q-z curves express respectively the evolution of the mobilised side friction and the mobilised base reaction with pile displacements. Pile was divided into segments connecting to each other by springs. The rigidity of the springs was a function of the surrounding soil properties at that section, especially Menard pressuremeter modulus. The analysis started from the lowest segment by assuming a displacement at pile toe. At each step, knowing the value of displacement and axial force at the bottom of the segment, one tried to estimate the displacement at the midst. Once the mentioned displacement was found, the axial load at the middle and on top of the segment and also the displacement on the segment head could be evaluated. These data could provide the essential input for starting the analysis of the upper segment, as the displacement and load on the head of the lower segment are that of the base of the upper one. At the end, arriving to the last segment, which is the extreme upper one, the value of axial load at its head should be equal to the load applied to the pile head. If that was not the case the steps have to be redone by assuming another initial load and displacement. In the thermo-mechanical case, first a pile under purely thermal loading was analysed. Knellwolf *et al*. (2011) took the benefit of existence of a null point along the pile around which pile contracts or expands while cooled or heated. The displacement at this point was set to zero, and the thermal deformation ($\varepsilon_{thermal}$) was equal to $\alpha\Delta T$. Again the displacement and axial stress were estimated at the

segments around the null point. Knowing the axial stress, the blocked axial strain, which is less than the free thermal deformation was calculated. The difference of the two strains (known as the 'observed strain') was set as the new $\varepsilon_{thermal}$ and calculation was repeated until the observed strain tends to zero. When a mechanical load was also added up, first the mechanical analysis was conducted and the mechanical deformation was obtained. Then, in the thermal analysis, the deformation at the null point was set to be the calculated mechanical deformation (instead of zero). The same steps as thermal analysis (as stated earlier) passed afterwards. It has to be noted that the major assumptions of this method are that the soil/pile interaction properties do not change with temperature, radial displacements of the pile are ignored and pile properties including coefficient of thermal expansion and elastic modulus of the pile are temperature independent. So, the same t-z curves commonly used could be applied in the thermo-mechanical analysis. The proposed numerical code was examined by simulating the in situ tests performed previously at Lausanne and London (Laloui *et al*., 2003, Bourne-Webb *et al*., 2009). A good agreement between experimental and numerical results was achieved. Pile axial strain measured in London test at the end of mechanical, cooling and heating phases are compared to the numerical ones in Figure 1.29.

Based on the load transfer method, Pasten & Santamarina (2014) presented a numerical algorithm to investigate the long-term behaviour of a pile under thermal cycles. The method is similar to the method proposed by Knellwolf *et al*. (2011) however instead of using current bilinear t-z curves which are based on constant shear stiffness value, they suggest a linear elastic-perfectly plastic model which considers stiffness increase with depth. Pile was divided into sub-segments with equal lengths. The upper element was analysed on the basis of the lower one. At the bottom of the i_{th} element, first the displacement was estimated and based on that, axial force was computed. Change in the element length (Δ_i) was then evaluated and the displacement on the element head was calculated. If thermal loads were also included, assuming a uniform pile temperature change, Δ_i was modified as $\alpha\Delta T$ minus mechanical contraction. Side friction at this element and axial load at its top were then estimated. Calculation continued until the last element where the axial force at the top should be equal to the load at pile head. Unlike the formulation proposed by Knellwolf *et al*. (2011), the null point was produced as a result and its position was not searched by iteration. Numerical results show that thermal cycles resulted in accumulation of plastic deformations, which could affect the long-term performance of this kind of piles. Also, a great part of plastic displacements appeared during the first thermal cycles.

Dupray *et al*. (2014) conducted a coupled multi-physical finite element modelling and used a 2D approach in order to study the behaviour of a group of energy piles from mechanical and energy point of view. The simulations were performed using the finite element code Lagamine (developed at the University of Liège). A parametric study was conducted during which effect of heat injection rate and the temperature of the pile on thermal losses was investigated. Effects of submitting only one pile in a group of piles to thermo-mechanical loading were also compared with the case where all the piles were loaded thermo-mechanically. Greater thermally induced stress values were observed in the former case.

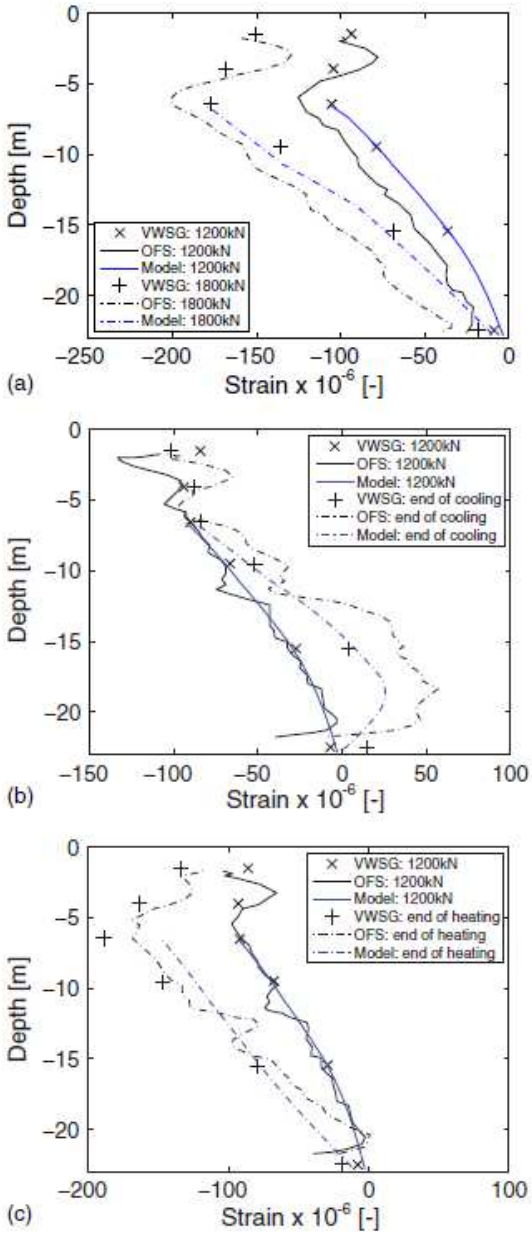

Figure 1.29 Modelled and measured strains at the end of (a) the mechanical loading phase (b) the cooling phase (c) the heating phase (Knellwolf *et al*., 2011)

1.7 Design approaches

With respect to energy piles, national, European and international standards have been proposed which focus mainly on the environmental issues of heat extraction/injection, energy-related aspects of thermal energy consumption and heat pump systems problems (SIA, 2005; Lapanje *et al*., 2010). No codes were yet released concerning the mechanical features of energy piles, which could be related to the insufficiency of experimental data on this type of pile. The Ground Source Heat Pump Association in the UK recommended a design approach on energy pile in 2012 (GSHP, 2012). Some design charts are addressed which have been developed on the basis of back calculation of the tested pile at Lambeth College where the pile lied on London clay (Bourne-Webb *et al*., 2009). Special care should be taken while applying the mentioned charts in other geological formations (GSHP, 2012). In the absence of geotechnical standards, engineers might apply safety factors, which could be up to twice the values used for classical piles (Nuth, 2008) that could impose extra construction costs to contractors (Nuth, 2008; Abuel Naga *et al*., 2014).

Some limited attempts have been made on producing practical design tools (e.g. computer programs) to analyse the behaviour of the pile under the coupled thermo-mechanical loading and to propose a design strategy. The existing numerical tools are based on load transfer method applying t-z functions, which express the mobilised side friction and pile tip reaction as a function of pile displacements (Knellwolf *et al*., 2011).

The algorithm presented by Knellwolf *et al*. (2011), which is based on the mentioned load transfer t-z functions and was discussed earlier in section 1.6.3, was implemented in Thermo-Pile program (Peron *et al*., 2010), a software for geotechnical design of energy piles. Assuming that pile and soil/pile interface properties are not temperature dependent, the classical t-z functions presented by Frank and Zhao (1982) were used in this program, while the mentioned assumptions might not be valid all the time (Abuel-Naga *et al*., 2014; Shoukry *et al*., 2011) and the comprehensiveness of the proposed model may be questioned.

Suryatriastuti (2013) proposed a new nonlinear t-z function to analyze the behaviour of a pile under thermal loading. Two sets of t-z functions are proposed; one for monotonic loading and the other for cyclic loading. The formulation takes into account the amplitude and the rate of interface cyclic degradation and the cyclic strain hardening/softening of interface. The t-z function was compared to the results of direct shear tests under cyclic loading to examine its functionality. The t-z function was then implemented into a computer program and the results were compared to their numerical results formerly obtained using a more complex 3D

analysis with specific (Modjoin) interface elements. The consistency of the two sets of results confirms the workability of the proposed t-z functions via a simpler and less time consuming calculation. However, the applicability of the proposed model is not yet confirmed by simulating full-scale tests on energy piles.

1.8 Conclusion

A literature review of energy piles with special emphasis on geotechnical aspects was conducted in order to provide a background for the current study. The response of the soil surrounding the pile and that of soil/pile interface to thermo-mechanical solicitations determine the mechanical behaviour of the pile. While numerous studies could be found in the literature on experimental investigation of the thermo-mechanical behaviour of soil, very limited data could be found on the effect of temperature on soil/pile interface response. The general behaviour of energy piles has been examined through in situ tests since 1998. However much more experimental results are needed in order to prepare a rich and reliable database on the performance of energy piles in different geological formations and under various thermal and mechanical loadings. The limited in situ experiments on the subject show explicitly the evolution of axial force distribution in the pile when thermal effects are added. Generally, heating leads to an increase in compressive forces while cooling results in a decrease. However, the quantity of axial force change depends on many parameters, such as pile head and toe restraint conditions, soil properties and magnitude of thermal loads.

Recently, the relevance of physical modelling of energy piles has been considered through centrifuge tests and small scale ones. The centrifuge tests performed until now on energy piles, show variation of pile bearing capacity and axial force distribution by thermal cycles. In spite of some disadvantages, small-scale tests (known also as 1g model tests) are easier to control, more economic and quicker than other experimental tools which make them interesting tools for conducting parametric studies. Energy piles have been less examined at this scale. Limited results available show that the model is able to capture soil/pile interaction during thermal cycles. Studies on a model pile in sand show that the pile behaviour remains thermo-elastic under rather light loads while irreversible deformations appear under heavier loads. Also, shaft resistance varies by applying thermal cycles.

CHAPTER 2
DEVELOPMENT OF PHYSICAL MODEL FOR ENERGY PILE

2.1 Introduction

A physical model for studying the mechanical behaviour of an energy pile is developed. The model is composed of a temperature-controlled pile installed inside a large container of compacted soil (similar to that used by Kalantidou *et al*., 2012). Compared to the model used by Kalantidou *et al*. (2012), more sensors were added, mechanical and thermal loading systems were enhanced. The pile was equipped with temperature sensors and strain gauges for measuring its axial force profile. The surrounding soil was dry Fontainebleau sand or saturated Kaolin clay. The pile was subjected to purely mechanical and thermo-mechanical loading and the effects induced in the pile and in the soil were tracked via sensors measurements. This chapter includes the detail on the model development and the adopted test procedures.

2.2 Experimental setup

The experimental setup is presented in Figure 2.1 and the detail on dimensions and sensors installation is shown in Figure 2.2. The pile was installed in a container, which was gradually filled with soil. A metal frame has been constructed such that it accommodates the soil container, support the load of the water tank and transfer it to the pile. A load cell was placed on the pile head. Three displacement transducers were attached to the pile head for measuring the total displacement during loading. Five strain gauges were adhered to the pile for measuring the axial stress in the pile. Three temperature transducers were stuck to the surface of the pile at various levels. Eleven temperature transducers were embedded in the soil to track temperature variation during the tests. Eight total pressure transducers were also used to measure the stress in different directions at various levels of soil.

The experiments were conducted in dry Fontainebleau sand or in saturated Kaolin clay. As the two mentioned soils, which are different in nature and also in hydraulic properties, are

expected to show different responses to thermo-mechanical loading, it would be interesting to examine the behaviour of the pile embedded in each one.

For loading the pile by head, a progressive loading was adopted by flowing water into the water tank, which was placed in the upper part of the frame. By letting more water enter into the tank, the applied load on top of the pile will increase. This gradual loading allows avoiding shocks that might happen during abrupt increase of load on pile head. Below, the main parts of the system are discussed in detail.

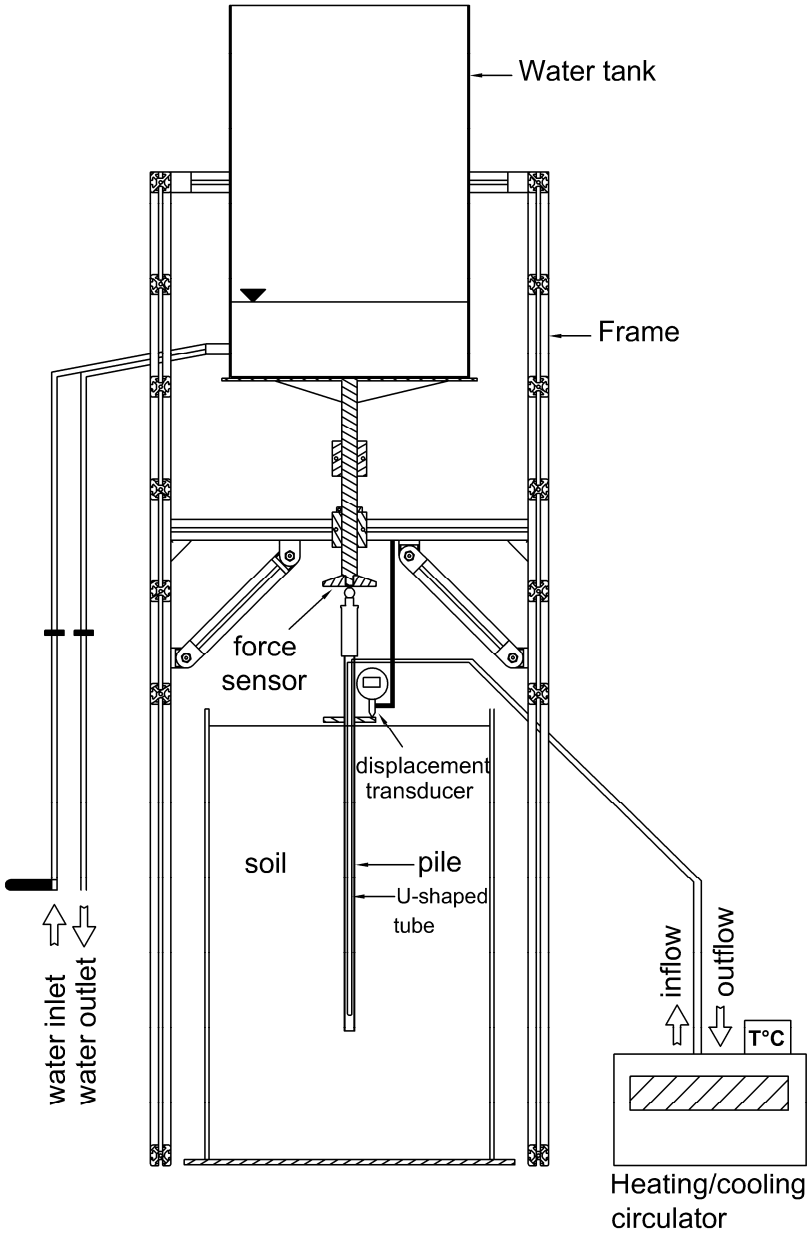

Figure 2.1 Experimental setup

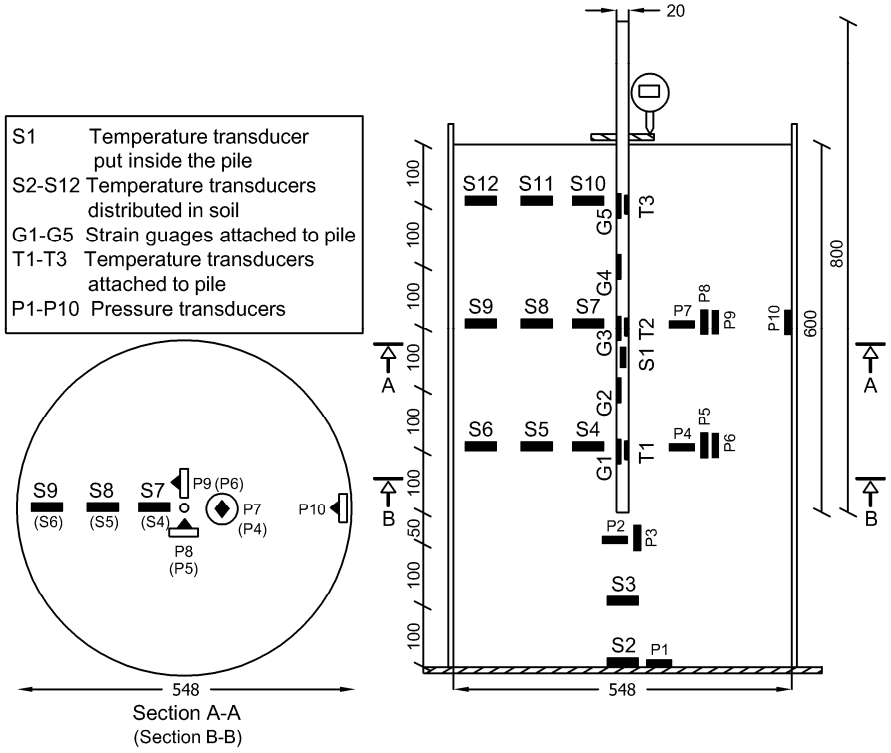

Figure 2.2 Sensors distribution

2.2.1 Model pile

2.2.1.1 Pile dimension and instrumentation

The model pile (shown in Figure 2.3) was a closed-end aluminium tube with outer and inner diameters of 20 and 18 mm, respectively. Six full-bridge strain gauges (G1 to G6) were attached to the outer surface of the pile at 100, 200, 300, 400, 500 and 600 mm from the pile toe, respectively. It should be noted that the gauge G6 was broke down at the very beginning of the experiments and was excluded. Three temperature transducers (T1, T2, and T3) were stuck to the pile at 100, 300, and 500 mm from the pile toe (Figure 2.4).

Figure 2.3 The model pile

Figure 2.4 Detail on strain gauges (G) and temperature transducers (T)

2.2.1.2 Full-bridge type strain gauges

The detail of the full-bridge strain gauge (G) is shown in Figure 2.5*a*. At each level, four strain gauges are arranged following the full-bridge configuration: two gauges measure the axial strain and two others measure the transversal strain of the pile surface. The idea is to measure resistance changes (ΔR) caused by an axial force along the pile and transforming it to strain. The resistance (R) and axial strain (ε_l) are linked via equation (2.1):

$$\frac{\Delta R}{R} = \beta \varepsilon_l \qquad (2.1)$$

where β is the gauge factor, which is equal to 2.13 for the utilised strain gauges.

To increase the accuracy of the measurements, the gauges were arranged following the Wheatstone bridge configuration (see Figure 2.5*b*). The bridge is powered by an electronic

source along the diagonal AC with voltage U_E. The output voltage is shown by U_A. The bridge is balanced (the output voltage $U_A = 0$) when:

$$\frac{R_1}{R_2} = \frac{R_3}{R_4} \tag{2.2}$$

At equilibrium, the voltage U_A is zero, but the variation of any of the resistances leads to a change of U_A. After Rosquoet (2004), in a full-bridge configuration, the sensibility of the measured signal is maximal and the effects of temperature are eliminated. A full bridge unbalanced by ΔR_i gives an output voltage of U_A which could be calculated by the following equation:

$$\frac{U_A}{U_E} = \frac{1}{4}\left(\frac{\Delta R_1}{R_1} - \frac{\Delta R_2}{R_2} + \frac{\Delta R_3}{R_3} - \frac{\Delta R_4}{R_4}\right) \tag{2.3}$$

Substituting from equation (2.1):

$$\frac{U_A}{U_E} = \frac{\beta}{4}(\varepsilon_1 - \varepsilon_2 + \varepsilon_3 - \varepsilon_4) \tag{2.4}$$

For the case of uniaxial tension (or compression), as shown in Figure 2.5*c*, gauges I1 and I3 are arranged along the axis of the uniaxial stress and measure the longitudinal deformation (ε_l) while gauges I2 and I4 are arranged in the orthogonal direction and measure the transversal deformation (ε_t). ε_l and ε_t are related to each other by the Poisson's ratio (ν): $\varepsilon_t = -\nu\varepsilon_l$.

Equation (2.4) is simplified as follows:

$$\frac{U_A}{U_E} = \frac{\beta}{2}(\varepsilon_l - \varepsilon_t) = \frac{\beta}{2}(1+\nu)\varepsilon_l \tag{2.5}$$

The axial force is then computed via equation (2.6), assuming that the metal pile has a linear elastic behaviour:

$$P = \varepsilon_l EA \tag{2.6}$$

in which A is the pile section area (A = 59.68 mm^2) and E is the elastic modulus of aluminium (E = 69 GPa).

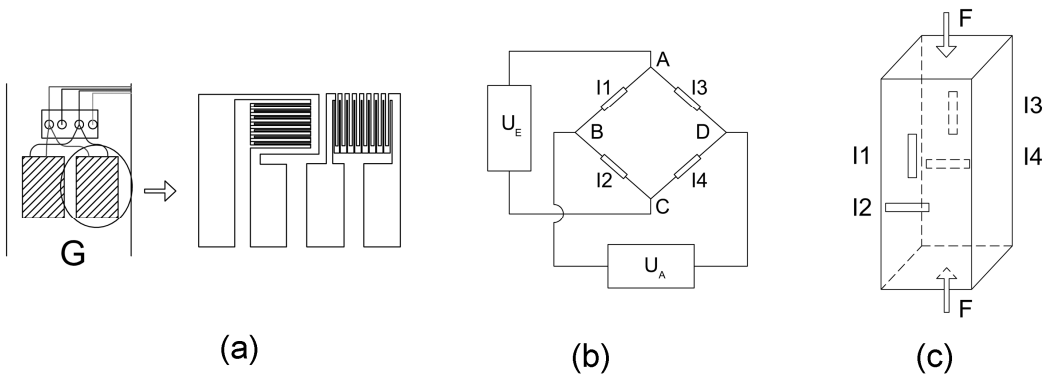

Figure 2.5 Detail of the full-bridge strain gauge: (a) installation on the pile surface; (b) behaviour under uniaxial compression of the pile; (c) full-bridge configuration.

2.2.1.3 Pile surface roughness

In order to have the maximum roughness at pile surface, a layer of sand was coated on its outside surface. To produce a homogeneous surface, the pile was first covered with Araldite glue (Figure 2.6*a*). It was then fixed by its toe on a sand layer already poured in a plastic tube. The tube was filled gradually with sand afterwards (Figure 2.6*b*). At last, the pile was fully surrounded by sand (Figure 2.6*c*). After 24 hours, when the glue was perfectly dried, the pile was driven out gently. It has to be noted that the sand utilised was the Fontainebleau sand, which was later used as one of the soils within which the pile is embedded.

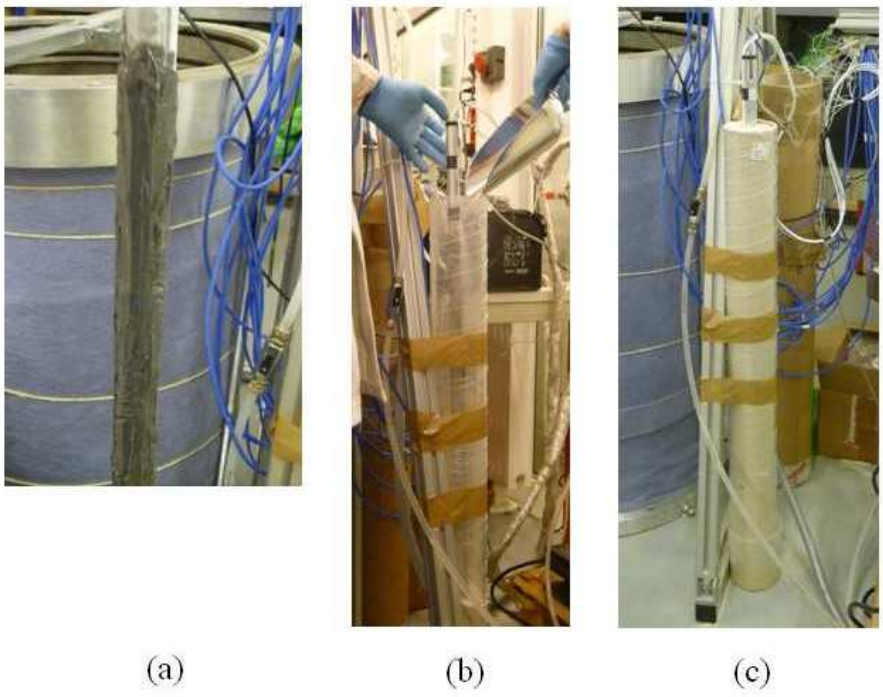

Figure 2.6 Pile surface coating by sand: (a) surface covering with glue; (b) pile installation and pouring sand; (c) leaving the pile in the sand to be fully coated

According to Fioravante (2002) the interface roughness could be normalised and upper and lower limits could be defined accordingly in order to distinguish whether the surface is smooth or rough. The normalised roughness is defined as:

$$R_n = R_t / D50 \quad (2.7)$$

where R_t is the maximum surface roughness in a length of L_m which varies between 0.8 and 2.5 mm (Figure 2.7*a*).

In the case of the mentioned model pile, assuming that the soil grains at the interface (which is made up of the same soil when the pile is embedded in Fontainebleau sand) were replaced by the median sized grain (D50), it could be deduced that R_t is equal to or greater than D50 (Figure 2.7*b*) . The R_n value would be at least 1. According to Fioravante (2002) For the R_n values less than 0.02, the interface is considered to be smooth while for the values great than 0.1 it is assumed to be rough. More side friction and dilatancy are expected to occur at rougher interfaces.

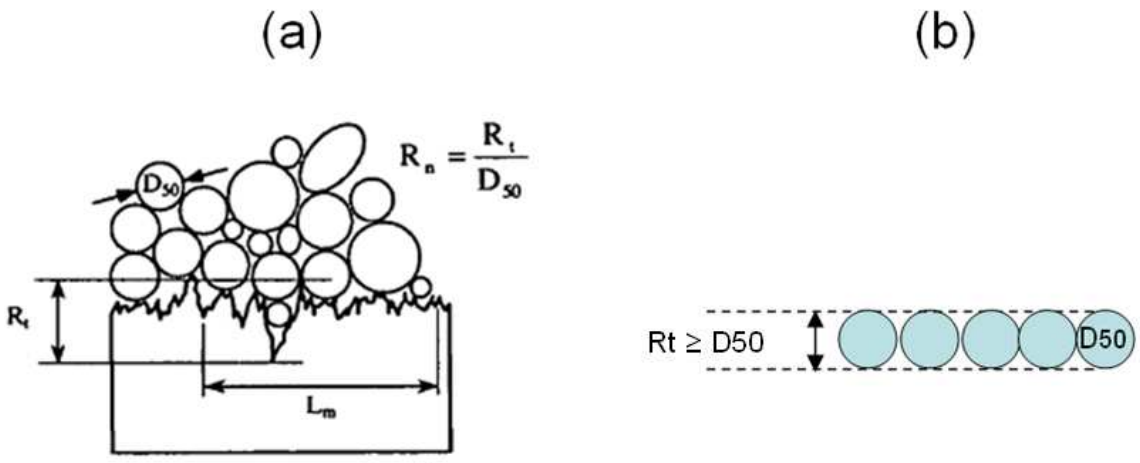

Figure 2.7 (a) Definition of R_n and R_t (Fioravante, 2002) (b) Estimated R_t on the model pile surface

In the case where the model pile was surrounded by Kaolin clay, as the grains were much finer (the grain size distribution of the soils will be shown later), R_n would be higher than in the previous case, which means that in the two cases, soil/pile interface was relatively rough.

2.2.1.4 Calibration of strain gauges

Before testing, strain gauges on the pile were calibrated under a relatively small load. Pile toe was fixed and it was loaded by its head. All the transducers have to show the same value

as the load cell, which was located at the pile head. Axial force recorded by the load cell and the ones evaluated via the measurements of the strain gauges and using Equation 2.5 and 2.6 are depicted as a function of time in Figure 2.8. The pile was subjected to a static load of 110 N at its head and it was heated from about 20°C to 25°C. The pile head load was selected small enough in order not to subject the pile to buckling. It should be noted that the minimum load which could be applied to the pile is equal to the weight of the loading system which was 100 N. It was not loaded incrementally to higher load values for the same reason. As could be detected in the figure, temperature did not affect the gauges measurements which confirms that the utilised strain gauges are temperature compensated. There exists a maximum difference of 20 N between the head load and the force values measured by gauges.

To interpret the tests results, Equation 2.5 is modified as follows:

$$(\frac{U_A}{U_E})_{test} - (\frac{U_A}{U_E})_{initial} = \frac{\beta}{2}(\varepsilon_l - \varepsilon_t) = \frac{\beta}{2}(1+\nu)\varepsilon_l \tag{2.8}$$

in which $(\frac{U_A}{U_E})_{test}$ is the value measured during the test and $(\frac{U_A}{U_E})_{initial}$ is the value recorded prior to the pile's installation in each experiment.

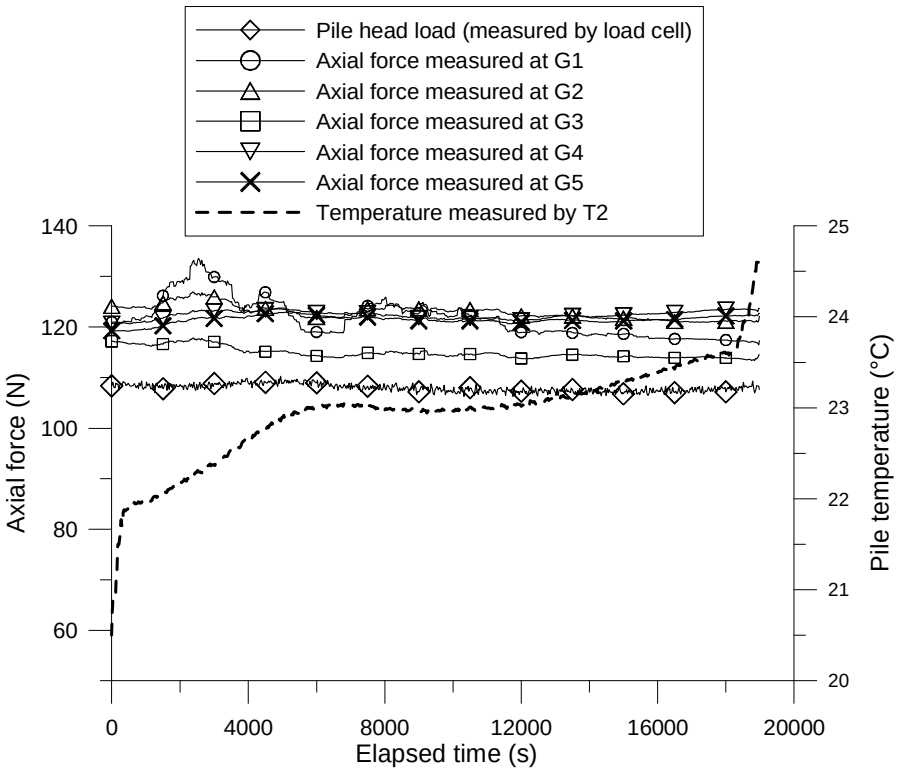

Figure 2.8 Strain gauges calibration

2.2.2 Temperature control

To control the pile temperature, a heating/cooling circulating bath of type Cryostat MX was used. The device allows the temperature control from -20°C to 150°C. The internal reservoir was filled with water and connected to the U-shaped tube that was inserted inside the pile (Figure 2.1). The U-shaped tube which works as heat carrier fluid pipe in the model energy pile is of aluminium and has an internal diameter of 2 mm. The pile was filled with water to ensure the temperature homogenisation during the tests. The soil container was covered by expanded polystyrene sheets to limit heat exchange between the soil and ambient air.

To monitor the temperature variations, other than the three temperature transducers that were attached to the surface of the pile (T1, T2, and T3), twelve temperature transducers of type PT1000 with an accuracy of ±0.3°C were placed in the soil. The transducers are composed of a steel stem with length of 50 mm and diameter of 5 mm and a silicon cable (Figure 2.9). One temperature transducer was placed inside the pile (S1), at 300 mm from the pile toe (Figure 2.2). The other temperature transducers (S2 to S12) were distributed at different levels in the soil. S2 was attached to the bottom of the soil container, at the centre. S3 was placed at 100 mm above S2 and 250 mm under the pile toe (Figure 2.10). At levels of 350 mm, 550 mm and 750 mm from bottom of the soil container, three temperature transducers were installed with distances of 50 mm, 150 mm, and 250 mm from the axis of the pile. Figure 2.11 depicts the installation of transducers S10, S11 and S12.

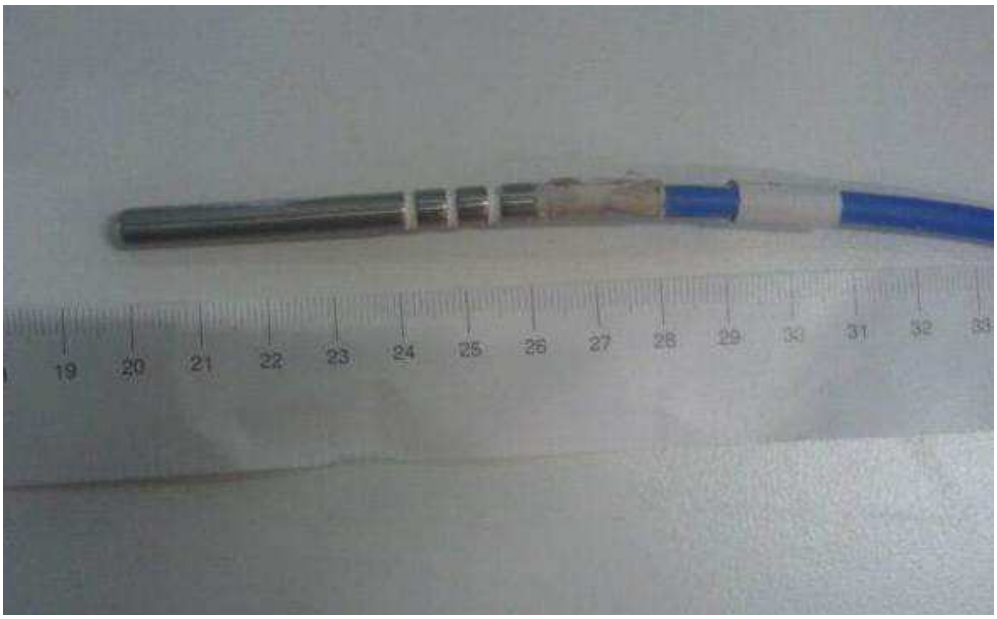

Figure 2.9 Detail on the utilised temperature transducer

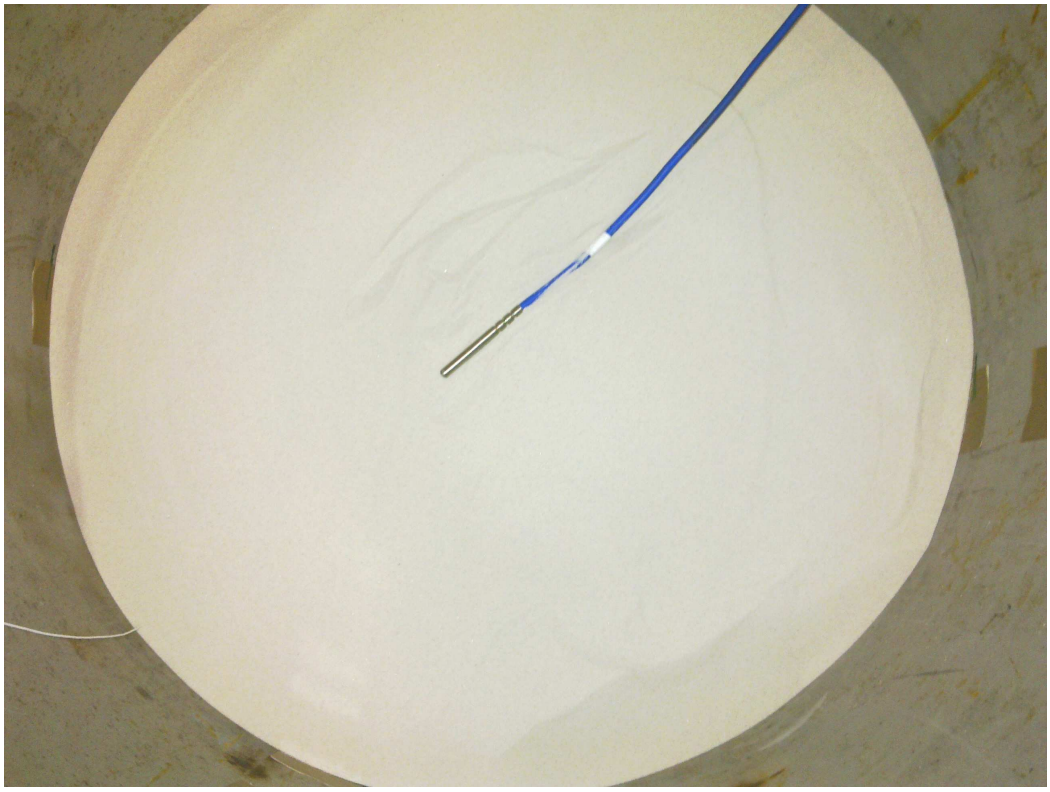

Figure 2.10 Installation of temperature transducer S3 on the compacted soil layer

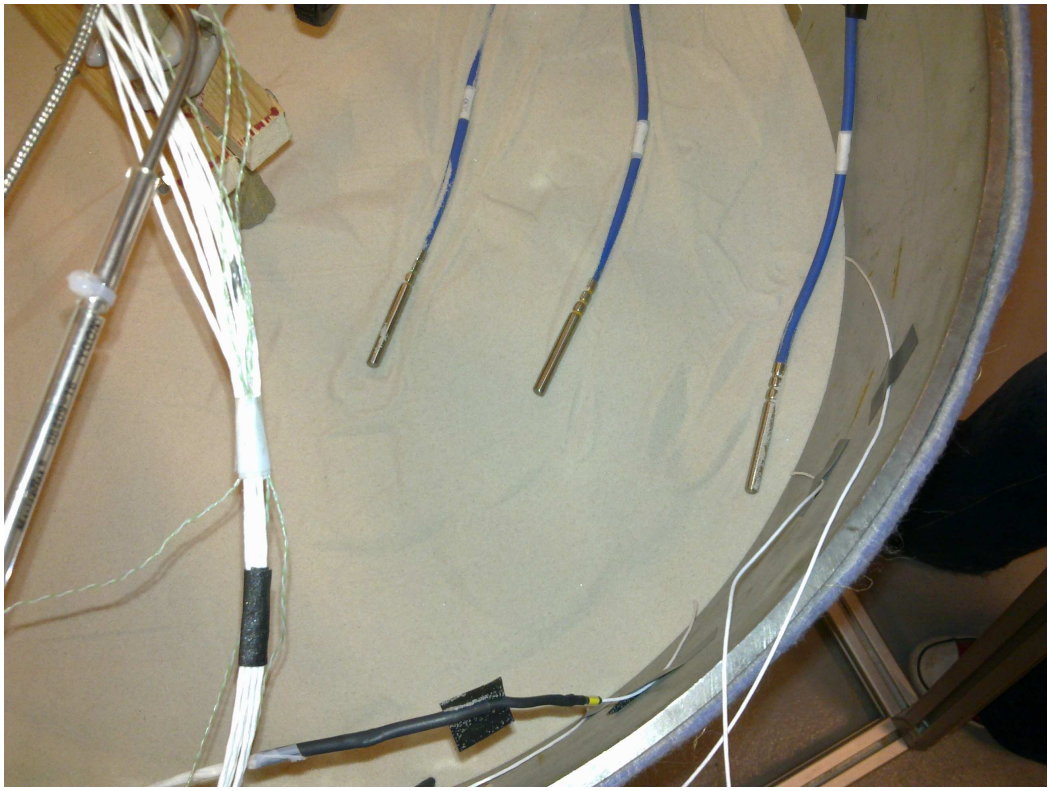

Figure 2.11 Installation of temperature transducers S10, S11 and S12 on the compacted soil layer

2.2.3 Total pressure measurement

In order to measure the total stress in the soil during the tests, ten pressure transducers (denoted by 'P' in Figure 2.2) were installed at different positions. The ultra-thin transducers used were of Kyowa (PS series) type. They have a diameter of 6 mm and a thickness of 0.6 mm (Figure 2.12) and are capable to measure the normal stress applied on their sensing surface in the range of 0 – 100 kPa with an accuracy of 1 kPa. Because of their fragile structure, the utilised pressure transducers were stuck to a solid plate which permits to protect them and at the same time makes it easier to install them in considered directions (Figure 2.13). Measurements which are expressed in voltage, could be converted into pressure via Equation 2.8:

$$TP(kPa) = \frac{U_A(mV)}{U_t(V)} \times \frac{capacity(kPa)}{ROV(mV/V)} \tag{2.8}$$

where *ROV* is the 'rated output voltage' and changes between 0.5 and 0.8 mV/V. The sensors capacity is 100 kPa.

One pressure sensor was attached to the bottom of the container (P1) as shown in Figure 2.2. The sensor P2 was used to measure the vertical stress 50 mm under the pile toe. Sensor P3 measured the horizontal stress at the same level. At the level of 350 mm above the soil container bottom, the sensors P4, P5, P6 were installed around the pile at a distance of 50 mm from the pile axis. The sensor P4 measured the vertical stress. The sensors P5 and P6 measured the horizontal stresses along two directions: towards the pile axis (P5), and perpendicular to this direction (P6). At the level of 550 mm above the soil container bottom, three sensors were installed around the pile at a distance of 50 mm from the pile axis and one sensor was fixed at the container wall (P10). P7 was used to measure the vertical stress at this depth. The sensing face of the sensors P8 and P10 was fixed towards the pile axis. The sensor P9 measured also the horizontal stress but in the direction that is perpendicular to that of P8. The locations of the sensors were chosen to capture the stress change around the pile and also to verify the boundary effects in the model.

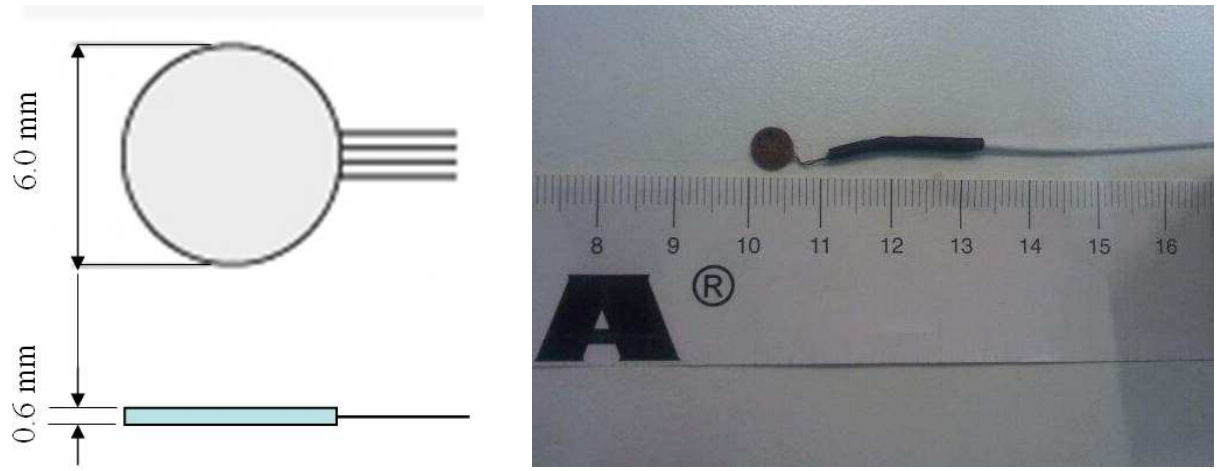

Figure 2.12 Detail on the pressure transducer shape and dimension

(a) (b)

Figure 2.13 (a) Detail on the structural protection of the pressure transducers (b) Installation of pressure transducers P7, P8 and P9 at the pile vicinity on the compacted soil layer

2.3 Experimental procedure for experiments on dry sand

2.3.1 Physical properties of Fontainebleau sand

The physical properties of Fontainebleau sand are as follows: particle density ρ_s = 2.67 Mg/m^3; maximal void ratio e_{max} = 0.94; minimal void ratio e_{min} = 0.54 (De Gennaro *et al.*, 2008); and median grain size D_{50} = 0.23 mm. Thermal conductivity and volumetric specific heat capacity, measured by 'KD2 Pro thermal Properties analyzer' device, were equal to 0.2 W/(mK) and 1.2 J/(m^3.K), respectively. The grain size distribution of the sand used is shown in Figure 2.14.

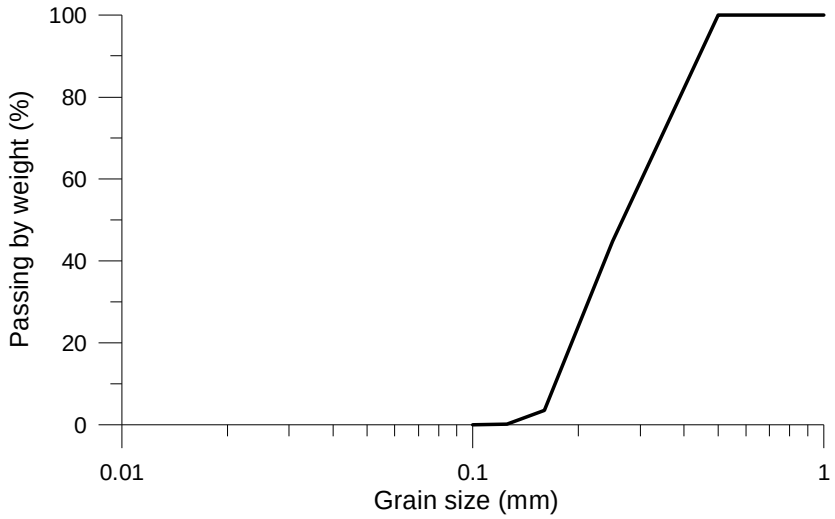

Figure 2.14 Grain size distribution of Fontainebleau sand

2.3.2 Installation

Soil compaction was started by layers of 100 mm, 100 mm and 50 mm in the soil container. A wooden tamper was used to compact dry sand at a dry unit weight of 15.1 kN/m^3, which corresponds to a relative density of 46%. It should be noted that the same value was used in De Gennaro *et al*. (1999). Considering its relative density, the sand could be classified as relatively loose (Said, 2006). The density was controlled by the mass of sand to be compacted and the thickness of each layer. The pile was then fixed at its position in the centre of the container with the help of a temporary support. This method of pile installation represents more closely that of non-displacement piles, which is mainly used in the technology of geothermal foundations. The U-shaped tube was then inserted into the pile, which was filled with water. After that, compaction was continued around the fixed pile in layers of 100 mm. The temperature and pressure transducers were placed at the pre-defined positions on the compacted soil layer as compaction proceeded. Six soil layers were compacted this way. The temporary support was therefore removed and pile was liberated. Afterwards, the displacement transducers and the force sensor were fixed at the pile head.

2.3.3 Test programme

2.3.3.1 Purely mechanical loading

The loading programme was adopted according to the French standard (AFNOR, 1999) on static axial pile loading. Based on the ultimate load of the pile, Q_{max}, the loading path is composed of three phases as illustrated in Figure 2.15: (1) the preparation phase which corresponds to a loading up to $0.1 \times Q_{max}$ for 15 min and unloading. The displacements

observed at this stage are related to perturbations occurred during soil compaction and pile installation and will be ignored; (2) the incremental loading up to $0.5\times Q_{max}$ by increments of $0.1\times Q_{max}$ which are maintained for 1 hour and unloading; (3) loading up to failure with increments of $0.1\times Q_{max}$ and unloading. It should be noted that in this phase the increments are kept for 30 min up to the axial load of $0.5\times Q_{max}$ and 60 min afterwards until failure. The conventional failure corresponds to a pile head settlement of 10% of the pile diameter (AFNOR, 1999), which is 2 mm in this case.

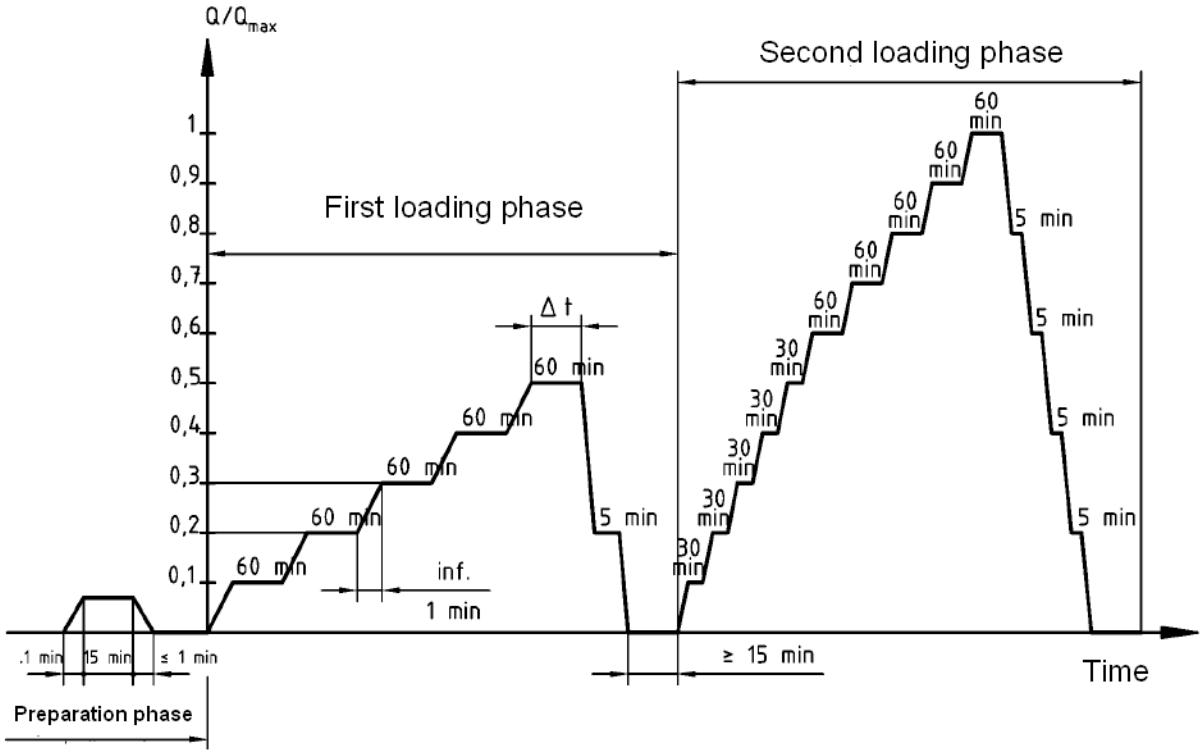

Figure 2.15 Loading procedure for purely mechanical tests (Test E1) on the pile in Fontainebleau sand

The ultimate load of the model pile was estimated at 500 N following the tests performed by Kalantidou *et al*. (2012) in similar conditions and also some preliminary tests on the existing system. During the preparation phase, the pile was loaded up to 100 N. This value is higher than $0.1\times Q_{max}$, recommended by the procedure but it corresponds to the total weight of the loading system (empty water tank, metallic support), which is the minimum load that could be applied on the model pile. For the second phase, the load was increased from 0 to 100, 150, 200, 250, 300, 350, 400, 450, 500 N.

2.3.3.2 Thermo-mechanical loading under two thermal cycles

In the thermo-mechanical tests, it was intended to subject the pile to thermal cycles under a constant axial load. The tests began by a mechanical loading phase in accordance with the loading procedure explained above. Once the desired load value was achieved and the corresponding time was over, it was kept unchanged until the end of the test. The mechanical loading phase depends on the pile head load value, defined in each test. In tests under 100, 150, 200 and 250 N, as the load values are less than $0.5 \times Q_{max}$, mechanical loading was limited to the preparation phase and first loading phase (Figure 2.16*b*). On the contrary, in the tests under loads greater than 250 N, the pile was submitted to preparation, first and second loading phases (Figure 2.16*c*). One test was also conducted under 0 N; the mechanical loading phase consisted of loading and unloading the pile in the preparation phase (Figure 2.16*a*).

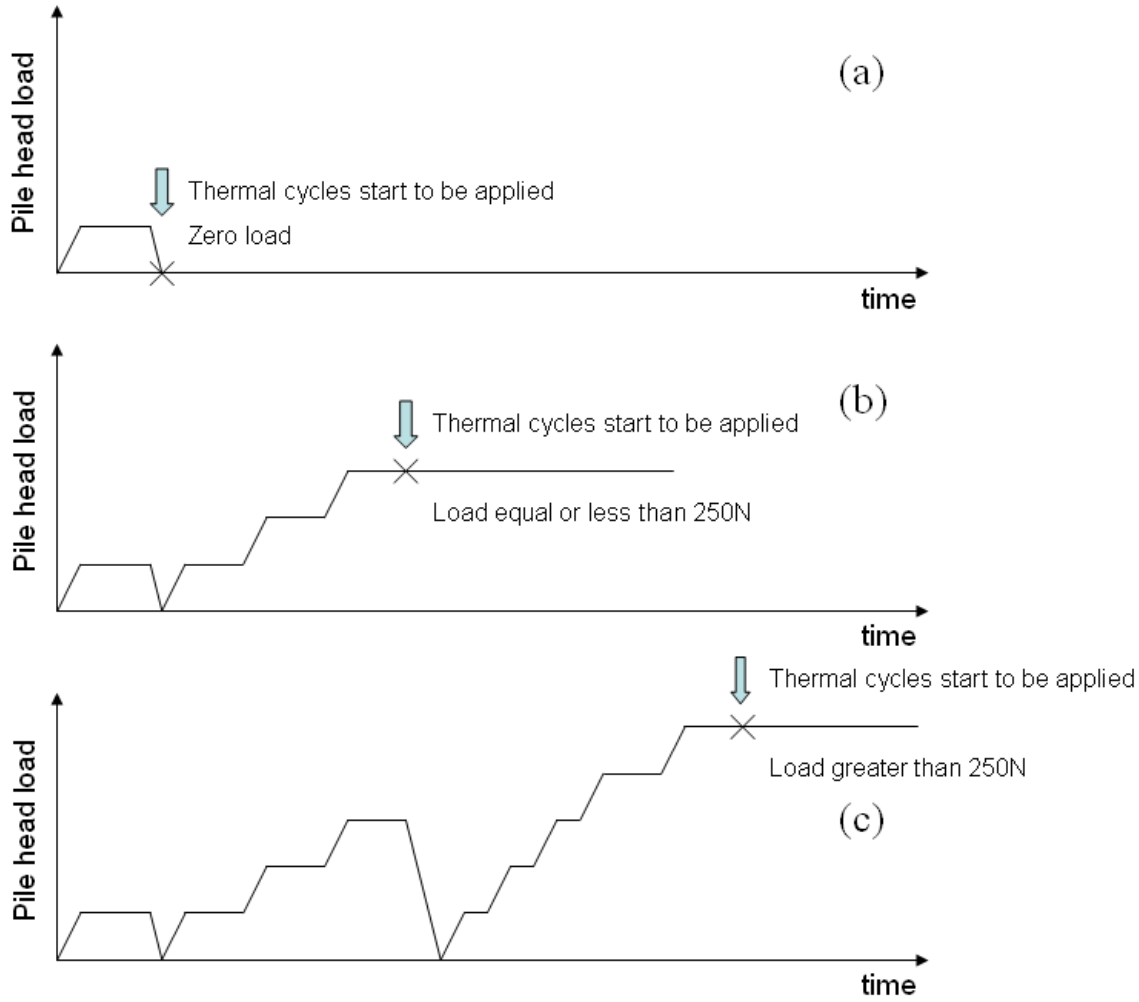

Figure 2.16 Loading procedure in thermo-mechanical tests on the pile embedded in sand under a pile head load of (a) 0 N (b) less than (or equal to) 250 N (c) More than 250 N

Under the target mechanical load, the heating/cooling circulating bath was turned on together with a peristaltic pump, which helped to increase the flow rate in the pipes. That way water at a certain temperature circulated at a rate of 0.1 L/s. Two thermal cycles were applied to the pile between 5°C and 35°C. Thermal loading was also conducted incrementally, by steps of 5°C. It was observed that after 1 h temperature changes in the pile stabilises, thus each step was maintained for 2 h. The duration was increased during nights or weekends. Six thermo-mechanical tests were conducted in this context. Testing programme is shown in Figure 2.17. In total, seven experiments have been performed (E1 to E7).

It should be noted that at the end of each test, the soil, the pile and all the transducers were removed. Soil was re-embedded according to the process described above before conducting the next test.

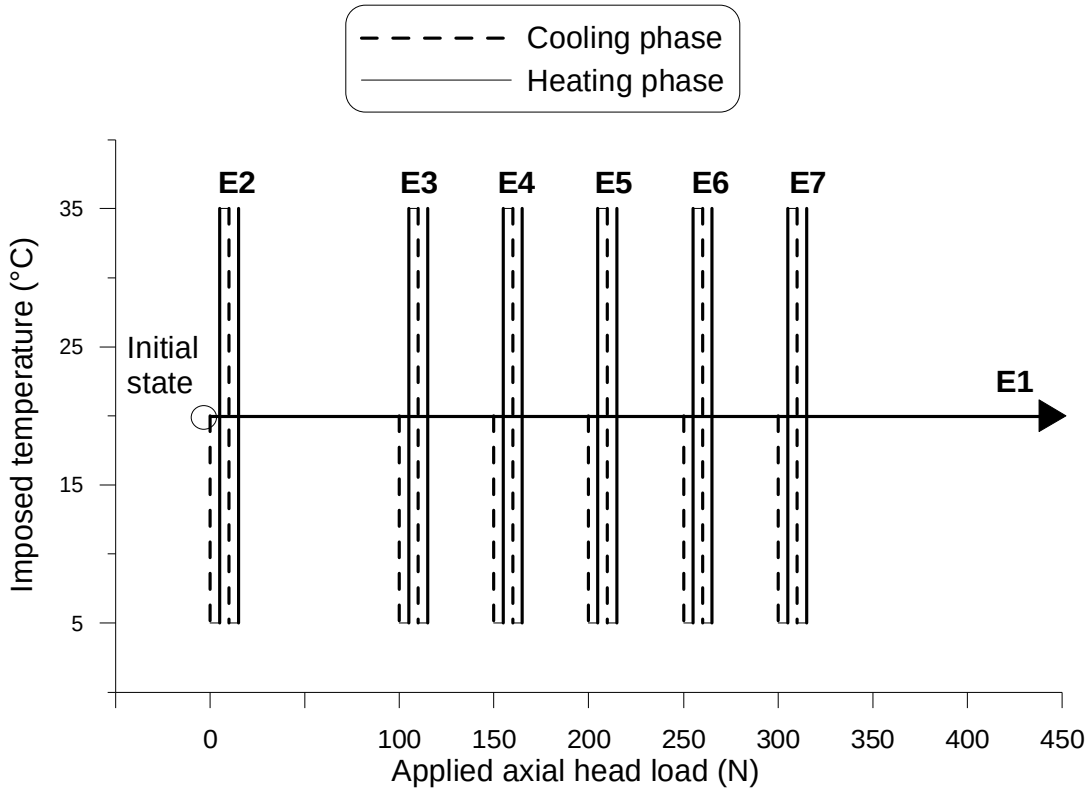

Figure 2.17 Test programme (pile in Fontainebleau sand)

2.3.3.3 Thermo-mechanical loading under several thermal cycles

In order to evaluate the effect of the heating/cooling cycles number on the performance of the model energy pile, one experiment was conducted under 30 thermal cycles. Considering each thermal cycle as the approximation of one year of the energy pile operation, 30 cycles could simulate the behaviour of the model pile within 30 years of its service. The pile was

subjected first to the mechanical load of 150 N (similar to test E4), which is 30% of the model pile ultimate load and thus could be considered as the model pile service load. Two thermal cycles were applied according to the loading programme performed in test E4. Thermal cycles were continued between 5°C and 35°C but this time the pile was subjected only to the extreme temperature values and thermal loading was not applied incrementally. Each step of thermal loading was maintained for 24 hours. The test conducted within this context will be referred to as test E8.

2.4 Experimental procedure for experiments on saturated clay

2.4.1 Physical properties of Kaolin clay

Kaolin clay commercially known as Speswhite China clay was selected for the experiments. Kaolin clay is a non-expansive permeable clay (Cekerevac, 2003; Savage, 2007), which makes it a suitable choice especially when tests are performed under a saturated state. Also, according to Cekerevac (2003), thermal effects on this type of clay could be distinguished from creep induced effects. The provided material is in the form of a refined powder with high whiteness and brightness. Particle size distribution of Kaolin clay, obtained by laser diffraction method, is shown in Figure 2.18.

Kaolin clay has a liquid limit w_L = 57%, a plastic limit w_P = 33%; and a particle density ρ_s = 2.60 Mg/m^3 (Frikha, 2010). Regarding its plasticity index of 24, the soil could be classified as MH or OH according to the Unified Soil Classification Scheme. Soil activity, which is calculated as the ratio of plasticity index to the percentage of grains less than $2\,\mu m$, is then equal to 0.3 that is relatively low. According to Vega & McCartney (2014), a soil with a low activity ratio does not contain a large amount of clay minerals that might be affected by temperature. Thermal conductivity and volumetric specific heat capacity, measured by 'KD2 Pro thermal Properties analyzer' device, were equal to 1.5 W/(mK) and 3.3 J/(m^{3}K) respectively.

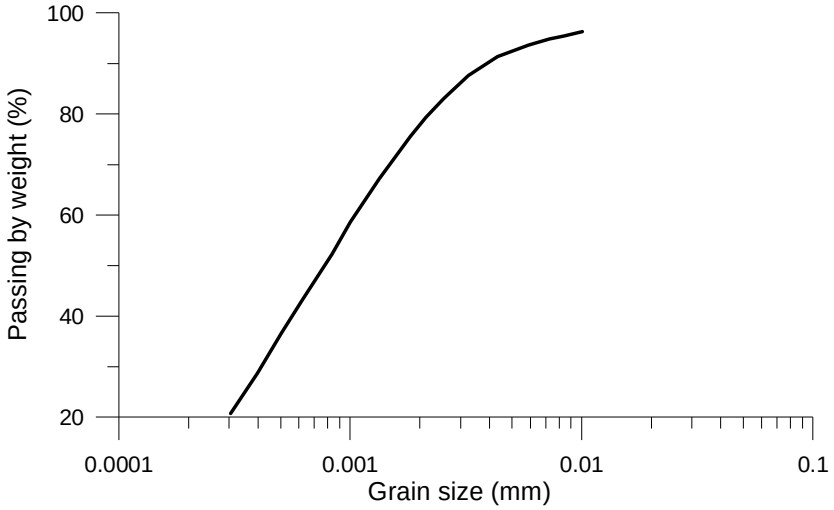

Figure 2.18 Grain size distribution of Kaolin clay

2.4.2 Installation

The soil was mixed with tap water at a water content of 33% in a large mixer in order to facilitate the compaction process. The prepared material was then maintained in hermetic boxes to ensure humidity homogenisation.

Soil compaction started with three layers of 100, 100 and 50 mm. A vibratory hammer was used to compact the soil at the dry density of 1.5 Mg/m^3 (the same value as the Fontainebleau sand). The sensors were placed in the soil according to Figure 2.2. The same locations were considered as in the experiments on sand. The pile was installed afterwards by means of a metallic fixation such that its toe touched the last soil layer. Soil compaction was continued with 100 mm thick layers around the pile (Figure 2.19 and Figure 2.20*a*). Once the compaction was finished (Figure 2.20*b*), saturation was started by injecting tap water from the bottom. The water container (see Figure 2.1) which was intended to be utilised for mechanical loading, was used to apply a sufficient hydraulic gradient at this stage via several tubes connected to the bottom of the soil container. Considering a hydraulic conductivity of $10^{-8} m/s$ for Kaolin Speswhite clay (Youssef, 1994; Al-Tabba *et al*., 1987) and under the hydraulic gradient of 2 m, the saturation time was estimated to be 32 days. During the saturation period, soil surface was covered to prevent water loss by evaporation. Since no measurement was conducted on the pore water pressure to ensure the achievement of a saturated state, soil was kept under the mentioned conditions for a long time of about 10 months which is widely longer than the calculated value. During the last 5 months, the soil was watered also from its top surface to enhance saturation and also to avoid any superficial suction.

Figure 2.19. First stages of clayey soil compaction

(a) (b)

Figure 2.20 (a) Last stages of clayey soil compaction (b) Final soil surface

2.4.3 Test programme

2.4.3.1 Purely mechanical loading

The pile was first subjected to purely mechanical loading. Axial loading was applied by increments of 50 N, as for the experiments on sand. Each increment was kept for 1 hour. Loading was continued until failure, which is 10% of the pile diameter (2 mm). The mechanical loading programme is depicted in Figure 2.21*a*. Two tests, referred to as F1 and F2 were conducted by applying the mentioned procedure to check the repeatability and to evaluate the ultimate load. As compaction and saturation procedures are difficult and time consuming, several tests were performed on the same system but within a 7 days interval. It is assumed that the excess pore water pressures generated by loading during a test would dissipate during this rest time and that the subsequent test would be conducted under almost the same conditions as the previous one. The results would be then comparable. Accordingly, once one test was finished, the pile was unloaded and the next test was performed one week later on the same system.

2.4.3.2 Thermo-mechanical loading under two thermal cycles

The thermo-mechanical loading programme was adopted according to the work of Akrouch *et al*. (2014). Similar to the experiments on sand, during thermo-mechanical tests, first the pile was subjected to a mechanical load, then thermal cycles were applied under a constant load value. Five tests, denoted by F3, F4, F5, F6 and F7, were performed under 100 N, 150 N, 200 N, 250 N and 300 N, respectively. In all the tests, the pile was mechanically loaded for 2 h, then the heating/cooling circulator was turned on to set the temperature at 35°C. After 2 h, the temperature was decreased to 20°C which is equal to ambient temperature. This step was also kept for 2 h. Cooling continued by changing the temperature at the circulator to 5°C and keeping it at this temperature for 2 h. In the last step of thermal loading, temperature at the circulator was increased to 20°C. Water at this temperature circulated for 2 h. Once one thermal cycle was finished, the pile was unloaded. The circulator continued to work at 20°C within 14 hours to avoid temperature changes in the pile. The subsequent test was started under another mechanical load value. Thermo-mechanical loading programme is shown in Figure 2.21*b*.

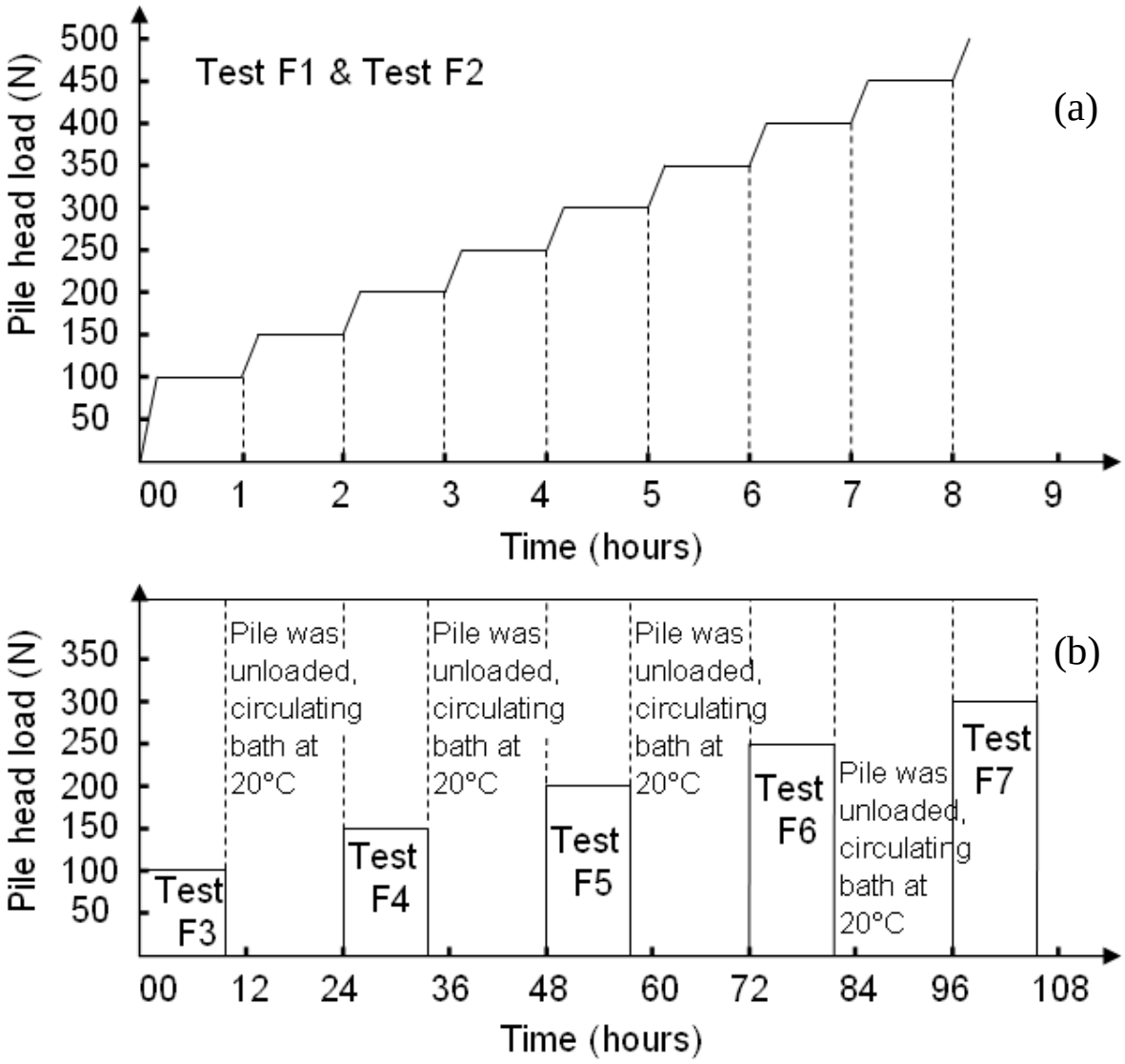

Figure 2.21 Loading programme (pile in Kaolin clay): (a) purely mechanical loading; (b) thermo-mechanical loading

2.5 Discussion

When working on physical model, special caution should be taken in order to minimise the boundary effects. Generally, the dimensions of the soil container should be large enough in order not to affect the principal mechanism observed in the pile. For the same reason enough space should be considered between the pile toe and the bottom of the container.

The dimensions of the soil container were 548 mm in diameter and 880 mm in height. Considering the dimensions of the pile, the ratio of diameter of soil specimen to the pile diameter is equal to 27.4. Thus the boundary effect is negligible according to Parkin & Lunne (1982) who suggest the minimum ratio of 20 for loose sands and 50 for dense sands. The distance between the pile toe and the base of the container was 250 mm, which is 12.5 times

greater than the pile diameter. In the work of Le Kouby *et al*. (2004), this distance was equal to 10 times the pile diameter.

Scale effects are more pronounced regarding the ratio between the pile diameter (20 mm) and the median diameter of sand particles (D_{50} = 0.23 mm); this ratio is equal to 87 in the developed model. Foray *et al*. (1998) propose the lower limit of 200, while Garnier and König (1998) reduce the ratio to 100 and Fioravante (2002) suggests 50. The mentioned ratio is much greater than the proposed limits in the case where the pile is embedded in Kaolin clay (as soil grain size is much smaller).

2.6 Conclusion

In this chapter, the development of a laboratory scale model on energy pile is shown. The model is composed of a model energy pile, a soil container, a loading frame and a temperature control system. The model pile is equipped with a heat carrier fluid pipe connected to the temperature control system. Pile could be loaded by its head mechanically. By circulating water at controlled temperature inside the pipes, its temperature could be changed at any time. That way a coupling thermo-mechanical loading could be achieved. The loading effects are tracked by strain gauges and temperature transducers in the pile and temperature and pressure transducers at various locations in the soil. In order to evaluate the effect of surrounding soil properties and hydraulic conditions on pile behaviour, the pile was embedded first in dry Fontainebleau sand and next in saturated Kaolin clay and was submitted to purely mechanical and thermo-mechanical loading. Experimental results will be presented in Chapter 3.

CHAPTER 3

EXPERIMENTAL RESULTS ON PHYSICAL MODEL

3.1 Introduction

Experimental results obtained on the physical modelling of a single energy pile are presented and discussed within this chapter. According to the experimental procedure described in Chapter 2, the model pile was first embedded in dry Fontainebleau sand and subjected to purely mechanical and combined mechanical and thermal loading. The response of the pile was investigated through measured pile head displacement, pile temperature and pile axial strain. The effects induced in the soil during mechanical and thermo-mechanical loading were explored via the measurement of temperature and total pressure. During test E1, the pile was subjected to incremental axial loading until failure. In tests E2, E3, E4, E5, E6 and E7, the pile underwent two cooling/heating cycles under a constant mechanical load, while in test E8, the number of thermal cycles was increased to 30 in order to examine the impact of thermal loading in the long term. The model pile was then installed in Kaolin clay which was saturated afterwards. Two tests (denoted by F1 and F2) during which the pile was loaded mechanically until failure were conducted. As described in Chapter 2, failure is defined as 10% of the pile's diameter which is equal to 2 mm in this study. In tests F3, F4, F5, F6 and F7, the pile was subjected to a constant axial load and one heating/cooling cycle.

3.2 Experimental results on the model pile in dry sand

As described in Chapter 2, the pile was loaded mechanically in test E1 and thermo-mechanically in test E2 through test E7. Experimental results consist of pile head displacement, pile axial load, soil total pressure and pile and soil temperature. It should be noted that some of the contents of this section have been published in Yavari *et al*., 2014*a*.

3.2.1 Behaviour under axial mechanical loading (test E1)

The results of test E1 are shown in Figure 3.1 to Figure 3.7. The axial forces, measured at the pile's head and at various locations along the pile (measured by strain gauges), are shown

versus elapsed time in Figure 3.1*a*. It should be noted that the strain gauge G4 has failed and data from this gauge was not available. The pile head displacement measured is shown in Figure 3.1*b*. The test was stopped when the pile head displacement reached 2 mm, which correspond to a pile head load of 450 N. It can be noted that the displacement transducer reacted immediately to load changes (there are no delayed effects).

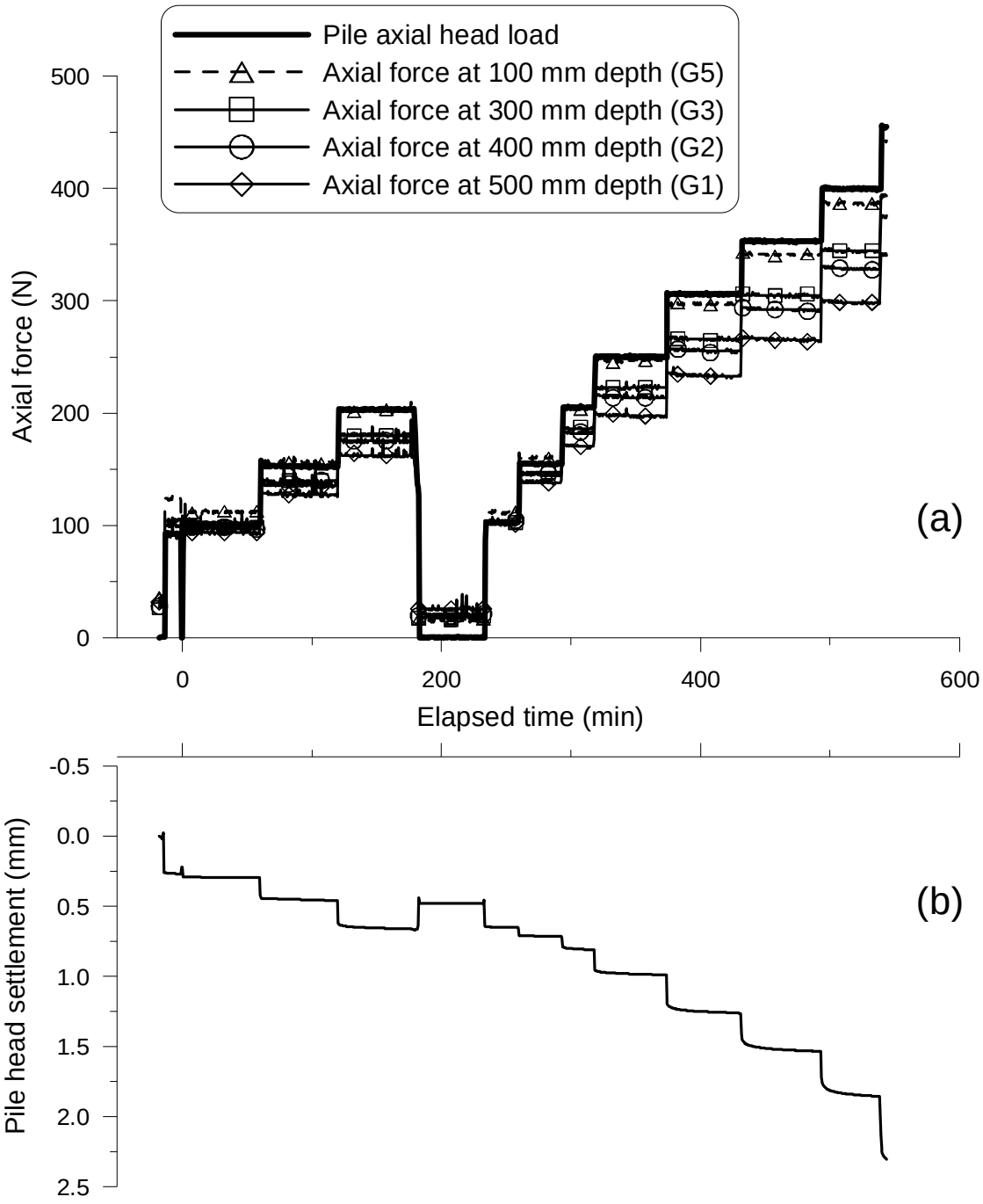

Figure 3.1 Results of test E1 : (a) pile head axial load and the axial forces measured at different levels along the pile (b) pile head displacement

Figure 3.2 shows the pile head displacement versus time for each loading increment in test E1. According to recommendation of AFNOR (1999) on this plot, time effect is evaluated in a period of 60 minutes. Thus for the loads less than $0.5\times Q_{max}$, the response of the pile in the first loading phase (detail in section 2.3.3.1) is considered. For heavier loads, the second loading phase is taken into account. The pile settled immediately as the load increased; the settlement continued during the following 60 minutes by a lower rate and reached a final value. A linear relationship between displacement and time in logarithmic scale seems to exist. Parameter α_n could be defined as follows (AFNOR, 1999):

$$\alpha_n = (S_{60} - S_{30}) / \log 2 \tag{3.1}$$

where S_{30} and S_{60} are displacement values at t = 30 min and t = 60 min under a constant load. The variation of α_n with axial load is plotted in Figure 3.3. A regular trend could not be observed, however the value of α_n is small and does not exceed 0.05 mm. The maximum α_n is achieved under 400 N, which is almost 90% of the ultimate load.

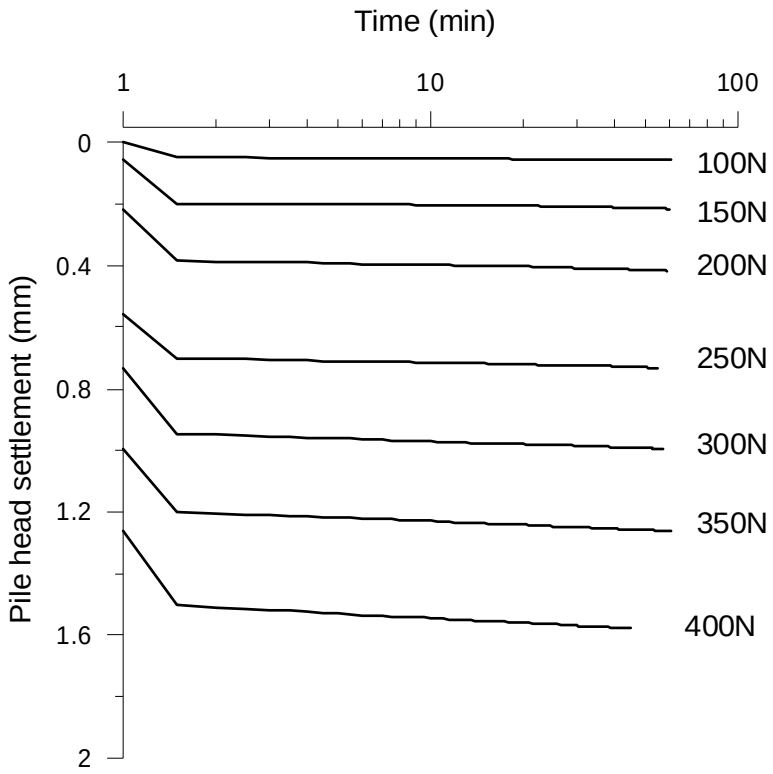

Figure 3.2 Pile settlement time dependency in test E1

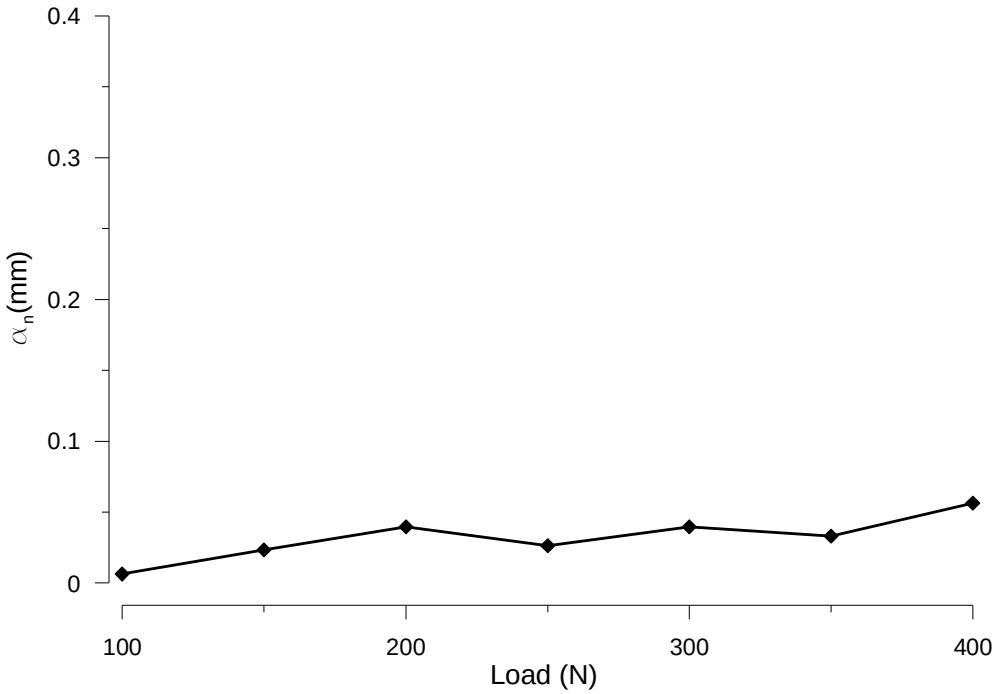

Figure 3.3 Variation of α_n by load in test E1

Figure 3.4 presents the curves of pile head displacement versus load obtained from test E1 and the mechanical part of the other tests. In tests E3 to E6, pile was loaded to 100 N, 150 N, 200 N and 250 N, respectively. Considering the ultimate load of 450 N, 50 % of the maximum load was 225 N, which is close to 250 N. Thus, in test E6, the unloading/reloading phase was neglected. On the contrary for test E7, as the target value of 300 N is definitely higher than 50 % of the maximum load, the pile was unloaded after 200 N and the second phase of loading, with exactly the same increments as in the purely mechanical test was performed. The results show that the experimental procedure leads to a good repeatability of the pile head displacement/axial load curve.

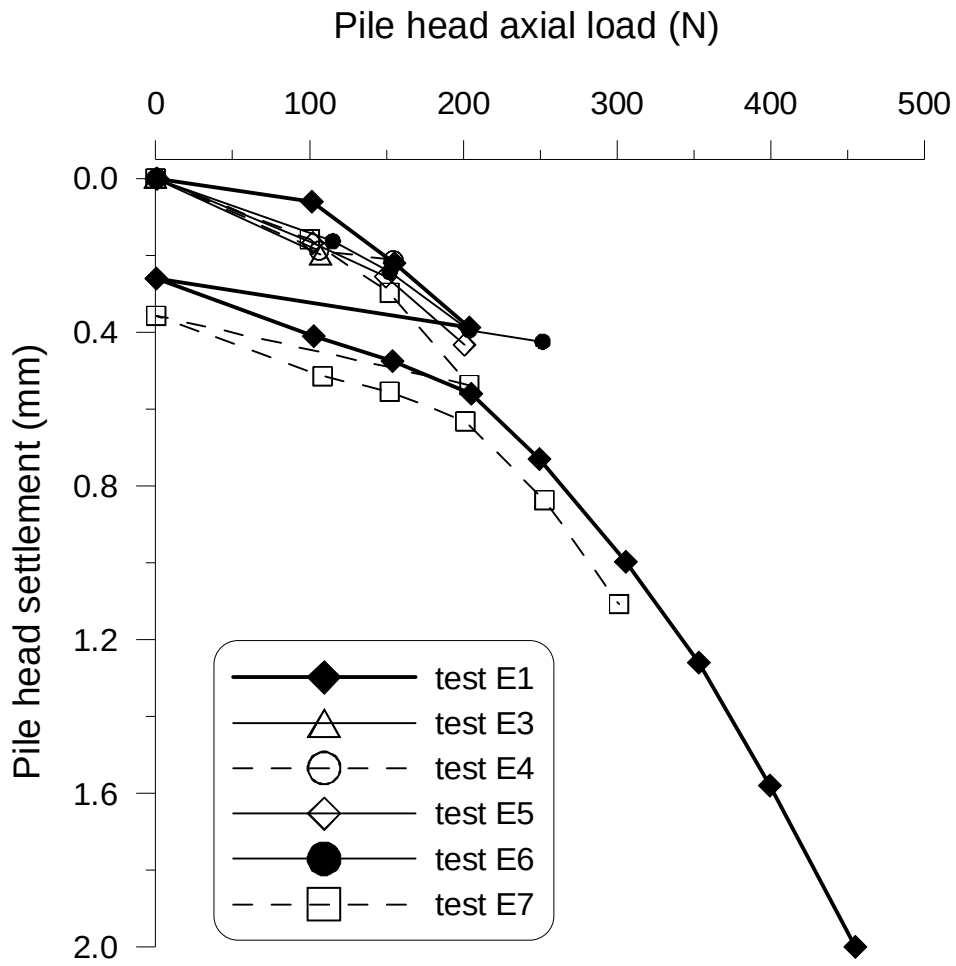

Figure 3.4 Load-settlement curves obtained from various tests in dry sand

In Figure 3.5 changes in soil pressure at different positions in the soil during test E1 could be observed. Ten pressure transducers were used during the test, among which six have operated. The pressure measured at the initial point of each curve is the value of stress just after the compaction of the sand layers in the container. It can then be compared to the conventional values γz for vertical stress and $K_0 \gamma z$ for horizontal stress at rest (where γ is the soil unit weight, γ = 15.1 kN/m^3; z is the depth; and K_0 is the coefficient of lateral earth pressure at rest, which could be assumed to be $K_0 = 1 - \sin\varphi$, about 0.44). For example, the initial measured and calculated stress at P2 are almost the same and equal to 10 kPa. The measured value at P3, about 7 kPa, is comparable to the calculated value of 5 kPa (considering that the accuracy of total pressure transducers is ±1 kPa). During the mechanical loading of test E1, only the soil pressures measured at P2 and P3, that were situated 50 mm below the pile toe, were significantly modified; pressure at P2 increased from 10 kPa to 45 kPa at the end of the test. The changes in soil pressure measured by other sensors were not significant.

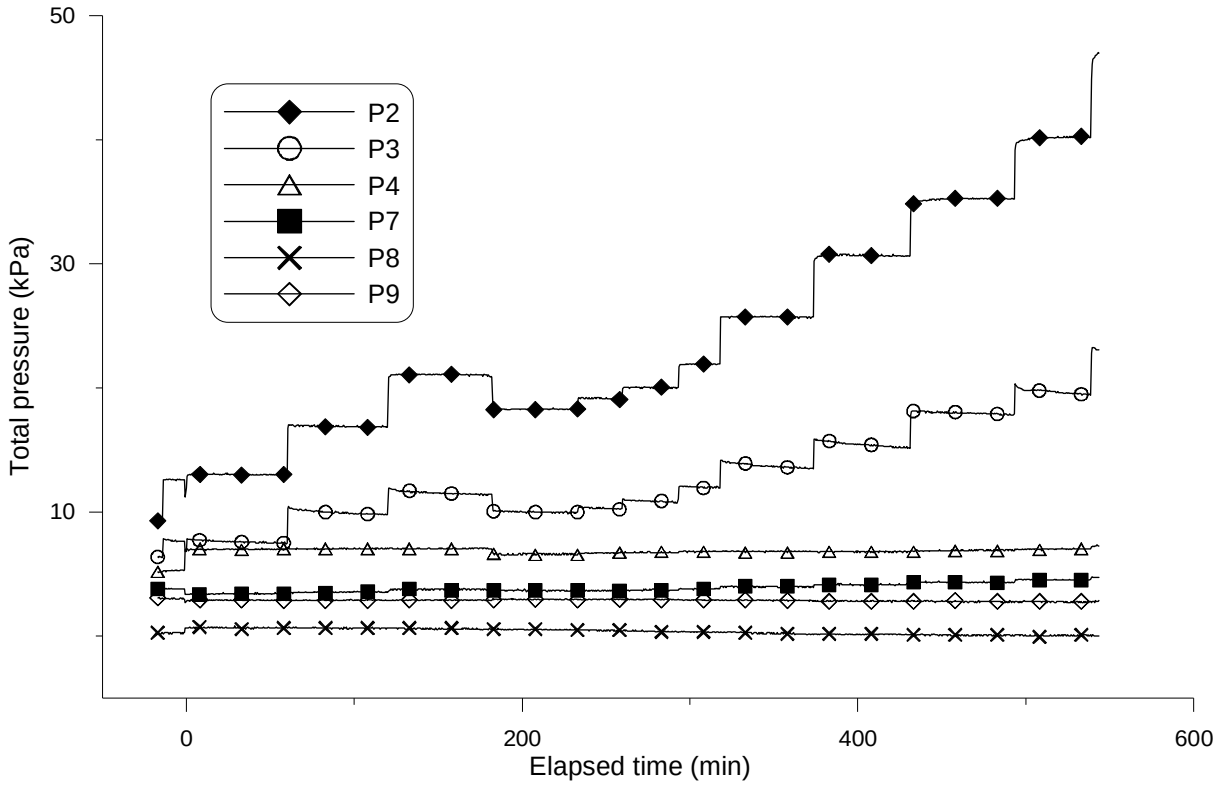

Figure 3.5 Results of test E1: total pressure changes versus elapsed time at different locations

In Figure 3.6, axial force distributions along the pile obtained at the end of each loading step in test E1 (Figure 3.1*a*) are plotted. The axial force profile corresponding to the initial state (obtained after the soil compaction) is also shown. This profile could indicate the pre-stress existing in the pile due to the effects of installation. As a partially linear decrease of the load with depth could be observed, the value of load at pile toe, where no gauges were installed, could be estimated by extrapolation from the two last measured forces at G1 (500 mm depth) and G2 (400 mm depth). The extrapolated part is shown in dashed lines. Under 100 N, the same force value (of 100 N) could be observed throughout the pile. In other words, no friction was yet mobilised at the soil/pile interface. As the load increases, the effect of mobilised friction becomes more significant; at 400 N of axial head load, about 70 % of the head load was transmitted to the pile toe. From Figure 3.6, four zones A, B, C, D could be defined to calculate the mobilised friction along the pile.

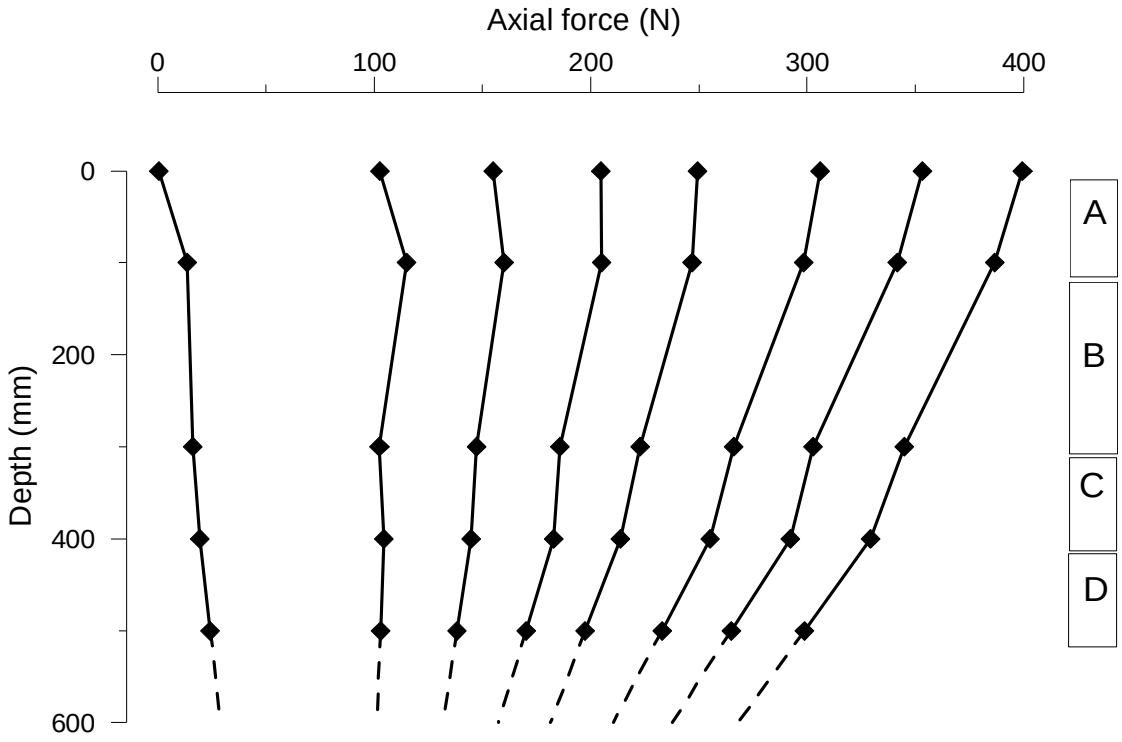

Figure 3.6 Results of test E1: axial force distribution along the pile

Figure 3.7 shows the friction mobilised along the pile versus pile head settlement for zones A, B, C and D (see Figure 3.6 for zones definition). Mobilised friction corresponds to the loss of axial load divided by the total area of the soil/pile interface at each zone. The results show that mobilised friction increased progressively with the pile head displacement during the first loading phase. When the pile was unloaded, the mobilised friction decreased and reached the initial value. By the second loading phase, it increased again. During the first loading steps this increase was much more significant but as failure approached, the slope of the curve became smaller. A sudden change in the friction values at higher depths (zones C and D) could be observed as failure was approaching.

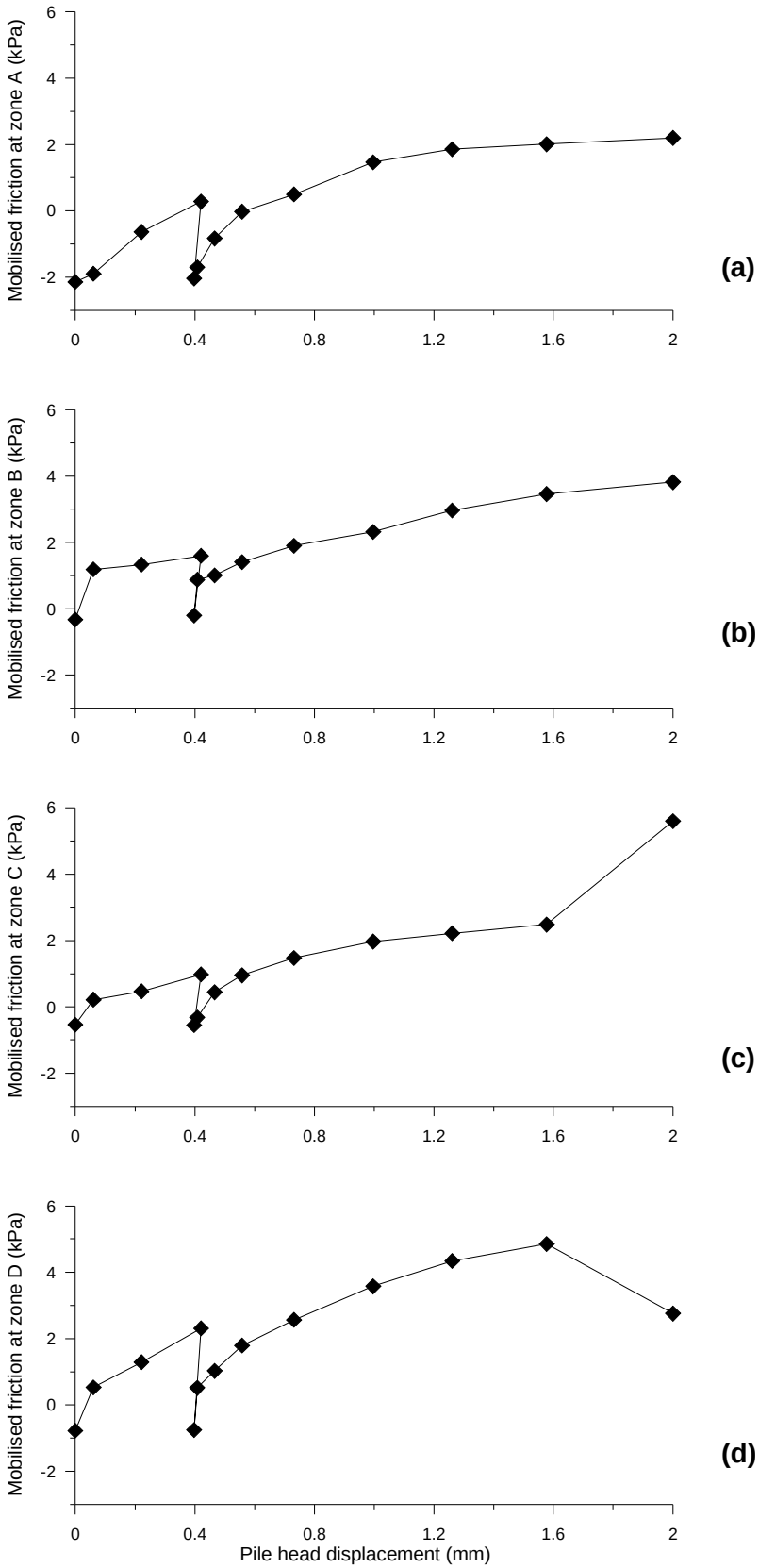

Figure 3.7 Results of test E1: mobilised friction along the pile: (a) at zone A; (b) at zone B; (c) at zone C; at zone D

3.2.2 Behaviour under thermal loading at constant axial load (tests E2 to E7)

In Figure 3.8, the temperature measured at various locations in test E2 is shown. The results obtained from the other tests were similar. Figure 3.8*a* shows the measurements of temperature along the pile. As mentioned above, T1 to T3 are the temperature sensors stuck to the pile and S1 is the one placed inside the pile. Two thermal cycles were applied as follows: a cooling phase down to 5°C was first conducted by increments of 5°C. Heating then started by the same increments up to 35°C. The minimum temperature recorded by S1 was 8°C and the maximum was 30°C. The T1 to T3 measurements, which are similar, varied from 12°C to 28°C. The temperature changes seemed to stabilise by the end of two hours during which the temperature remains unchanged. The data recorded by the other sensors distributed in the soil are presented in Figure 3.8*b* to Figure 3.8*e*. S2 was fixed to the bottom of the container while S3 was situated 100 mm below the pile toe. At these levels temperature seemed not to be influenced by the pile temperature changes. Sensors S4, S7 and S10, which were placed nearby the pile but at depths of 500 mm, 300 mm and 100 mm, show a total temperature change of about 5°C between the end of cooling and the end of the heating phases. The changes of temperature measured by the others sensors were less significant. In addition, it can be noted that the temperature changes measured at three depths and at the same distance from the pile were quite similar; S4, S7, S10 recorded the same temperatures during the test. This is also the case for the sets S5-S8-S11 and S6-S9-S12.

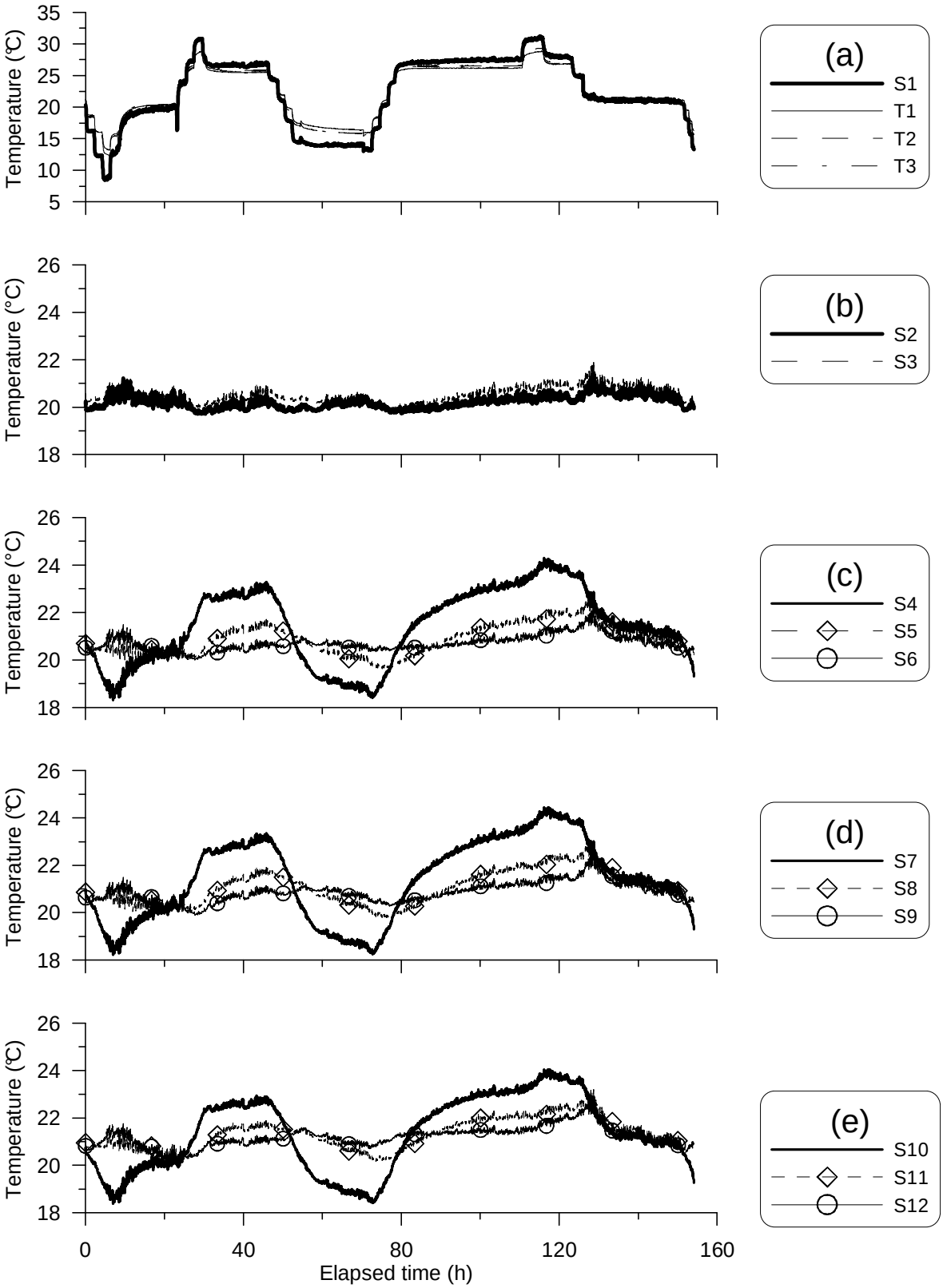

Figure 3.8 Temperature changes in test E2: (a) at the pile surface and inside the pile; (b) at the bottom of the container and 50 mm below the pile; (c) at 500 mm depth; (d) at 300 mm depth; (e) at 100 mm depth

Pile head displacement variations versus elapsed time during the thermal cycles are shown in Figure 3.9(*a, c, e, g, i, k*) for tests E2, E3, E4, E5, E6, E7, respectively. In order to achieve 'thermal settlements' in the test, once the pile displacement stabilised under mechanical loading and prior to thermal loading, displacement transducers were zeroed. In Figure 3.9*(b, d, f, h, j, l*), the results of these tests are shown in terms of pile head settlement versus pile temperature (measured by the temperature gauges stuck on the pile surface). In these figures, the pile thermal expansion curve, which expresses the deformation of a pile restrained at toe, but free in other directions under a temperature change, is also plotted for comparison purposes. The slope of this curve is then equal to α (linear expansion coefficient, $\alpha = 23\times10^{-6}$/°C for aluminium). For test E2 where the pile was not loaded axially, the results show pile head heave during heating and settlement while cooling. The relationship between pile head settlement and pile temperature is reversible and follows the pile thermal expansion curve (Figure 3.9*b*). In Figure 3.9*c* pile head displacement under a small value of load (100 N, almost 20 % of the ultimate resistance of the pile) is shown (test E3). During the first cooling phase, the pile settled. It heaved as it was subjected to heating but did not recover the settlement due to the cooling phase. Exactly the same trend could be observed in the second cycle. The cumulated settlement also could be observed in the temperature-settlement curve in Figure 3.9*d*. Larger displacements were encountered in the first cycle (especially during the first cooling). The magnitude of the settlement became smaller in the following cycle, but the trend remained similar. The slope of the first cooling phase was steeper than that of the second cooling phase. The latter was similar to the slope of the pile thermal expansion curve. The slopes of the two heating phases were similar and smaller than that of the cooling phases. The same observations could be made from the results of the other tests (E4, E5, E6, and E7).

In Figure 3.10, the interval of the pile head displacement obtained during the thermal phase (shown in Figure 3.8) is plotted together with the load-settlement curve of test E1 as a reference curve. Initial points are shown by circles and pile head displacement variation during thermal loading is shown by arrows. It is noted that the initial points can be different from the load-settlement curve due to the variation of the load-settlement curve between various tests (see Figure 3.4). For the three tests at low axial load (E2, E3, and E4), the interval of pile head settlement during thermal cycles remained smaller than 0.3 mm. For the tests at heavier axial load (E5, E6, and E7), the intervals were much larger (close to 0.6 mm).

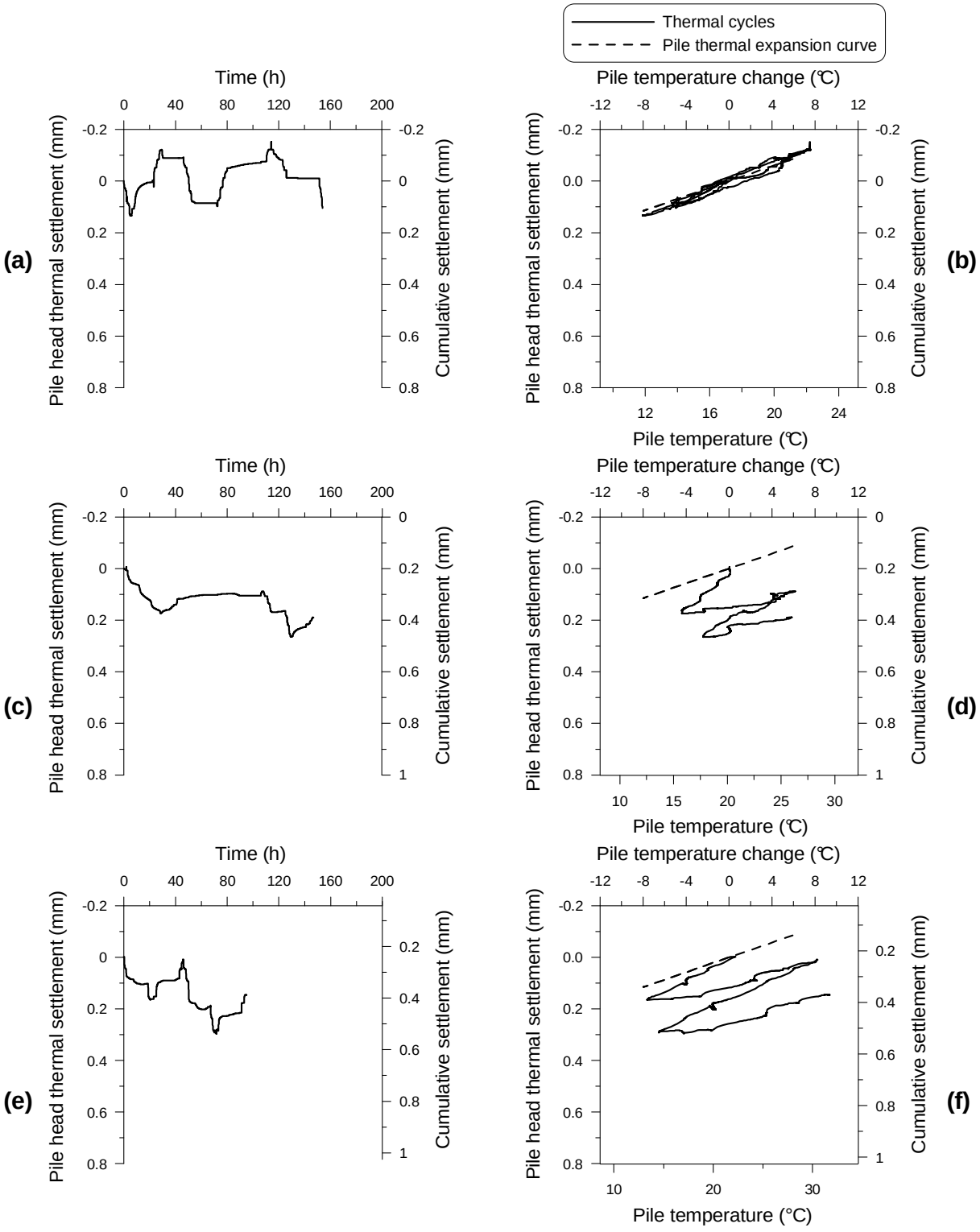
Thermal cycles
Pile thermal expansion curve
(a)
Time (h)
Pile head thermal settlement (mm)
Cumulative settlement (mm)
(b)
Pile temperature change (℃)
Pile temperature (℃)
(c)
(d)
(e)
(f)
Pile temperature (°C)

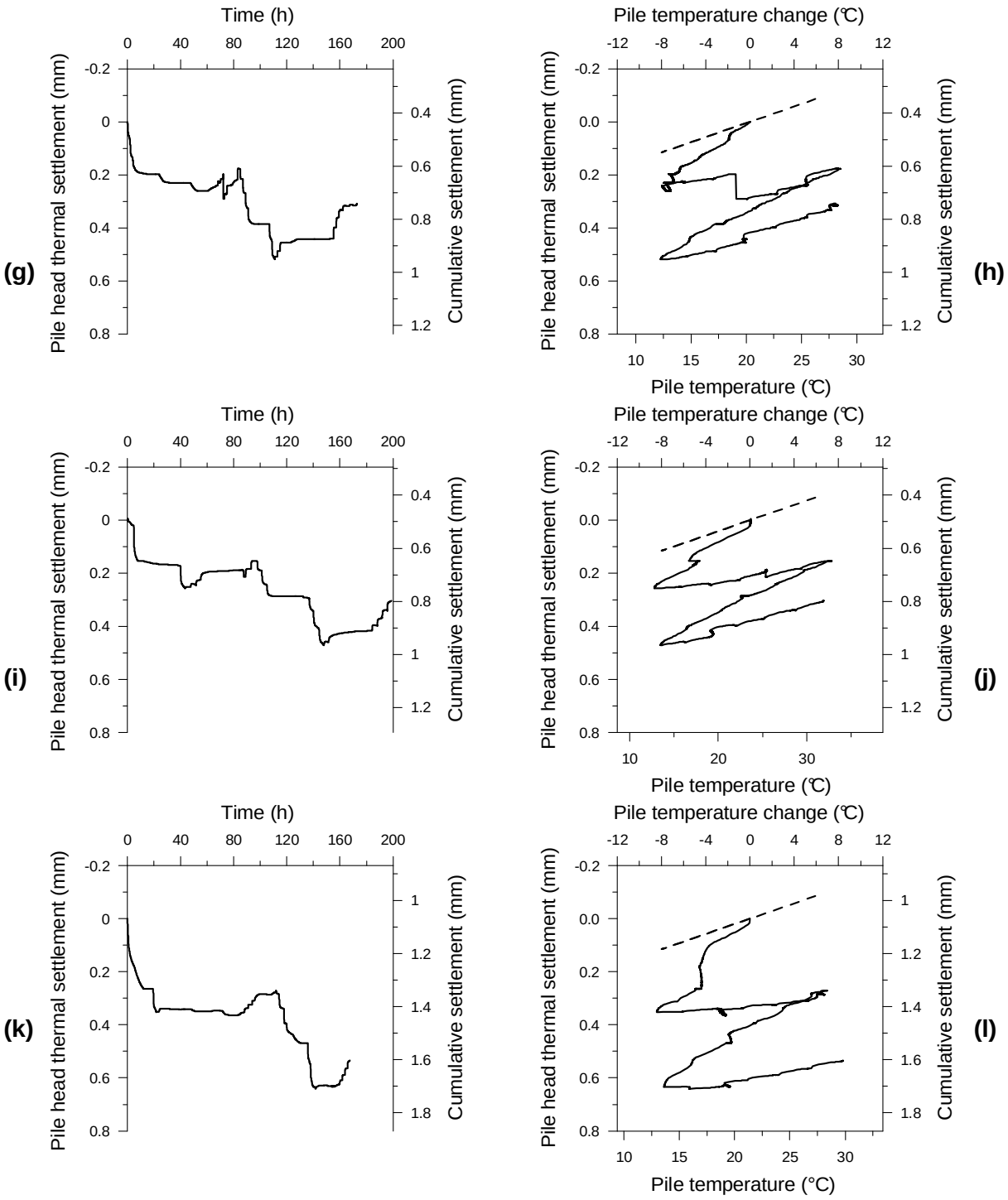

Figure 3.9 Pile thermal settlement versus elapsed time during tests: E2(a), E3(c), E4(e), E5 (g), E6(i), and E7(k); pile head settlement versus pile temperature in tests E2(b), E3(d), E4(f), E5(h), E6(j), and E7(l).

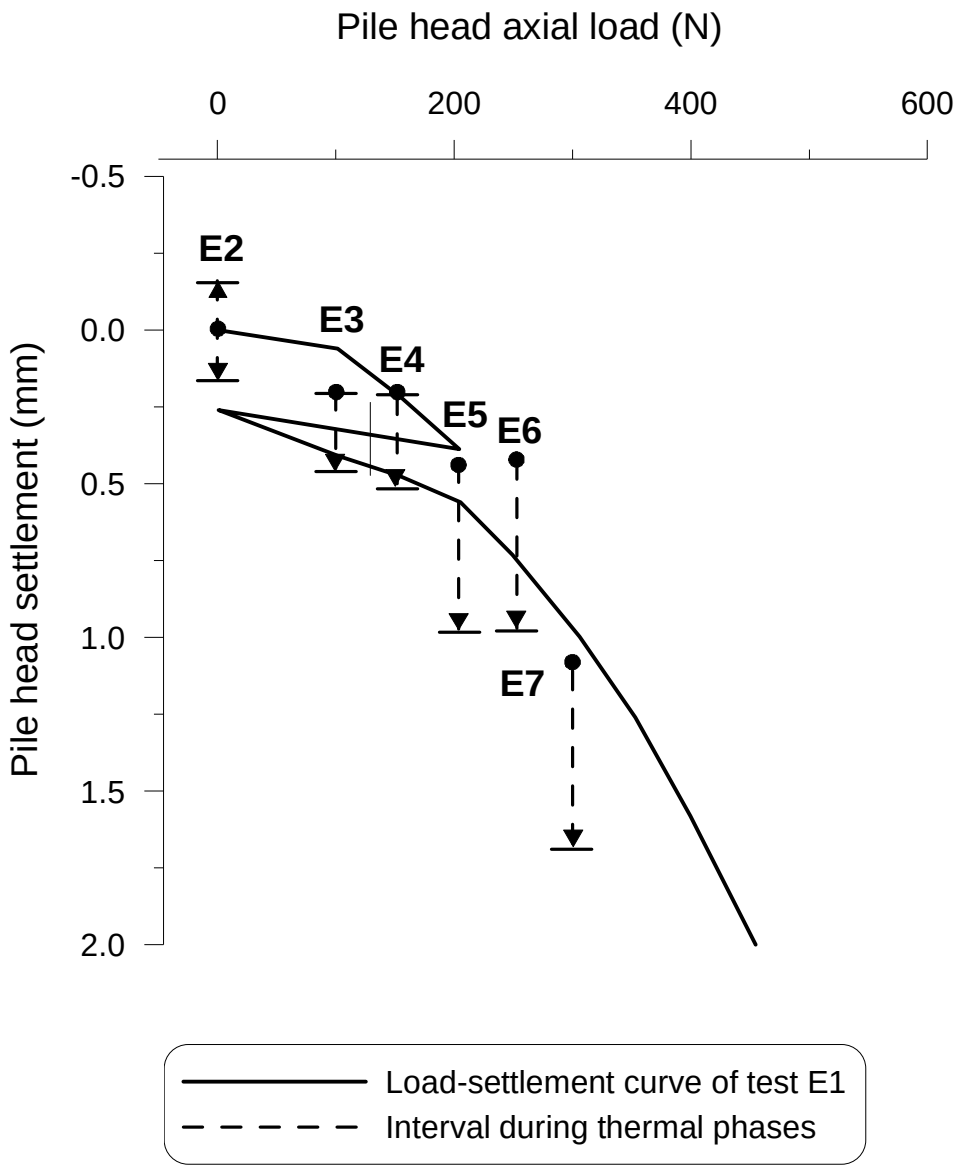

Figure 3.10 Interval of pile head settlement during thermal phase

In Figure 3.11*a*, soil pressure and pile temperature are plotted versus elapsed time for the thermal phase of test E2. For P2 and P3, the pressure decreased during the first cooling (this decrease was about 5 kPa at P2 and 1.5 kPa at P3). In the other positions (P4 to P9) which measure the soil pressure around the pile, pressure increased by cooling, decreased by heating and was slightly reduced during the period for which the temperature was maintained constant. In Figure 3.11*b*, soil pressure and pile temperature are plotted versus elapsed time in the thermal phase of test E6. For P2 (situated below the pile toe), the results show that heating increased the soil pressure and the effect of the cooling phase was not significant. For the other sensors, the effect of the heating/cooling phases was not clear but soil pressure at all levels increased slightly while cooling and decreased with subsequent heating. The same

observations can be noted from other tests with an axial load at the pile head during the thermal cycles.

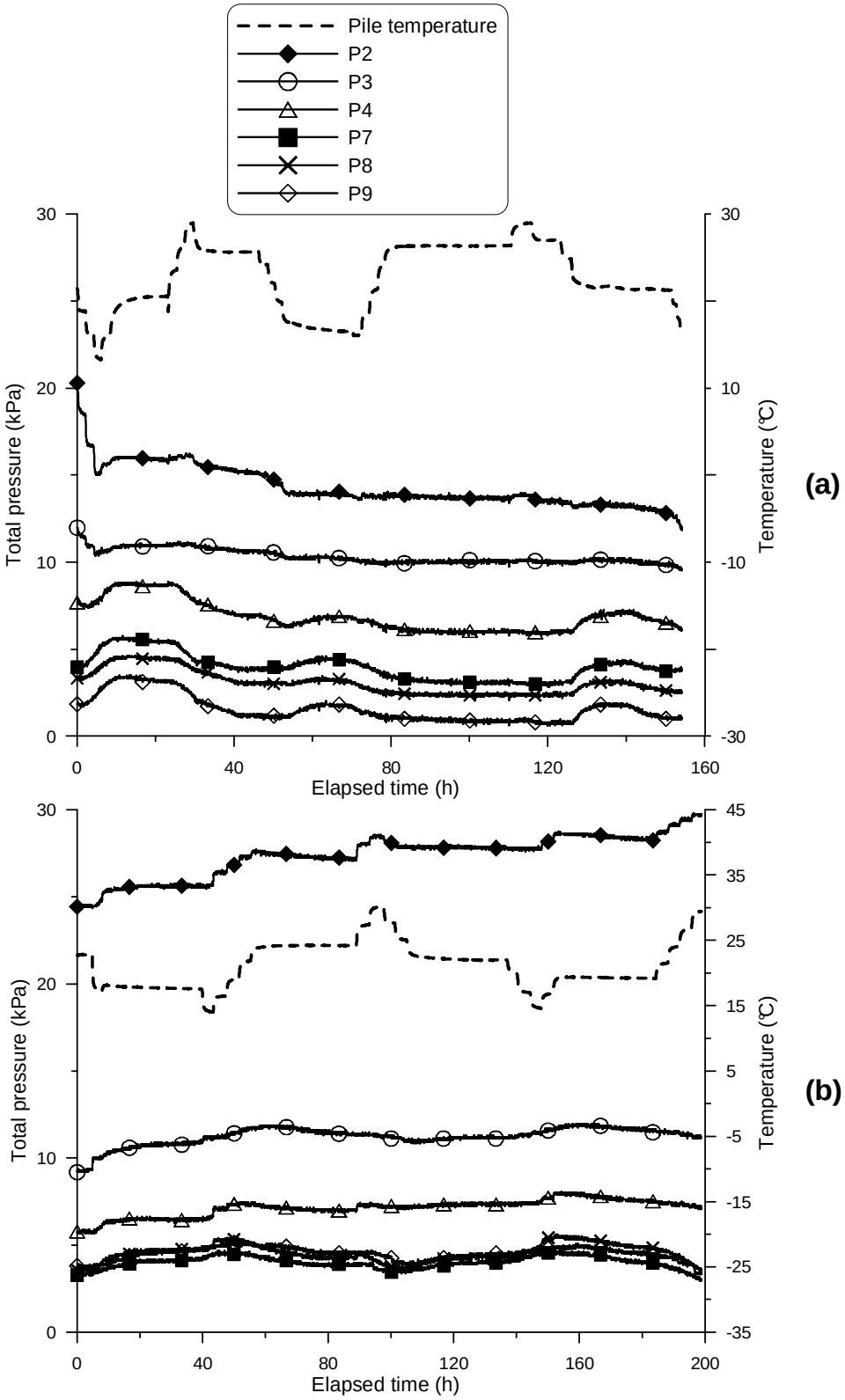

Figure 3.11 Total pressure and temperature versus elapsed time during thermal phase: (a) test E2; (b) test E6

The axial forces and pile temperature measured along the pile for test E2 during the thermal phase are shown in Figure 3.12*a*. It can be noted that cooling increased the axial force at all levels and the latter decreased during heating. In addition, significant changes in axial force were observed during some phases where the temperature was kept constant for a long time (35 h – 45 h; 55 h – 75 h; 85 h – 95 h). The results of test E6 are plotted in Figure 3.12*b*. By cooling the pile at t = 5 h, the axial forces at all levels increased. Between t = 10 h and t = 40 h the temperature was not changed but the axial forces decreased. After this period, when the pile was cooled again, the axial forces increased again. During the subsequent heating, until t = 60 h, the axial forces decreased progressively. The results of other tests were similar and two conclusions could be drawn: (i) cooling increases the axial force and heating decreases the axial force; (ii) in some cases, where the pile temperature was kept constant for a long time, significant changes in axial forces can be observed (a strong time dependency can be seen).

In Figure 3.13, the axial force profiles along the pile are plotted for all the thermo-mechanical tests. The profile mentioned as ‘mechanical’ in the figures was obtained just before that the thermal cycles started. There were four other profiles measured at the end of the cooling and heating processes. According to Figure 3.13(*a, b, c*), under lighter axial loads (0 N to 150 N, tests E2, E3, and E4), by the end of the first cooling, the axial forces along the pile were higher than those at the end of the mechanical phase. Subsequent heating decreased the axial forces. The latter were smaller than those measured initially on the mechanical profile. The same trend was visible during the second thermal cycle. In addition, for the tests E2 and E4, it seems that the pile lost all the additional axial force it has gained while cooling during subsequent heating. For the tests at heavier axial loads (200 N in test E5, 250 N in test E6, 300 N in test E7), the first cooling phase led to axial force increase along the pile, which was followed by a decrease during subsequent heating. Nevertheless, axial forces remained higher than those of the initial mechanical profile. In other words, axial forces have been accumulating progressively during the thermal cycles.

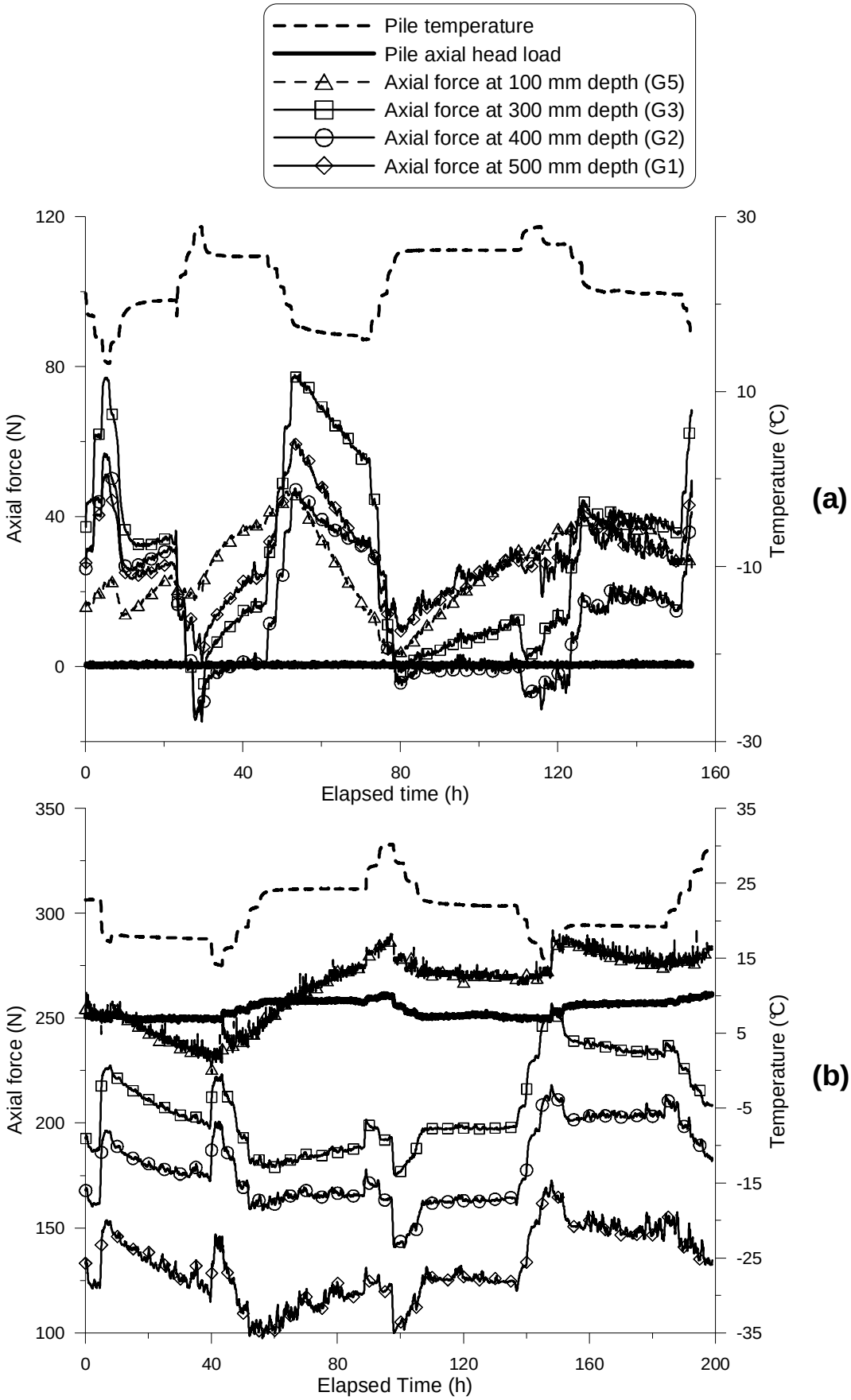

Figure 3.12 Axial forces and temperature during thermal phase: (a) test E2; (b) test E6

On the basis of obtained pile axial forces, the curves of mobilised friction versus pile head displacement during thermal phases were plotted. The results of tests E2 and E6 are represented in Figure 3.14. As can be seen in Figure 3.14*a* to Figure 3.14*d* (test E2), the curves obtained in successive cooling and heating phases form a loop, which is compatible with the axial load profiles shown in Figure 3.13*a*. The same reversibility was observed in Figure 3.9*b*, where the thermal displacements were plotted versus pile temperature. The thermo-elastic behaviour of the pile under nil axial load could also be seen in mobilised friction curves. Conversely, no visible regularity was noted in the results of test E6, where the axial head load was 250 N (Figure 3.14*e*-*h*). Only at zone B (Figure 3.14*f*) a clear tendency could be observed: mobilised friction decreased by cooling and increased by heating. Obviously mobilised friction was sensitive to the pile temperature and changed with thermal cycles.

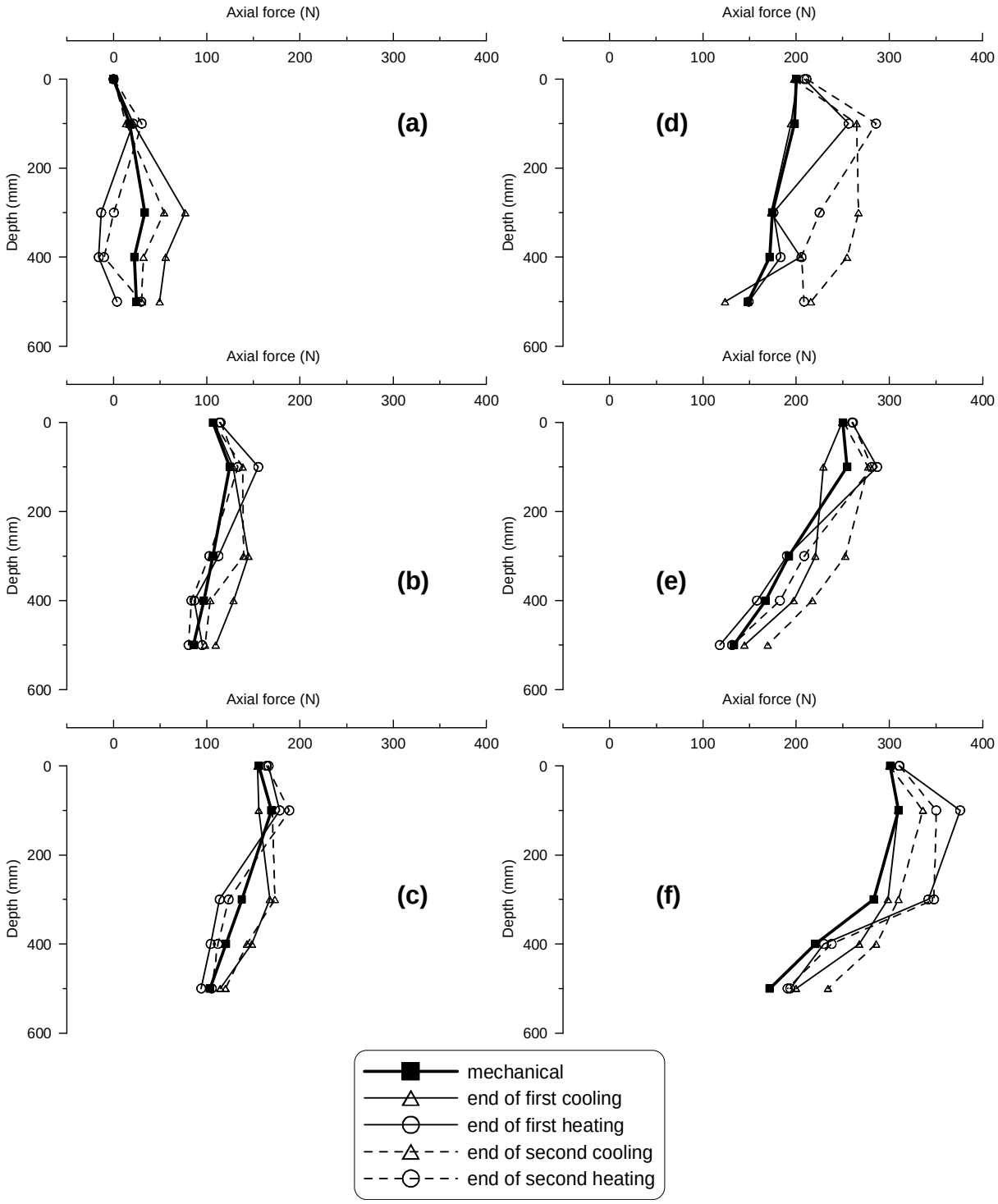

Figure 3.13 Axial force distribution along the pile (a) in test E2 (b) in test E3 (c) in test E4 (d) in test E5 (e) in test E6 (f) in test E7

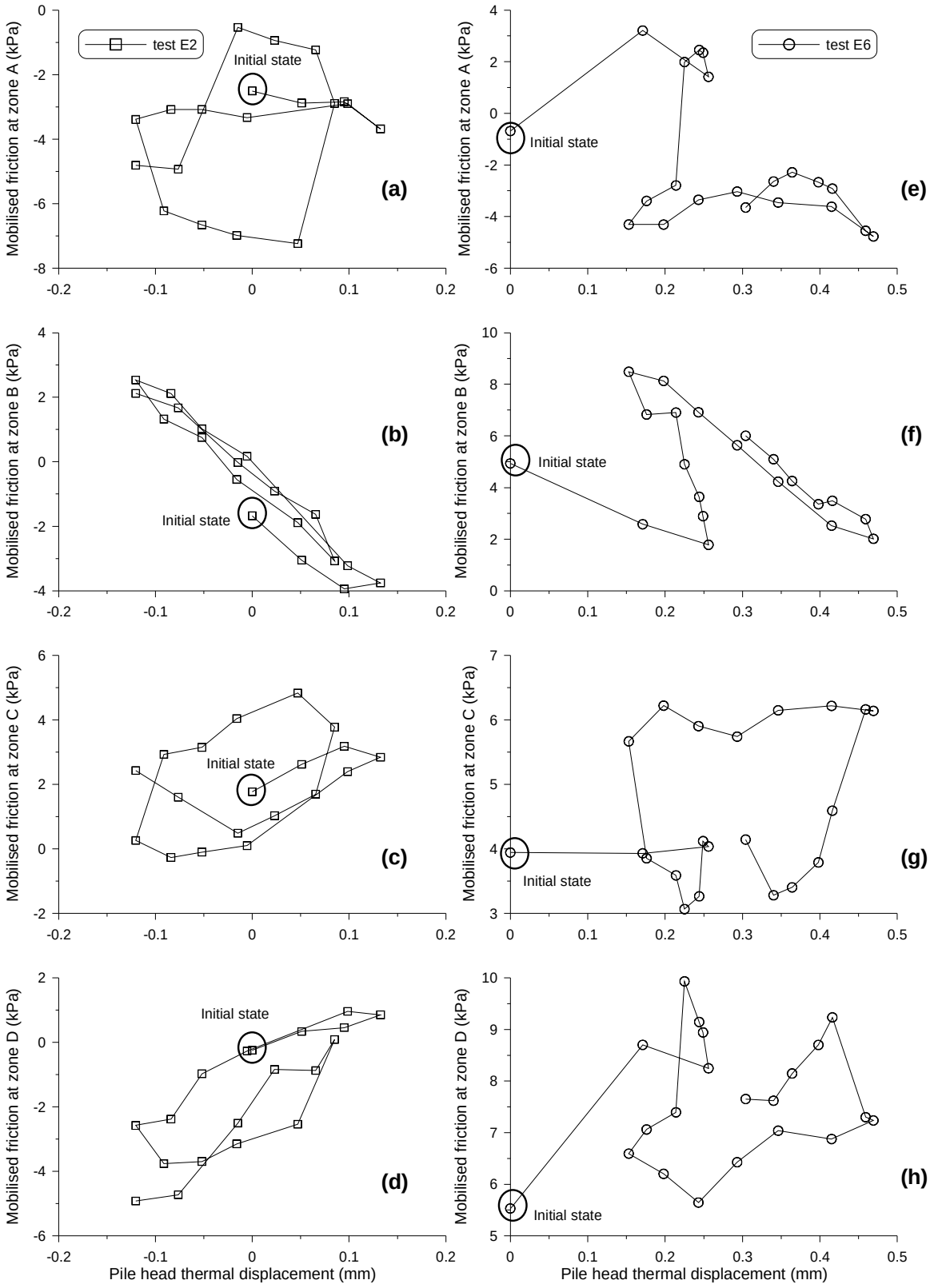

Figure 3.14 Mobilised friction along the pile during thermal phase: (a, b, c, d) test E2; (e, f, g, h) test E6

3.2.3 Behaviour under 30 thermal cycles (test E8)

In test E8, similar to test E4, the pile was loaded to 150 N and subjected to two thermal cycles between 5°C and 35°C. The two first thermal cycles were performed by increments of 5°C. The pile was then subjected to 28 additional cooling/heating cycles. During these cycles, pile was subjected only to the extreme values (5°C and 35°C), with no intermediate steps. Pile temperature measured at three positions (transducers T1, T2 and T3) is shown in Figure 3.15. As could be seen, pile temperature varied between 12°C and 33°C. Temperature values measured by the three transducers are almost superposed.

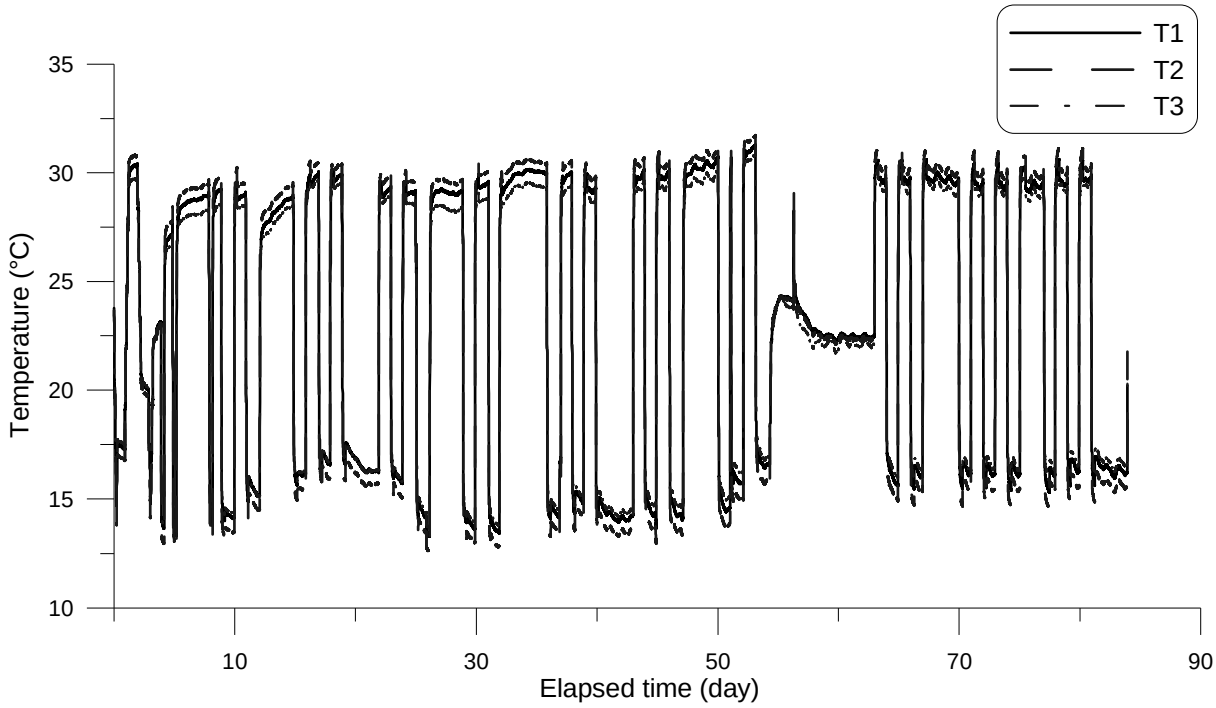

Figure 3.15 Temperature changes in test E8 at the pile surface and inside the pile

Pile thermal settlement versus time is plotted in Figure 3.16*a*. The pile settled with a higher rate during the first cycles while the rate relaxed afterwards. Figure 3.16*b* shows the pile thermal settlement as a function of its temperature. The pile settled when it was cooled and heaved during the subsequent heating. By the end of the thirteenth cycle, pile settlement reached 3 mm. In the same figure, the pile thermal expansion curve is also plotted. The slope of the pile settlement curve approached that of the pile thermal expansion curve, as thermal cycles proceeded.

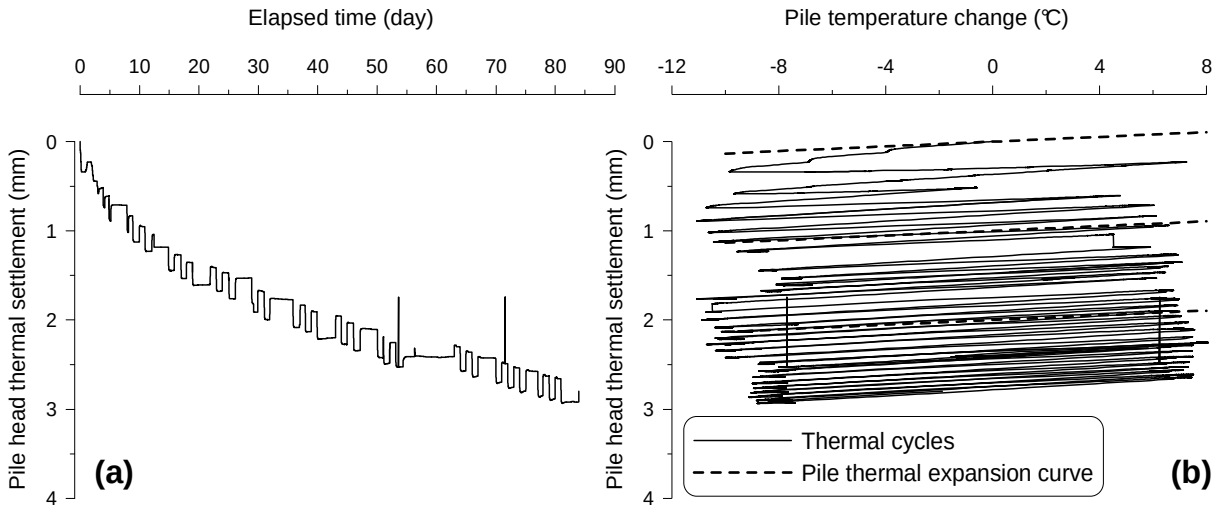

Figure 3.16 Results of test E8: (a) pile thermal settlement versus elapsed time; (b) pile head settlement versus pile temperature

Figure 3.17 shows total pressure changes during thermal cycles. Total pressure measured at positions P4 to P9 at the vicinity of the pile showed slight variation with time. Initial pressure values at P2 and P3 were about twice the predicted value (γz and $K_0 \gamma$z respectively). The pressure measured below the pile toe (at P2 and P3) increased during the first two cycles; the increasing trend continued with a less significant rate. By the end of the last thermal cycle, the pressure measured at the aforementioned positions was almost 1.5 times the initial pressure. At other positions, there existed some small fluctuations in measured values when the pile was heated or cooled, but as a general trend it could be concluded that thermal cycles did not impose significant changes to soil total pressure at the considered positions.

Variation of axial force measured by each gauge during successive cycles is plotted in Figure 3.18. Strain gauges responded immediately to temperature changes, however their measurements did not stabilise once temperature stopped to change (for example between t = 1300 h and t = 1500 h, pile temperature was constant and equal to 23°C while axial force changed). Cooling increased compressive forces while heating led to axial force decrease. Axial force distribution in the pile is depicted in Figure 3.19. Similar to Figure 3.13, the profile obtained at ambient temperature and under 150 N of axial load was referred to as the 'mechanical' one. By the first cooling, compressive forces in the pile increased; the lower half of the pile was more affected. The subsequent heating led to a decrease in compressive forces. The profiles obtained at the end of the last cooling and heating phases are shown in the same plot. As could be observed, higher compressive forces were generated in the pile at this stage comparing to the first cycle, while the effect of cooling was more pronounced.

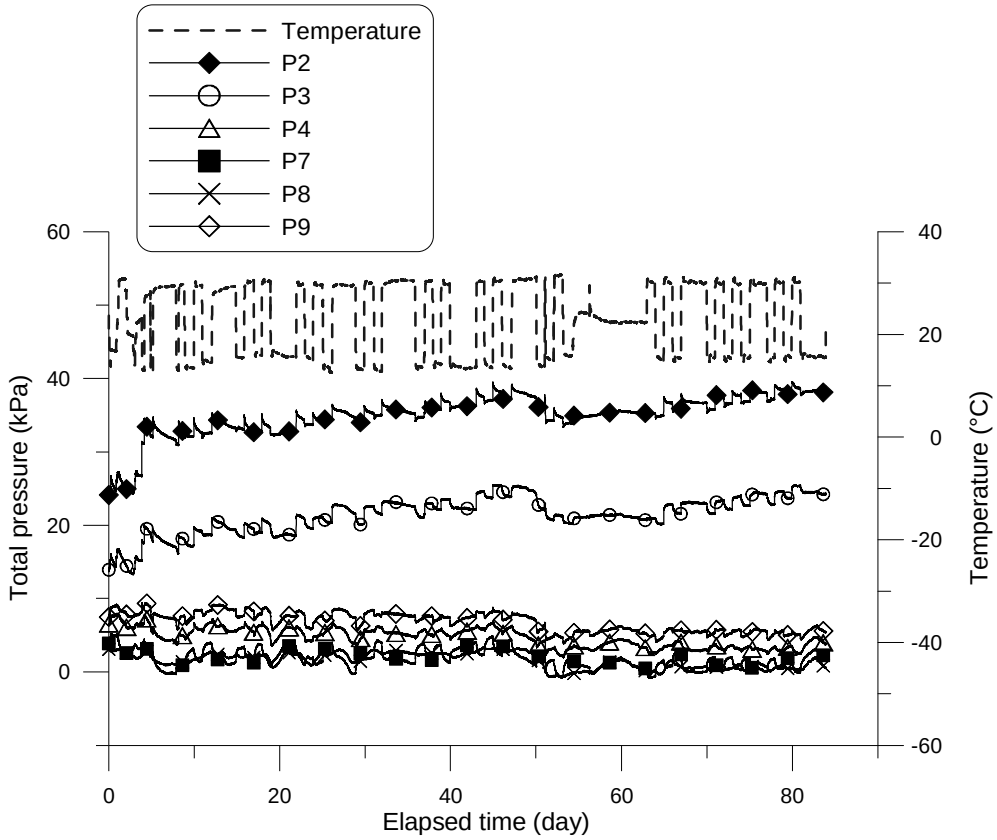

Figure 3.17 Total pressure and temperature versus elapsed time during thermal phase of test E8

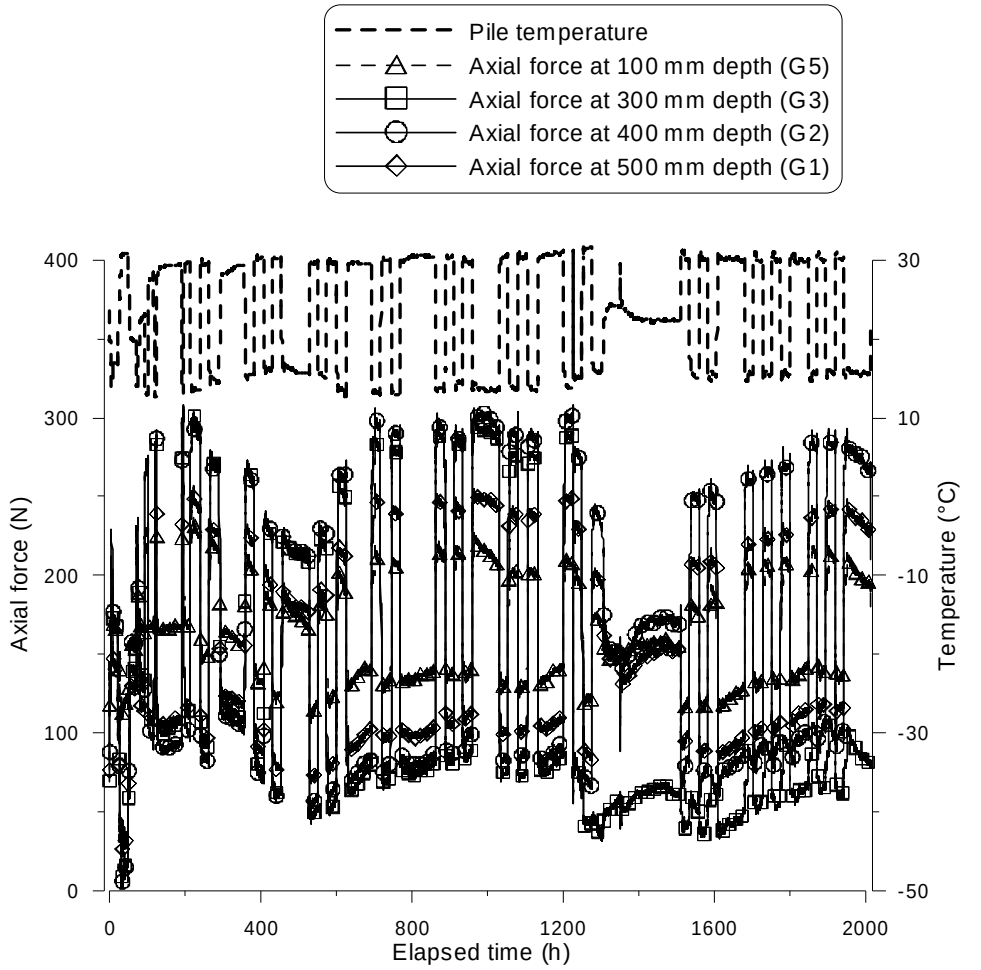

Figure 3.18 Axial forces and temperature during thermal phase in test E8

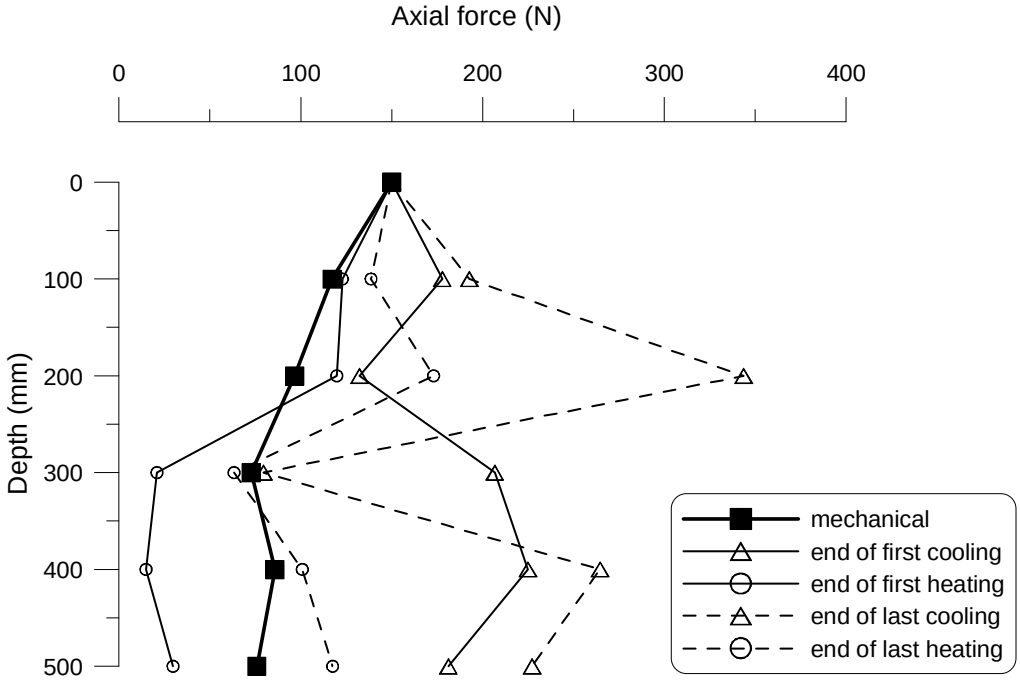

Figure 3.19 Axial force distribution along the pile in test E8

3.3 Experimental results on the model pile in saturated clay

In the last part of the experiments, the pile was surrounded by clay and loaded mechanically and thermo-mechanically. The pressure transducers and the strain gauges seem to have been damaged during the compaction and saturation procedures and no data was obtained in terms of total stress in the soil and axial force in the pile. The experimental results consist in pile displacement and soil and pile temperature.

3.3.1 Behaviour under mechanical axial loading (tests F1 & F2)

Figure 3.20 through Figure 3.23 show the response of the pile to purely mechanical loading. Two tests were performed by loading the pile axially up to failure. Load was increased by increments of 50 N, while each increment was maintained for 1 hour. Loading procedure in test F1 could be detected in Figure 3.20*a*. Pile settlement in test F1 could be followed in Figure 3.20*b*. Pile settlement became sensible after 400 N and reached 2 mm (which is equal to 10% of pile diameter and corresponds to the conventional pile displacement at failure) under 537 N. Ultimate load could be then estimated equal to 537 N.

Effect of time on pile response to loading increments could be detected in Figure 3.21. Under lighter load values, pile settlement stabilised within one hour. More visible creep effect can be detected under heavier loads. Similar to the case of sand (Figure 3.2), there exists an exponential relationship between pile displacement and time under a constant load value, while time effects are more pronounced in the case of clay, such that the value of α_n (defined according to Equation 3.1) increases continuously and reaches 0.3 under 500 N (93% of the ultimate load) in Figure 3.22. According to AFNOR (1999) in order to compute the creep load (Q_C), the linear parts of the beginning and the end of the curve are extended to an intersection, the bisector of the angle between them intersects the curve at the point Q_C. The creep load was equal to 430 N.

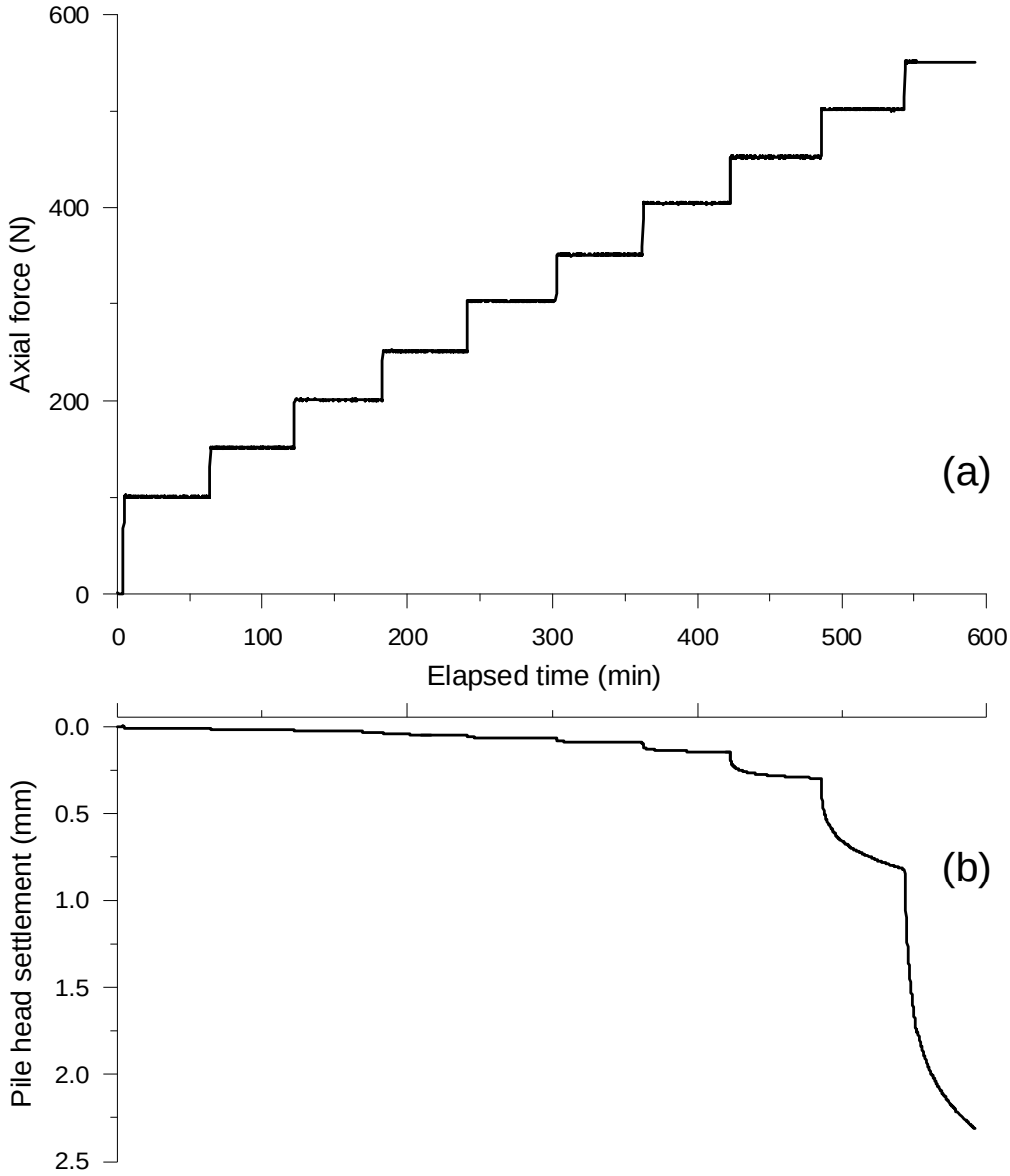

Figure 3.20 Results of test F1: (a) pile head axial load (b) pile head displacement

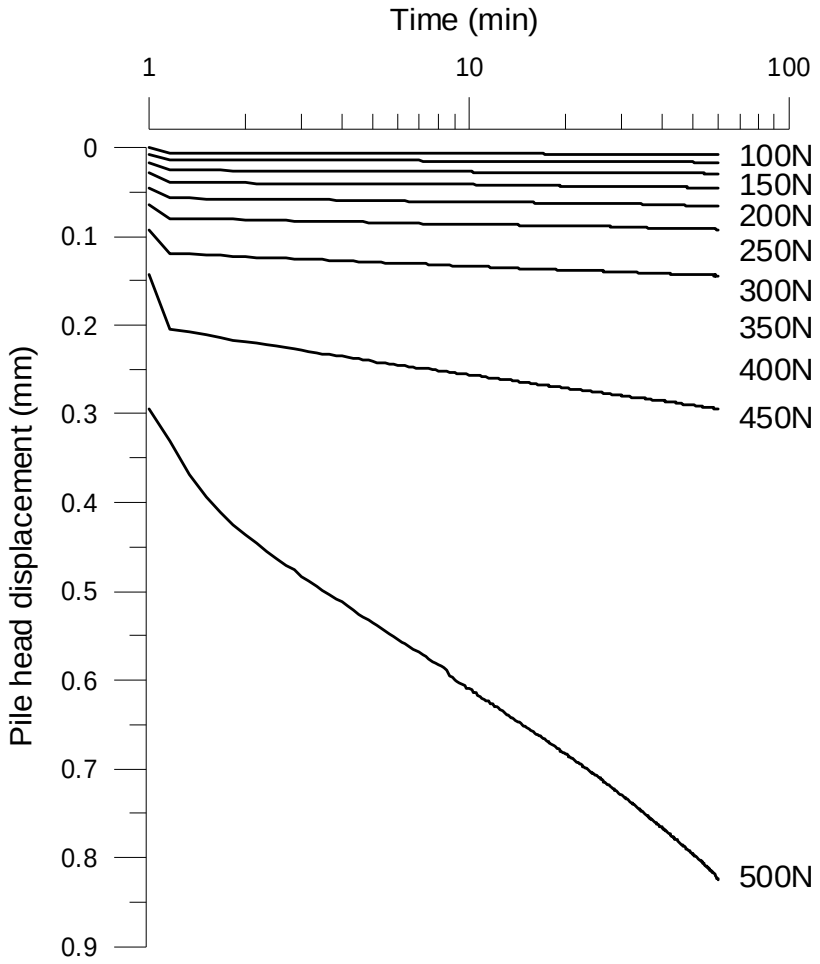

Figure 3.21 Pile settlement time dependency in test F1

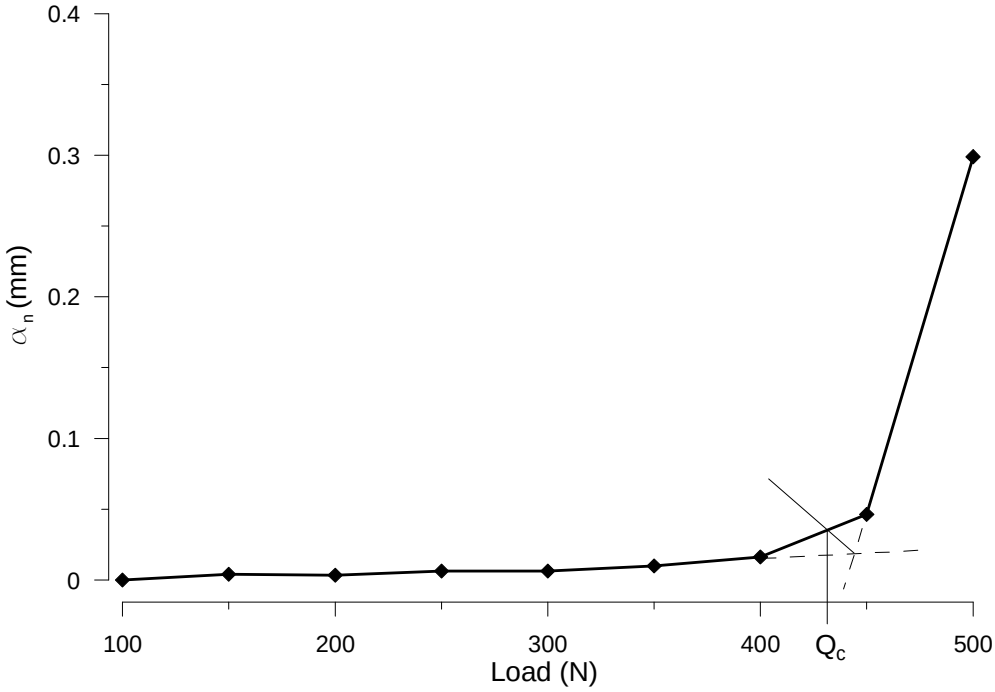

Figure 3.22 Variation of α_n by load in test F1

Pile load-settlement curves obtained in tests F1 and F2 are depicted in Figure 3.23. Because of some technical problems, test F2 was stopped before that failure occurred. The repeatability of the mechanical tests could be confirmed by the good coherence between the two curves. The value of the ultimate load in the two tests was the same and equal to 537 N.

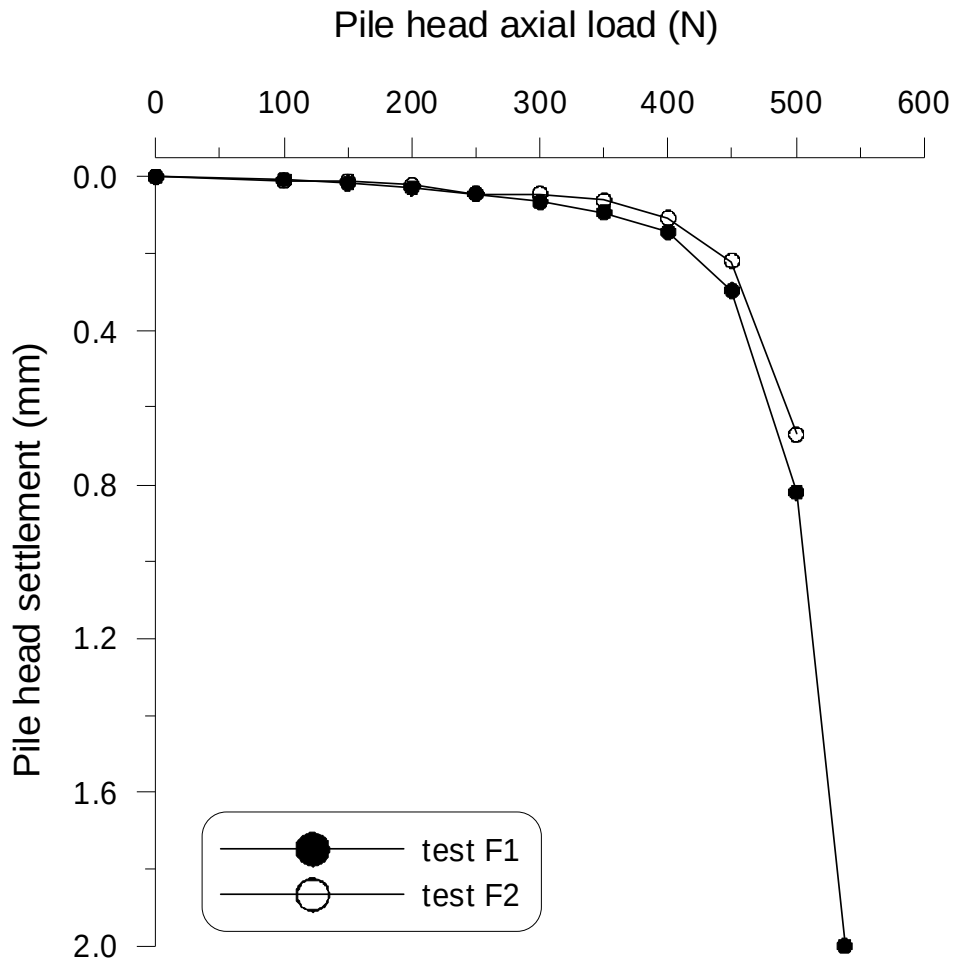

Figure 3.23 Load-settlement curves obtained via tests F1 & F2

3.3.2 Behaviour under thermal loading (tests F3 to F7)

According to the thermo-mechanical loading procedure described in section 2.4.3.2, five tests were performed under a constant load value and one thermal cycle. The experimental results of this family of tests could be observed in Figure 3.24 to Figure 3.26. In each test, the pile was loaded axially. After two hours the circulating bath started to work at 35°C and the pile was heated for two hours. In order to cool the pile, bath temperature was set first to 20°C and then to 5°C during the next four hours. The thermal cycle was completed by heating the pile back to ambient temperature, which is about 20°C. The pile was unloaded at this stage while pile temperature was kept constant by keeping the bath working at 20°C during the next

14 hours, before the following test could start. Pile temperature change recorded by transducers T1, T2 and T3 and temperature sensor S1 during the whole procedure mentioned above is shown in Figure 3.24*a*. Temperature values detected by S1 varied between 10°C and 32°C. Maximum and minimum values recorded by the transducers on the pile's surface were 14°C and 26°C. Temperature changes in the soil at different positions could be seen in Figure 3.24*b-e*. There existed some fluctuations in temperature measurements at these positions, however temperature values measured by S2 and S3 (below the pile toe) did not seem to be dependent on pile's temperature and are almost 20°C throughout the test. The same statement could be made on temperature measurements at S5, S6, S8, S9 and S11, which were located at distances higher than 100 mm from the pile's surface. Closer to the pile, at S4, S7 and S10, the temperature was less stable and changed as the pile's temperature varied, such that the highest and lowest measured temperature values recorded were 18.5°C and 23°C.

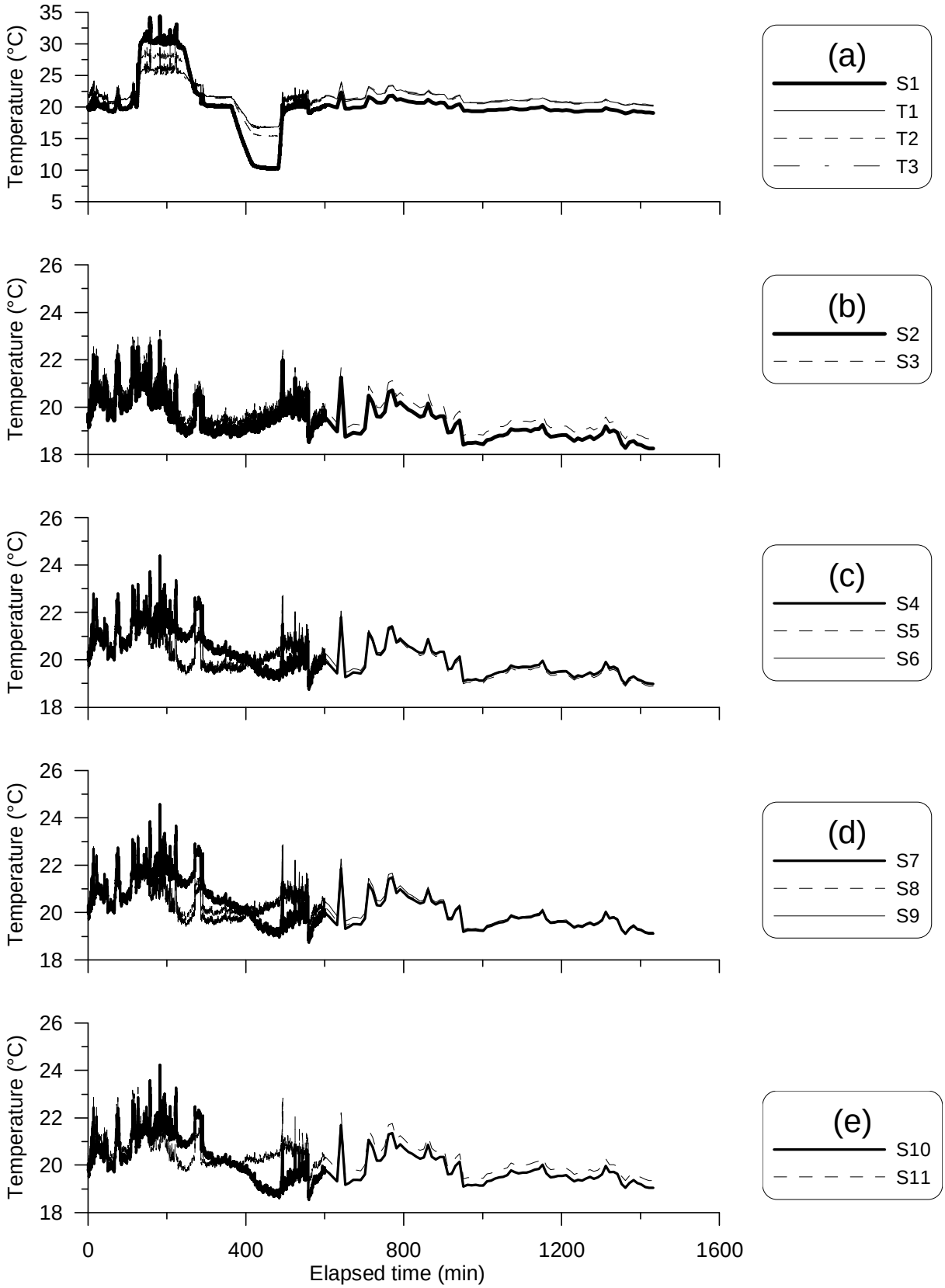

Figure 3.24 Temperature changes in test F3: (a) at the pile surface and inside the pile; (b) at the bottom of the container and 50 mm below the pile; (c) at 500 mm depth; (d) at 300 mm depth; (e) at 100 mm depth

Pile head total settlement in tests F3 through F7 could be seen in Figure 3.25(*a, c, e, g, i*). As could be observed, the pile settled under the mechanical load in the first two hours (120 min) of the test. The settlement was greater in the pile under a heavier load (comparing Figure 3.25*i* to Figure 3.25*a*, for example). The pile began to heave while heated from 20°C to 35°C. It settled during the subsequent cooling down to 5°C and heaved again during the last heating (back to 20°C). A distinct step could be detected at t = 600 min, when the pile was unloaded; except in test F4 (Figure 3.25*c*). Pile displacement continued at a smaller rate afterwards. In tests F3, F4 and F5, pile final settlement was almost zero; which indicates that the pile had returned to its initial position within the 14 hours after having been unloaded. This value was higher in tests F6 and F7 where pile was loaded by a heavier mechanical load.

Pile head settlement versus temperature during a complete thermal cycle (between t = 120 min and t = 600 min in Figure 3.25*a, c, e, g* and *i*) is exhibited in Figure 3.25*b, d, f, h*, and *j*, respectively. The pile thermal expansion curve is also plotted. Its slope is equal to α. The pile reacted immediately to temperature change and heaved with the first heating; however its displacement was naturally less than that of a free pile. It settled when it was cooled. The slope of the cooling branch of the pile thermal settlement curve was steeper than that observed during heating. Pile underwent a more significant settlement when cooled under heavier loads (comparing Figure 3.25*i* to Figure 3.25*a*, for example). The pile heaved in the next heating phase; the slopes of the two heating branches were almost equal. Under 100 N, 150 N and 200N, the pile behaviour was almost thermo-elastic (Figure 3.25*b*, Figure 3.25*d* and Figure 3.25*f*); the pile displacement at the end of the thermal cycles was not exactly zero but it was very small. Under 250 N and 300 N (Figure 3.25*h* and Figure 3.25*j*), more significant irreversible deformation could be detected once thermal cycles were stopped.

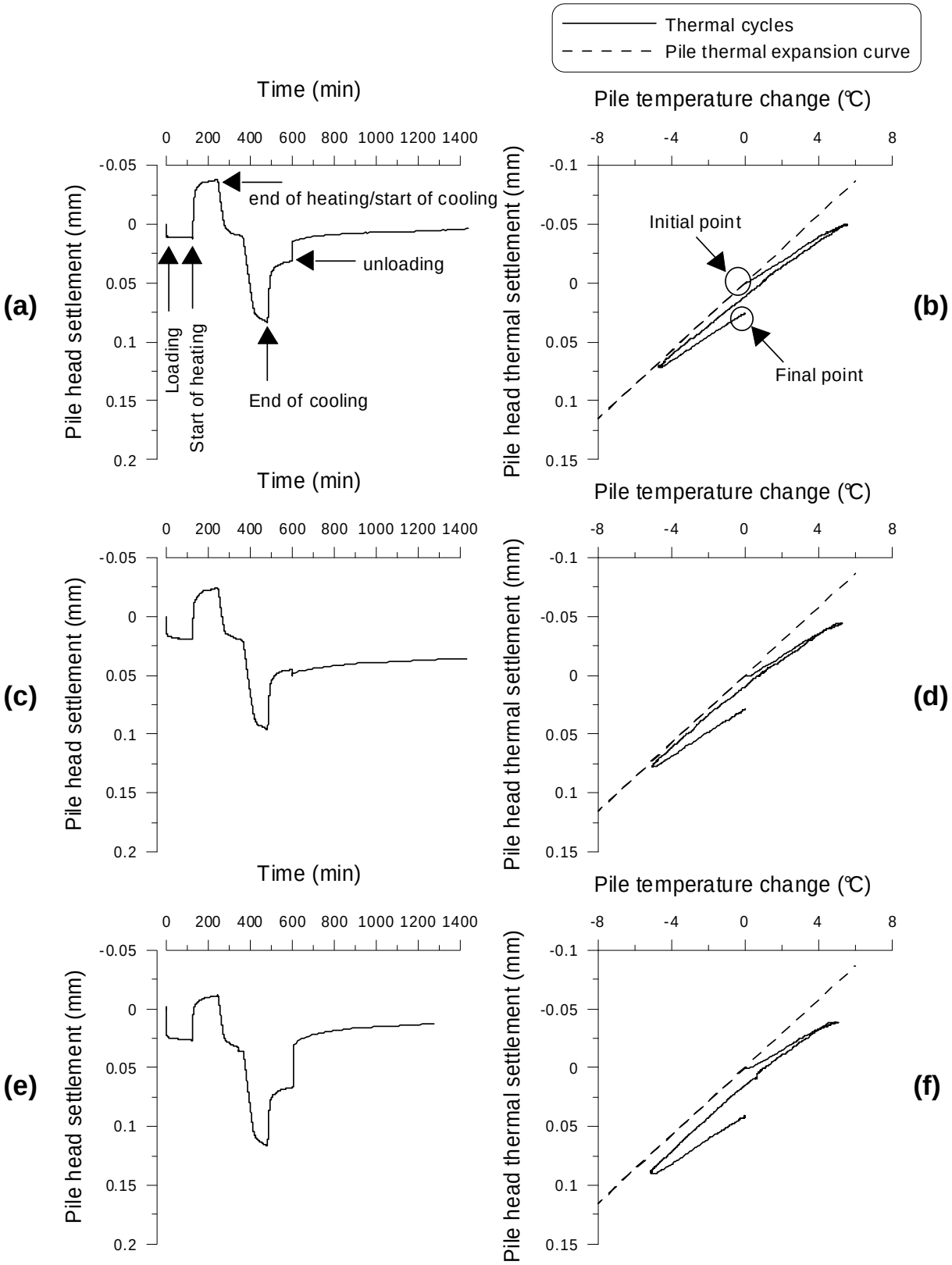
Thermal cycles
Pile thermal expansion curve
Time (min)
Pile head settlement (mm)
Pile temperature change (°C)
Pile head thermal settlement (mm)
end of heating/start of cooling
unloading
Loading
Start of heating
End of cooling
Initial point
Final point
(a)
(b)
(c)
(d)
(e)
(f)

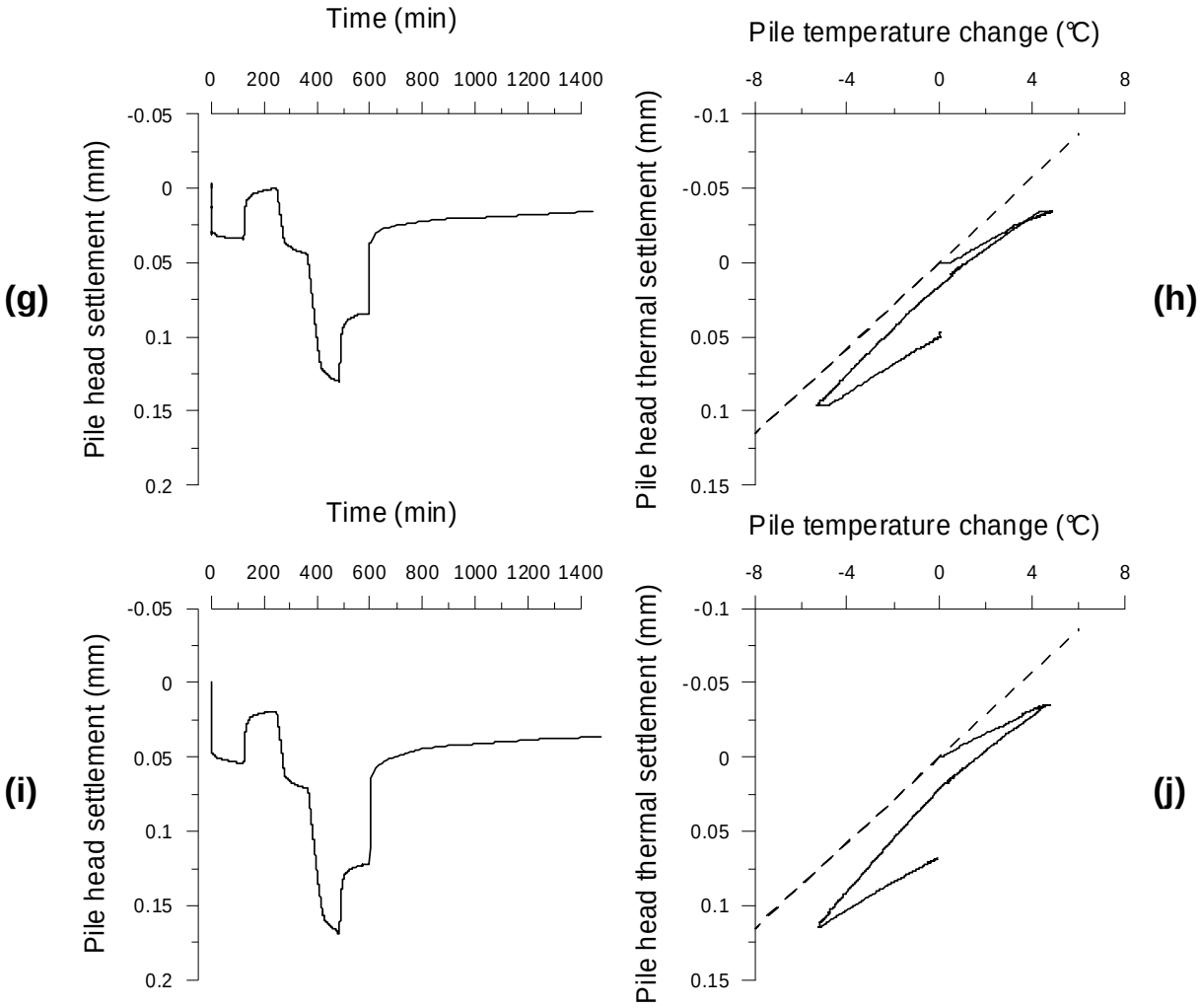

Figure 3.25 Pile total settlement versus elapsed time during tests: F3(a), F4(c), F5(e), F6(g), F7(i); pile head thermal settlement versus pile temperature in tests F3(b), F4(d), F5(f), F6(h), F7(j)

Maximum and minimum values of pile settlement under the thermo-mechanical loading could be detected in Figure 3.25. The evolution of the load-settlement curve obtained under purely mechanical loading, within the thermal cycle could be plotted on the basis of these values, as in Figure 3.26. The points obtained in the mechanical loading phase in each test correspond to the pile head displacement at t = 120 min in Figure 3.25*a*-*i* (shown as 'initial point' in Figure 3.25*a*) and are shown by circles in Figure 3.26. The evolution of each point is shown by dashed lines. Pile displacement after one complete cycle, which was referred as 'final point' in Figure 3.25, is shown by triangles in Figure 3.26. Once again, it could be observed that under rather light loads, the pile underwent more heave by heating. More settlement was expected under heavier loads. The ratio of the 'final' value to the maximum absolute value observed during the test (extremities of the dashed lines) at each load increment is computed and the result is exhibited in Figure 3.27. A linear increase in the ratio with the pile load could be detected. It could be deduced that under 100 N (0.19×Q_{max}), 37%

of the pile displacement within one thermal cycle was irreversible, while under 300 N ($0.56 \times Q_{max}$), only 37% of the pile displacement was reversible.

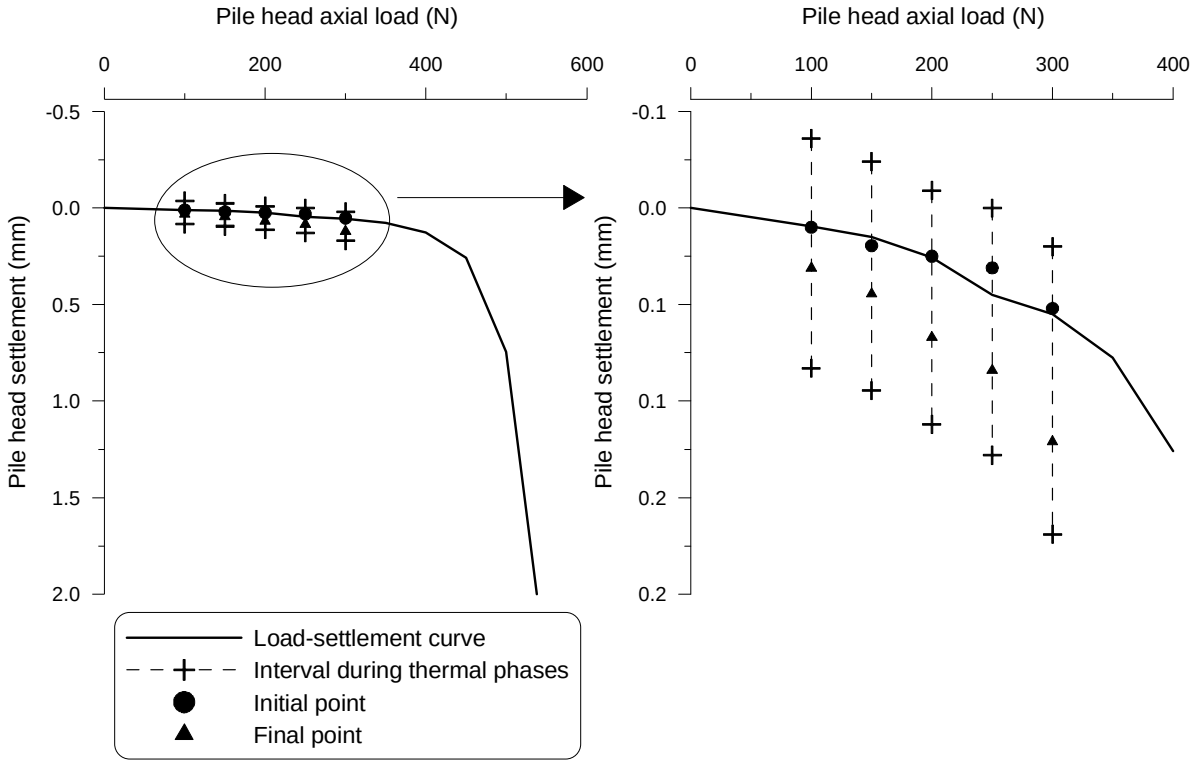

Figure 3.26 Interval of pile head settlement during thermal phase

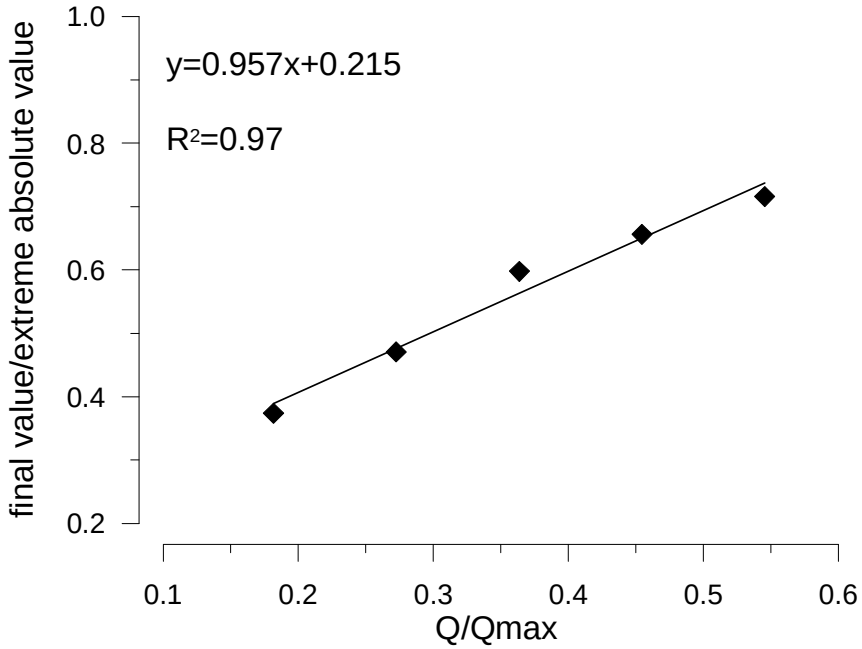

Figure 3.27 Comparison of the final displacement value to the maximum absolute displacement value (according to Figure 3.26)

3.4 Discussion

In physical modelling and when sands are studied, the soil specimen is usually prepared by pluviation. This method is applied in calibration chambers in order to achieve the best homogeneity (Baudouin, 2010; Choi *et al*., 2010; Dupla *et al*. 2008; Le Kouby, 2003). In the present experimental work, considering the dimensions of the frame (see Figure 2.1), which accommodated the totality of the system components, it was not possible to use a pluviation method to prepare the soil sample. By the way, good repeatability of the load-settlement curves was found (Figure 3.1) confirming that controlling dry density by layer was good enough.

As mentioned in some previous studies (Jardine *et al*., 2009; Zhu *et al*., 2009; Talesnick, 2012), utilising pressure transducers in sand could not always lead to satisfactory measurements. The tiny fragile structure of the total pressure transducers makes set up difficult while pouring sand on the existing layer to compact the next layer. This explains why in the present study among the ten pressure transducers only six have operated throughout the test. In both the mechanical and thermo-mechanical phases, P2 and P3 were the most affected ones. Actually, considering the position of P2 and P3 (both 50 mm below the pile toe, one oriented vertically and the other oriented horizontally), one could conclude that a large part of the head load was transmitted to its toe. This statement could be confirmed via the axial force profiles of test E1 (Figure 3.5), where the axial force at pile toe represents more than 70 % of the axial head load.

The thermo-mechanical tests on sand showed that only under nil axial load a perfectly thermo-elastic behaviour could be noted (Figure 3.8). The heavier was the load applied at the pile head, the more irreversible settlement was observed. That led to the accumulation of pile settlement, which continued as thermal cycles proceeded as seen in test E8. When the pile was subjected to numerous thermal cycles, it settled at a rather high rate during the first cycles. The rate decreased during the following cycles but did not stabilise within 30 cycles. Although the cyclic loading in the performed tests was of thermal nature, it could be comparable to mechanical cyclic loading tests reported in many studies on model piles (Tali, 2011; Benzaria *et al*., 2013). According to Benzaria *et al*. (2013), cyclic loading reduces the side friction between the pile and the sand and permanent displacements are observed at pile head. In the present study, significant thermally-induced displacement at pile toe led to progressive compaction of the sand and as the cycles continued, side friction loss was compensated by end bearing mobilisation. It could be then concluded that settlement rate

should decrease after some cycles, as it is the case in the results of test E8. Continuous settlement is also compatible with the trend observed in soil pressure measurements at P2 and P3 (50 mm below the pile toe) in Figure 3.10 and Figure 3.17. The vertical pressure increased at these points, especially during heating, which confirms the restrained longitudinal expansion of the pile at its toe. Other pressure transducers, installed close to the pile, showed an increase of pressure during heating and a decrease while cooling. The same governing pattern could be seen in the measurements of axial force along the pile under thermo-mechanical loading (the axial force increased by cooling and decreased by heating in Figure 3.13). As the temperature sensors showed (Figure 3.7), the temperature of the soil around the pile changed with the pile temperature. The soil pressures measured at this region (measurement of all the pressure transducers except P2 and P3) were therefore dependant on the volume changes in the pile and in the soil. As no uniform stress was applied on top of the soil specimen, the soil was free to expand at its surface. Reduction of soil pressure could be explained by the fact that the soil column around the pile was free to expand at its surface. Considering the pile, its radial expansion while heating would not therefore be restrained by the expanding surrounding soil. In that way stress in the pile was released.

To summarise, it seems that until 150 N of head load ($0.3\times Q_{max}$) the behaviour of the pile embedded in sand remained thermo-elastic under two cooling/heating cycles. From 0 N up to 150 N of pile head load, a pseudo-thermo-elastic behaviour could be observed in the axial force profiles. Considering the mechanical (initial) profile as the reference curve, the profiles obtained after thermal phases oscillate around this curve. As a consequence, the variation of axial forces induced by cooling was compensated by heating. The interval of the pile head displacement during thermal cycles at an axial load higher than 150 N was twice as high as that at a lower axial head load (Figure 3.9). The axial force profiles changes also become larger under more significant loads. The irreversible settlement at the pile head after thermal cycles can be then attributed to irreversible strains in the soil surrounding the pile toe and the soil/pile interface. At heavier axial loads, the stress state in these zones is closer to the failure state. Thermal cycles modify the stress state at these zones and may induce plastic strain (due to grains rearrangements). As a consequence, irreversible settlement can be observed.

As mentioned above, the effects of temperature cycles on the mechanical behaviour of energy pile can be considered using two aspects: (i) thermal expansion of the pile and the soil; (ii) thermo-hydro-mechanical coupling in the surrounding soil. In the present study where dry sand was used, the thermo-hydro-mechanical coupling can be ignored assuming that temperature changes have no effect on the mechanical properties of sand. In this case, only

the thermal expansion of the pile and that of the soil can be used to explain the observed phenomenon.

Considering the tests performed on the model pile in saturated clay, good repeatability between two identical tests could be observed in terms of the load-settlement curves. The ultimate load was 537 N which is 1.2 times the corresponding value for the pile in sand. Creep increased with axial load (similar to the results of Bond & Jardine, 1995 and Konrad & Roy, 1987). Especially under heavier axial loads (more than 50% of the ultimate load) significant creep settlements could be observed (Figure 3.21). As Edil & Mochartt (1988) deduce from their tests on a floating model pile in saturated clay, the immediate settlement is almost elastic. The time dependent component of the total displacement could be attributed mainly to slip at soil/pile interface and consolidation of the surrounding soil. In a floating pile in clay, the slip term plays the main role (Edil & Mochartt, 1988). As no measurements on the pile axial force distribution (and thus the load transfer) was available in the present study, it could not be stated clearly whether the pile was of floating or end-bearing type.

Regarding the pile thermal displacement versus pile temperature (Figure 3.25), pile heaved when it is heated and settled when it was cooled. Globally, pile settled continuously with the applied thermal cycles. The amount of irreversible deformation increased with load. The original pile load-settlement curve underwent important evolution when thermal effects were also included (Figure 3.26). In fact, it could be stated that in this case, thermo-mechanical effects on the surrounding clayey soil were no more negligible. As it was discussed in detail in section 1.4, volume change in soil is dependent on its temperature and applying thermal cycles leads to accumulated plastic strains (Vega & McCartney, 2014). Especially in this case, as the soil could be considered to be normally consolidated, both heating and cooling induce contraction (Abuel-Naga *et al*., 2007, Tang *et al*., 2008), which might help in pile continuous settlement. Unfortunately, strain gauges and pressure transducers were damaged during the preparation phase and the saturation procedure which led to loosing data in terms of stress in the pile and in the soil.

3.5 Conclusion

The mechanical behaviour of energy pile was investigated through a physical model. At the first stage to simplify the problem, dry sand was used as the surrounding soil. Different thermo-mechanical tests were performed following the same procedure: loading the pile incrementally until a target value, keeping the load constant at this stage and applying two thermal cycles to the pile. One test was also conducted under the calculated service load and

thirty cooling/heating cycles. Different transducers located in the soil and on the pile surface monitored the induced thermal effects. The following conclusions can be drawn:

- Under the conditions of the present work, more than 70 % of the axial head load was transferred to the pile toe.
- Soil pressures measured just below the pile toe were significantly influenced by the mechanical and thermal loadings. The changes of total pressure at other positions were negligible.
- Mobilised friction at the soil/pile interface gradually increased with the initial mechanical loading and was significantly modified during the subsequent thermal cycles.
- During two thermal cycles under constant axial head load, for a head load lighter than 30 % of the pile resistance, thermo-elastic behaviour of the pile could be observed. For heavier head load, significant cumulative settlement could be observed and axial force at pile toe gradually increased.
- Pile continued to settle as thermal cycles proceeded and more permanent displacements were observed. More compressive forces were generated in the pile by the subsequent cooling and heating cycles. However, as for the two first thermal cycles, cooling the pile led to higher compressive loads (comparing to heating). Soil pressure at pile toe increased with thermal cycles number, while at other positions total pressure did not change with pile temperature.
- Under purely mechanical loading, pile response did not show a significant time dependency, while significant are observed on the response of the pile under combined thermal and mechanical loading.

Next, the tests were conducted on the model pile embedded in saturated clay. Total pressure transducers and strain gauges were damaged during the saturation procedure and no measurements were available in terms of pile and soil stresses. Pile head displacement and pile and soil temperature were monitored during the tests. In the two first tests, the pile was subjected to incremental axial loading. Five experiments were then conducted during which the pile was subjected to a constant axial load and one heating/cooling cycle. The analysis of the experimental results shows that:

- Pile ultimate load was equal to 537 N, which is 1.2 times the ultimate load in the case of sand.
- Pile heaved during heating and settled during the subsequent cooling. The following heating induced a heave while the pile did not return to the initial position, where

thermal displacement was equal to zero. Even under the lightest tested mechanical load (100 N, or $0.2 \times Q_{max}$), irreversible displacement appeared whose quantity increased as the pile head load augmented.

- Time dependency of pile head displacement was visible under purely mechanical loading. Creep rate increased as the pile head load approached to its ultimate value. Creep load was equal to 430 N.

CHAPTER 4

EFFECT OF TEMPERATURE ON SHEAR STRENGTH OF SOIL AND SOIL/STRUCTURE INTERFACE

4.1 Introduction

In this chapter, the shear behaviour of soils and that of soil/concrete interface is investigated through direct shear tests at various temperatures. Conventional shear apparatus is equipped with a temperature control system. Three temperature values were considered (5°C, 20°C and 40°C). These values correspond to the range of temperature near energy geo-structures. Direct shear tests were performed at normal stress values ranging from 5 kPa to 100 kPa. The shear behaviour of Fontainebleau sand, Kaolin clay, and Kaolin clay/concrete interface was investigated.

4.2 Experimental setup

A direct shear apparatus (VJ Tech type) equipped with a temperature control system was used to investigate the shear behaviour of soil and soil/concrete interface. A general view of the system is shown in Figure 4.1. A copper tube was accommodated in the shear box container and connected to a heating/cooling circulating bath (Figure 4.2*a*). Water with controlled temperature circulated inside the copper tubes via the circulator. These tubes were plunged in water inside the shear box container. This system allowed controlling the temperature of soil specimen inside the cell. Two thermocouples were installed in the container: one below the shear box and the other at the water surface. The thermocouples allow confirming that the target temperature of the sample is achieved and the temperature is homogeneous inside the cell. The container was thermally insulated using expanded polystyrene sheets (Figure 4.2*b*). The soil (or soil/concrete) was sandwiched between two porous stones and two steel porous plates.

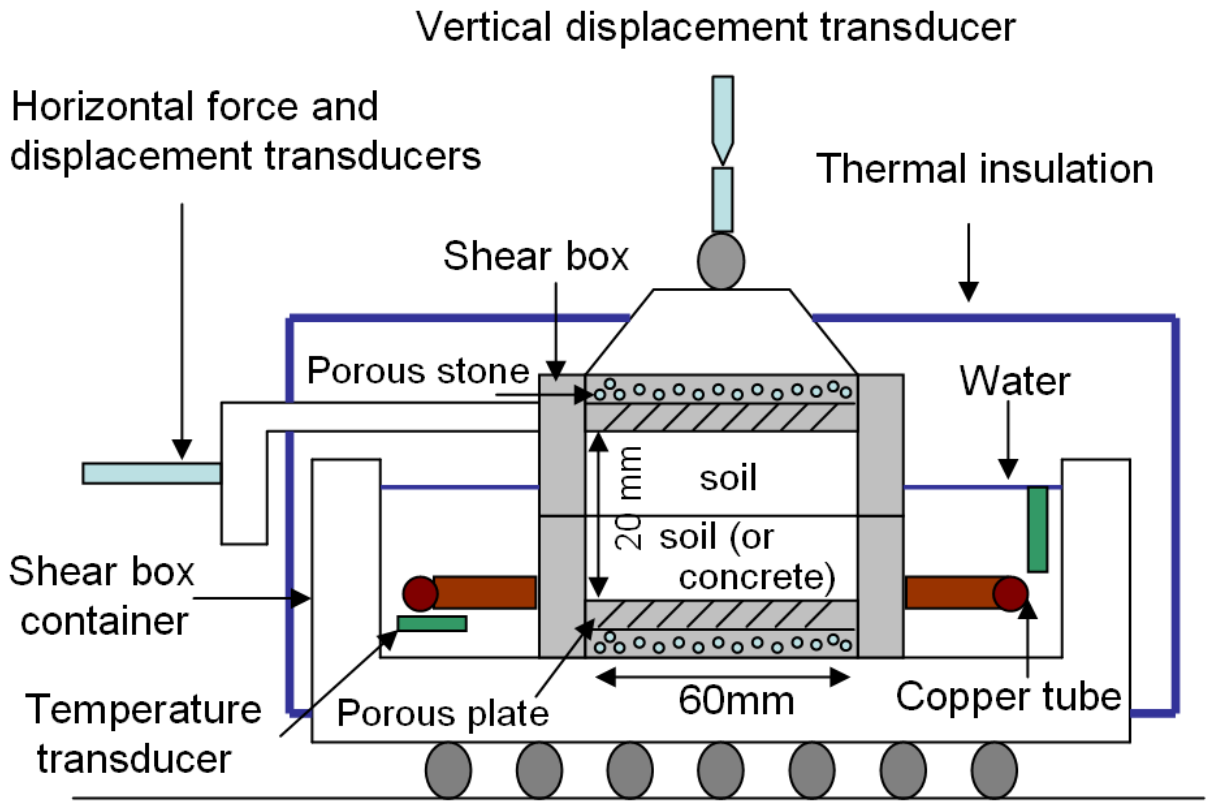

Figure 4.1 Direct shear apparatus with temperature control system

Figure 4.2 (a) View of the shear box with copper tubes and water inside (b) Thermal insulation of the shear box

4.3 Materials studied

In the present work, tests were performed on Fontainebleau sand, Kaolin clay, and Kaolin clay/concrete interface. The physical properties of Fontainebleau sand are the same as described in Chapter 2: particle density ρ_s = 2.67 Mg/m^3; maximal void ratio e_{max} = 0.94;

minimal void ratio e_{min} = 0.54 (De Gennaro *et al*., 2008); and median diameter D_{50} = 0.23 mm. The grain size distribution of the sand used is shown in Figure 2.9. To perform direct shear tests, sand was directly poured into the shear box and slightly compacted at a dry density of 1.51 Mg/m^3. This value, corresponding to a relative density of 46%, is similar to that in the work of De Gennaro *et al*. (1999) and Kalantidou *et al*. (2012).

The Kaolin clay has a particle density ρ_s = 2.60 Mg/m^3, a liquid limit w_L = 57% and a plastic limit w_P = 33% (Frikha, 2010). The grain size distribution of Kaolin clay, obtained by laser diffraction method, is also shown in Figure 2.13. To prepare a soil sample, the clay powder was mixed with deionised water at 1.5 w_L and then consolidated in an oedometer cylinder (with an internal diameter of 100 mm) under a vertical stress of 100 kPa. At the end of the consolidation phase, the soil sample was removed from the cylinder and cut into blocks of dimensions 60 x 60 x 20 mm and inserted into the shear box for testing the shear behaviour of clay.

To test the clay/concrete interface, the thickness of the sample was reduced to 10 mm. A piece of concrete with a thickness of 10±2 mm was cut and firmly fixed to the lower half of the shear box. The maximum roughness detectable through photos is in the order of 0.7 mm (see Figure 4.3). It should be noted that the same piece of concrete was used in all interface tests. In other words, roughness value has not changed from one test to another.

In any case, once the sample was placed in the shear box, the shear box container was filled with water and samples were saturated within a certain time which varied between 15 minutes (for sand) and 30 minutes (for clay). Shear tests were intended to be performed on saturated samples.

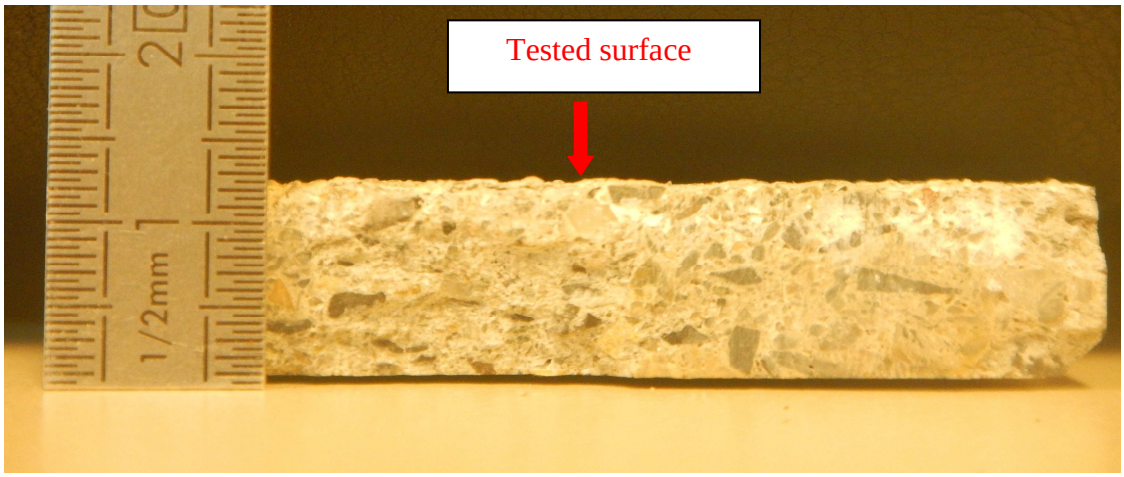

Figure 4.3 Concrete plate used for studying clay/concrete interface

4.4 Thermo-mechanical loading paths

The choice of the thermo-mechanical loading path is of great importance in the case of clay, as it is a generally accepted idea that its response depends highly on the loading history. The loading paths applied are shown in Figure 4.4. For each test, after the installation of the system, a normal stress of 100 kPa was applied to the sample (path A-B); this value is equal to the pre-consolidation pressure of clayey sample. Loading was applied by steps of 20 kPa. Load was increased once the vertical displacement changes stabilised. The soil temperature was then increased from the initial value (20°C) to 40°C by increments of 5°C (path B-C). Each increment was kept for 15 minutes. Once temperature reached 40°C, it was kept constant for two hours in order to permit the dissipation of the excess pore water pressure induced by heating. Test results in this part show that vertical displacement stabilises within this time. In total, it could be stated that soil was heated +20°C in 3 hours (or approximately 7°C in 1 hour). This value of 40°C corresponds to the maximal value of temperature tested in the present work. For shearing tests at 40°C (Figure 4.4*a*), the normal stress was decreased to the desired value (path D-E). After 30 minutes when volume changes after unloading was stabilised, the sample was sheared. For shearing tests at 20°C (Figure 4.4*b*) and 5°C (Figure 4.4*c*), the soil temperature was first incrementally decreased to the desired temperature (path C-D). Each increment, of 5°C, took approximately 30 minutes. Cooling was performed at almost the same rate as heating (7°C/hr). Finally, the normal stress was decreased to the desired value (path D-E) prior to shearing. In order to ensure that appropriate heating and cooling rates are considered, the work of Sultan *et al*. (2002) on thermal consolidation of Boom clay was taken into account. In their study, soil samples with height of 76 mm, diameter of 38 mm and hydraulic conductivity of $10^{-12} m/s$ were utilised. Heating and cooling rates were equal to 0.1°C/15 min (almost 0.4°C/hr). According to the one-dimensional consolidation theory, consolidation time (*t*) is proportional to H^2/K, where '*H*' is the sample height (or drainage path, more precisely) and '*K*' is the soil hydraulic conductivity. Thus;

$$\frac{t_{BoomClay}}{t_{KaolinClay}} = \frac{H^2_{BoomClay}/K_{BoomClay}}{H^2_{KaolinClay}/K_{KaolinClay}} = \frac{76^2/10^{-12}}{20^2/10^{-8}} \approx 10^5$$

It could be then concluded that thermal consolidation in the case of this study could be performed at 10^5 times faster rates. The rate of 7°C/hr considered in this work seems therefore to be acceptable.

The interest of the adopted thermo-mechanical loading protocol could be clarified in Figure 4.5. It is noteworthy that the notation of '*LY*' for the loading yield surface comes from the work of Cui *et al*. (2000). Laloui & François (2009) used the bounding surface theory and took the yield surface as the bounding surface and changed also the notation to '*BS*'. The initial loading yield surface is shown as LY_i. According to the proposed thermo-mechanical path, soil is first loaded to its preconsolidation pressure which is equal to 100 kPa (path A-B). Heating the soil (in this case from 20°C to 40°C, path B-C) moves the yield surface towards LY_f. The elastic domain is thus enlarged. Cooling (path C-D), unloading to a lower normal load (path D-E) and shear will then take place in the new elastic zone.

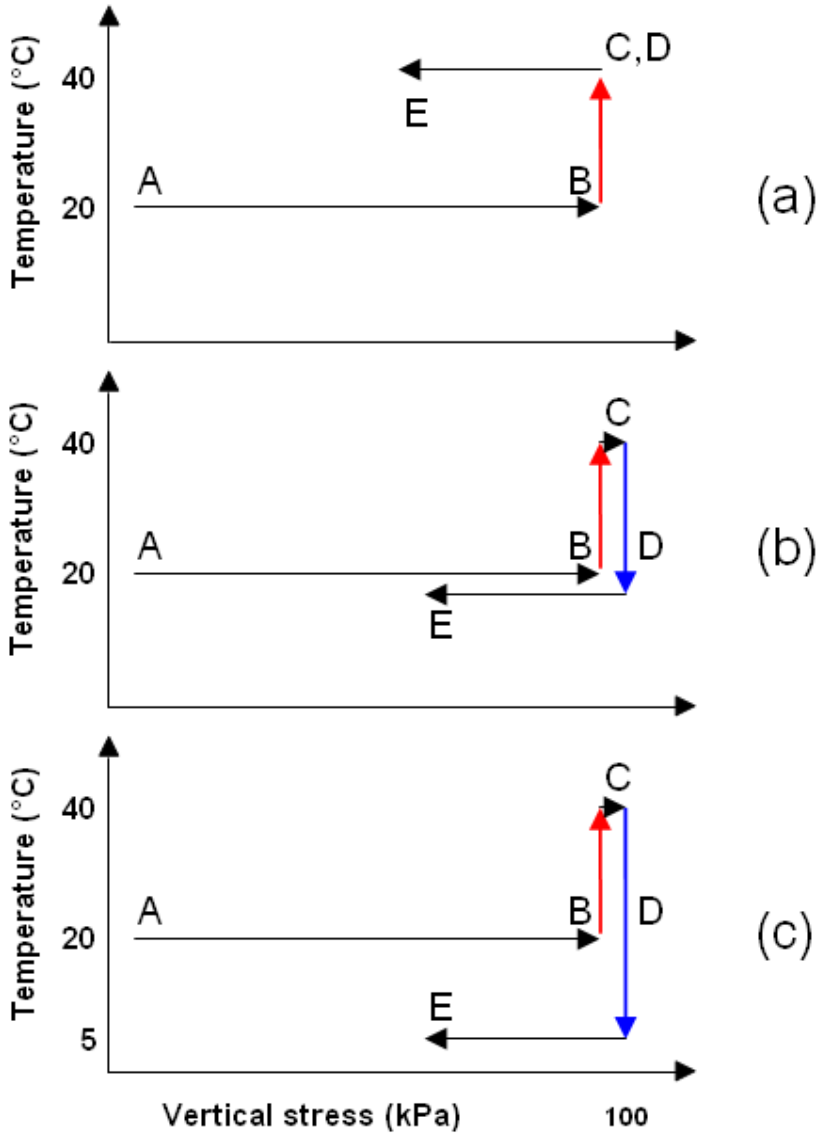

Figure 4.4 Thermo-mechanical loading paths: (a) tests at 40°C; (b) tests at 20°C; (c) tests at 5°C

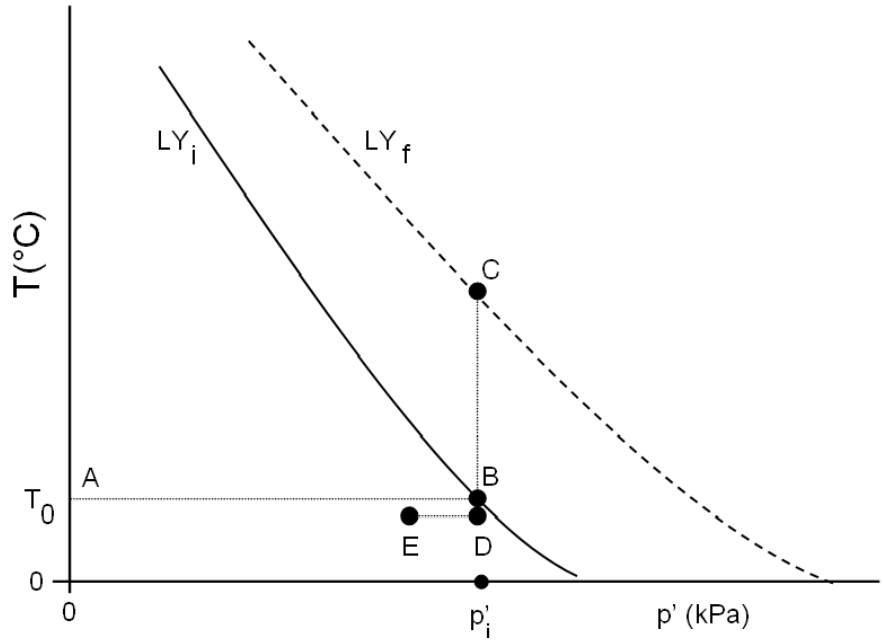

Figure 4.5 Evolution of the loading yield surface (*LY*) in *T-p'* plan

For the tests on clay or clay/concrete interface, shearing rate was chosen small enough in order to ensure that no excess pore pressure was generated during the test and the sample was sheared under drained conditions. The maximum shear rate could be defined on the basis of the consolidation curve and the value of t_{100} (in minutes). According to the French standard code on direct shear testing (AFNOR, 1994), the corresponding equation, which gives the shear rate, is as follows:

$$V_{\max} = \frac{125}{t_{100}} [\mu\text{m/min}] \tag{4.1}$$

From the consolidation phase (path A-B), the value of t_{100} can be estimated at 9 min. The shear rate was thus set to 14 μm/min (following Equation 4.1).

For granular soils the shear rate could be higher as the consolidation is faster. In the tests on sand the shear displacement was applied at the rate of 0.2 mm/min (according to AFNOR, 1994). The maximal shear displacement at which shearing stops is set to 6 mm. This value is 10% of the soil specimen dimension in the shear direction.

4.5 Thermal calibration

Calibration procedure was performed prior to testing in order to eliminate the unwanted temperature effects. Instead of the soil specimen, a steel cylinder with an external diameter of 60 mm and a thickness of 20 mm was installed inside the shear box. A normal stress of 100

kPa was applied. A complete thermal cycle according to the procedure explained in the previous part (Figure 4.4*c*) between 20°C, 40°C and 5°C was conducted. The purpose was to evaluate the effect of temperature on the horizontal and vertical load and displacement transducers measurements (as depicted in Figure 4.6) and subtracting them from the results of the main tests on soil and soil/concrete interface. However according to Figure 4.6 temperature does not affect significantly the corresponding values (±1 kPa in stress measurements and ±0.04 mm in displacement measurements) .

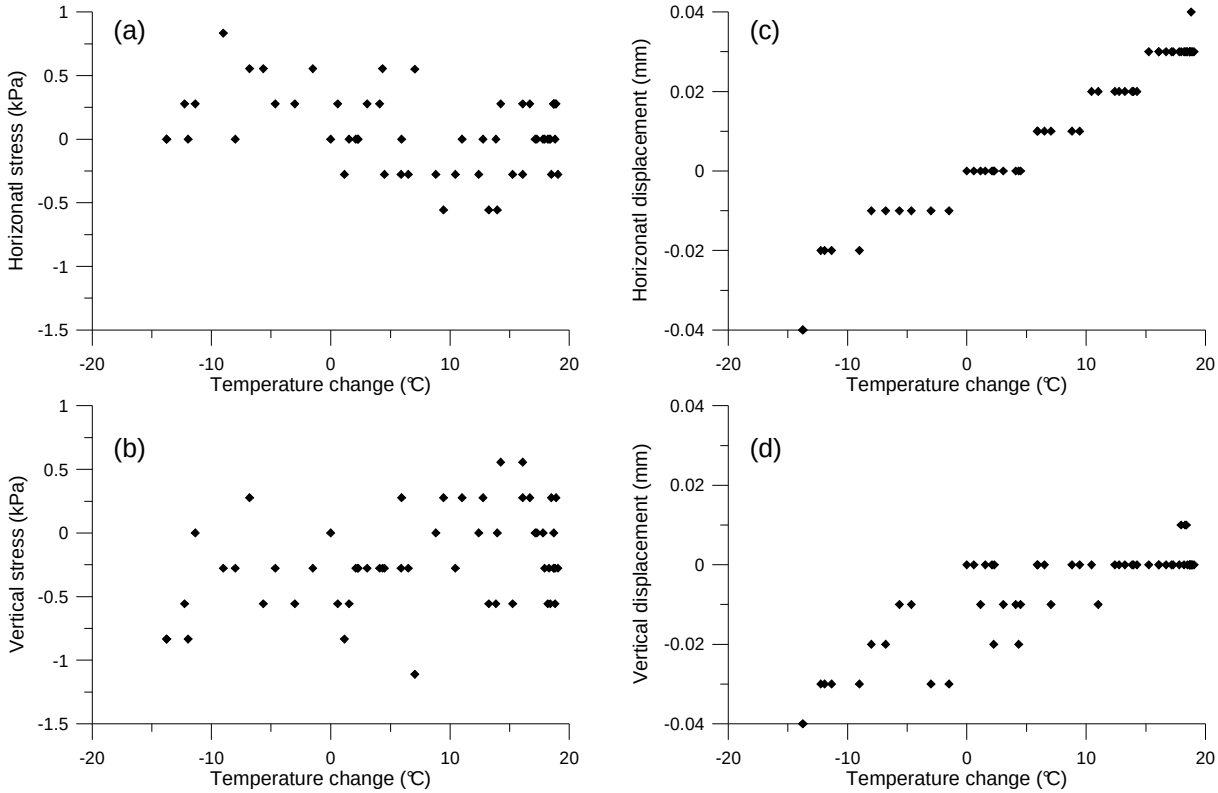

Figure 4.6 Transducers measurements versus temperature change in thermal calibration test, measurement of: (a) horizontal stress; (b) vertical stress; (c) horizontal displacement; (d) vertical displacement

4.6 Experimental results

4.6.1 Tests on sand

Results of shear tests on sand at different temperatures are shown in Figure 4.7 to Figure 4.9. Under each normal stress and each temperature two tests were conducted in order to check the repeatability of the experiments. Experimental results at 5°C are exhibited in Figure 4.7. As could be seen in Figure 4.7*a*, no peak value could be detected on the shear strength/horizontal displacement curves and the failure is of ductile type, except for one test

under 80 kPa, where a softening behaviour could be observed. Figure 4.7*b* shows the vertical displacement during the shear process. Under higher normal stresses there exists a contracting phase followed by a dilating one. When load was smaller, soil at the interface tended to dilate from the beginning to the end of the shear process. However quantitatively, the repeatability of the tests in terms of vertical displacement was less than for the shear stress. Maximum shear strength observed as a function of normal stress is shown in Figure 4.7*c*. Failure is of Mohr-Coulomb type with no cohesion and with a friction angle of 35.8°.

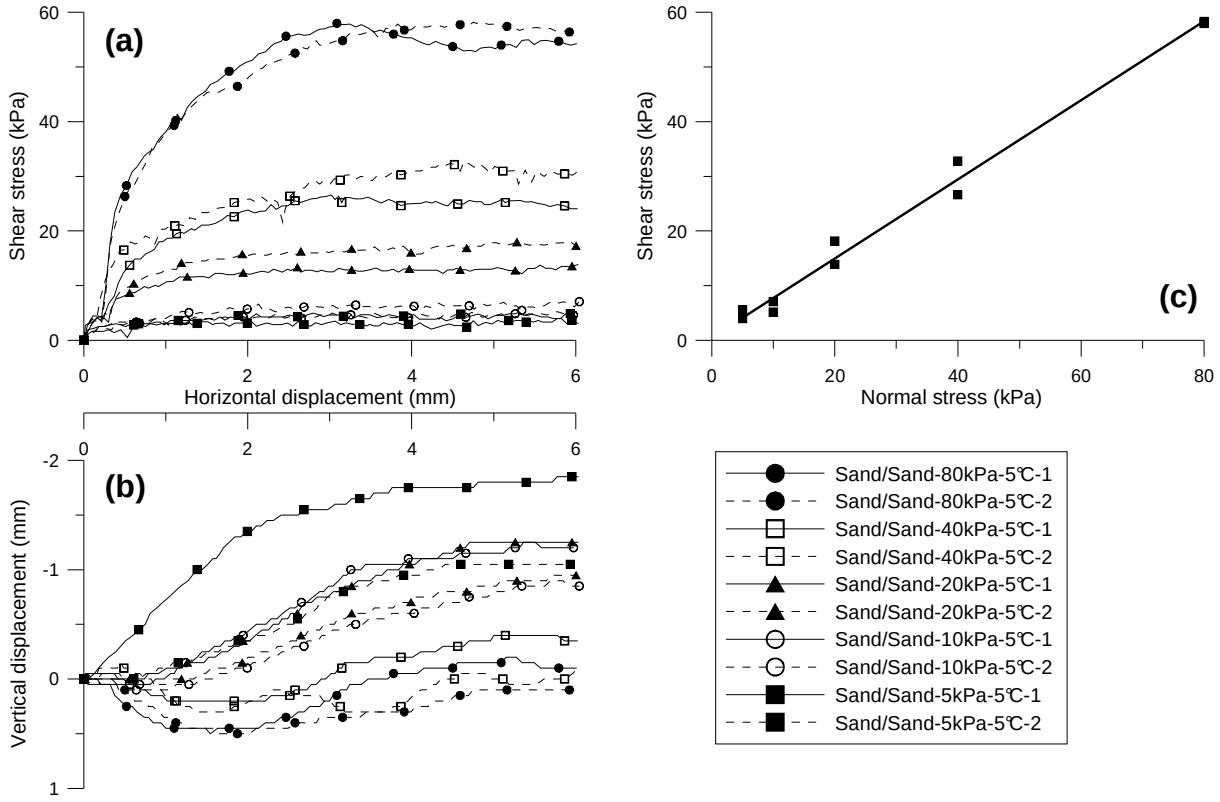

Figure 4.7 Experimental results on Fontainebleau sand at 5°C: (a) shear stress versus horizontal displacement; (b) vertical displacement versus horizontal displacement; (c) shear strength envelope

Experimental results on sand at 20°C are shown in Figure 4.8. As in the case of 5°C, under 5 kPa up to 40 kPa of normal stress, the behaviour was of ductile type and no peak shear strength could be spotted (Figure 4.8*a*). The peak behaviour was observed on one the two tests at 80 kPa of normal stress. The vertical displacement behaviour (Figure 4.8*b*) is similar to that at 5°C; under normal stress values of 80 kPa and 40 kPa, soil tended to contract at first, then it began to dilate. The peak strength envelope is shown in Figure 4.8*c*. A very good agreement between tests under the same normal stress value could be detected at 5, 10 and 40

kPa. Failure is again of Mohr-Coulomb type. Friction angle equals 34.8° and soil is almost cohesionless.

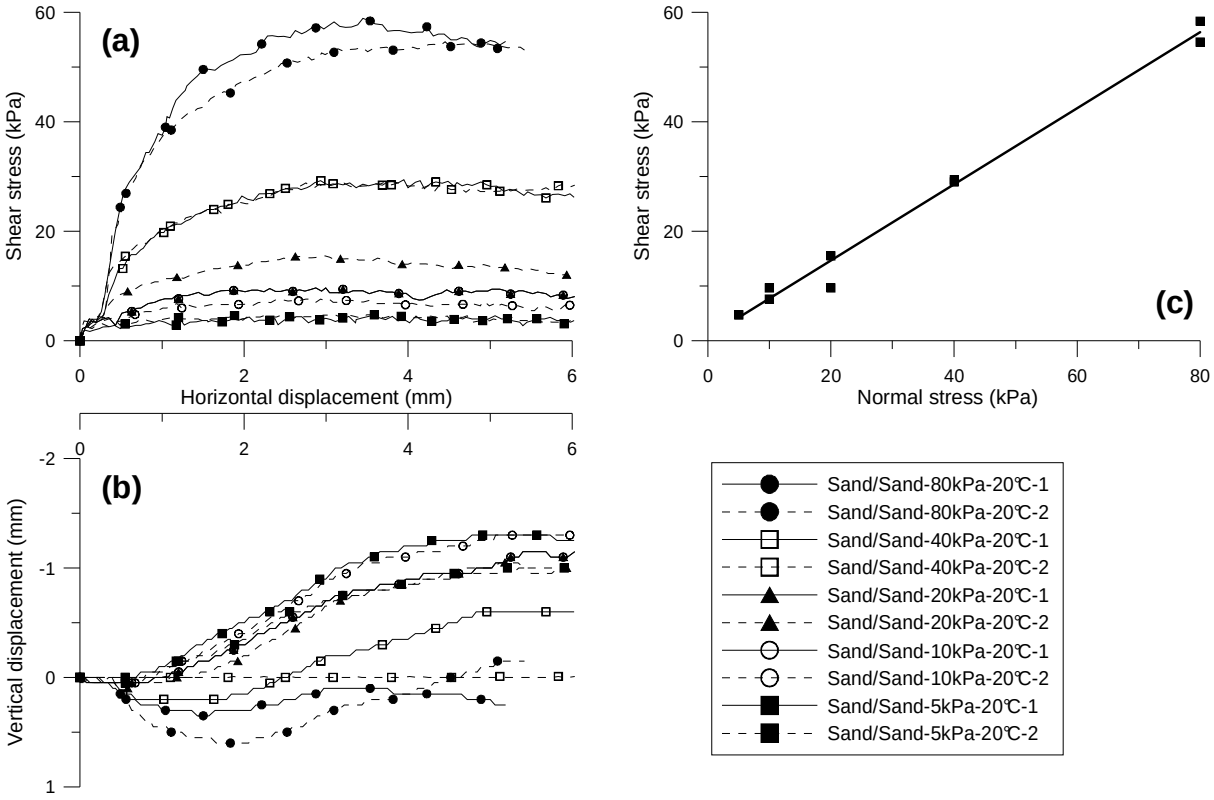

Figure 4.8 Experimental results on Fontainebleau sand at 20°C: (a) shear stress versus horizontal displacement; (b) vertical displacement versus horizontal displacement; (c) shear strength envelope

The results of tests at 40°C are exhibited in Figure 4.9. Similar observations to that at 5°C and 20°C can be noted: discrepancy on the vertical displacement/horizontal displacement curves (Figure 4.9*b*); good repeatability on the peak strength/normal stress plot (Figure 4.9*c*); a Mohr-Coulomb type failure which results a friction angle of 35.1° and a null cohesion.

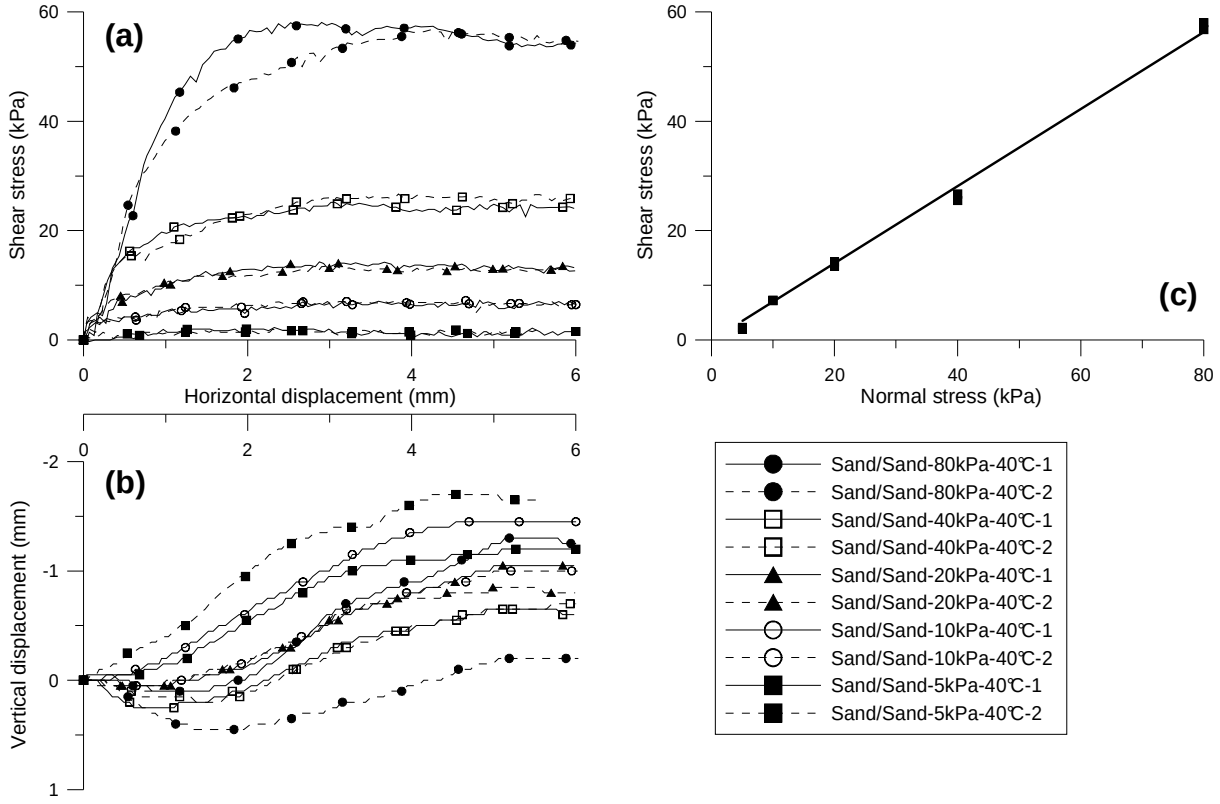

Figure 4.9 Experimental results on Fontainebleau sand at 40°C: (a) shear stress versus horizontal displacement; (b) vertical displacement versus horizontal displacement; (c) shear strength envelope

4.6.2 Tests on clay and clay/concrete interface

Results on clay and clay/concrete interface at 5°C are shown in Figure 4.10. In Figure 4.10*a*, clay/concrete interface shows peak strength under different values of normal stress, while no peak value could be detected on clay. Results on vertical displacement versus horizontal one are shown in Figure 4.10*b*. For both clay and clay/concrete interface, under 40, 80 and 100 kPa, vertical deformation was contracting. Under smaller normal stresses (5, 10 and 20 kPa), a dilating phase could be detected. Vertical deformation of clay was almost twice higher than that observed on clay/concrete interface under the same normal stress. Peak and residual shear strength of clay and that of clay/concrete interface are shown in Figure 4.10*c*. The strength envelope of clay locates above that of clay/concrete interface.

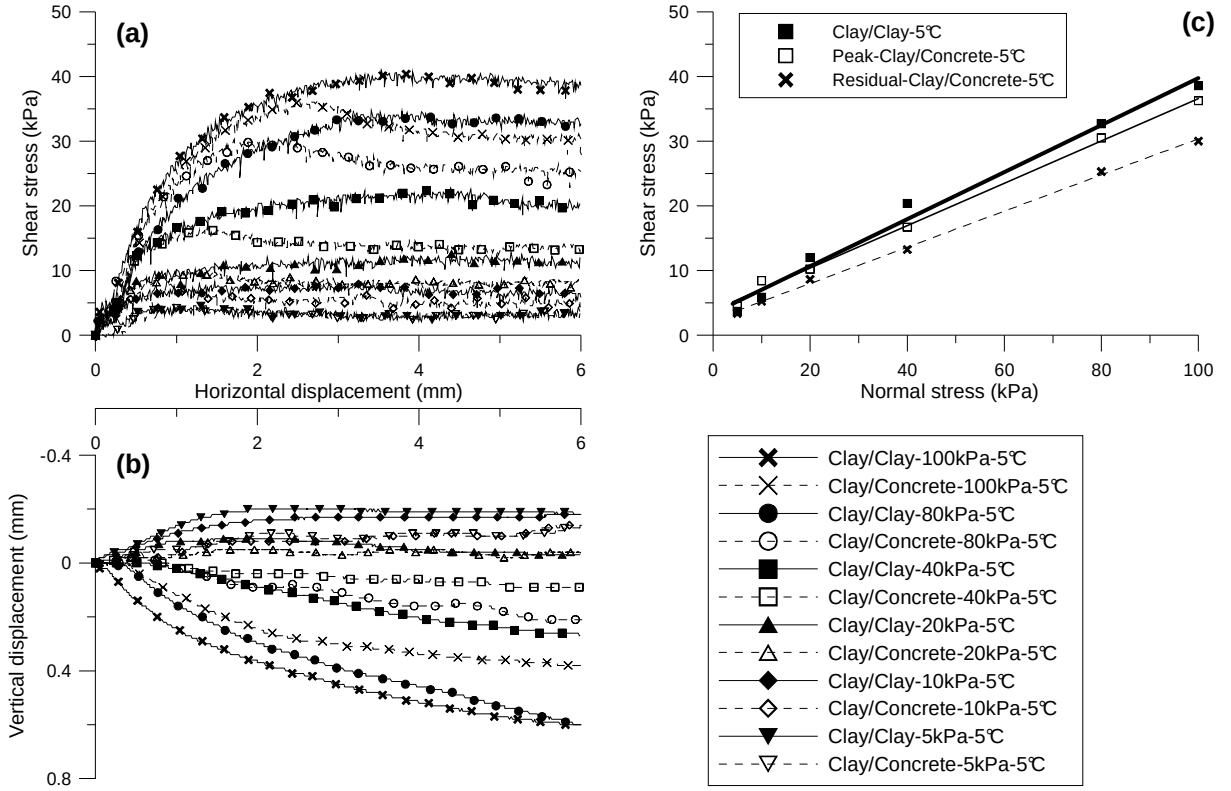

Figure 4.10 Experimental results on Kaolin clay and Kaolin clay/concrete interface at 5°C: (a) shear stress versus horizontal displacement; (b) vertical displacement versus horizontal displacement; (c) shear strength envelope

Results at 20°C are shown in Figure 4.11. The same observation as at 5°C (Figure 4.10*a*) is valid for Figure 4.11*a*. In addition, the softening behaviour of clay/concrete interface is more pronounced under normal stress values of 40, 80 and 100 kPa. Figure 4.11*b* shows that the vertical displacement of clay/clay was about twice higher than that of clay/concrete interface. At 40, 80 and 100 kPa of normal stress the soil tended to contract while it dilated at lower normal stresses. Peak and residual shear strength envelopes are shown in Figure 4.11*c*. As at 5°C (Figure 4.10*c*), smaller shear strength values correspond to clay/concrete interface.

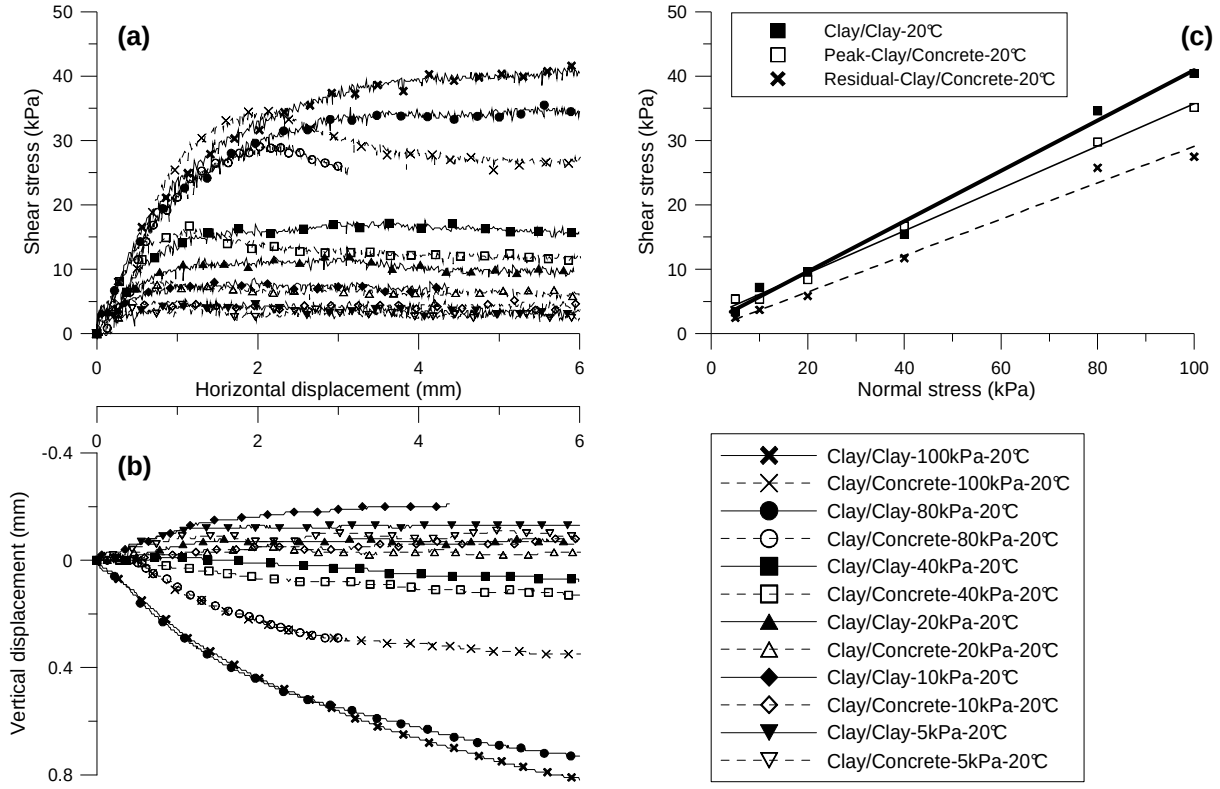

Figure 4.11 Experimental results on Kaolin clay and Kaolin clay/concrete interface at 20°C: (a) shear stress versus horizontal displacement; (b) vertical displacement versus horizontal displacement; (c) shear strength envelope

Results on shear stress versus horizontal displacement of clay and that of clay/concrete interface at 40°C are exhibited in Figure 4.12*a*. As in the cases at 5°C and 20°C, a softening behaviour is observed for clay/concrete interface while a ductile type is observed for clay. Results on vertical displacement versus horizontal one at 40°C are shown in Figure 4.12*b*. In both clay/concrete interface and clay/clay tests, under 40, 80 and 100 kPa, sample tended to contract during the shear process while dilation was observed at smaller normal stress. The difference between the shear envelope of clay and the peak-strength envelope on clay/concrete interface is quite small at 40°C (Figure 4.12*c*).

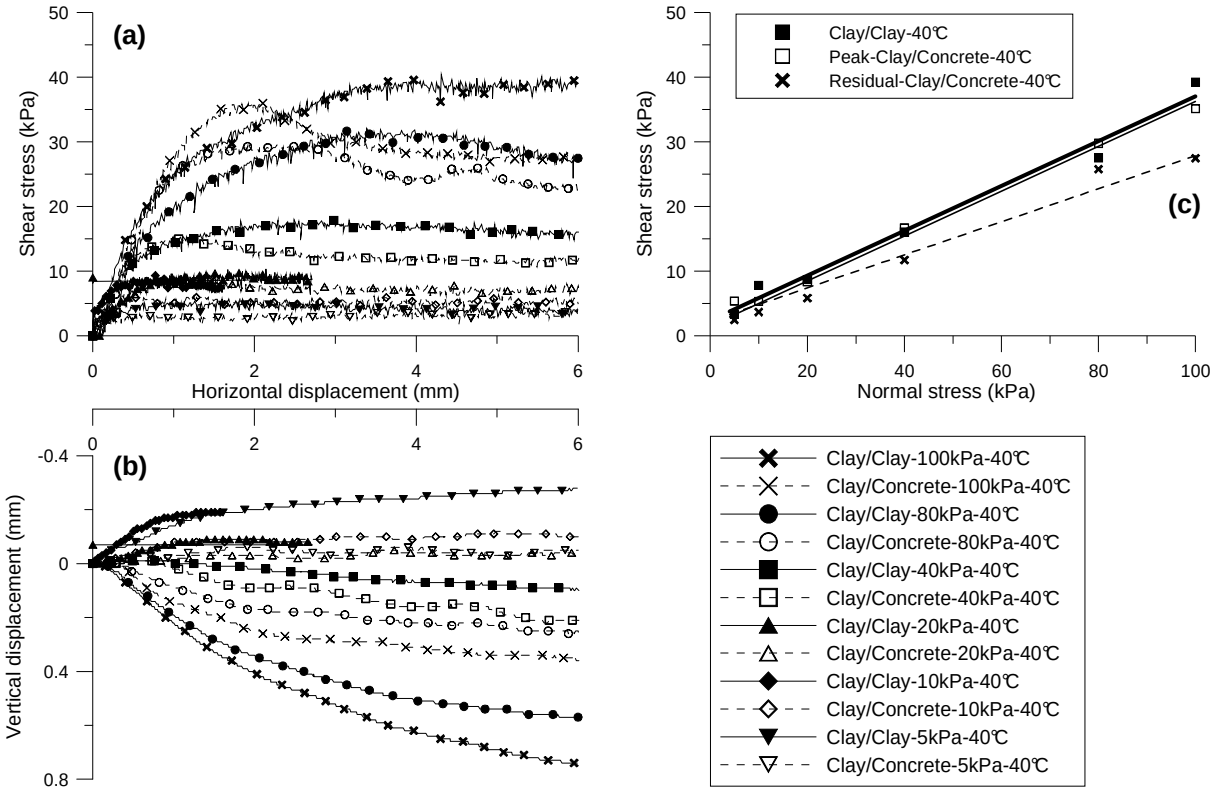

Figure 4.12 Experimental results on Kaolin clay and Kaolin clay/concrete interface at 40°C: (a) shear stress versus horizontal displacement; (b) vertical displacement versus horizontal displacement; (c) shear strength envelope

In order to evaluate the effect of temperature on shear strength parameters (friction angle and cohesion), all the results are shown in Figure 4.13. It could be concluded that the effect of temperature on the friction angle was quite small and the trend was not clear (Figure 4.13*a*). For sand, the friction angle decreased slightly from 5°C to 20°C, while in the range of 20°C and 40°C it did not change. Effect of temperature on the angle of friction of clay and the residual friction angle of clay/concrete interface was similar; it slightly increased from 5°C to 20°C and decreased from 20°C to 40°C. The friction angle of clay was higher than the peak-strength friction angle of clay/concrete (except at 40°C). The cohesion measured on clay and clay/concrete interface was quite small, of the order of a few kPa (Figure 4.13*b*) with small variation between 5°C and 40°C. The residual cohesion of clay/concrete interface and that of clay showed a small decrease between 5°C and 20°C and a slight increase between 20°C and 40°C. The cohesion of clay was generally higher than the residual cohesion of clay/concrete interface (except at 40°C). With respect to peak cohesion value on clay/concrete interface, the cohesion value decreased in the range between 5°C and 40°C (from 4 kPa to 2 kPa).

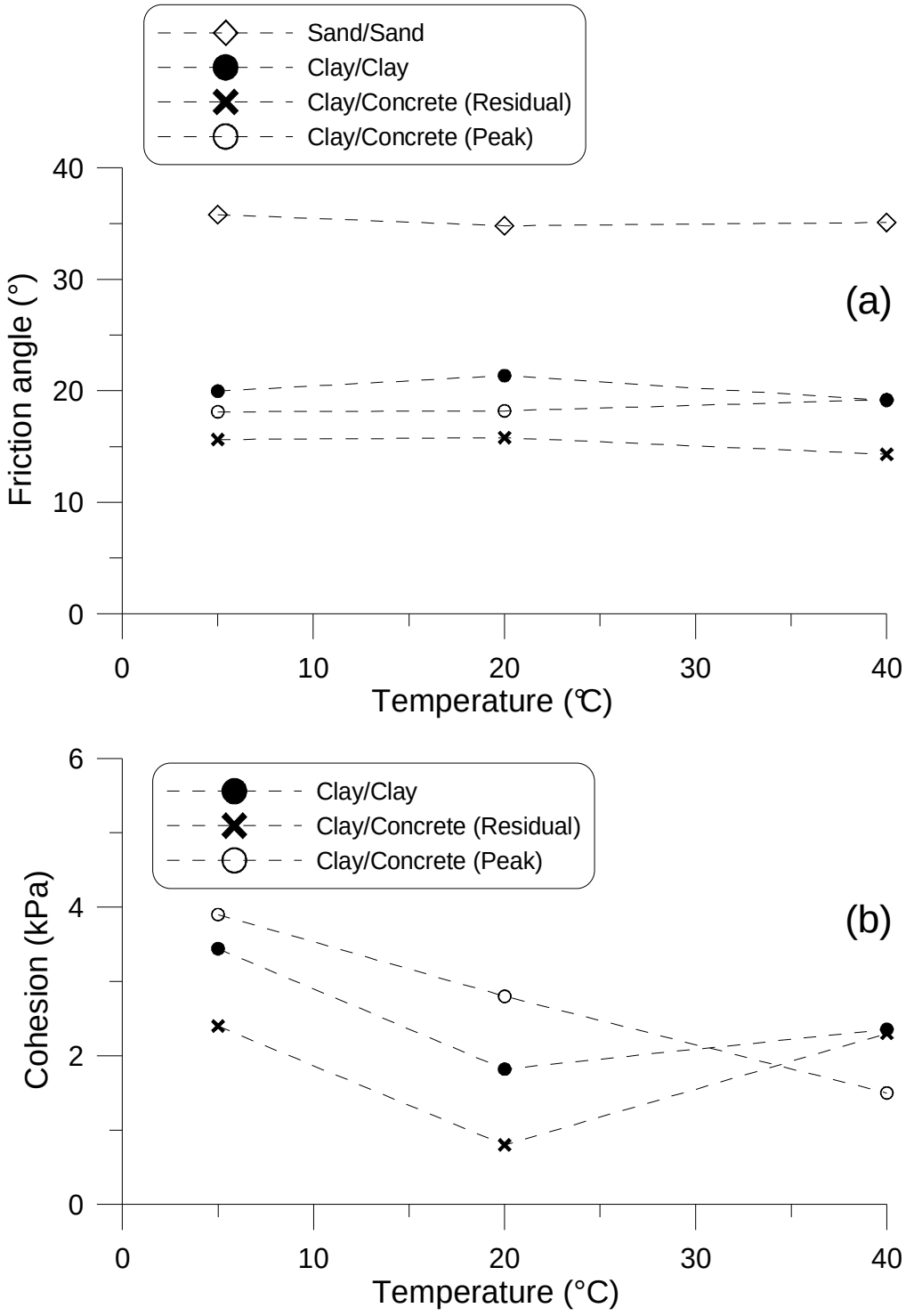

Figure 4.13 Effect of temperature on (a) friction angle and (b) cohesion

4.7 Discussion

For the tests on sand, all the tests have been duplicated. The results show good repeatability in terms of shear stress versus horizontal displacement. That allows obtaining reliable results in terms of shear strength. Nevertheless, the repeatability in terms of vertical displacement versus horizontal one was less obvious. Actually, this result is related to the volume change in the sheared zone, but the thickness of the sheared zone can vary from one test to the other. For the tests on clay and clay/concrete interface that are more time consuming, only one test has been conducted at each temperature and normal stress. The relationship between the shear strength and the normal stress could be well correlated with a linear function, which allowed determining the friction angle and the cohesion. These observations show equally the reliability of the obtained results.

The thermo-mechanical loading procedure in tests on clay and clay/concrete interface was applied by considering the thermo-mechanical behaviour of clay. Actually, prior to shearing, the sample was heated to 40°C under its preconsolidation pressure (100 kPa). Heating leads to the mobilisation of the loading yield surface to the right in *T-p'* plan. The samples were cooled afterwards to the target temperature (5°C or 20°C), unloaded and sheared. That way, one could state that all the samples where sheared starting from the elastic domain and thus the results will be comparable to each other. Heating and cooling were applied under drained conditions.

In order to better analyse the effect of temperature on soils friction angle, the results of the present study are plotted together with that obtained from others in the same figure (Figure 4.14). The results from the existing studies show that the effect of temperature on soils friction angle was quite small. In addition, at higher temperature, the friction angle could be higher in some cases and lower in others. These observations were similar to that obtained in the present work. On the other hand, the range of applied temperature in the previous studies varied between 20°C and 100°C, which is the range when considering the geological radioactive waste disposal. In the present work, these conclusions were extended to lower temperature (5°C), which corresponds to the problem of energy geo-structures.

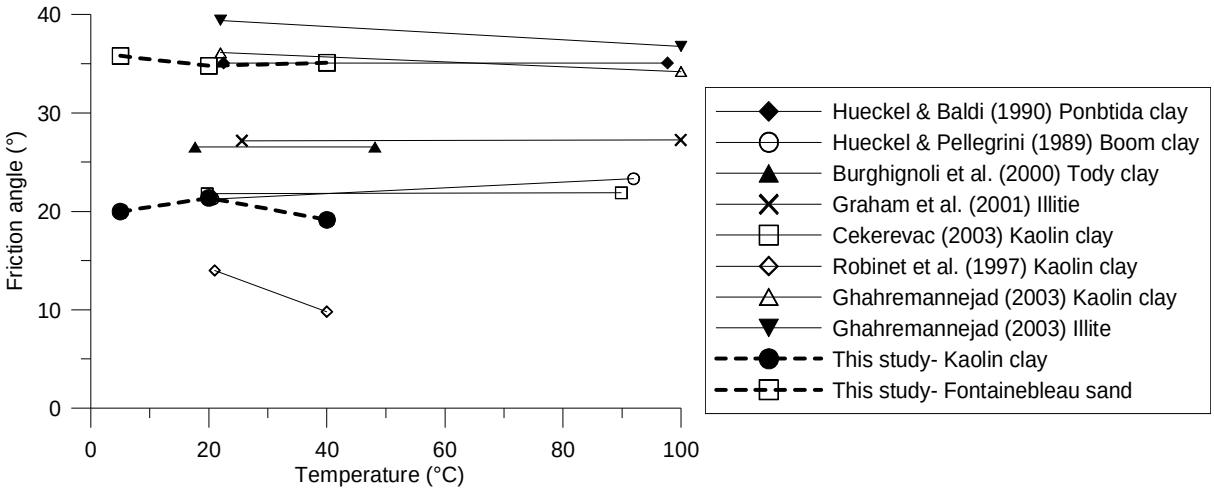

Figure 4.14 Effect of temperature on friction angle

The results on clay/concrete interface show a softening behaviour during shearing. In addition, the results show that the peak-strength friction angle of the clay/interface was slightly lower than that of clay (except at 40°C). As shown by previous studies (Tsubakihara & Kishida, 1993; Rouaiguia, 2010; Taha & Fall, 2013), the interface behaviour was dependent on the surface roughness. By increasing the roughness, the corresponding shear stress curve would approach to the shear stress evolution in clay itself. After Rouaiguia (2010), the relatively plane surface of concrete makes clay particles reorient easily once reaching the maximum shear strength. The particles would then be aligned in the developed sheared zone and the shear stress decreases. This might explain the softening behaviour observed on clay/concrete interface. In the present work, vertical settlement of the clay sample was about twice of that of clay/concrete. That can be explained by the fact that the thickness of the clay sample used in clay/clay tests was twice that of the clay utilised in clay/concrete interface.

In the work of Di Donna & Laloui (2013*b*) on illite clay/concrete interface, the peak friction angle increased between 20°C and 60°C, while the residual value decreased slightly in the same temperature range. That is also the trend observed in the present work between 20°C and 40°C. Regarding the cohesion value on illite clay/concrete interface in the work of Di Donna & Laloui (2013*b*), a significant increase in residual and peak values was observed as the temperature increased from 20°C to 60°C. Also, peak and residual values were close to each other at a constant temperature value; the corresponding values were about 8 kPa at 20°C and 19 kPa at 60°C. No regular tendency on residual cohesion variation, neither on clay nor on clay/concrete interface, was observed in the range of 5°C and 40°C in the present work. The peak cohesion of clay/concrete interface decreased as the temperature increased.

4.8 Conclusions

Shear behaviour of sand, clayey soil and that of clay/concrete interface at various temperatures was investigated through direct shear tests. The shear box apparatus was equipped with a temperature control system. The samples were consolidated under 100 kPa and sheared under a controlled temperature. Samples were then sheared at 5°C, 20°C and 40°C. The results show that friction angle (and the shear strength) of sand was almost independent of temperature in the range of 20°C and 40°C. The friction angle was slightly higher at 5°C comparing to 20°C. The effect of temperature on clay was not significant; at 20°C the friction angle was slightly higher and the cohesion was slightly lower than that at 5°C and 40°C.

The shearing behavior of clay/concrete interface showed a softening behaviour. The peak friction angle of clay/concrete interface was lower than that of clay. This value increased slightly when temperature increased from 20°C to 40°C but it remained constant when temperature decreased from 20°C to 5°C. Regarding the residual friction angle of clay/concrete interface, the values at 5°C and 20°C were similar and higher than that at 40°C. Small cohesion values were observed on clay and clay/concrete interface. higher residual values were measured on clay than on clay/concrete interface. Minimum residual cohesion was obtained at 20°C while higher values were observed at lower and upper temperatures. Peak cohesion of clay/concrete interface was greater than the residual one (except at 40°C) and decreased between 5°C and 40°C.

CHAPTER 5

FINITE ELEMENT ANALYSIS OF ENERGY PILES

5.1 Introduction

In the first part of this chapter dedicated to numerical studies, a commercial numerical code (Plaxis 8.2) was used to simulate the mechanical behaviour of energy piles under thermo-mechanical loading. The thermal load was simply simulated by imposing volumetric strains calculated from the coefficient of thermal expansion of the material on the pile. Simulation was performed for two existing in-situ experiments and one experiment performed using physical modelling in laboratory.

In the following part, another commercial code (CESAR-LCPC) in which temperature effects are also included was selected. The behaviour of the energy pile in the physical model under thermo-mechanical solicitation (as discussed in Chapter 2) is examined numerically. Purely mechanical loading was performed by applying load increments to the pile's head until failure. In thermo-mechanical tests, pile was first loaded incrementally and then subjected to two thermal cycles between 10°C and 30°C. The thermo-mechanical effects induced in the pile and in the soil were obtained in terms of soil total pressure and temperature, pile axial load and pile head displacement. The numerical results were compared to the experimental ones.

5.2 Mathematical formulation of a thermo-mechanical problem

Herein, a thermo-mechanical model which is only coupled in terms of thermally induced volume changes is chosen. It is assumed that strength and stiffness parameters of the considered material are constant and do not change with temperature. In general, the solution of such a thermo-mechanical problem is achieved in two parts: the first part is based on solving the heat equation, valid at any point of the structure:

$$C_v \frac{\partial T}{\partial t} - \text{div}\left(\text{k}\left(\text{grad}\, T\right)\right) = 0 \tag{5.1}$$

with C_v the volumetric heat capacity, k the thermal conductivity, T the temperature and t the time.

During the second part, the mechanical response of the structure is calculated which should satisfy the following well-known equations:

- the balance of momentum:

$$\mathrm{div}\underline{\underline{\sigma}} + \rho \underline{g} = 0 \tag{5.2}$$

With $\underline{\underline{\sigma}}$ stress tensor, ρ soil density and $\underline{g}$ gravitational acceleration vector.

- and the constitutive equation:

$$\underline{\underline{\sigma}} = \mathbb{C} : (\underline{\underline{\varepsilon}} - \underline{\underline{\varepsilon}}^{p} - \underline{\underline{\varepsilon}}^{th}) + \underline{\underline{\sigma}}^{0} \tag{5.3}$$

where $\mathbb{C}$ is the fourth-order isotropic linear elastic stiffness tensor, $\underline{\underline{\sigma}}^{0}$ is the initial stress tensor, $\underline{\underline{\varepsilon}}$, $\underline{\underline{\varepsilon}}^{p}$ and $\underline{\underline{\varepsilon}}^{th}$ are total deformation, plastic deformation and thermal deformation tensors and are defined as follows:

- Strain-displacement equation:

$$\underline{\underline{\varepsilon}} = \frac{1}{2}(\mathrm{grad}\underline{u} + \mathrm{grad}\underline{u}^{T}) \tag{5.4}$$

$\underline{u}$ is the displacement vector.

- Associated flow rule:

$$\underline{\underline{\varepsilon}}^{p} = d\lambda \frac{\partial f}{\partial \underline{\underline{\sigma}}} \tag{5.5}$$

with f the yield function, which must satisfy the consistency condition $f(\sigma) = 0$ and $df = 0$, $d\lambda \geq 0$ is the plastic multiplier.

- Thermal expansion in an isotropic material:

$$\underline{\underline{\varepsilon}}^{th} = \alpha \Delta T \underline{\underline{1}} \tag{5.6}$$

α is the coefficient of thermal expansion.

Boundary conditions are formulated as follows:

$$(\underline{\underline{\sigma}}.\underline{n})_i = \underline{\Gamma}_i^{\,d} \text{ on } \partial\Omega_{\Gamma_i} \tag{5.7}$$

$$\underline{u}_i = \underline{u}_i^{\,d} \quad \text{on } \partial\Omega_u \tag{5.8}$$

$$T = T^d \quad \text{on } \partial\Omega_T \tag{5.9}$$

$$q = q^d \quad \text{on } \partial\Omega_q \tag{5.10}$$

with Γ_i^d and u_i^d the imposed stress and displacement vectors components, and T^d and q^d the imposed temperature and heat flux, at given and distinct space regions.
Once the parameters are known, a finite element code could be used to solve the system of equations.

5.3 A first and simple strategy to model energy piles

The numerical results presented in this section have been published in Yavari *et al*., 2014*b*.

5.3.1 Considered case studies

A commercial finite element code well-suited for geotechnical analyses was used to model the mechanical behaviour of energy piles under thermo-mechanical loadings. Temperature effects are not included in Plaxis 8.2. Thermal loading was therefore simply simulated by imposing on the pile volumetric strains corresponding to temperature changes. The numerical simulations were compared to the existing data on in-situ and physical model tests.

Three existing experimental studies have been considered. The first one corresponds to the in-situ tests reported by Laloui *et al*. (2003) and is referred to as 'Lausanne test'. A pile situated below a building under construction was equipped with a heating system, load cells, strain gauges, and thermometers. The drilled pile diameter was 0.88 m and its length was 25.8 m. The geological profile is summarised in Table 5.1. At various stages of the construction of the building, the temperature of the pile was increased by approximately 15°C and then the system was let cool down to the initial temperature. The first test (T1) was performed before starting the construction when the pile head was free to move. The other tests (T2 to T7) correspond to the heating/recovery test at the end of each construction stage. The results obtained show pile head displacement and variation of axial strain along the pile under different head loads during heating/recovery tests.

The second study considered is that presented by Bourne-Webb et al. (2009) and Amatya *et al*. (2012) and will be referred to as 'London test' within this chapter. A loading-test pile, 0.55 m in diameter and 23 m in length, including pipe loops for temperature control was installed in London Clay. After applying a constant mechanical load at the pile head, a cooling/heating cycle was applied to the pile; the temperature of the fluid circulating in the pile was varied between -2.5°C and 36°C. Temperature and strains were measured at various locations along the pile during the thermo-mechanical loading. The movement at the pile head was also recorded.

In the third work, Kalantidou *et al*. (2012) studied the soil/pile interaction while changing the temperature of the pile through a small-scale model. A model pile, which was a closed-end aluminium tube of 20 mm in external diameter and 600 mm in length, having its surface coated with sand, was embedded in compacted dry sand. After applying the axial load on the pile's head, the pile was heated from 25°C to 50°C and the system was let cool down to 25°C. The pile temperature and the pile head displacement were monitored.

More detail on the mentioned experiments could be found in Chapter 1.

5.3.2 Introduction of the numerical model

The models are considered to be axisymmetric. The dimensions are exactly the same as those of experiments. In the case of in situ tests, the extension of the simulated domain is chosen large enough to avoid boundary effects (at least 30 times the pile diameter). In the case of the physical model (Kalantidou *et al*., 2012), the dimensions of the soil container are precisely known and the same sizes are chosen in the numerical simulation. As an example, the mesh used for simulating Lausanne test is shown in Figure 5.1.

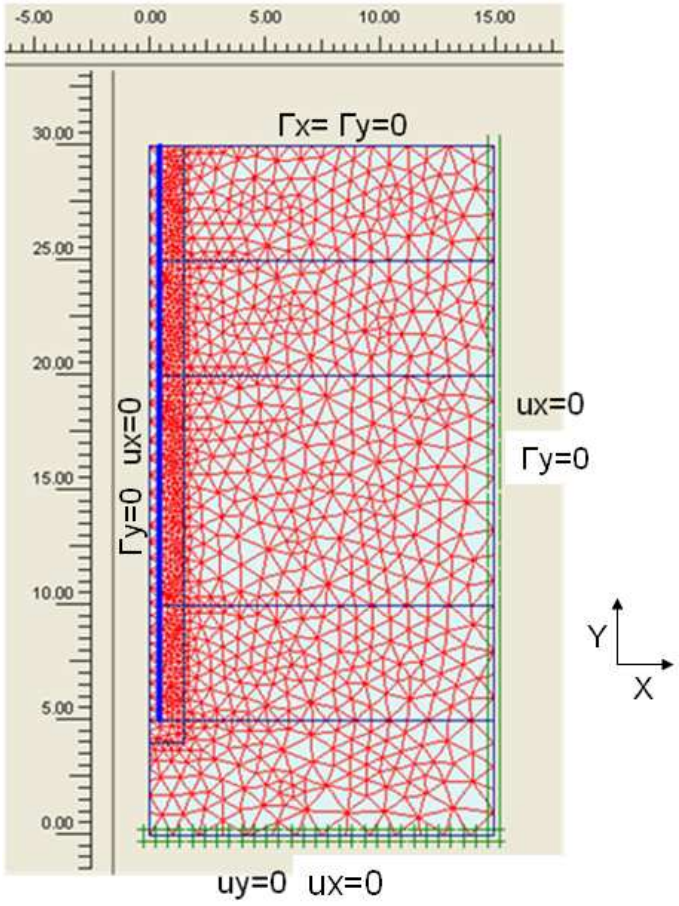

Figure 5.1 Utilised mesh and boundary conditions in the case of Lausanne test

The pile was modelled as an isotropic linear elastic non-porous material. For the soil, an isotropic linear elastic material with a failure criterion of Mohr-Coulomb type is chosen. The constitutive drained parameters and the drainage conditions are summarised in Tables 5.1 and 5.2. To analyse undrained behaviour, one of the possible methods which could be applied by Plaxis is the one based on effective parameters. In fact, the total (undrained) stiffness matrix ($\mathbb{C}$) is defined as follows:

$$\mathbb{C} = \mathbb{C}' + \frac{K_w}{n}\underline{\underline{1}} \tag{5.11}$$

Where $\mathbb{C}'$ is the effective stiffness matrix, K_w is the bulk modulus of water and n is the porosity.

Instead of specifying the components of $\mathbb{C}$, one could specify $\mathbb{C}'$ and K_w. Total stress will be then calculated as follows:

$$\Delta\sigma = \mathbb{C}\left(\Delta\varepsilon - \Delta\varepsilon^{P} - \Delta\varepsilon^{th}\right)$$

Table 5.1. Constitutive parameters of the soil in the case studies

Case study	London test		Lausanne test					Physical model
Material	Made ground (sand and gravel)	London clay	Alluvial soil	Alluvial soil	Sandy gravelly moraine	Bottom moraine	Molasse	Fontainebleau sand
Depth (m)	0-4	> 4	0-5.5	5.5-12	12-21.7	21.7-25.1	25.1-31	0-0.85
Drainage condition	Drained	Undrained	Drained	Drained	Drained	Drained	Undrained	-
γ (kN/m^3)	19	20	20	19.5	20	22	25.5	15.1
c' (kPa)	0	20	5	3	6	20	4	0
φ'	35°	25°	30°	27°	23°	27°	25°	36.5°
ψ	0°	0°	0°	0°	0°	0°	0°	0°
E (MPa)	13	70	260	260	450	630	3000	340
ν	0.3	0.3	0.3	0.3	0.35	0.35	0.22	0.30

γ, c, φ, ψ, E and ν are unit weight, cohesion, friction angle, dilation angle, elastic modulus and Poisson's ratio

Table 5.2. Constitutive parameters of the pile in the case studies

Case study	London test	Lausanne test	Physical model
Pile diameter (m)	0.550	1.000	0.020
E (GPa)	40.0	29.2	13.0
ν	0.20	0.20	0.33
α_v (10^{-6}/°C)	25.5	30.0	69.0

α_v is the volumetric coefficient of thermal expansion

The parameters and the drainage conditions for the case of Lausanne test are chosen according to numerical studies of Laloui *et al.* (2006). For the case of London test, parameters and drainage conditions are chosen following Amatya *et al.* (2012), Reeves *et al.* (2006) and Karakus & Fowell (2005). For the case of the physical model, the soil parameters are chosen according to the ones proposed by De Gennaro *et al*. (2008) for Fontainebleau sand. Regarding the dilatancy angle (ψ) as the manual compaction method used in the work of Kalantidou et al. (2012) was different than the pluviation method applied by De Gennaro *et al*. (2008), dilatancy angle was deduced from the manual compaction test performed by Combarieu (1999) on the same sand.

To evaluate the pile stiffness, considering that the model pile was an empty cylinder of aluminium, the modulus of elasticity is calculated for the equivalent section. According to Figure 5.2, the value of E_{eq} should be calculated such that Equation 5.11 is satisfied:

$$A_0 E_0 = A_{eq} E_{eq} \tag{5.11}$$

with A_0 =59.69 mm^2, A_{eq} =314.16 mm^2 and E_0 =69 GPa.

E_{eq} is thus equal to 13 GPa.

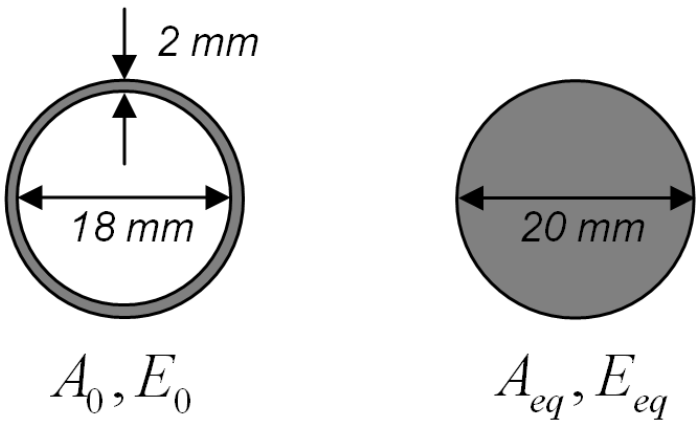

Figure 5.2 Original and equivalent pile sections in the case of an empty tube pile

For the three cases, the soil/pile interface was considered perfectly rough; in other words, no interface element was added. This assumption does not seem unrealistic considering the concrete surface of the in-situ piles and the sand-coated surface of the small scale model pile (see section 2.2.1.3). It should be noted that the interface elements are usually used when studying soil/pile interaction under complex mechanical loading, including cyclic and lateral ones (Yang & Jeremic, 2005; Nogami *et al.*, 1992; Said et al., 2009). In the present study, the mesh is refined in this zone, where significant stress gradients are expected.

To simulate thermal effects on the mechanical behaviour, the volumetric thermal deformation $\alpha_v \Delta T$ corresponding to temperature change ΔT was imposed to the pile, where α_v is the volumetric coefficient of thermal expansion and is equal to three times the lineal coefficient of thermal expansion. For simplicity, spatial variation of temperature along the pile was neglected in simulations and a mean value was considered in each step. In a first approach, the thermal expansion of the soil was not considered. This decoupling between thermal and mechanical effects permits to use existing numerical codes and to perform simple computations.

Initial stresses are calculated on the basis of the soil and pile unit weight and the depth of the soil layer and pile length. The coefficient of earth pressure at rest (K_0) is taken as 1-sinφ'. Applied boundary conditions could be observed in Figure 5.1. At lateral boundaries, horizontal displacements are blocked. Lateral boundaries are stress free in the perpendicular direction. Vertical fixities are applied at the bottom of the mesh.

To model the boundary conditions at the pile head in the experiments of Bourne-Webb *et al.* (2009) and Kalantidou *et al.* (2012), only the axial force (equal to that imposed in the experiments) was applied. In the case of Laloui *et al.* (2003), as the pile head was restrained by the building, axial force equal to that measured at the pile head during each step was imposed.

5.3.3 Numerical simulation

The results obtained from test presented by Laloui *et al.* (2003) and the simulation results are shown in Figure 5.3 and Figure 5.4. Seven heating/recovering cycles were applied; each cycle corresponds to a stage of the construction of the building. Figure 5.3*a* presents the change of mean temperature along the pile for each heating/recovering cycle. In Figure 5.3*b*, the pile head displacement during these cycles is presented. Pile axial strains measured at various depths are shown in Figure 5.3*c-f*. Comparison between the simulation and the

experimental results shows that the mechanical behaviour of the pile can be predicted correctly not only in terms of pile head displacement but also in terms of axial strain at various depths.

For further comparison, the axial strain profiles (measured and modelled) along the pile at the end of each heating (or recovering) step are shown for the first test (T1) where construction was not started yet (Figure 5.4*a* and Figure 5.4*b*). In Figure 5.4*c* and Figure 5.4*d*, temperature values measured and modelled along the pile are shown. Strain profiles show generally good agreement between the simulation and the measured ones, although in the actual test the behaviour seems rather reversible in the recovery phase. Discrepancies between simulation and experimental data can be explained partly by the difference in the temperature profiles.

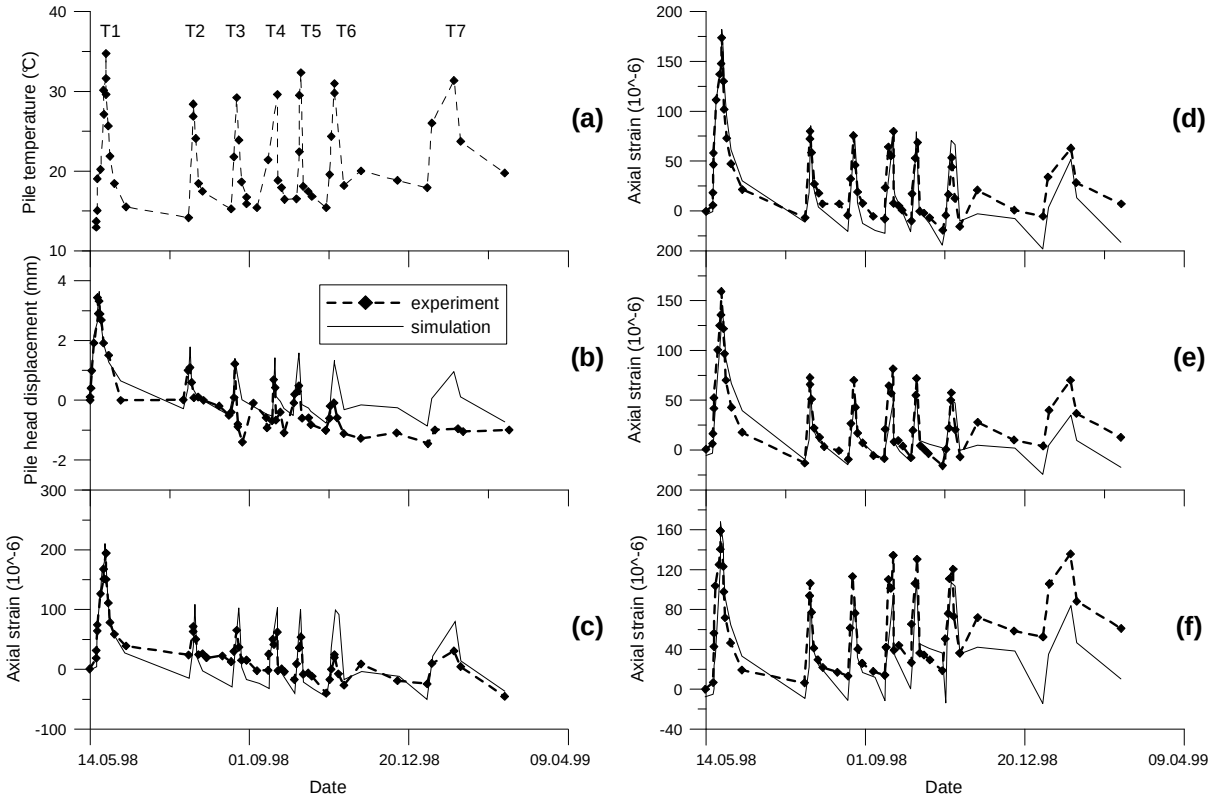

Figure 5.3 Results of Lausanne test: (a) Pile temperature; (b) Pile head displacement; (c) Pile axial strain at 2.5 m depth; (d) Pile axial strain at 10.5 m depth; (e) Pile axial strain at 16.5 m depth; (f) Pile axial strain at 24.5 m depth

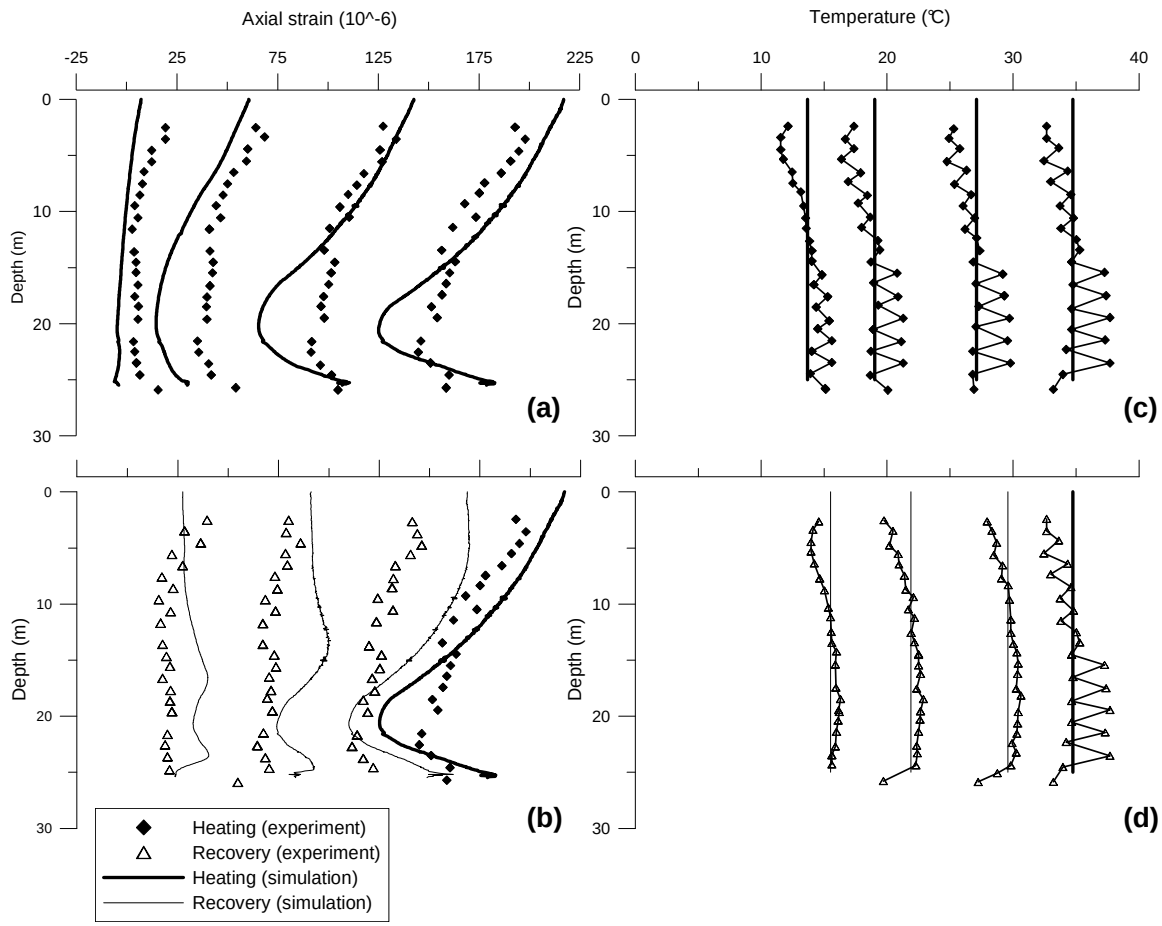

Figure 5.4 Results of Lausanne test: (a) Pile axial strain distribution during heating; (b) Pile axial strain distribution during recovering; (c) Temperature evolution of pile during heating; (d) Temperature evolution of pile during recovery

The results obtained from the tests presented by Bourne-Webb *et al*. (2009) are shown in Figure 5.5 and Figure 5.6. During the test, the pile was first loaded to 1800 kN and then unloaded. Reloading was performed up to 1200 kN. From the initial temperature (20°C), the pile was cooled with a circulating fluid at a temperature of about -2.5°C kept constant for about one month. Then the fluid was heated to about 36°C (Figure 5.5*a*). In Figure 5.6.a, the temperature changes measured along the pile (as detailed in Bourne-Webb *et al*., 2009) are shown for the end of the cooling phase and the end of the subsequent heating phase. It is observed that the cooling phase decreased the average pile temperature by 18°C and that the pile temperature is 9°C higher than the initial one at the end of the heating phase. In Figure 5.5*b*, pile head displacement during different stages is shown. A good agreement between numerical and experimental results could be observed during mechanical and cooling steps while simulations overestimate pile head heave during heating. In Figure 5.6*b*, the axial strain profiles along the pile are plotted for three stages: end of the mechanical loading, end of the

cooling, and end of the heating phases. The simulation is in good agreement with results recorded by strain gauges (after Amatya *et al.*, 2012) during the distinct phases.

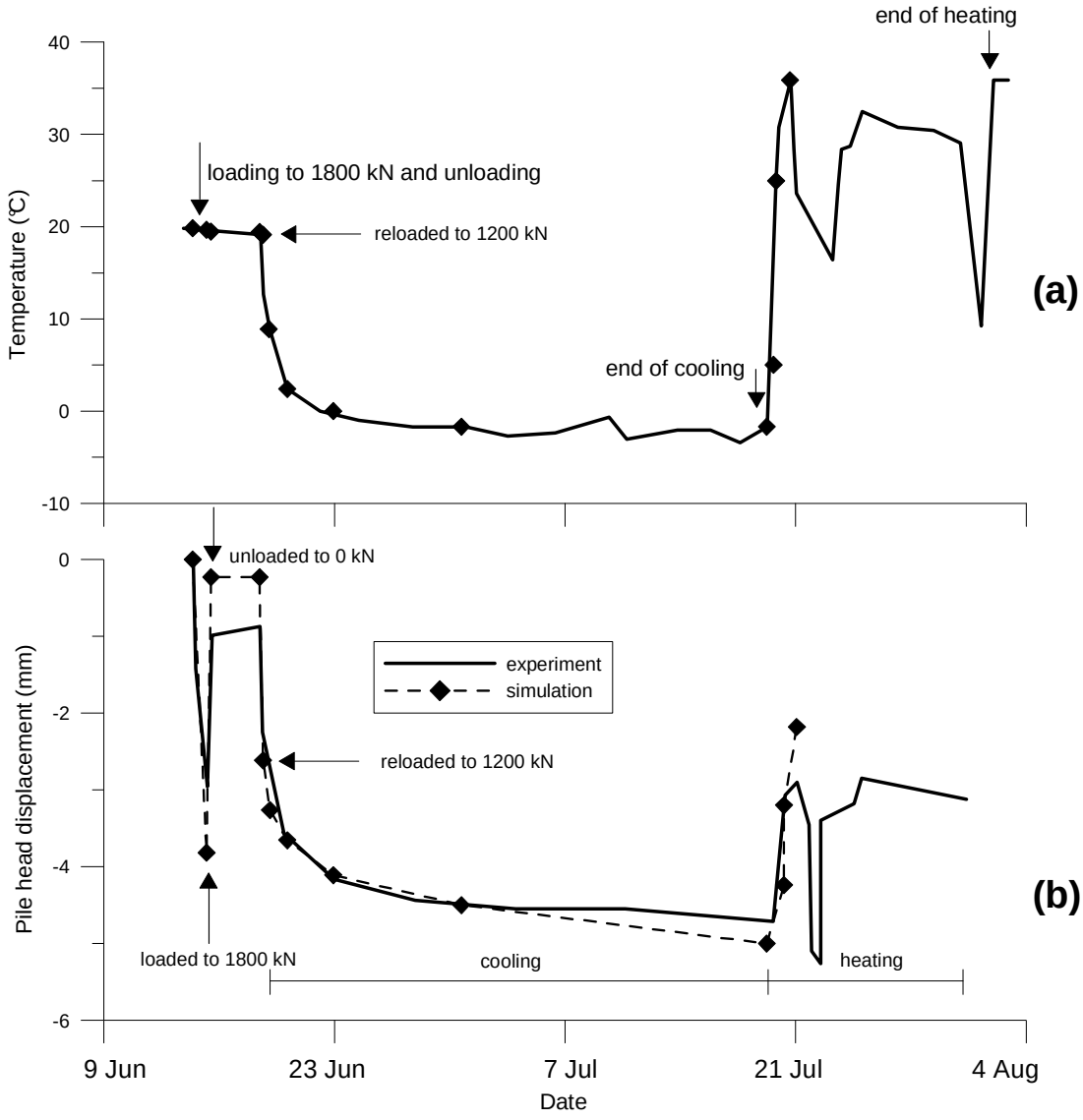

Figure 5.5 Results of London test: (a) temperature of the circulating fluid; (b) pile head displacement

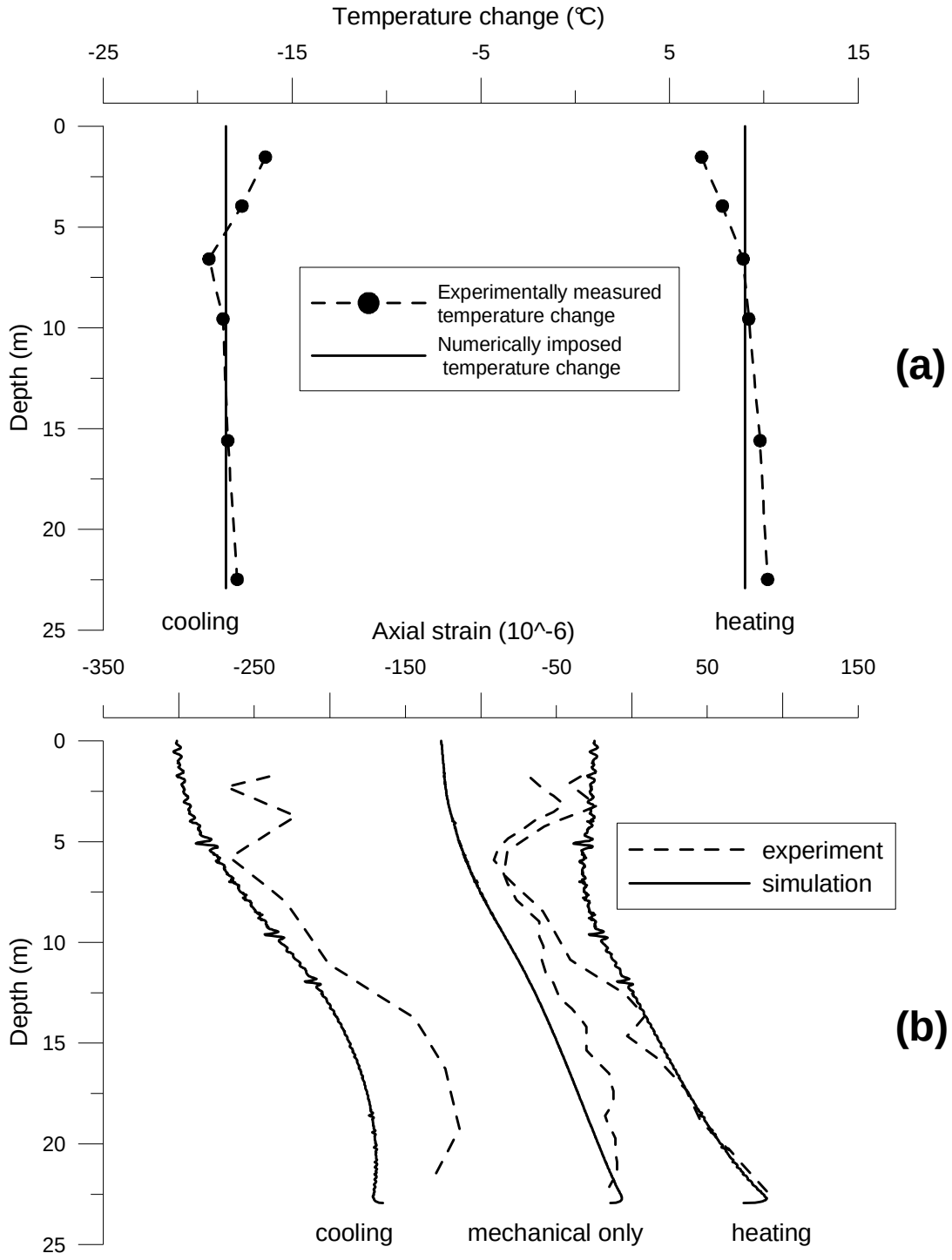

Figure 5.6 Results of London test: (a) profile of temperature along the pile; (b) pile axial strain distribution

The load-settlement curve obtained from the work of Kalantidou *et al*. (2012) is shown in Figure 5.7. Experimental and numerical curves are in acceptable consistency. The results obtained during the heating/recovering tests under constant load are shown in Figure 5.8. It should be noted that 'thermal settlement' in each test is obtained by removing the mechanical

settlement of the pile under the corresponding load, which was obtained at the end of the mechanical loading step and just before that thermal loading begins to be applied. As could be observed, without the pile head load (Figure 5.8*a*) the simulation is similar to the experimental results. Under 200 N of pile head load (Figure 5.8*b*), a large disparity between the two sets of curves could be observed. During the first heating, pile heave is about twice higher in the test. Besides, the pile behaviour seems more reversible compared to the numerical results. On the contrary, at 400 N and 500 N of pile head load (Figure 5.8*c*), a good compatibility could be found. It should be stated that in 1g-physical models, geostatic stress levels are relatively low; this increases experimental inaccuracies and modelling difficulties and could explain some of the discrepancies observed above.

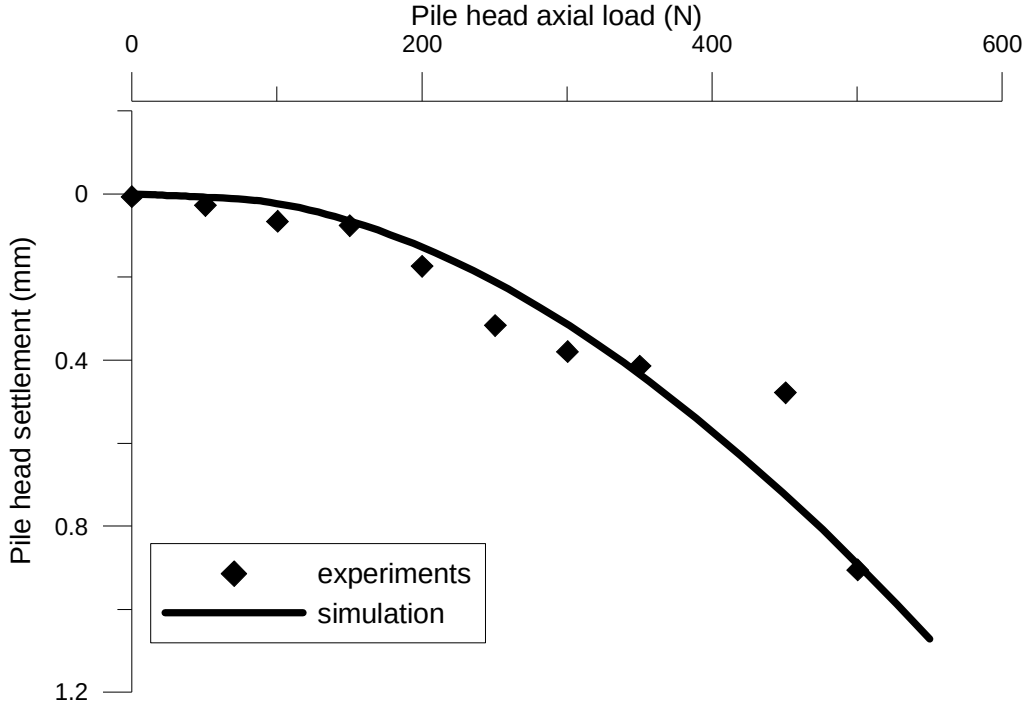

Figure 5.7 Results of the small-scale test: load-settlement curve

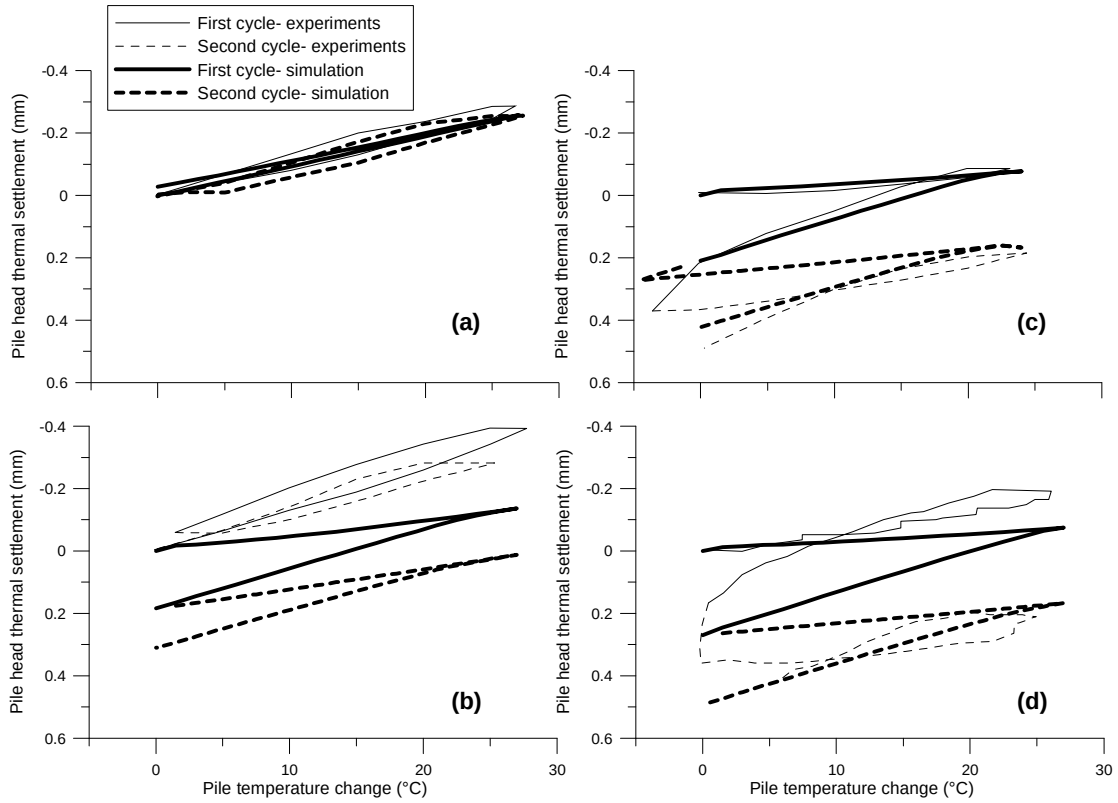

Figure 5.8 Results of the small-scale test: Temperature-settlement curves under different head loads: (a) 0 N; (b) 200 N; (c) 400 N; (d) 500 N

5.3.4 Discussion

Mechanical behaviour of an energy pile is affected by the thermal volume change in the pile and in the soil, soil and pile parameters changes due to temperature changes, and sensitivity of soil/pile interface characteristics to thermal loading (Laloui *et al.*, 2006). In the first part of the numerical studies, for the sake of simplicity, only the pile's thermal volume change is taken into account. A commercial code which is used by thousands of consulting engineers worldwide and is renowned for its simplicity and accurate soil constitutive models is chosen. Another decoupling procedure was also used before by Knellwolf *et al.* (2011). The present study shows generally good agreement between experimental data and numerical simulation. This means that the mechanical behaviour of the pile is mainly governed by its thermal volume change and the thermal volume change in the soil has less influence. The disparity between experimental results and simulation could be explained first by the assumption that the temperature of the pile is homogenous. The second reason can be related to the lack of interface element in the numerical simulation. The results obtained in this study could encourage the geotechnical engineers to use the same software in modelling the behaviour of an energy pile.

It is important to distinguish ‘cooling’ and ‘recovery’ notions. In the experiments of Laloui *et al*. (2003) and also the mentioned small-scale test, the pile temperature decreased freely with time and not by imposing low temperatures directly. In other words the speed of thermal loading was smaller in the recovery method, which is comparable to drained mechanical loadings in general. Time effects related to loading phases are not accounted for in our approach. That might be one source of the overestimation of irreversible deformations by the model in the recovery phase of Lausanne test. Another point is that application of thermal volume changes to the pile while no thermal volume changes are considered for the surrounding soil might induce a more abrupt response of the pile. In practice, in the presence of heat diffusion from the pile to the soil, the temperature field (and the consequent volumetric expansions or contractions) would be more uniform, which could lead to more uniform axial deformation distribution, as observed in the experiments presented by Laloui *et al*. (2003).

In the second part of the numerical studies, it was intended to simulate the tests performed on the small scale model within this research (as presented in Chapters 2 and 3) and compare the mechanisms observed in the experiments and in the numerical model. The numerical work aims to provide a better understanding on the model pile behaviour; as discussed in Chapter 3, the experimental results contradict somehow the ones obtained on real scale energy piles until now, chiefly in terms of pile axial force variation by heating and cooling. The finite element code was changed for multiple reasons. By simulating the performed tests it was not only planned to evaluate the mechanical behaviour of the pile but also to model the heat diffusion in the soil and compare the temperature values tracked by transducers to the computed ones. Thus a numerical code with the ability of considering thermal effects was needed. Besides, as the experiments were performed at a small scale, thermal volume change in the soil may also play a more significant role. In order to take into account these effects, the same method as the one used in Plaxis could not be applied because contrary to the pile, the soil temperature change (and thus the corresponding volumetric thermal strains) is not constant and is a function of time and distance from the pile.

5.4 Numerical modelling by CESAR-LCPC

5.4.1 Introduction of the numerical model

As a computational tool, CESAR-LCPC program, which is a general finite element calculation code dedicated primarily to civil engineering problems, was used. The mentioned

code was utilised in order to simulate the experiments shown in Chapters 2 and 3. As the problem is of an axisymmetric nature, the problem could be reduced to a two-dimensional one. The dimension of the pile and the soil container were adopted according to the real conditions (as shown in Figure 2.1). The mesh consisted of 2509 6-node triangular elements (5098 nodes in total). The generated mesh is shown in Figure 5.9. At the vicinity of the pile, where shear strain localisation is susceptible to happen (Saggu & Chakraborty, 2014b), the mesh was refined.

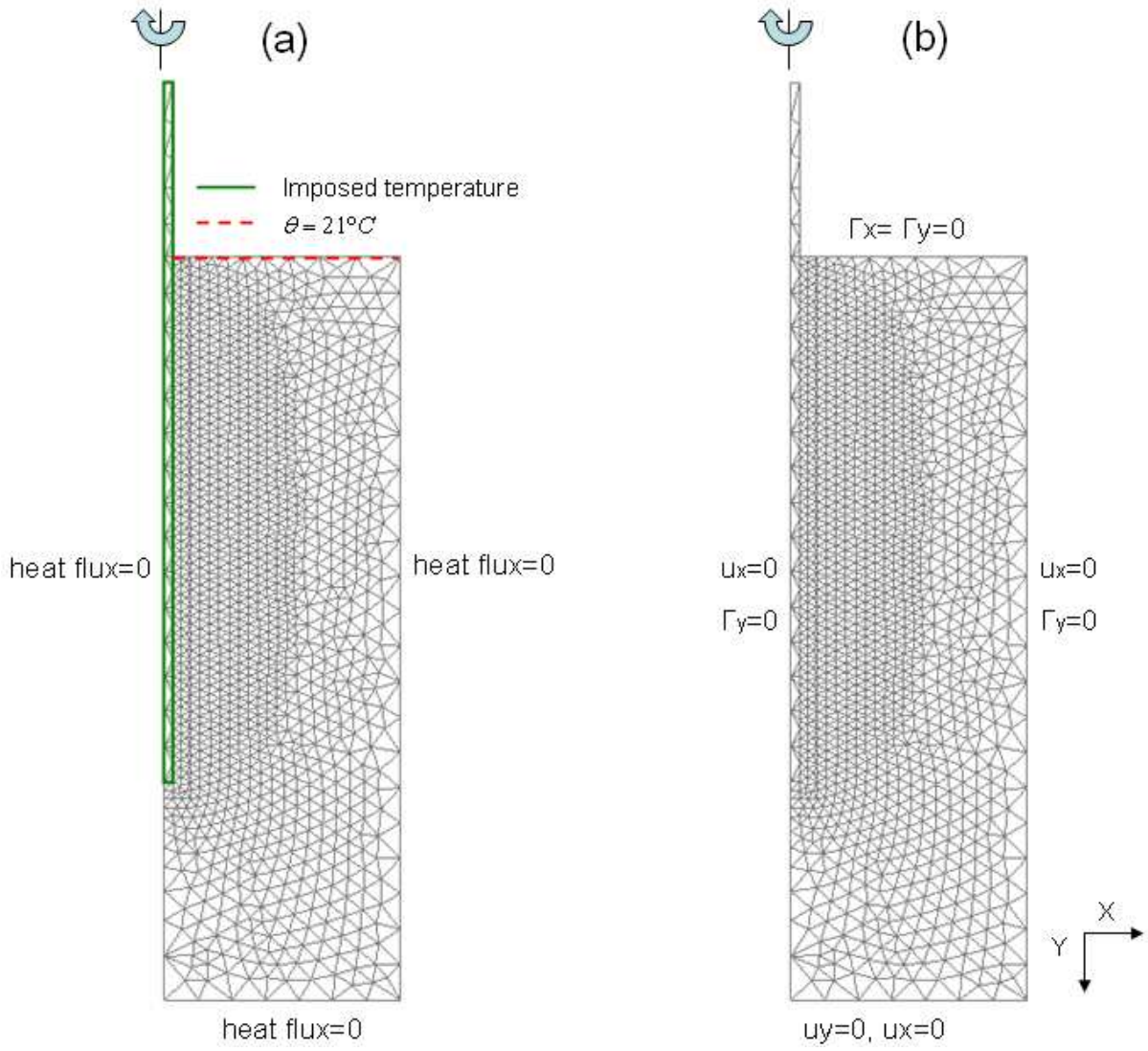

Figure 5.9 (a) Thermal boundary conditions and (b) mechanical boundary conditions for the small scale tests analysed with CESAR-LCPC code.

The mechanical and thermal parameters of soil and pile are shown in Table 5.3. The parameters of the pile are the ones previously chosen for modelling the tests performed by

Kalantidou *et al*. (2012) as a pile with the same dimension and characteristics was utilised in the present experiments. The pile was modelled as an isotropic linear elastic material. Concerning the soil, thermal parameters were measured on dry Fontainebleau sand during the experiments using the 'KD2 Pro thermal Properties analyzer'. A standard Mohr-Coulomb type failure criterion was assigned to the soil. The mechanical parameters were basically chosen according to the work of De Gennaro *et al*. (2008), with the same considerations as in the case of modelling the experiments of Kalantidou *et al*. (2012), in section 5.3.2. No interface elements were added, which corresponds to a perfect at the soil/pile interface.

Table 5.3. Constitutive parameters of soil and pile for the physical model

Mechanical and thermal parameters	Soil	Pile
γ (kN/m^3)	15.1	11.7
E (MPa)	340	13000
ν	0.30	0.33
c' (kPa)	0.10	-
φ'	34°	-
ψ	0.5°	-
k (W/(m°C))	0.2	237
C_v (10^6 Wsec/ m^3 °C))	1.2	2.4
α (10^{-6}/°C)	1	23

In the calculation code used, the DTLI calculation module of CESAR-LCPC allows to calculate the evolution of the temperature field of a structure subjected to a thermal loading, which is applied in terms of thermal boundary conditions. The heat transfer problem could be solved under transient or permanent regimes.

The calculation module MCNL allows modelling materials whose behaviour is elasto-plastic (with or without hardening) or non-linear elastic. In general, the solution of a problem addressed by MCNL is independent of time. The calculation module MCNL allows, in a single calculation, to decompose the applied load, as well as non zero imposed displacements, in increments which could be equal or not.

With respect to thermal boundary conditions, the axis of symmetry is an adiabatic boundary. The elements which are submitted to a constant temperature are shown in Figure 5.9*a*. A constant temperature of 21°C was applied to the soil top surface which is equal to ambient temperature during the experiments. The temperature applied to the pile wall was

constant at each phase and was defined according to thermal steps applied in the corresponding experiment. Heat exchange at the right hand side and the bottom of the mesh was cancelled; a zero heat flux was imposed to these regions. As it was aimed to perform the calculations under a transient regime, an initial temperature was also needed. The initial temperature of the overall structure was set to 21°C .

Concerning the mechanical initial conditions, initial stresses were defined by soil unit weight (which is 15.1 kN/m^3) and the depth of the soil layer. The coefficient of earth pressure at rest (K_0) was set to 0.44, which is equal to $1-\sin\varphi'$ (Jáky's equation). As the soil in the experiment was not an overconsolidated one, the formulation utilised should be representative of the at rest coefficient (Boháč *et al.*, 2013). In terms of mechanical boundary conditions, the horizontal displacements were restricted on the right and left hand side of the mesh. Lateral boundaries were also stress free in the perpendicular direction. At the bottom, vertical fixities were applied. Thermal and mechanical boundary conditions are shown in Figure 5.9.a and Figure 5.9.b, respectively.

Simulation of each thermal test started by generating temperature fields according to the experimental thermal loading programme. Thermal loading programme applied in test E2 is shown as an example in Figure 5.10. Temperature values are the ones recorded by the temperature transducer on the pile surface, shown by T1 in Figure 5.10. In order to simulate these thermal steps, 19 phases were created, which are denoted 'th_i'. A transient regime was chosen for the thermal analysis, which considers the time during which the corresponding temperature increment was applied to the pile. The initial temperature field at each stage is actually the final temperature field in the previous one.

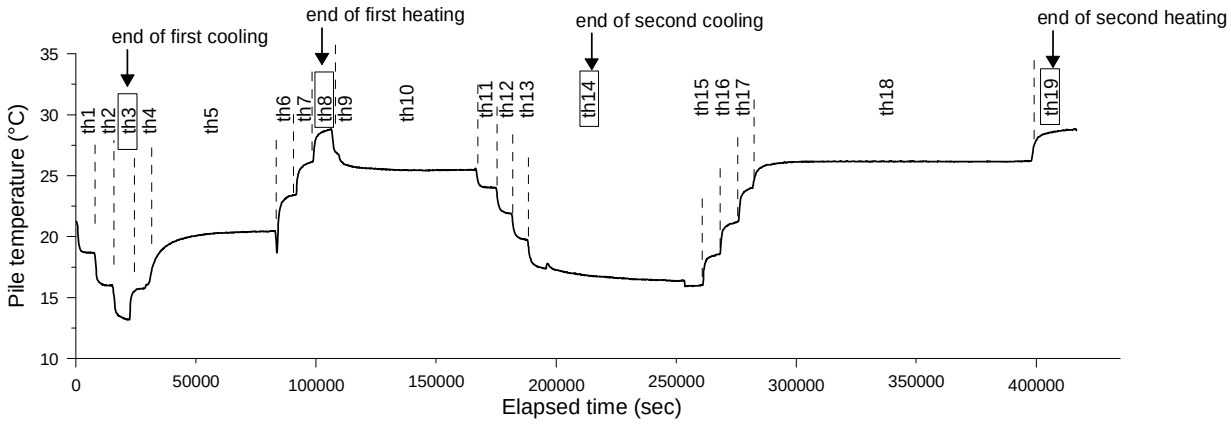

Figure 5.10 Thermal loading programme in test E2

Mechanical loading was composed of five successive dependent stages. Each phase initiated on the basis of the results of the last one. Detailed description of the stages is shown in Table 5.4. In the purely mechanical loading stage (which is represented by 'M' in Table 5.4), load was applied to the pile head incrementally. The increments are the same as the ones applied during the concerning experiment. The subsequent stage aimed to calculate the response of the structure subjected to the first cooling phase. Generally speaking, in order to add up thermal effects, thermal dilation coefficient of the pile and the soil, a reference temperature according to which temperature changes are calculated and a temperature field were entered as inputs. The reference temperature in stage THM1, which calculates the response of the structure at the end of first cooling, was equal to ambient temperature (21°C) and the temperature field provided as input was the one created in th_3. To perform the calculation in the subsequent heating stage, which is denoted by THM2 in Table 5.4, reference temperature could be no more equal to 21°C; as the pile and the soil at its vicinity were already cooled, a uniform temperature could not be attributed to the total structure. In order to get rid of this temperature non-uniformity, a new temperature field was first created which is equal to the difference between the temperature field at the end of heating and that at the end of cooling (th_8 - th_3). Doing so, the reference temperature could be taken as zero. The same procedure was applied on stages THM3 and THM4. It should be noted that in the mechanical analysis, the response of the structure was evaluated only at the end of cooling and heating procedures and the intermediate thermal steps were ignored. In simulating test E8, 60 thermo-mechanical stages were introduced to represent 30 thermal cycles.

Table 5.4. Loading path applied in simulating test E2

Loading stage	Reference temperature	Initial temperature field	Final temperature field
M	21°C	-	-
THM1 (end of first cooling)	21°C	-	th_3
THM2 (end of first heating)	0°C	th_3	th_8
THM3 (end of second cooling)	0°C	th_8	th_{14}
THM4 (end of second heating)	0°C	th_{14}	th_{19}

5.4.2 Numerical simulation of tests E1 to E7

Figure 5.11 through Figure 5.13 show the results of test E1, which was a purely mechanical test. Load-settlement curve observed in the experiment is compared to the one obtained via the simulation in Figure 5.11. A good compatibility between the two curves could be observed, while generally, the pile settlement is greater in the experiments than in the simulation, under the same load value. Considering 2 mm (which is equal to 10% of the pile diameter) as the pile head displacement at failure (AFNOR, 1999), the ultimate load value is the same in the simulation and the experiment and equal to 450 N.

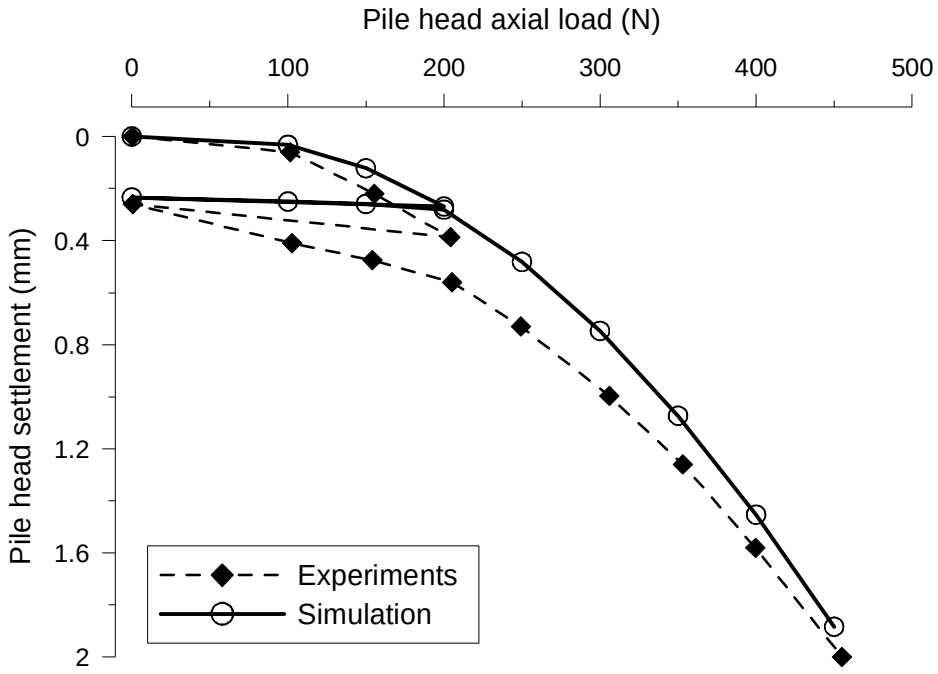

Figure 5.11 Measured and calculated load-settlement curve (test E1)

Total pressure values at different positions in the soil are shown in Figure 5.12. Pile head load at each increment is shown in Figure 5.12*a*. The initial stress point, which shows the pressure value at time 0, is the value of the pressure at rest. The initial values of vertical stress should be equal (or comparable) to the predicted value of γz (where γ=15.1 kN/m^3), while the horizontal stress is about $K_0 \gamma z$. From this point of view, experimental initial vertical and horizontal stress values below the pile (at positions P2 and P3, shown in Figure 5.12*a* and Figure 5.12*b*) are slightly greater than the ones obtained via simulation. Numerical and experimental vertical stress increase as the head load value increases (Figure 5.12*a*). The corresponding values are also close to each other. According to Figure 5.12*b* horizontal stress

tends to increase by loading steps both in numerical and experimental results, while the quantitative difference between the results is more pronounced than in the case of vertical stress (Figure 5.12*a*). Vertical stress measurements in different depths at the vicinity of the pile could be observed in Figure 5.12*c* and Figure 5.12*d*. Initial stress values are superposed and good compatibility continues during the subsequent loading increments. Either in the simulation and in the experiments, the stress value is independent of pile head load. Horizontal stress variation near the pile at depth of 300 mm (position P8) is shown in Figure 5.12*e*. It seems that there was a problem in the measurements as the values, from the initial one to the last one, are almost zero. With respect to the numerical results, horizontal stress does not change with the pile head load level. The radial stress evolution at the same depth during the test could be observed in Figure 5.12*f*. A good consistency between experimental and numerical values could be detected. In general, stress level in the soil is more sensitive to the pile head load at the pile toe than in the zones near the pile skin.

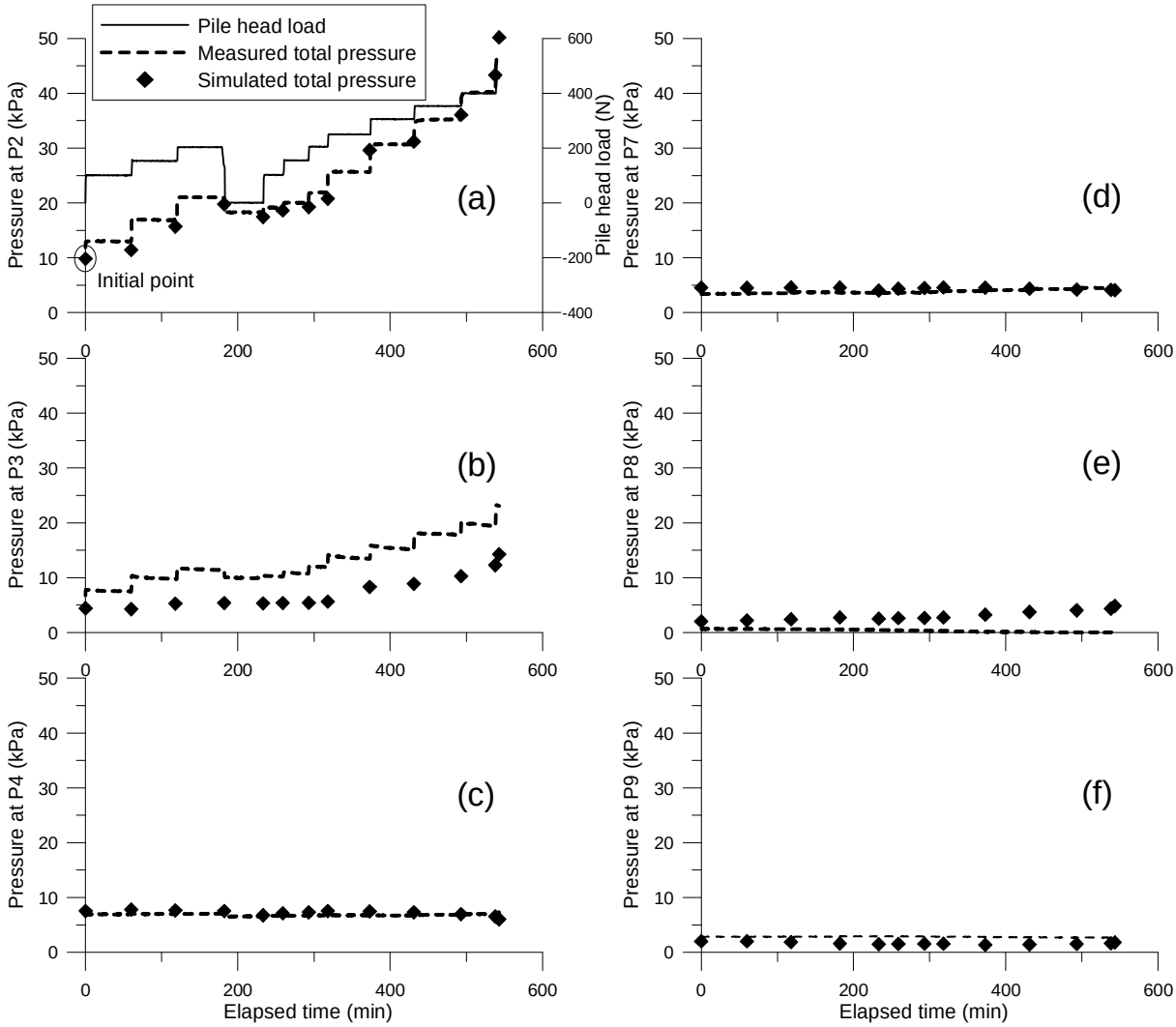

Figure 5.12 Measured and calculated curves: Total pressure changes in test E1 at: (a) P2; (b) P3; (c) P4; (d) P7; (e) P8; (f) P9

Axial load distribution along the pile under different head load values is presented in Figure 5.13. The slope of the load distribution curve gives an idea on the mobilised lateral friction. A gentler slope indicates that more friction has been mobilised. According to the numerical results, until 100 N of head load, almost 100% of the head load is transferred to the pile toe. As the head load increases, lateral friction mobilises and under 400 N, the pile toe supports 50% of the load. While in the experimental load distribution profiles, even under 200 N, 90% of the head load is sent to the pile toe. At 400 N of load, only 25% of the head load is carried by lateral friction and the rest is transferred to the pile toe.

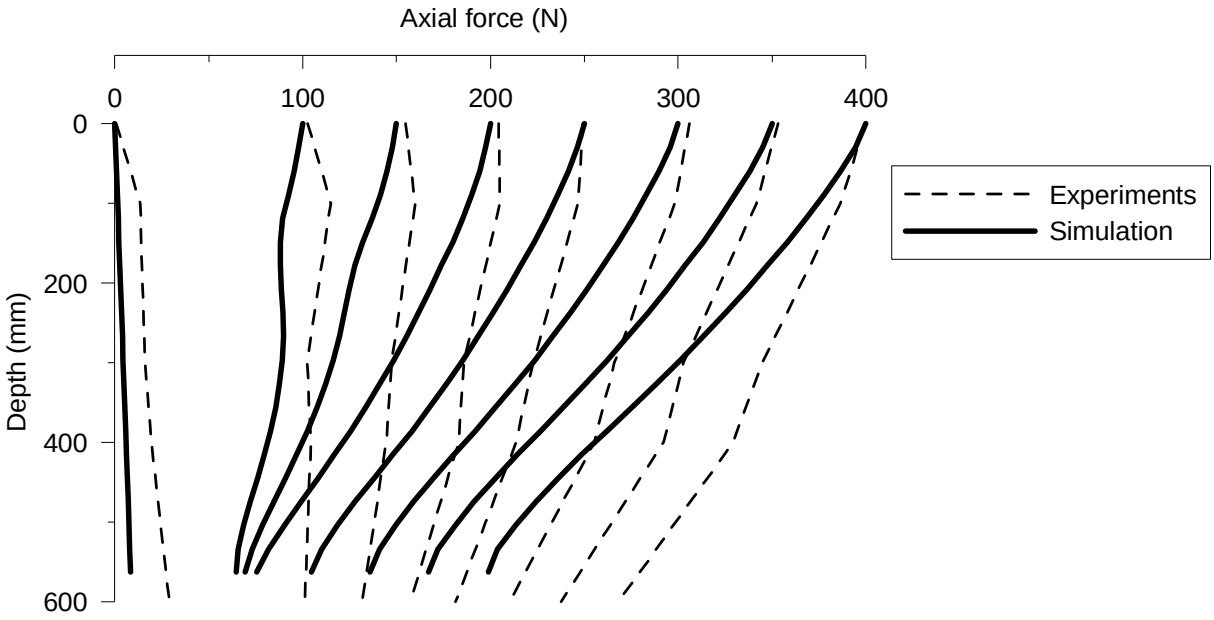

Figure 5.13 Axial force distribution along the pile (test E1)

The results of the thermo-mechanical experiments (test E2 to test E7) are exhibited in Figure 5.14 to Figure 5.20. The temperature fields obtained at the end of first cooling (stage th_3) and the one calculated at the end of first heating (stage th_8) in test E2 are exhibited in Figure 5.14*a* and Figure 5.14*b*, respectively. Temperature distribution in the soil at the depth of 300 mm is plotted in Figure 5.15. The experimental curves are the ones measured during test E2 under the thermal loading programme shown in Figure 5.10. In the simulation, the same thermal loading programme was applied to the pile. As expected, soil temperature is less stable and more sensitive to the pile temperature changes at 50 mm from the pile wall, where transducer S7 is located. This could be investigated in Figure 5.15*a* both in experimental and numerical results. At greater lateral distances, where transducers S8 and S9 are located (Figure 5.15*b* and Figure 5.15*c*), soil temperature does not change significantly during thermal cycles. Experimental and numerical results are in a good quantitative agreement. Numerical values at S2 and S3 are slightly higher than the experimental ones. There exists a difference of 0.5°C at the start which indicates that the initial temperature field has not been uniform in the soil in the experiment while a uniform one was considered in the numerical model.

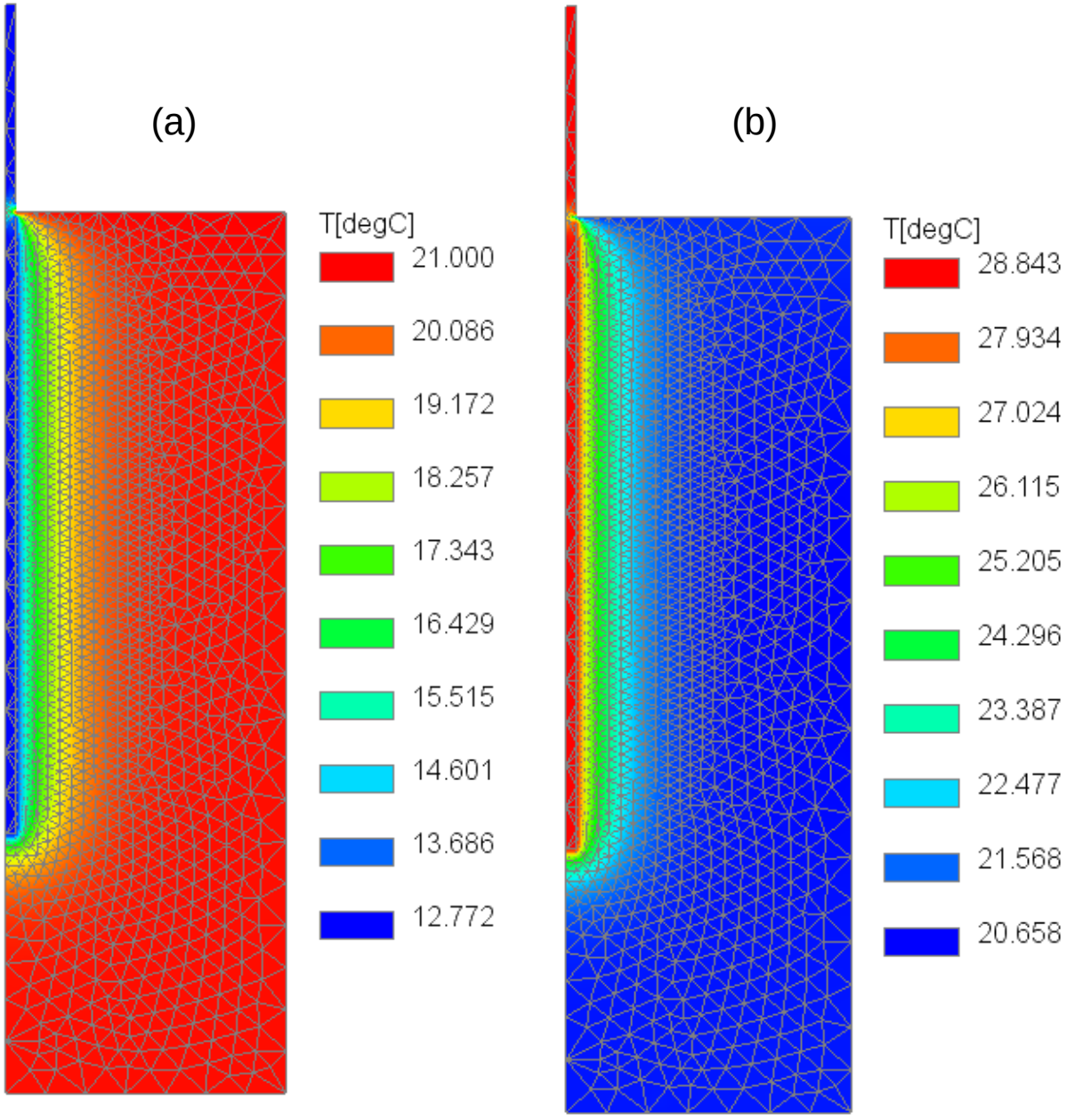

Figure 5.14 Simulated temperature fields in test E2: (a) at the end of first cooling (b) at the end of first heating

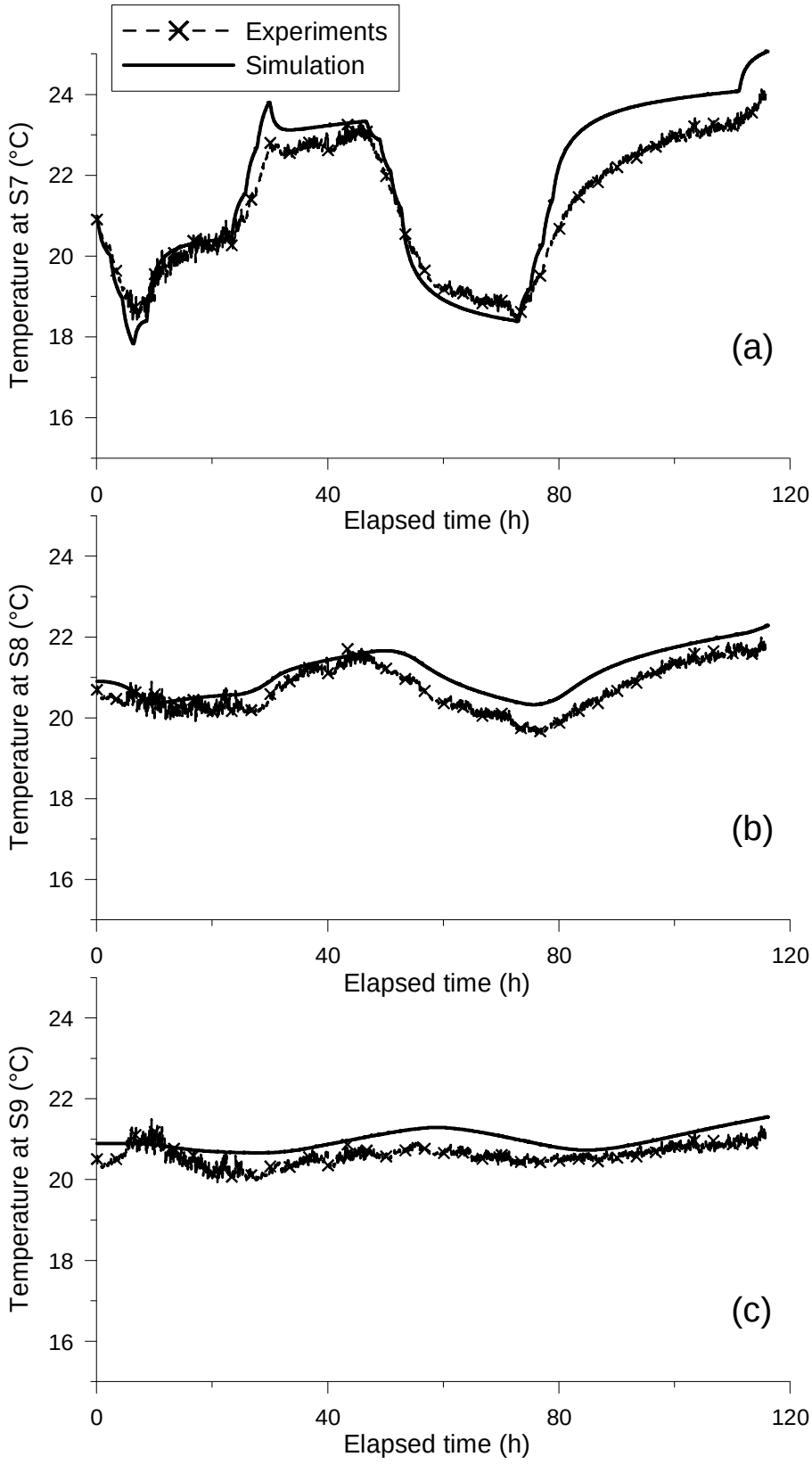

Figure 5.15 Temperature variation in test E2 at depth of 300 mm at the lateral distance of: (a) 50 mm from the pile, (b) 150 mm from the pile, (c) 250 mm from the pile

Pile settlement during thermal cycles under different head load values is analysed subsequently. In the experiments, in order to capture thermal displacements, the displacement transducers were zeroed just before the application of thermal cycles and therefore the displacement values resulting from the mechanical phase were neglected. Before comparing experimental and numerical results, some corrections were made on the experimental data. In Figure 5.16, pile head displacement versus temperature measured during test E2 through test E7 is shown in dashed lines. Pile head settles down during the first cooling phase. It tends to heave during the succeeding heating phase, while the displacement does not return to zero. The same observation remains valid on the second cooling and heating cycle. That means pile continues to settle as thermal cycles proceed. What is unusual in these curves is that the settlement during the first cooling is almost linear and has a certain slope, but it does not go on continuously on the same line; some steps could be observed in the curves during which the temperature change is constant but the pile settlement continues. This phenomenon is more visible in Figure 5.16*f* which plots the pile settlement under 300 N. During the first cooling, once the temperature change reaches -4°C, the pile settlement is equal to 0.1 mm. Temperature remains unchanged but the pile continues to settle down to 0.3 mm. The curve resumes its regular trend afterwards and pile settles with the same slope as before. Time effects could explain this observation. As stated in the experimental loading programme, each thermal loading step was maintained for at least two hours. As the tests continued during the night (or sometimes weekend), it was not possible to keep the rhythm and continue with the same timing steps (see Figure 5.10). As a consequence, the pile was subjected to some constant temperature during a long time, while its settlement does not stabilise. In numerical simulations time effects are not considered. In order that the experimental results be comparable to numerical ones, time effects should be removed. The thick lines in Figure 5.16 are plotted using the initial and final temperature change values and the governing slopes in the cooling and heating phases which was obtained regarding the raw data (dashed lined curves).

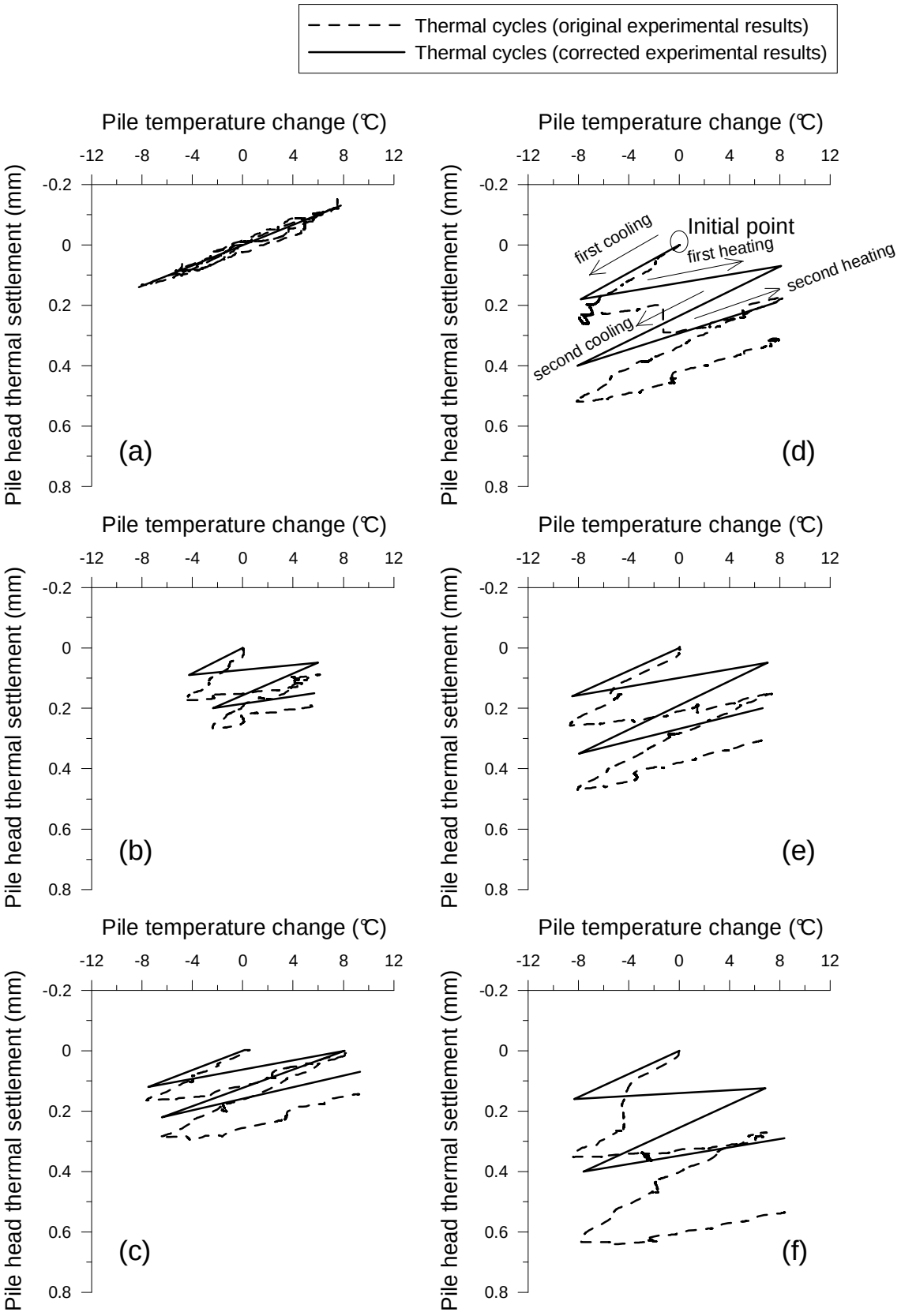

Figure 5.16 Pile thermal settlement versus pile temperature; raw and corrected data obtained from tests: E2(a), E3(b), E4(c), E5(d), E6(e), E7(f)

Pile settlement versus temperature obtained via simulation is then compared to the corrected experimental one in Figure 5.17. Other than these two curves, pile thermal expansion curve is also plotted. The latter expresses the expansion or contraction of a pile that is restricted by its toe and is free to move in the other direction. It is noted that this pile will be called the 'free pile' within this chapter. The slope of the curve is then equal to α (thermal expansion coefficient of the pile which is equal to 23×10^{-6}/°C). This slope could be compared to the slope of the first cooling in simulation and experiments. As could be seen in Figure 5.17*a*, that pile behaviour under 0 N is thermo-elastic both in numerical and experimental models. Quantitatively, pile settlement and heave are greater in the experiment. During cooling, pile experimental settlement is also greater than the case of the free pile, while the pile head settles less in simulation. As plotted in Figure 5.17*b*-*d*, numerical pile settlement during the first cooling is compatible with the pile thermal expansion curve. Pile settles more in this phase in the experiments (test E3 to test E5). By successive heating, pile heaves. Under 100 N of load (Figure 5.17*b*) until 200 N (Figure 5.17*d*), pile head returns to its initial state according to numerical results, while in the experiments even under 100 N, the pile heave during the first heating does not compensate its settlement during the first cooling. Under 250 N (Figure 5.17*e*) and 300 N (Figure 5.17*f*) both in the simulation and the experiments, pile displacement remains positive during the first heating and pile does not return to its initial position. As could be observed in Figure 5.17*b* through Figure 5.17*f*, pile settles by the second cooling phase, both in the simulation and in the experiment. The slope of the second cooling is the same as the first one in the experiment while the slope of the first cooling is steeper than the second one in the numerical curves. Slopes of the first and second heating are steeper in the simulation than in the experiments. Both numerically and experimentally, pile continues to settle during thermal cycles and as the head load value increases more irreversible deformations are produced.

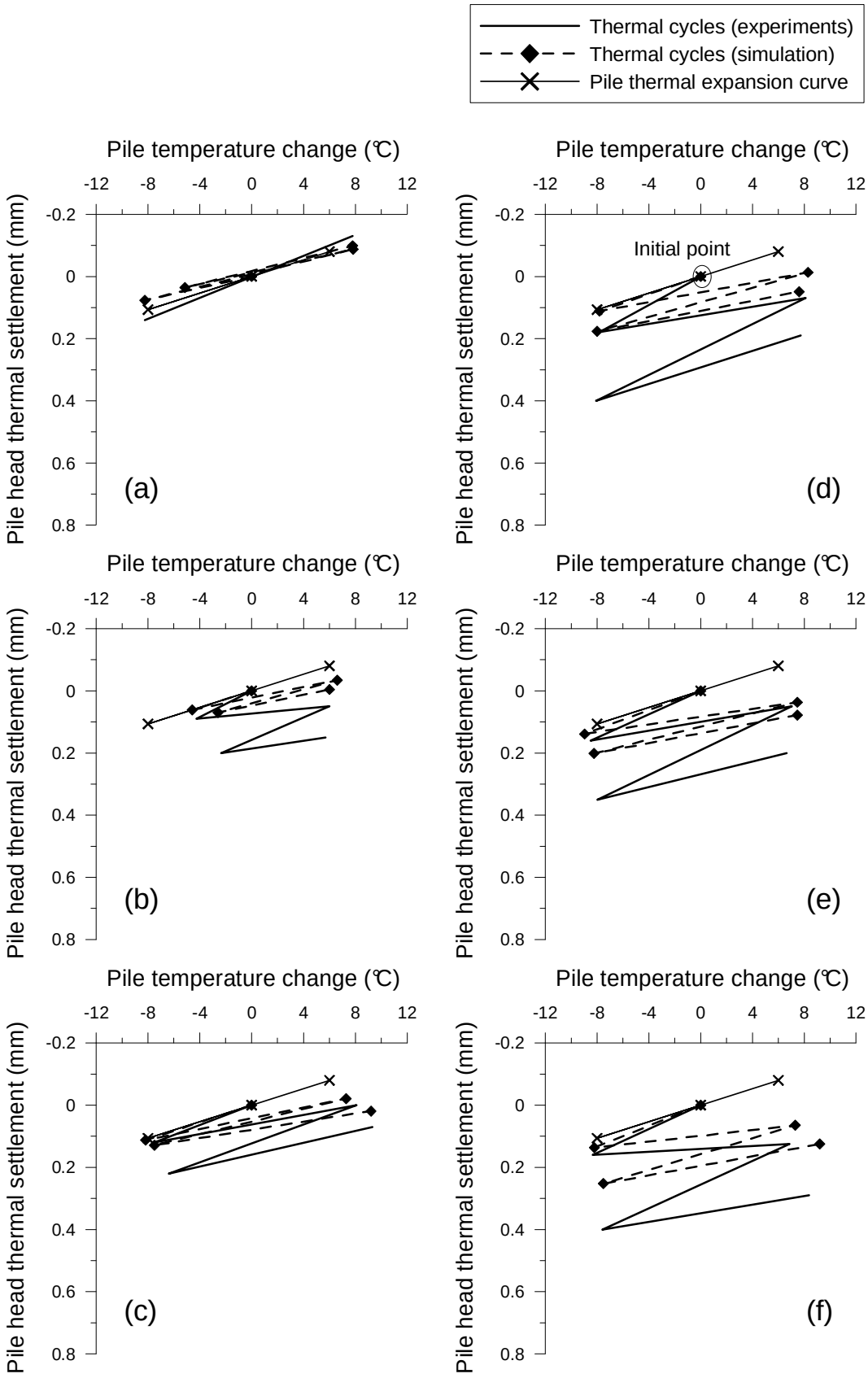

Figure 5.17 Pile thermal settlement versus pile temperature during tests**:** E2(a), E3(b), E4(c), E5(d), E6(e), E7(f)

Total pressure evolution during thermal cycles at different positions in test E2 is shown in Figure 5.18. As in Figure 5.12, the initial point should be comparable to γ z for vertical stress and $K_0 \gamma$z for horizontal one. From this point of view, there exists some sort of error in the measurements of transducers P2 and P3, referring to Figure 5.18*a* and Figure 5.18*b*. Apart from that, considering Figure 5.18*a*, vertical pressure decreases by the first cooling both in simulation and experiments. The reduction value is the same and about 5 kPa (which is about 50% of the initial stress value considering the numerical results and 25% of the initial stress value considering the experimental results) in both cases. Vertical pressure continues to decrease by thermal cycles. By heating, numerical vertical pressure increases and approaches the initial value. The same trend as observed on the first cooling and heating could be made also on the second cycle. Horizontal pressure measured at P3, shown in Figure 5.18*b*, seems to be insensitive to temperature. This is also the case in the simulation results. Referring to Figure 5.18*c-f*, numerical and experimental curves are in good quantitative correspondence. As a general conclusion, pressure in the soil at the pile vicinity does not change significantly as the pile temperature changes neither in the simulation nor in the experiments.

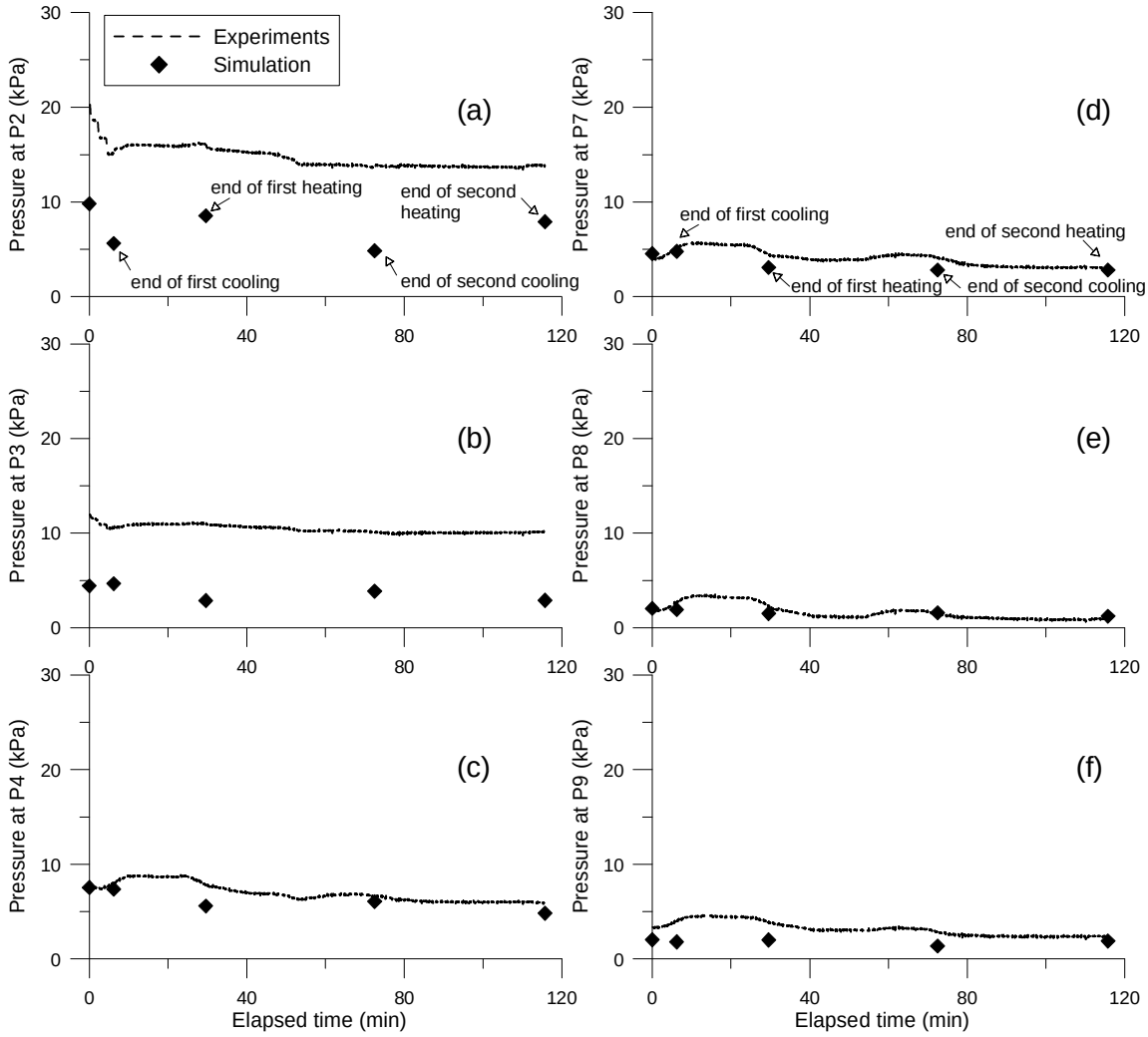

Figure 5.18 Total pressure variation by thermal cycles in test E2 at: (a) P2; (b) P3; (c) P4; (d) P7; (e) P8; (f) P9

Total pressure variation by thermal cycles in test E7 is exhibited in Figure 5.19. As a general conclusion, temperature effects are negligible on the total pressure value at positions P3 through P9, as could be seen in Figure 5.19*b-f*. This is also the case at the simulated pressure values at P2; until the first heating, pressure value does not change. By the second cooling it decreases a little and increases to the previous value by the next heating phase. While in the experimental results at the same position, a governing increasing trend by thermal cycles could be detected.

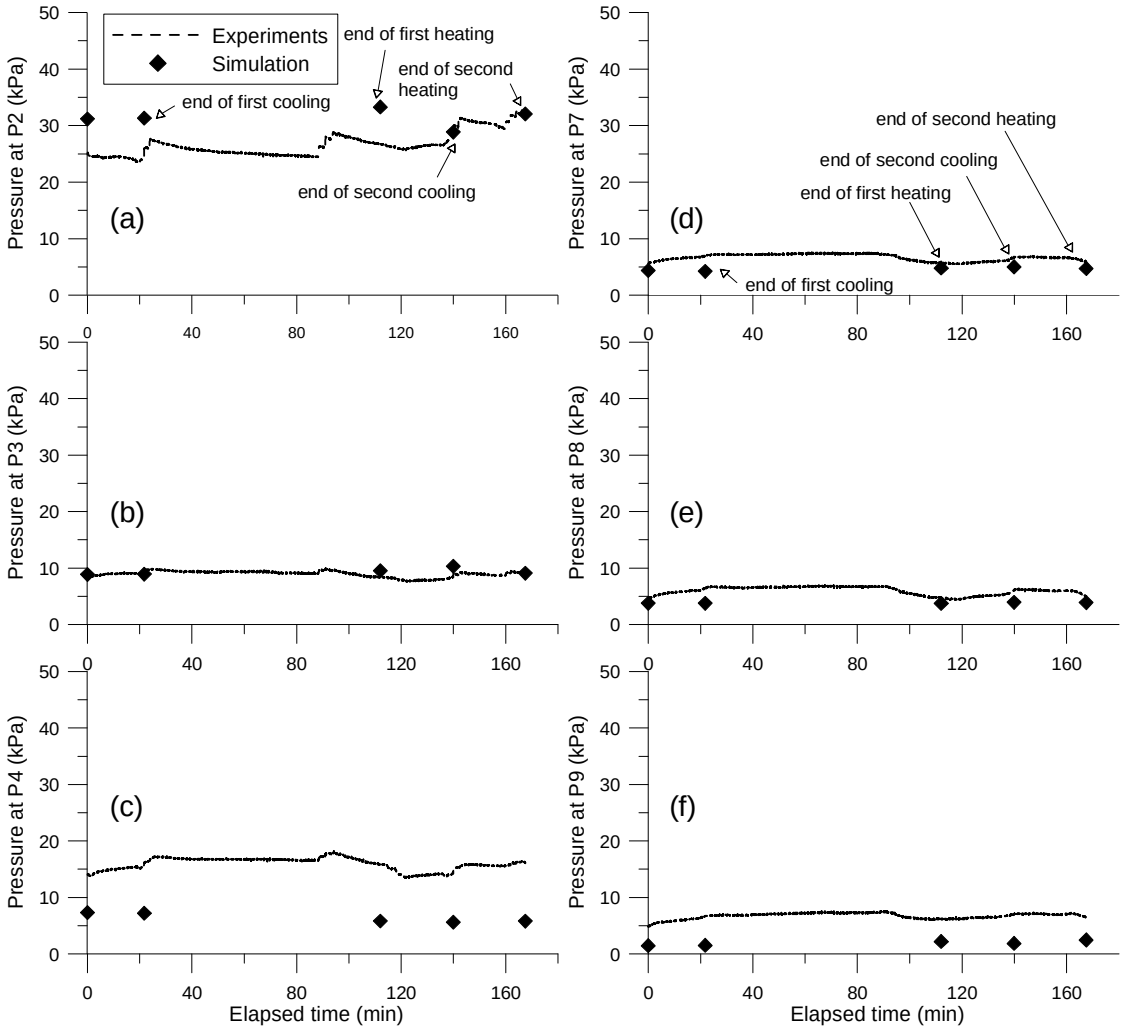

Figure 5.19 Total pressure variation by thermal cycles in test E7 at: (a) P2; (b) P3; (c) P4; (d) P7; (e) P8; (f) P9

Axial load distribution along the pile in test E2 through test E7 is plotted in Figure 5.20. Two sets of curves could be detected: experimental (which is shown by dashed lines) and numerical (which is represented by thick lines). Each set is composed of five curves: the first one is the reference one, which is obtained after that the pile mechanical incremental loading is finished and it is ready to be subjected to thermal cycles. The curve is denoted by 'mechanical'. The other four curves plot the axial load distribution obtained at the end of first cooling, first heating, second cooling and second heating. Figure 5.20*a* shows the results of thermal loading on the pile with no head load. The non-zero axial load values along the pile on the experimental 'mechanical' profile could be explained by the presence of pre-stresses in the pile due to installation. The numerical values are naturally equal to γ_p z A where γ_p is the pile unit weight, z changes between 0 and l (the pile length), and A is the pile section ($3.1\times10^{-4}\,\mathrm{m}^2$). Regarding numerical curves, tensile forces (negative values) are generated in

the pile as it is cooled. When it is heated afterwards, compressive forces are produced which are greater than the initial values detected on the 'mechanical' profile. The same load distribution as under first cooling is observed on second cooling. This is also the case on the first and second heating while compressive forces are slightly greater in the second heating. Regarding experimental results, exactly an inverse trend is observed; heating produces tensile forces while cooling generates compressive forces. Also, the absolute values of the axial force decrease as thermal cycles proceed. As a consequence, the profiles obtained at the end of second cooling and second heating are closer to the initial profile. Under a non-zero load value (Figure 5.20*b-f*) the trends observed on numerical profiles under zero load stays unchanged; as the pile is cooled compressive forces in the pile decrease comparing to the concerning 'mechanical' profile and as it is heated compressive forces increase. The effect of heating is more pronounced on the load distribution curves. Except in the case of 200 N (Figure 5.20*d*), the two profiles obtained at the end of first and second cooling are almost superposed while the additional compressive forces are more important at the end of second heating than after the first one. The axial force at the pile toe is affected by thermal loading, especially under relatively lower loads (Figure 5.20*b*, Figure 5.20*c* and Figure 5.20*d*). According to Figure 5.20*b-f*, there exists a point on the profiles obtained at the end of heating phases, where the slope changes. This point is located at depth of 280 mm and its position does not change with the head load value. When it comes to experimental axial load distribution profiles, it is not easy to find a regular tendency. But globally, the same observation as the case of zero load (Figure 5.20*a*) could be made: cooling leads to axial force increase while heating leads to axial force decrease. Also, when applying thermal cycles on the pile under rather heavy loads (300 N, Figure 5.20*f*), the axial forces along the pile increase as thermal cycles go on. Pile toe is also more affected by thermal cycles when it is subjected to rather heavy mechanical loads.

Evolution of the plastic zone around the pile under 0 N and 300 N and for the first two thermal cycles is shown in Figure 5.21 and Figure 5.22. Under no mechanical load, the plastic zone spreads at the contact zone and even at the soil surface by the initial cooling (Figure 5.21*b*). The plastic zone propagates in the soil when the pile is heated afterwards (Figure 5.21*c*) while the soil around the upper half of the pile is more affected. The plastic zone does not change significantly by the following thermal cycle (Figure 5.21*d* and Figure 5.21*e*), except that a larger area close to the soil surface is affected. Under 300 N of mechanical load, the plastic zone is spread at the pile vicinity and at the pile toe (Figure 5.22*a*). First cooling affects particularly lower depths of the soil near the pile (Figure 5.22*b*) and the soil surface.

Subsequent heating leads to spread the plastic points at the contact zone (Figure 5.22*c*). Same as the previous case, the plastic zone extension does not change sensibly during the next cooling/heating cycle (Figure 5.22*d* and Figure 5.22*e*).

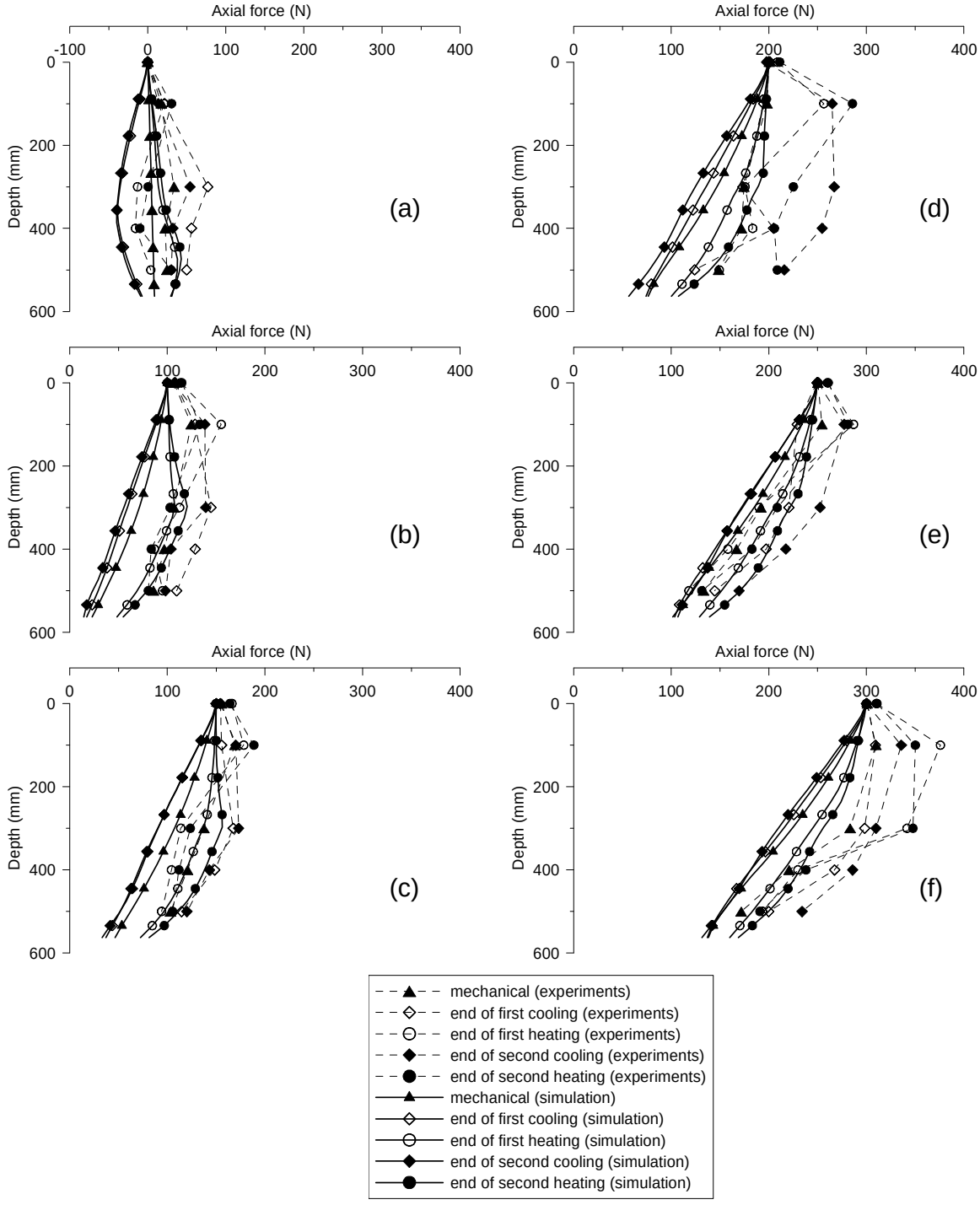

Figure 5.20 Axial load distribution along the pile in tests: E2(a), E3(b), E4(c), E5(d), E6(e), E7(f)

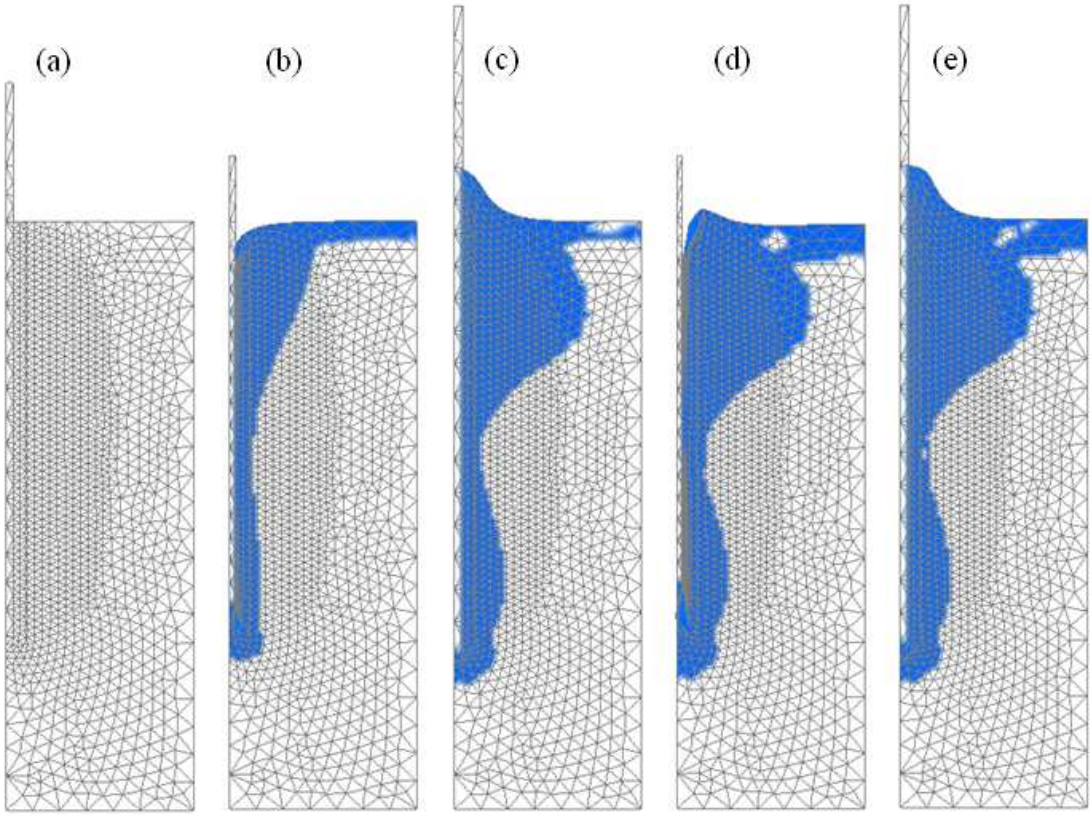

Figure 5.21 Plastic zone evolution under 0 N at the end of : (a) purely mechanical phase (b) first cooling phase (c) first heating phase (d) second cooling phase (e) second heating phase. In all subfigures, the mesh is deformed according to displacements (amplification factor = 500).

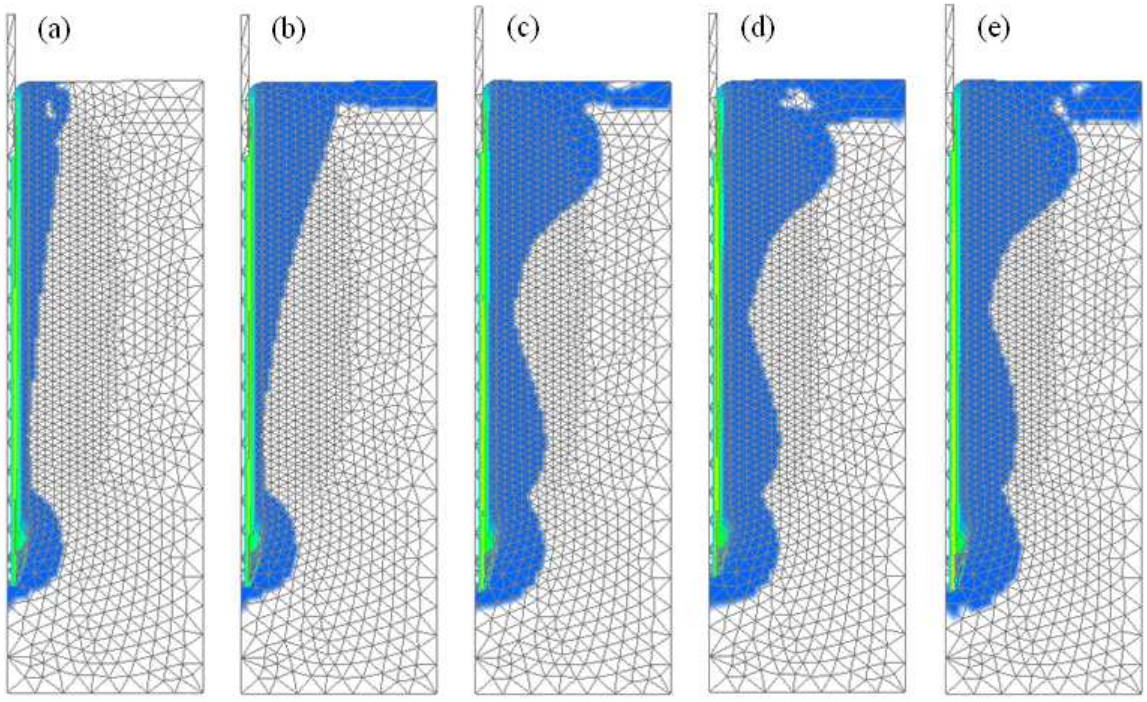

Figure 5.22 Plastic zone evolution under 300 N at the end of: (a) purely mechanical phase (b) first cooling phase (c) first heating phase (d) second cooling phase (e) second heating phase. In all subfigures, the mesh is deformed according to displacements (amplification factor = 500).

5.4.3 Simulation of test E8

Figure 5.23 depicts the pile thermal settlement versus pile temperature change. Pile head thermal settlement measured during 30 thermal cycles in test E8 was first corrected in order to eliminate the time effects, as explained before on Figure 5.16. Both the original and corrected curves are exhibited.

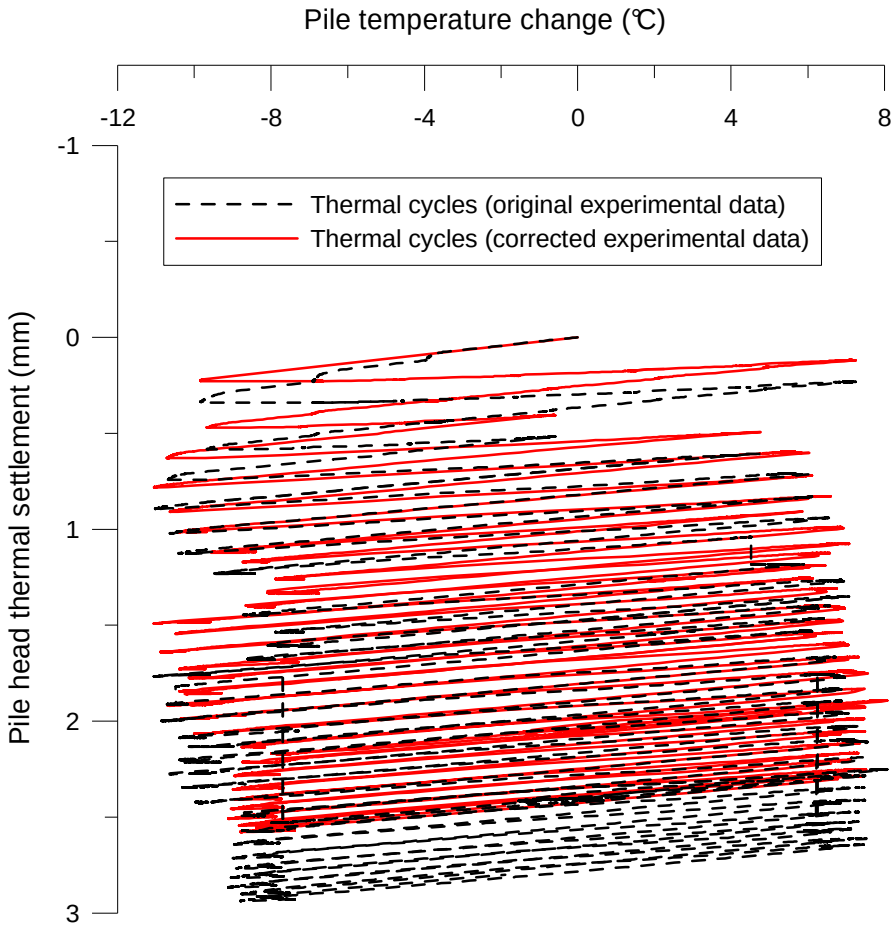

Figure 5.23 Pile thermal settlement versus pile temperature: raw and corrected data obtained from test E8

The corrected curve is then compared to the pile thermal settlement curve obtained via simulation and the expansion curve of a free pile in Figure 5.24. As could be seen, the pile continues to settle with thermal cycles in the test and in the simulation. However the pile settlement is much higher in the experiment. Figure 5.25 spots clearly the quantitative difference between the two sets of thermal settlements. The pile settlement at the end of each cycle in the simulation and in the test is plotted by empty and filled symbols, respectively. As could be observed, both the model pile and the modelled one undergo the highest settlement during the first ten cycles. After that the settlement continues more slowly and it seems that

the modelled pile will reach an accommodation state within some further cycles. In contrast, the pile in the test settles down more abruptly by thermal cycles and it seems that stabilisation procedure is further long.

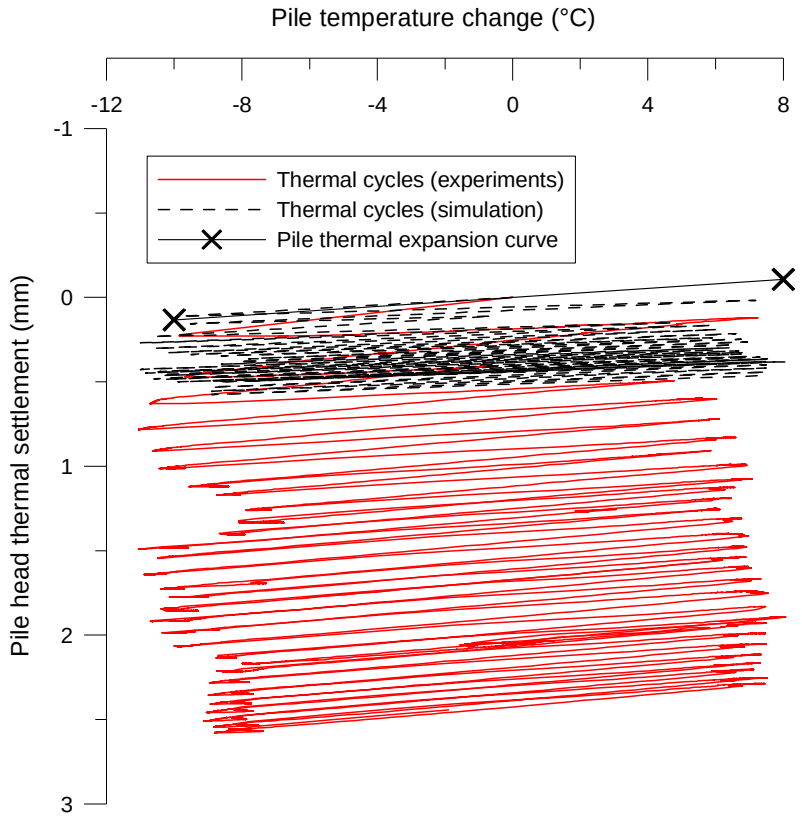

Figure 5.24 Pile thermal settlement versus pile temperature during test E8

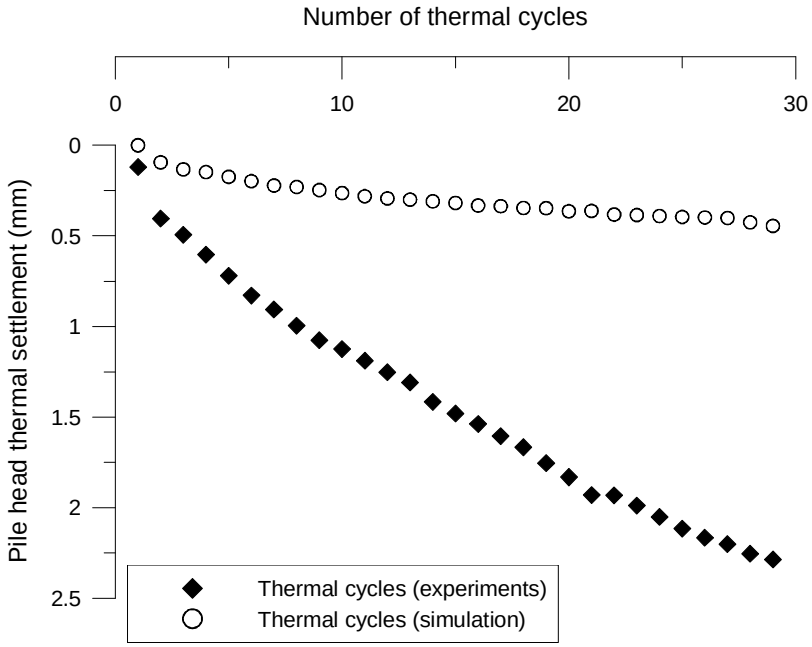

Figure 5.25 Pile head settlement versus thermal cycles

Axial load distribution in the pile is depicted in Figure 5.26. The numerical and experimental curves obtained at the purely mechanical test, the first and the last cooling and heating cycles are compared. In the simulated pile compressive forces decrease as the pile is cooled for the first time and increase by the subsequent heating phase. As thermal cycles follow, the initial mechanical axial force profile is more affected such that important tensile loads are generated in the pile by the last cooling. Also, more compressive forces are generated by the last heating phase. However, the impact of cooling in the long term is more pronounced than heating. Similar to the case of the pile under two thermal cycles (Figure 5.20), an inverse trend is detected on the experimental results: compressive loads decrease by initial heating and increase by initial cooling. Again according to the experimental results, compressive forces increase in the pile as thermal cycles proceed.

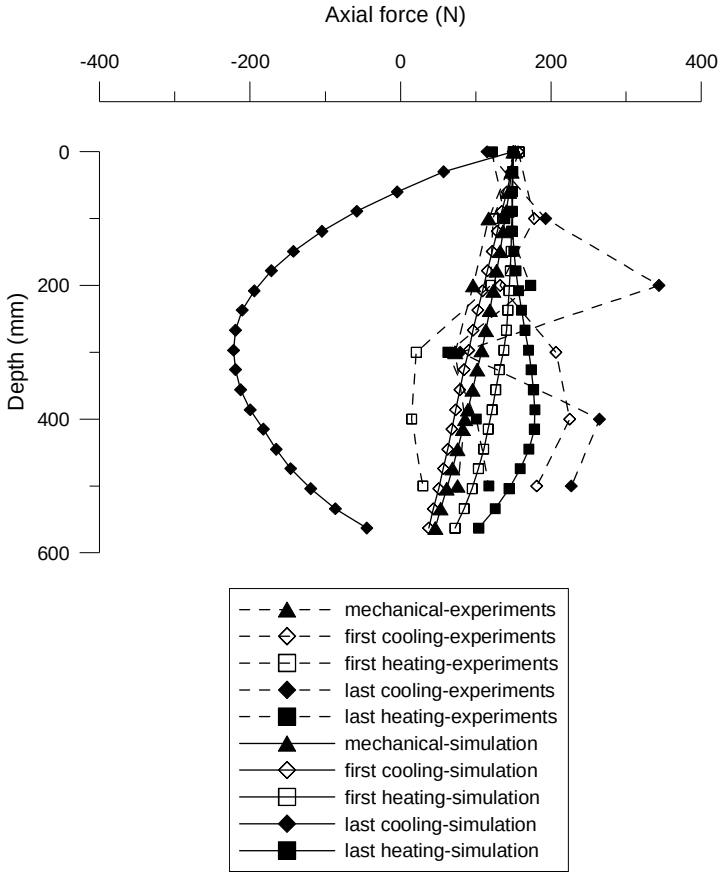

Figure 5.26 Axial load distribution along the pile in test E8

The plastic zone developed in the soil at the end of loading phases is shown in Figure 5.27. Plastic zone propagates near the pile by the end of the mechanical loading (Figure 5.27*a*). Cooling the pile leads to extension of plastic zone especially in the upper half of the pile (Figure 5.27*b*). Soil surface is also affected in this phase. By heating, plastic zone continues to

develop while there exists a point in the pile near which the plastic zone remains the same (Figure 5.27*c*). Extension of the plastic zone at final cooling and heating phases (Figure 5.27*d* and Figure 5.27*e*) is almost the same. Comparing to the first thermal cycle (Figure 5.27*b* and Figure 5.27*c*), plastic zone propagates deeper in the soil near the soil surface. Also, a larger area at the pile toe is affected.

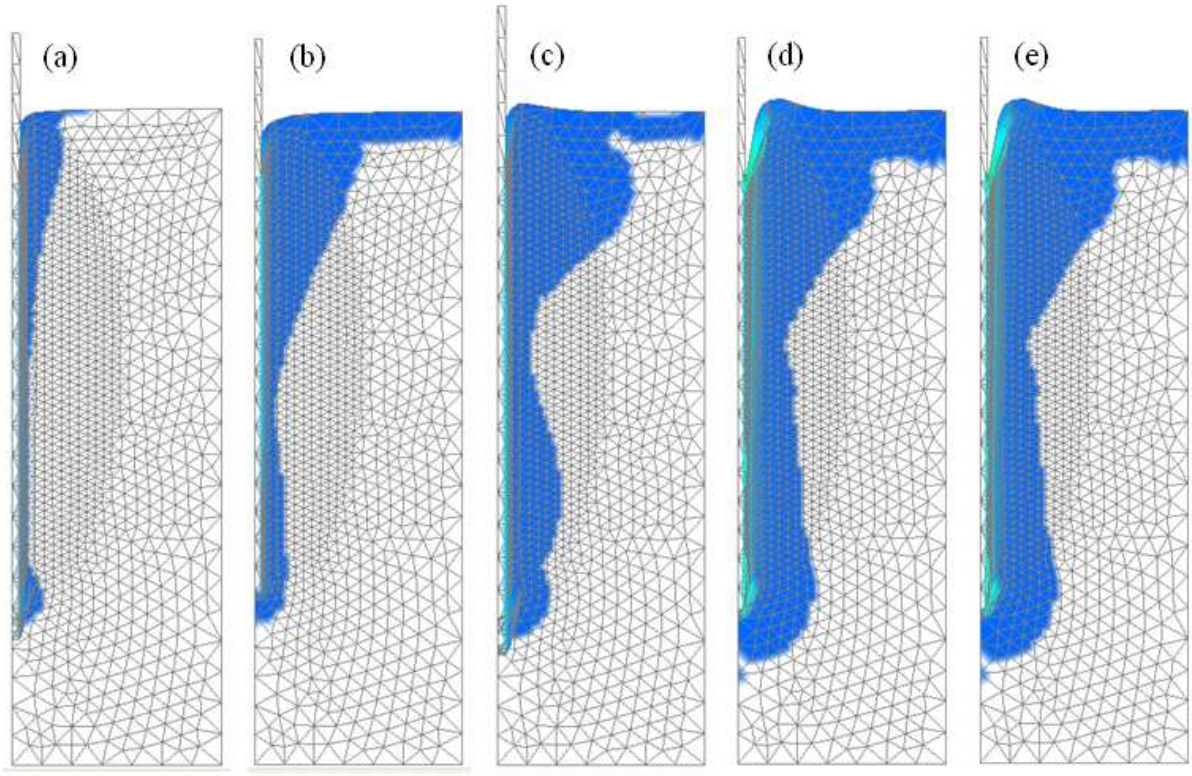

Figure 5.27 Plastic zone evolution under 150 N at the end of : (a) purely mechanical phase (b) first cooling phase (c) first heating phase (d) last cooling phase (e) last heating phase. In all subfigures, the mesh is deformed according to displacements (amplification factor = 500).

5.4.4 Discussion

In order to have a better understanding of the disparities between the results of the physical and the numerical model under purely mechanical loading, load-settlement curves and axial load distribution profiles should be taken into account at the same time (Figure 5.11 and Figure 5.13). According to Figure 5.11 , pile behaviour in unloading from 200 N to 0 N and reloading to 200 N is reversible in the numerical model while the two branches of unloading and reloading are not superposed in the experimental results. Also, the pile settles more in the experiment than in the simulation which means that the finite element model is stiffer. Looking at Figure 5.13, lateral friction plays a more important role in the numerical curves, which implies that less proportion of the head load is transmitted to the pile toe. It could be

then concluded that the considered perfect contact between the soil and the pile was not representative of the contact situation in the test. Also on the experimental axial load profiles, until 200 N (about 45% of the ultimate load), it is only the pile toe that is affected by loading. In other words, lateral friction was not mobilised below 45% of the ultimate load. From this point of view, it seems that the physical model was representative of an end bearing pile while the behaviour of the simulated pile resembles to a semi-floating pile.

With respect to thermo-mechanical tests, Figure 5.15 shows that the numerical model was able to simulate the temperature fields in the thermo-mechanical test. This shows that thermal parameters and boundary conditions were compatible with the test conditions. Besides, heat transfer occurred by conduction only, which was expected as soil had been dry sand and other mechanisms such as convection or advection were not significant.

In terms of mechanical behaviour under two thermal cycles, some major discrepancies between experimental and numerical results were detected. Regarding Figure 5.16 which illustrates pile thermal settlement versus pile temperature, the physical model shows significant creep during thermal cycles. This creep -or time effect in a broader sense- that may be enhanced by temperature increases, manifests as the continuous variation with time of a mechanical quantity (which could be soil total pressure, pile displacement and pile axial force in the case of this study) under a constant temperature. This time dependency could be also detected in experimental results on total pressure in Figure 5.18 and Figure 5.19; there exists some periods were temperature had been constant but total pressures continued to change (stress relaxation). By removing the apparent creep from thermal settlement curves, more quantitative resemblance is achieved between the numerical and experimental results in Figure 5.17, while the thermal settlement of the pile in the simulation is always smaller than in the tests, which was also the case in mechanical settlement (Figure 5.11). Considering Figure 5.17*a*, pile behaviour remained elastic in both cases under purely thermal loading. The slope of the simulated curve is less than that of the free pile, which indicated that in the numerical model, not only the pile head but also the pile toe moves. Consequently, when the pile is cooled, it contracts and when it is heated it expands from both ends in the numerical model. On the contrary, the slope of the experimental curve is smaller than that of a free pile. In other words it undergoes more important thermal deformation comparing to a free pile restrained by its end, which seems difficult to explain. Under 100, 150 and 200 N of head load (Figure 5.17*b*, Figure 5.17*c* and Figure 5.17*d* respectively) slope of the numerical curve during the first cooling is the same as that of a free pile, while more settlement is observed on the experimental curve. The observation could be justified only in one case: in the numerical

model, pile acts like a free pile during the first cooling; it contracts from its head, so that the side friction is mobilised along the pile especially on the upper part while pile toe is not particularly affected. In the experiments, pile contracts by its head and at the same time it continues to settle under the existing mechanical (head) load.

Better clarification could be provided by Figure 5.28. The response of a free pile during a thermal cycle is shown in Figure 5.28*a*. Figure 5.28*b* and Figure 5.28*c* show the observed pile behaviour under the first thermal cycle in the simulations and in the experiment. Δ_i and $\Delta_i^{'}$ denote respectively the pile displacement at the end of cooling and at the end of heating. The initial state, shown by $\Delta T = 0$, is defined as follows: pile settlement has stabilised under the last increment of mechanical loading in a certain test and the pile is ready to be subjected to thermal cycles. Considering that pile head settlements under mechanical loading were similar in numerical and experimental results (Figure 5.11), the same initial states could be imagined in both cases, as it is the case in Figure 5.28*b* and Figure 5.28*c* at $\Delta T = 0$. The pile has a length of l_1 in both cases. It is aimed to compare the pile numerical and experimental displacements with that of a free pile with the same length of l_1 which is only fixed by its toe and is free to move in other directions (Figure 5.28*a*). Δ_1, Δ_2 and Δ_3 denote respectively head displacement of the free pile, the model pile in simulation and the model pile in the test at the end of first cooling. According to Figure 5.17, up to 200 N of mechanical load, Δ_1 is equal to Δ_2 and smaller than Δ_3. Logically, pile head in the test could not contract more than a free pile, thus there should exist some movement at the pile toe, while in the simulation pile toe does not move. This is also compatible with Figure 5.20 where cooling has not a serious effect on axial force at pile toe. By the subsequent heating, pile head expansion is more significant in the simulations than in the experiments ($\Delta_2^{'}$ is very small and is smaller than $\Delta_3^{'}$ according to Figure 5.17) which might indicate that pile downward movement in the experiment is even facilitated by its expansion from its toe ($\Delta_4^{'}$ is greater than Δ_4, $\Delta_5^{'}$ is very small). Thus, vertical stress measured during the test at P1 (Figure 5.19*a*) continues to increase. When the mechanical load increases to 250 N and 300 N (Figure 5.17*e* and Figure 5.17*f*) pile settlement in the simulations during the first cooling approaches to the experimental one (Δ_2 is almost equal to Δ_3 and is greater than Δ_1); mechanical load is large enough to make the pile toe move downward. During the heating phase that follows, pile heave in the experiment is smaller than that in the simulations ($\Delta_2^{'}$ is smaller than $\Delta_3^{'}$).

However $\Delta_5^{'}$ is no more equal to zero, as the axial force profiles (Figure 5.20) show a load transfer in the pile which must result in some settlements at pile toe.

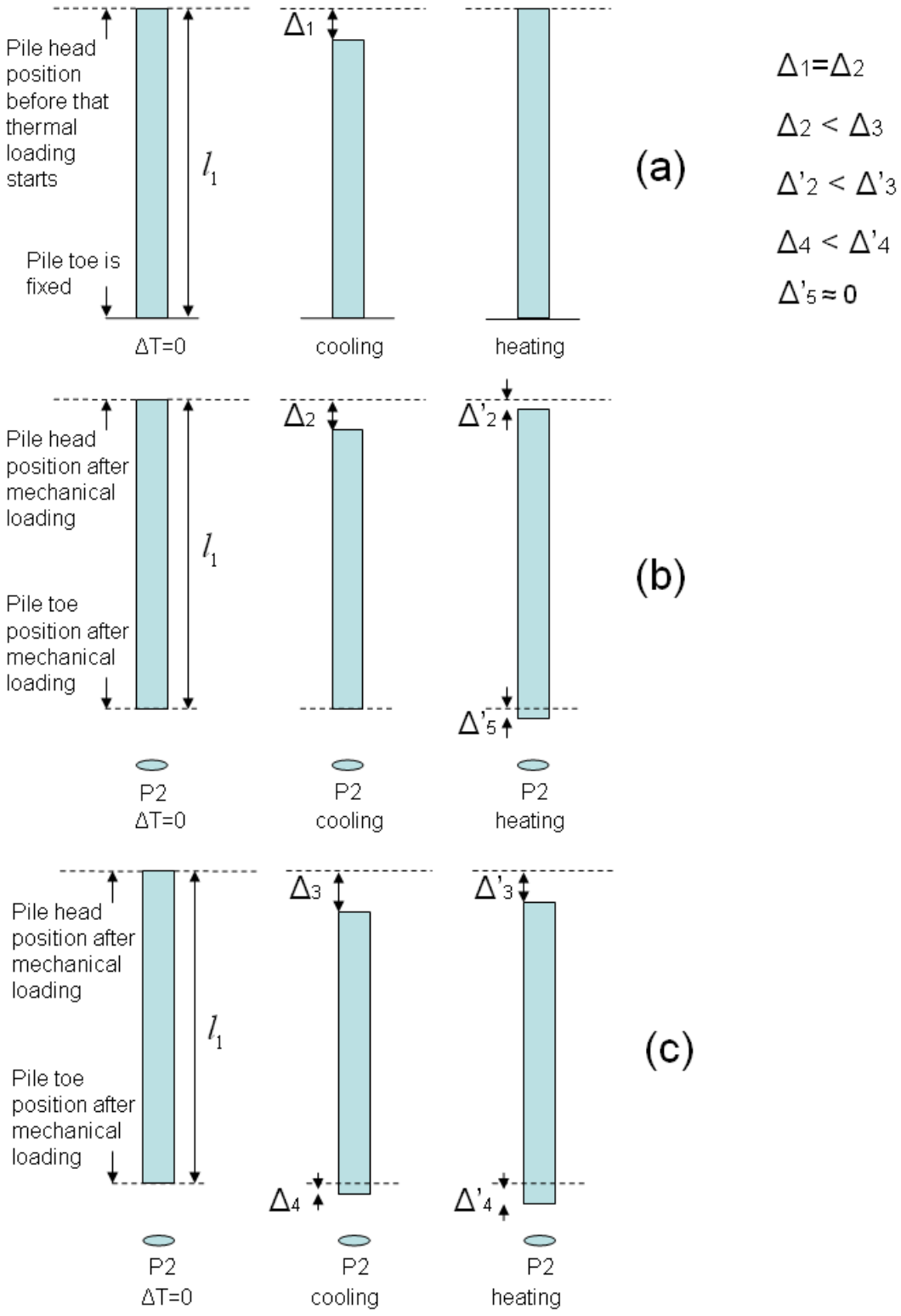

Figure 5.28 Prospective mechanisms for pile behaviour under a load less than 200N and a thermal cycle: (a) a free pile (b) pile in the simulations (c) pile in the experiment

The difference between numerical and experimental axial load distribution profiles (Figure 5.20) is more complicated to be explained. The compressive stresses in the simulated pile decrease when it is cooled and increase when it is heated. The same trend was observed in the previous studies on simulation of in-situ (real scale) piles (Laloui *et al*., 2006, Suryatriyastuti, 2013), however the profile obtained at the mechanical phase seems to be more sensitive to heating than to cooling. The additional compressive stresses seem to increase as thermal cycles proceed. On the contrary, the profiles obtained at the end of first and second cooling are not very distant. On the other hand, no special tendency could be deduced from experimental axial load profiles. Under rather light loads (up to 150 N), compressive loads decrease by heating and increase by cooling. Under heavier loads, compressive stresses increase by thermal cycles; cooling induces compressive stresses to.

Considering the results of the thermo-mechanical loading test under 30 cooling and heating cycles, the simulated pile settlement is much less than that of the tested pile (Figure 5.24). It seems that pile settlement stabilises within the first cycles in the numerical model, while the pile in the experiment continues to settle with an important rate (Figure 5.25). The mechanisms could be compared on the basis of Figure 5.28: pile toe continues to push through the soil as thermal cycles proceed in the experiment while the modelled pile deforms mainly by its head. This could also be detected in Figure 5.27 which depicts the plastic zone development in the soil. The plastic zone is larger at lower depths, soil surface is also highly affected. With respect to axial force distribution in the pile (Figure 5.26), it seems that the trend observed in numerical results within two cycles (Figure 5.20) remains the same as the number of cycles increases: cooling leads to a decrease in compressive forces while heating leads to an increase. Heating has more visible effects on the axial force profiles within the first cycles (Figure 5.20), but in the long term the effect of cooling is more pronounced; the decrease in compressive forces is so important that significant tensile forces are produced in the pile. Quantitatively, the compressive force increase at the end of the last heating is not that important (Figure 5.26).

To summarise, it could be stated that the simulated pile is more dependent on the lateral friction than on the pile tip. The perfect contact assumed between the pile and soil elements makes the finite element model stiffer and more resistant. While the pile in the experiment is submitted to a lower frictional resistance, also at its toe the tip resistance is not high enough so that even under a very low mechanical load (100 N which is about 20% of the ultimate load) pile settlement continues during thermal cycles. More attention should be paid to the definition of an appropriate interface model. Globally, the small-scale test pile was subjected

to low lateral stresses. Besides, with no mechanical loading on the soil surface, the thermal volumetric changes in the pile were not prevented by the soil body. It seems that the purely mechanical test could be well simulated by adding up interface elements, while the thermal tests seem more complicated and may require the definition of a more appropriate numerical model.

5.5 Conclusion

A commercial finite element code for geotechnical design was first used for simulating a pile under thermo-mechanical loadings. Temperature effects are not included in the code. Instead, an equivalent thermal volumetric deformation was applied to the pile. This simplified method was examined by simulating two in-situ tests on energy piles and one laboratory physical model test. The numerical results were compared to the ones measured during the experiments. The observations show that the simulations are in good agreement with the experiments.

At the observed scale, the proposed method seems to produce satisfactory results in simulating the mechanical behaviour under coupled thermo-mechanical loadings. It could be used as a simple method in design procedures when fully coupled analyses methods are not envisioned.

Secondly, a series of thermo-mechanical tests and one purely mechanical experiment conducted on the pile in the physical model were simulated using a finite element numerical code which considers also thermal effects (contrary to the first code). In terms of purely mechanical tests, the code was able to predict satisfactorily the pile behaviour.

Thermal diffusion in the soil was simulated successfully, which indicates that on the one hand, the governing mechanism of heat transfer in the soil mass has been conduction and on the other hand, the assumptions made on thermal boundary conditions, such as existing no heat transfer via soil container’s wall, were compatible with the test conditions.

Pile settlement by cooling and its heave by heating were observed in both calculated and measured settlement-temperature curves. The pile in the experiments showed serious creep, which could not be taken into account in the simulations. By removing these time effects, more quantitative similarity was achieved between experimental and numerical pile head displacement values. The pile continued to settle down by thermal cycles both in the simulations and in the tests. More plastic deformation was generated under larger pile head load. However the pile settlement value was larger in the experiment. It seems that in the numerical model, the pile toe was less affected by thermal loading (especially under a non-

zero head load value) which could be due to the perfect adherence attributed to the pile/soil contact zone. While the pile in the experiments seems to be less restricted by the surrounding soil and continued to settle during thermal cycles. Regarding pile force distribution in the numerical model, heating led to an increase in compressive loads and cooling led to a decrease. No regular trend could be deduced from the corresponding experimental curves.

GENERAL CONCLUSION AND PERSPECTIVES

The primary aim of this PhD project was to investigate the soil/energy pile interaction mechanism through a small-scale model. A model pile (length of 800 mm and external diameter of 20 mm) was equipped with strain and temperature gauges. Strain gauges are of full bridge type in order to be compensated by temperature. The main interest of this strain gauge type is that they provide a relatively direct measurement of axial stress in the pile. The pile was first embedded in dry Fontainebleau sand (compacted manually) and then in saturated Kaolin clay (compacted by means of a vibratory hammer). Temperature transducers were spread into the soil at different levels and at different distances parallel to the pile axis. Pressure transducers were installed mainly in the vicinity of the pile. The pile was mechanically loaded at its head first and subjected to one, two or more thermal cycles.

The main conclusions which could be drawn from the pile's behaviour when it is embedded in dry sand are:

- Under purely mechanical loading, more than 70% of the pile head load was carried by its toe. The participation of side friction in load transfer was rather weak.
- Subjecting the pile to thermal cycles changed the axial force distribution. The first cooling led to an increase in compressive forces, while the subsequent heating decreased them. The next cooling/heating cycle increased compressive forces. The observed trend is in contrast with that observed in full-scale energy piles found in the literature review.
- Under rather light loads (up to 30% of the pile ultimate load), the behaviour of the pile remained thermo-elastic in terms of axial force distribution. A sort of symmetry between cooling and heating could be detected in these plots.
- In terms of pile settlement induced by temperature, a ratcheting behaviour could be observed as thermal cycles proceeded. The amount of irreversible deformation increased with the mechanical load to which the pile was subjected during thermal cycles. In the test where 30 thermal cycles were applied, an accommodation state could be observed from the 10^{th} cycle.

- The physical model presented significant creep under thermo-mechanical loading. Time effects could be detected in axial force, total pressure and thermal displacement measurements, where no stabilisation could be detected under a constant temperature value.

Coming to the pile behaviour in saturated clay, the following conclusions could be drawn:

- Time effects (creep) were visible in the mechanical loading stage, the creep rate increased with the pile head load.
- As it was the case in sand, thermal cycle led to the appearance of permanent settlements of the pile, with a magnitude increasing with the pile head load.

Shear behaviour of soils and that of soil/concrete interface was investigated through a modified direct shear apparatus at various temperature values. Three temperature values were considered (5°C, 20°C and 40°C). These values correspond to the range of temperature near energy piles. Direct shear tests were performed at normal stress values ranging from 5 kPa to 100 kPa. The results show that:

- The effect of temperature on the shear strength parameters of sand, clay and clay/concrete interface was negligible.
- Softening was observed during shearing of clay/concrete interface, while the behaviour of sand and clay was of ductile type.
- The (peak) shear strength of clay/concrete interface was generally smaller than that of clay.

A commercial finite-element code (Plaxis) was used to simulate a pile under thermo-mechanical loading. Thermo-mechanical loading was simulated by imposing an equivalent thermal volumetric deformation on the pile. Based on the experimental results on the shear box, it was also assumed that mechanical parameters of the soil and those of the soil/pile interface are temperature independent. Thermally-induced volume changes in the soil were ignored. The simplified method was examined by simulating two in situ tests on energy piles and one laboratory physical model (found from the literature review). The numerical results were compared to experimental measurements. The proposed method seems to provide satisfactory results in simulating mechanical behaviour of real scale energy piles; axial strains in the pile and pile head displacement were satisfactorily predicted. Then it could be concluded that at the full scale, the dominant mechanism resulting from thermo-mechanical loading is the volume change in the pile. Considering the physical model, the experimental results were limited to pile head settlement. From this point of view, the numerical results

were close to the experimental ones. However it is not evident that the good agreement also exists in terms of axial force distribution.

Another finite element code (CESAR-LCPC) with the ability to consider temperature effects was used to simulate the tests performed on the model pile in sand during this PhD project. Numerical results were compared with temperature sensors measurements. Good predictions were achieved in terms of heat transfer in the soil. On the contrary, the model was not able to reproduce the thermo-mechanical behaviour of the pile in terms of load transfer, which implies that a more complete model including interface elements should be used. Also, the model used may have to be revised in order to be adaptable to the pile subjected to a rather low range of stress, as it is the case in the physical model.

Considering the limitations of small-scale tests (in general and also in this special case), some modifications in the model and in the experimental procedure could be proposed for further researches:

- Applying a uniform load to the soil surface in order to increase the pressure level in the soil. Running a parametric study by changing the surface load value in order to quantify its effect on the pile's mechanical response.
- Revising the compaction method to ensure a homogenous compaction especially at the vicinity of the pile.
- Utilising another type of pressure sensors (more efficient one). Measuring pressure in the soil at more locations with special attention to the soil container wall. That way boundary effects previously checked on purely mechanical loading of the pile might be modified in order to be adapted to the case of thermo-mechanical loading.
- Supplying the model pile with an appropriate displacement transducer at its toe. In the present study the pile displacement was monitored only at its head.
- Using a new model pile with other type of strain gauges but exactly the same dimension and surface coating, submitting it to the same thermo-mechanical loading paths. Analysing the results and comparing the load transfer mechanism to the one observed in this study in order to confirm the observed mechanism (increase in axial force by cooling and decrease by heating).
- Studying in more detail the effect of time on the pile's behaviour under thermo-mechanical solicitation.

Regarding the performed shear tests, the following perspectives can be suggested:

- Evaluating the shear behaviour of the soil and soil/concrete interface under thermal cycles.
- Adding local measurement of pore pressure.
- Repeating the tests on rougher surfaces.

The numerical model could be explored more in details by:

- Simulating the tests performed on the pile in clay.
- Adding interface elements to the present model beside any other attempts in order to improve the comparison between the experimental and numerical results.
- Working on a constitutive model for the interface (under thermo-mechanical solicitation).

REFERENCES

Abuel-Naga, H., Raouf, M.I.N., Raouf, A.M.I. & Nasser, A.G. 2014. Energy piles: current state of knowledge and design challenges. *Environmental Geotechnics*. DOI: 10.1680/envgeo.13.00019.

Abuel-Naga, H., Bergado, D.T., Bouazza, A., & Ramana, G.V. 2007. Volume change behaviour of saturated clay under drained heating conditions: experimental results and constitutive modelling. *Canadian Geotechnical Journal* **44**(8): 942-956.

Adam, D. & Markiewicz, R. 2009. Energy from earth-coupled structures, foundations, tunnels and sewers. *Géotechnique* **59**(3) : 29–236.

AFNOR, NF p 94-071-1. 1994. Essai de cisaillement rectiligne à la boite, Partie 1 : cisaillement direct. *French Code*.

AFNOR, NF P 94 -150. 1999. Essai statique de pieu sous effort axial. *French Code*.

Akrouch, G.A., Sanchez, M. & Briaud, J.L. 2014. Thermo-mechanical behaviour of energy piles in high plasticity clays. *Acta Geotechnica* **9**(3): 399–412.

Al-Tabbaa, A. & Wood, D.M. 1987. Some measurements of the permeability of kaolin. *Géotechnique* **31**(4): 499-503.

Amatya, B., Soga, K., Bourne-Webb, P., Amis, T. & Laloui, L. 2012. Thermo-mechanical behaviour of energy piles. *Géotechnique* **62**(6): 503–519.

Amis, T. & Loveridge, F. 2014. Energy piles and other thermal foundations for GSHP. *REHVA Journal*: 32-35.

Arson, C., Berns, E., Akrouch, G., Sanchez, M., & Briaud, J.L. 2013. Heat Propagation around Geothermal Piles and Implications on Energy Balance. *Energy Book Series (1)*: "Materials and processes for energy: communicating current research and technological developments", ISBN (13): 978-84-939843-7-3.

Bandos, T., Montero, A., Fernandez, E., Santander, J.L.G., Isidro, J.M., Perez, L., Fernandez de Corboda, P.J. & Urchueguia, J.F. 2009. Finite line-source model for borehole heat exchangers: effect of vertical temperature variations. *Geothermics* **38**: 263-270.

Banks, D. 2008. An introduction to thermogeology : ground source heating and cooling. Blackwell Publishing, Ltd, Oxford, UK; 2008. DOI: 10.1002/9781444302677.ch2.

Baldi, G., Borsetto, M., Hueckel, T. & Tassoni, E. 1985. Thermally induced strain and pore pressure in clays. *International Symposium on Environmental Geotechnology*, Allentown, Pennsylvania, pp. 391-420

Baudouin, G. 2010. Sols renforcés par inclusions rigides: modélisation physique en centrifugeuse de remblais et de dallage. *Ph.D. thesis*, Université de Nantes, France. 285 pages.

Benzaria, O., Puech, A. & Le Kouby, A. 2013. Essais cycliques axiaux sur des pieux forés dans des sables denses. *Proceedings of 18th ICSMGE*, Paris.

Boënnec, O. 2009. Piling on the energy. *GeoDrilling International*.

Boháč, J., Mašín, D., Malát, R., Novák, V. & Rott, J. 2013. Methods of determination of K_0 in overconsolidated clay. *Proceedings of the 18th International Conference on Soil Mechanics and Geotechnical Engineering, Paris 2013.*

Bond, A. J. & Jardine, R. J. 1995. Shaft capacity of displacement piles in a high OCR clay. *Geotechnique* **45**(1): 3-23.

Bourne-Webb, P., Amatya, B., Soga, K, Amis, T., Davidson, C. & Payne, P. 2009. Energy pile test at Lambeth College, London: geotechnical and thermodynamic aspects of pile response to heat cycles. *Géotechnique* **59**(3): 237–248.

Brandl, H. 2006. Energy foundations and other thermo-active ground structures. *Géotechnique* **56**(2): 81–122.

Brandl H. 2013. Thermo-active ground-source structures for heating and cooling. *Procedia Engineering* **57**(2013): 9-18.

BRGM. 2005. Les enjeux des géosciences. Fiche de synthèse scientifique n°10, Avril 2005.

Burghignoli, A., Desideri, A. & Miliziano, S. 2000. A laboratory study on the thermomechanical behaviour of clayey soils. *Canadian Geotechnical Journal* **37**(4): 764-780.

Campanella, R.G. & Mitchell, J.K. 1968. Influence of temperature variations on soil behavior. *Journal of the Soil Mechanics and Foundation Engineering Division* **94**(8): 709–734.

Cekerevac, C. 2003. Thermal effects on the mechanical behaviour of saturated clays: an experimental and constitutive study. *Ph.D. thesis*, EPFL, Lausanne, Switzerland. 258 pages.

Cekerevac, C., & Laloui, L. 2004. Experimental study of thermal effects on the mechanical behaviour of a clay. *International Journal for Numerical and Analytical Methods in Geomechanics* **28**(3): 209–228.

Cervera, C.P. 2013. Ground thermal modelling and analysis of energy pile Foundations. *Master thesis*, Aalto University, Finland.

Chin, J.T. & Poulos, H.G. 1996. Tests on model jacked piles in Calcareous sand. *Geotechnical Testing Journal* **19**(2): 164-180.

Choi, S.K., Lee, M.J., Choo, H., Tumay, M.T. & Lee, W. 2010. Preparation of a large size granular specimen using a rainer system with a porous plate. *Geotechnical Testing Journal* **33**(1): 45-54.

Combarieu, O. 1999. Caractérisation mécanique d'un massif de sable compacté Cohérence des essais réalisés. *Bulletin de liaison des laboratoires des Ponts et Chaussées* **219**: 69-73.

Cui, Y.J., Sultan, N., & Delage, P. 2000. A thermomechanical model for saturated clays. *Canadian Geotechnical Journal* **37**(3): 607-620.

Cui, Y.J., Le, T.T., Tang, A.M., Delage, P., & Li, X. L. 2009. Investigating the time-dependent behaviour of Boom clay under thermomechanical loading. *Géotechnique* **59**(4): 319-329.

De Gennaro, V., Frank, R., Pande, G.N., Canou J. 1999. Finite element modelling of model piles in calibration chamber. *7th International Symposium on Numerical Models in Geomechanics*, Graz, Balkema, pp. 419-424.

De Gennaro, V., Frank, R., & Said, I. 2008. Finite element analysis of model piles axially loaded in sands. *Rivista Italiana Di Geotechnica* **2**: 44–62.

De Moel, M., Bach, P.M., Bouazza, A., Singh, R.M. & Sun, J.L.O. 2010. Technological advances and applications of geothermal energy pile foundations and their feasibility in Australia. *Renewable & Sustainable Energy Reviews* **14**(9): 2683-2696.

Diao, N., Li, Q. & Fang, Z. 2004. Heat transfer in ground heat exchangers with groundwater advection. *International Journal of Thermal Sciences* **43**: 1203–1211.

Di Donna, A. & Laloui, L. 2013a. Pieux énergétiques. *Bulletin technique de la Suisse romande*. Tracés N°3.

Di Donna, A., & Laloui, L. 2013b. Advancements in the geotechnical design of energy piles. *International Workshop on Geomechanics and Energy* – The Ground as Energy Source and Storage, Lausanne, Switzerland.

Dove, J.E., & Jarrett, J.B. 2002. Behaviour of dilative sand interfaces in a geotribology framework. *Journal of Geotechnical and Geoenvironmental Engineering* **128**(1): 25-37.

Dupla, J.C., Canou, J. & Dinh, A.Q. 2008. Caractérisation de mélanges de sables d'Hostun. Rapport PN ASIRI n°2.08.3.07.

Dupray, F., Laloui, L. & Kazangba, A. 2014. Numerical analysis of seasonal heat storage in an energy pile foundation. *Computers and Geotechnics* **55**: 67–77.

Ebnöther, A. 2008. Energy piles the European experience. *GeoDrilling International*.

Edil, T.B. & Mochart I.B. 1988. Creep response of model pile in clay. *Journal of Geotechnical Engineering* **114** (11): 1245-1260.

Esen, H., Inalli, M. & Esen, Y. 2009. Temperature distributions in boreholes of a vertical ground-coupled heat pump system. *Renewable Energy* **34**: 2672–2679.

Eslami, H., Rosin-Paumier, S., Abdallah, A. & Masrouri, F. 2014. Influence de la variation de la température sur les paramètres pressiomètrique d'un sol compacté. *Journées Nationales de Géotechnique et de Géologie de l'Ingénieur JNGG2014.*

Fioravante, V. 2002. On the shaft friction modelling of non displacement piles in sand. *Soils and Foundations* **42**(2): 23–33.

Fioravante, V. 2011. Load transfer from a raft to a pile with an interposed layer. *Géotechnique* **61**(2): 121-132.

Foray, P., Balachowski, L. & Rault, G. 1998. Scale effect in shaft friction due to the localisation of deformations. *Proceedings of the International Conference Centrifuge 98*, Tokyo, T. Kimura, O. Kusakabe, J. Takemura, Balkema, Rotterdam, Vol. **1**, pp. 211-216.

Franchomme, G., Rosin-Paumier, S. & Masrouri, F. 2013. Evaluating the impact of thermal variations on the penetration test parameters. *Proceedings of the first Pan-American conference on unsaturated soils, Cartagena de Indias, Colombia*: Advances in Unsaturated Soils, Caicedo B et al. (eds.), Taylor & Francis Group, London (2013) 371-376.

Frank, R. & Zhao, S.R. 1982. Estimation par les paramètres pressiométriques de l'enfoncement sous charge axiale des pieux forés dans les sols fins. *Bulletin de Liaison du Laboratoire des Ponts et Chaussées* **119** : 17-24.

Frikha, W. 2010. Etude sur modèle physique du renforcement d'une argile molle par colonnes ballastées. *Ph.D. thesis*, Ecole Nationale des Ingénieurs de Tunis (ENIT), Tunisie. 250 pages.

Fromentin, A., Pahud, D., Laloui, L. & Moreni, M. 1999. Pieux échangeurs: conception et règles de pré-dimensionnement. *Revue Française de Génie Civil* **6** : 387-421.

Garnier, J. & König, D. 1998. Scale effects in piles and nail loading tests in sand. *Proceedings of the International Conference Centrifuge 98*, Tokyo, T. Kimura, O. Kusakabe, J. Takemura, Balkema, Rotterdam, Vol. **1**, pp. 205-210.

Ghahremannejad, B. 2003. Thermo-mechanical behaviour of two reconstituted clays. *Ph.D. thesis*, University of Sydney, Australia. 225 pages.

GHSP 2012. Thermal pile design, installation and materials standards. Ground Source Heat Pump Association, http://www.gshp.org.uk/GSHPA_Thermal_Pile_Standard.html.

Graham, J., Tanaka, N., Crilly, T., & Alfaro, M. 2001. Modified Cam-Clay modelling of temperature effects in clays. *Canadian Geotechnical Journal* **38**(3): 608-621.

Hamidi, A., Tourchi, S., & Khazaei, C. 2014. Thermomechanical constitutive model for saturated clays based on critical state theory. *International Journal of Geomechanics*. DOI:10.1061/(ASCE)GM.1943-5622.0000402.

Hammoud, F., & Boumekik, A. 2006. Experimental study of the behaviour of interfacial shearing between cohesive soils and solid materials at large displacement. *Asian Journal of civil engineering (building and housing)* **7**(1): 63-80.

He, M. 2012. Numerical Modelling of Geothermal Borehole Heat Exchanger Systems. *Ph.D. thesis*, De Montfort University, Leicester, UK. 205 pages.

Holden, J.C. 1991. History of the first six CRB calibration chambers. *Proceedings of the 1st International Symposium on Calibration Chamber Testing*, Potsdam, NY, U.S.A.

Hong, P.Y., Pereira, J.M., Tang, A.M., & Cui, Y.J. 2013. On some advanced thermo-mechanical models for saturated clays. *International Journal for Numerical and Analytical Methods in Geomechanics* 37: 2952 – 2971. DOI: 10.1002/nag.2170.

Horikoshi, K., Matsumoto, T., Hashizumb, Y., Watanabe, T. & Fukuyama, H. 2003. Performance of piled raft foundations subjected to static horizontal loads. *International Journal of Physical Modelling in Geotechnics* **2**: 37-50.

Hueckel, T., & Pellegrini, R. 1989. Modeling of thermal failure of saturated clays. *International Symposium on Numerical Models in Geomechanics NUMOG*, pp. 81-90.

Hueckel, T., & Baldi, G. 1990. Thermoplasticity of saturated clays: experimental constitutive study. *Journal of Geotechnical Engineering* **116**(12): 1778–1796.

Hueckel, T., Francois, B., & Laloui, L. 2009. Explaining thermal failure in saturated clays. *Géotechnique* **59**(3): 197–212.

Jardine, R.J., Zhu B., Foray P. & Dalton C.P. 2009. Experimental arrangement for investigation of soil stresses developed around a displacement pile. *Soils and Foundations* **49**(5): 661-673.

Kalantidou, A., Tang, A.M., Pereira, J.M., & Hassen, G. 2012. Preliminary study on themechanical behaviour of heat exchanger pile in physical model. *Géotechnique* **62**(11): 1047 –1051.

Karakus, M. & Fowelleb, R.J. 2005. Back analysis for tunnelling induced ground movements and stress redistribution. *Tunnelling and Underground Space Technology* **20**(6): 514-524.

Katzenbach, R., Clauss, F., Waberseck,T. & Wagner, I. 2008. Coupled numerical simulation of geothermal energy systems. *Proceedings of the 12th International Conference of International Association for Computer Methods and Advances in Geomechanics (IACMAG).*, pp. 1170-1179.

Katzenbach, R., Clauss, F. & Rochée, S. 2013. Analysis of the freeze thaw performance of geothermal heat exchanger borehole grout materials. *Proceedings of the 18th International Conference on Soil Mechanics and Geotechnical Engineering, Paris 2013.*

Knellwolf, C., Peron, H. & Laloui, L. 2011. Geotechnical analysis of heat exchanger piles. *Geotechnical and Geoenvironmental Engineering* **137**(10): 890–902.

Konrad, J.M. & Roy, M. 1987. Bearing capacity of friction piles in marine clay. *Géotechnique* **37**(2): 163-175.

Krishnaiah, S., & Singh, D. N. 2004. Centrifuge modelling of heat migration in soils. *International Journal of Physical Modelling in Geotechnics* **4**(3), 39–47.

Kuntiwattanakul, P., Towhata, I., Ohishi, K., & Seko, I. 1995. Temperature effects on undrained shear characteristics of clay. *Soils and Foundations* **35**(1): 147-162.

Laloui, L. & Cekeravac, C. 2003. Thermo-plasticity of clays: an isotropic yield mechanism. *Computers and Geotechnics* **30**(8): 649–660.

Laloui, L & François. B. 2009. Acmeg-t: soil thermoplasticity model. *Journal of Engineering Mechanics* **135**: 932–944.

Laloui, L., Moreni, M., Fromentin, A., Pahud, D. & Steinmann, G. 1999. Heat exchanger pile :effect of the thermal solicitations on its mechanical properties. *Proceedings of the European Geothermal Conference*, Basel.

Laloui, L., Moreni, M. & Vulliet, L. 2003. Comportement d'un pieu bi-fonction, fondation et échangeur de chaleur. *Canadian Geotechnical Journal* **40**(2) : 388 – 402.

Laloui, L., Nuth, M. & Vulliet, L. 2006. Experimental and numerical investigation of the behaviour of a heat exchanger pile. *International Journal for Numerical and Analytical Methods in Geomechanics* **30**(8): 763 – 781.

Lapanje, A., Rajver, D. & Székely, E. 2010. Geothermal heat pumps manual. Operational Programme Slovenia-Hungary 2007-2013.

Lee, C.K. & Lam, H.N. 2007. Effects of groundwater water flow direction on performance of ground heat exchanger borefield in geothermal heat pump systems using 3-D finite difference method. *Proceedings: Building Simulation 2007*. pp. 337-341

Le Kouby, A. 2003. Comportement de micropieux modèles en chambre d'étalonnage. Application aux effets de groupe et aux sollicitations cycliques. *Ph.D. thesis*, Ecole Nationale des Ponts et Chaussées, France. 394 pages.

Le Kouby, A., Canou, J. & Dupla, J.C. 2004. Behaviour of model piles subjected to cyclic axial loading, Cyclic Behaviour of Soils and Liquefaction Phenomena. Triantafyllidis (ed), Taylor & Francis Group, London, pp. 159-166.

Lemos, L. J. L., & Vaughan, P. R. 2000. Clay interface shear resistance. *Géotechnique* **50**(1): 55-64.

Li, M. & Lai, A.C.K. 2012. Heat-source solutions to heat conduction in anisotropic media with application to pile and borehole ground heat exchangers. *Energy* **96**: 451–458.

Loveridge, F. & Powrie, W. 2013. Performance of Piled Foundations Used as Heat Exchangers. *Proceedings of the 18th International Conference on Soil Mechanics and Geotechnical Engineering, Paris 2013.*

Lubliner, J., Oliver, J., Oller, S. & Onate, E. 1989. A plastic-damage model for concrete. *International Journal of Solids and Structures* **25** (3):299–326.

Lupini, J. F., Skinner, A.E., & Vaughan, P.R. 1981. The drained residual strength of cohesive soils. *Géotechnique* **31**(2): 181-213.

Ma, X. & Grabe, J. 2010. Efficiency Increase of Soil Heat Exchangers due to Groundwater Flow and Air Injection Wells. *Proceedings World Geothermal Congress 2010,* Bali, Indonesia, pp. 25-29.

Mayne, P.W., Coop, M.R., Springman, S., Huang, A.B. & Zornberg, J. 2009. GeoMaterial Behavior and Testing. *Proceedings of the 17th International Conference on Soil Mechanics & Geotechnical Engineering*, Vol. **4**, pp. 2777-2872.

McCartney, J. S., & Murphy, K. D. 2012. Strain distributions in full scale energy foundations. *DFI J* **6**(2), 28–36.

McCartney, J.S. & Rosenberg, J. 2011. Impact of Heat Exchange on Side Shear in Thermo-Active Foundations. Proceedings of the Geo-Frontiers 2011 Conference, Jie H., Daniel E., Alzamora P.E. ASTM, Geotechnical Special Publications (GSP) 211: 488 – 498.

Mohajerani, M., Delage, P., Sulem, J., Monfared, M., Tang, A.M., & Gatmiri, B. 2014. The Thermal Volume Changes of the Callovo–Oxfordian Claystone. *Rock Mechanics and Rock Engineering* **47**(1): 131–142.

Monfared, M., Sulem, J., Delage, P., & Mohajerani, M. 2011. A laboratory investigation on thermal properties of the Opalinus claystone. *Rock Mechanics and Rock Engineering* **44**(6): 735–747.

Moritz, L. 1995. Geotechnical properties of clay at elevated temperatures. Swedish Geotechnical Institute, Report no. 14. 69 pages.

Murphy, K.D., McCartney, J.S. & Henry, K.S. 2014. Evaluation of thermo-mechanical and thermal behaviour of full-scale energy foundations. *Acta Geotechnica*. DOI: 10.1007/s11440-013-0298-4.

Nogami, T., Otani, J., Konagai, K., & Chen, H. 1992. Nonlinear soil-pile interaction model for dynamic lateral motion. *Journal of Geotechnical Engineering* **118**(1): 89–106.

Nuth, M. 2008. International realisation of ground energy. *GeoDrilling International*.

Okyay, U.S., Dias, D., Thorel, L. & Rault, G. 2014. Centrifuge modelling of a pile-supported granular earth-platform. *Journal of Geotechnical and Geoenvironmental* Engineering 140(2). DOI: 10.1061/(ASCE)GT.1943-5606.0001004.

Pahud, D., Fromentin, A. & Hubbuch, M. 1999. Heat exchanger pile system of the Dock Midfield at the Zürich Airport. Detailed Simulation and Optimisation of the Installation. Final report. Swiss Federal Office of Energy, Switzerland.

Paik, K., & Salgado, R. 2004. Effect of pile installation method on pipe pile behaviour in sands. *Geotechnical Testing Journal* **27**(1): 78 – 88.

Parkin, A.K. & Lunne, T. 1982. Boundary Effects in the Laboratory Calibration of a Cone Penetrometer for Sand. *Proceedings of the 2nd European Symposium on Penetration Testing*, Vol. **2**, pp. 761–768.

Pasten, C. & Santamarina, J.C. 2014. Thermally induced long-term displacement of thermoactive piles. *Journal of Geotechnical and Geoenvironmental Engineering* 140(5). DOI: 10.1061/(ASCE)GT.1943-5606.0001092.

Peron, H., Laloui, L., Knellwolf, C., Nuth M., Silvani, C. 2010. Geotechnical design of heat exchanger piles. *GSHP Association Research Seminar: Current and Future Research Into Ground Source Energy*, Milton Keynes, United Kingdom.

Recordon, E. 1993. Déformabilité des sols non saturés à diverses températures. *Revue Française de Géotechnique* **65**: 37-56.

Reeves, G.M., Sims, I. & Cripps, J.C. 2006. Clay Materials Used in Construction. The Geological Society, Engineering Geology Special Publication. No. 21.

Robinet, J.C., Pasquiou, A., Jullien, A. & Belanteur, N. 1997. Expériences de laboratoire sur le comportement thermo-hydro-mécanique de matériaux argileux remaniés gonflants et non gonflants. *Revue Française de Géotechnique* **81**: 53-80.

Rosquoet, F. 2004. Pieux sous charge latéral cyclique. *Ph.D. thesis*, Ecole Centrale de Nantes, France. 327 pages.

Rouaiguia, A. 2010. Residual shear strength of clay-structure interfaces. *International Journal of Civil & Environmental Engineering* **10**(3): 6-18.

Saggu, R. & Chakraborty, T. 2014a. Thermal analysis of energy piles in sand. *Geomechanics and Geoengineering: An International Journal*. DOI: 10.1080/17486025.2014.923586.

Saggu, R. & Chakraborty, T. 2014b. Cyclic thermo-mechanical analysis of energy piles in sand. *Geotechnical and Geological Engineering*. DOI: 10.1007/s10706-014-9798-8.

Said, I. 2006. Comportement des interfaces et modélisation des pieux sous charge axiale. *Ph.D. thesis*, Ecole Nationale des Ponts et Chaussées, France. 274 pages.

Said, I., De Gennaro, V. & Frank, R. 2009. Axisymmetric finite element analysis of pile loading tests. *Computers and Geotechnics* **36**: 6–19.

Saix, C., Deviller,s P., & El Youssoufi, M. S. 2000. Elément de couplage thermomécanique dans la consolidation de sols non saturés. *Canadian Geotechnical Journal* **37**(2): 308-317.

Sakr, M. & El Naggar, M. H. 2003. Centrifuge modelling of tapered piles in sand. *Geotechnical Testing Journal* **26**(1).

Sanner B. 2001. Shallow geothermal energy. *GHC Bulletin* **22**(4): 19-25.

Savage P.F. 2007. Evaluation of possible swelling potential of soil. *Proceedings of the 26th Southern African Transport Conference* (SATC 2007), South Africa, pp. 277-283.

Savvidou, C., & Britto, A.M. 1995. Numerical and experimental investigation of thermally induced effects in saturated soils. *Soils and Foundations* **35**(1): 37-44.

Shakir, R.R., & Zhu, J. 2009. Behaviour of compacted clay-concrete interface. *Frontiers of Architecture and Civil Engineering in China* **3**(1): 85– 92.

Shoukry, S.N., William, G.W., Downie, B. & Riad, M.Y. 2011. Effect of moisture and temperature on the mechanical properties of concrete. *Construction and Building Materials* **25**(2): 688–696.

SIA Documentation D 0190. 2005. Utilisation de la chaleur du sol par des ouvrages de foundation et de soutenement en beton. Guide pour la conception, la réalisation et la maintenance.

Stwart, M. & McCartney, J.S. 2014. Centrifuge modeling of soil-structure interaction in energy foundations. *Journal of Geotechnical and Geoenvironmental Engineering*. DOI: 10.1061/(ASCE)GT.1943-5606.0001061.

Sultan, N., Delage, P., & Cui, Y.J. 2002. Temperature effects on the volume change behaviour of Boom Clay. *Engineering Geology* **64**(2–3): 135–145.

Suryatriyastuti, M. E. 2013. Numerical study of the thermo-active piles behaviour in cohesinless soils. *Ph.D. thesis*, Université Lille 1, France. 176 pages.

Suryatriyastuti, M. E., Mroueh, H. & Burlon, S. 2012. Understanding the temperature-induced mechanical behaviour of energy pile foundations. *Renewable & Sustainable Energy Reviews* **16**: 3344–3354.

Taha, A., & Fall, M. 2013. Shear behaviour of sensitive Marine clay-concrete interfaces. *Journal of Geotechnical and Geoenvironmental Engineering* **139**(4): 644-650.
Talesnick, M.L. 2012. A different approach and result to the measurement of K0 of granular soils. *Géotechnique* **62**. DOI: http://dx.doi.org/10.1680/geot.11.P.009.

Tali, B. 2011. Comportement de l'interface sols-structure sous sollicitations cycliques. Application au calcul des fondations profondes. *Ph.D. thesis*, Ecole Nationale des Ponts et Chaussées, France.

Tang, A.M., Cui, Y.J., & Barnel, N. 2007. A new isotropic cell for studying the thermo-mechanical behaviour of unsaturated expansive clays. *Geotechnical Testing Journal* **30**(5): 1-8.

Tang, A.M., Cui, Y.J., & Barnel, N. 2008. Thermo-mechanical behaviour of a compacted swelling clay. *Géotechnique* **58**(1): 45–54.

Thorel, L., Rault, G., Garnier, J. Murillo, C., Gaudicheau, P., Néel, A. & Favraud, C. 2008. Mesures en macrogravité sur modèles réduits d'ouvrages géotechniques. BLPC n° 273.

Tsubakihara, Y., & Kishida, H. 1993. Frictional behaviour between normally consolidated clay and steel by two direct shear type apparatuses. *Soils and Foundations* **3**(2): 1-13.

Tsubakihara, Y., Kishida, H., & Nishiyama, T. 1993. Friction between cohesive soils and steel. *Soils and Foundations* **33**(2): 145-156.

Vega, A. & McCartney, J.S. 2014. Cyclic heating effects on thermal volume change of silt. *Environmental Geotechnics*. DOI: 10.1680/envgeo.13.00022.

Vuataz, F., Gorhan, H. & Geissmann, M. 2003. Promotion of geothermal energy in Switzerland:a recent programme for a long-lasting task. *European Geothermal Conference EGC 2003, Szeged, Hungary.*

Wang, B, Bouazza, A. & Haberfield, C. 2011. Preliminary observations from laboratory scale model geothermal pile subjected to thermo-mechanical loading. *Proceedings of the Geo-Frontiers 2011 Conference*, Jie H., Daniel E., Alzamora, P.E.. ASCE, pp. 430-439.

Weinstein, G.M. 2008. Long-term behaviour of micropiles subject to cyclic axial loading. *Ph.D. thesis*, Polytechnic University, Brooklyn, Newyork. 373 pages.

Yang, Y., Datcheva, M., König, D., Schanz, T. 2014. Heat transfer in a geothermal heat-pump system – an analytical assessment. *Géotechique Letters* 4: 139-144. DOI: 10.1680/geolett.13.00058.

Yang, Z. & Jeremić, B. 2005. Study of soil layering effects on lateral loading behavior of piles. *Journal of Geotechnical and Geoenvironmental Engineering* **131**(6): 762–770.

Yari, M. & Javani, N. 2007. Performance assessment of a horizontal-coil geothermal heat pump. *International Journal of Energy Research* **31**(3): 288–99.

Yavari, N., Tang, A.M., Pereira, J.M., & Hassen, G. 2014a. Experimental study on the mechanical behaviour of a heat exchanger pile using physical modelling. *Acta Geotechnica* **9**(3): 385–398.

Yavari, N., Tang, A.M., Pereira, J.M. & Hassen, G. 2014b. A simple method for numerical modelling of mechanical behaviour of an energy pile. *Géotechique Letters* 4: 119-124. DOI: 10.1680/geolett.13.00053.

Youssef, E. 1994 Etude théorique et expérimentale du flambement des pieux. *Ph.D. thesis*, Ecole Nationale des Ponts et Chaussées, France. 271 pages.

Zhang, L., McVay, M.C. & Lai, P. 1998. Centrifuge testing of vertically loaded battered pile groups in sand. *Geotechnical Testing Journal* **21**(4): 281-288.

Zhu, B., Jardine, R.J. & Foray, P. 2009. The use of miniature soil stress measuring cells in laboratory applications involving stress reversals. *Soils and Foundations* **49**(5): 675-688.